

Calibration and Implementation of the AASHTO Mechanistic-Empirical Pavement Design Guide in Arizona



Arizona Department of Transportation Research Center

Calibration and Implementation of the AASHTO Mechanistic-Empirical Pavement Design Guide in Arizona

SPR-606

September 2014

Prepared by:

Michael I. Darter

Leslie Titus-Glover

Harold Von Quintus

Biplab B. Bhattacharya

Jagannath Mallela

Applied Research Associates, Inc.

100 Trade Centre Dr., Suite 200

Champaign, IL 61820

Prepared for:

Arizona Department of Transportation

206 S. 17th Ave.

Phoenix, AZ 85007

in cooperation with

U.S. Department of Transportation

Federal Highway Administration

This report was funded in part through grants from the Federal Highway Administration, U.S. Department of Transportation. The contents of this report reflect the views of the authors, who are responsible for the facts and the accuracy of the data, and for the use or adaptation of previously published material, presented herein. The contents do not necessarily reflect the official views or policies of the Arizona Department of Transportation or the Federal Highway Administration, U.S. Department of Transportation. This report does not constitute a standard, specification, or regulation. Trade or manufacturers' names that may appear herein are cited only because they are considered essential to the objectives of the report. The U.S. government and the State of Arizona do not endorse products or manufacturers.

Technical Report Documentation Page

1. Report No. FHWA-AZ-14-606		2. Government Accession No.		3. Recipient's Catalog No.	
4. Title and Subtitle Calibration and Implementation of the AASHTO Mechanistic-Empirical Pavement Design Guide in Arizona				5. Report Date September 2014	
				6. Performing Organization Code	
7. Author Michael I. Darter, Leslie Titus-Glover, Harold Von Quintus, Biplab B. Bhattacharya, and Jagannath Mallela				8. Performing Organization Report No.	
9. Performing Organization Name and Address Applied Research Associates, Inc. 100 Trade Centre Drive, Suite 200 Champaign, IL 61820				10. Work Unit No.	
				11. Contract or Grant No. SPR 000-1(169) 606	
12. Sponsoring Agency Name and Address Arizona Department of Transportation 206 S. 17th Ave. Phoenix, AZ 85007				13. Type of Report & Period Covered FINAL REPORT 2008-2012	
				14. Sponsoring Agency Code	
15. Supplementary Notes Prepared in cooperation with the Federal Highway Administration.					
16. Abstract This report documents efforts of the Arizona Department of Transportation (ADOT) to implement the American Association of State Highway and Transportation Officials (AASHTO) DARWin-ME pavement design guide in Arizona. The research team also prepared a practical stand-alone user's guide that provides guidance for obtaining inputs, conducting design, and establishing the recommended pavement design. Implementation focused on identifying the desired pavement design application of flexible hot-mix asphalt (HMA) pavements, composite pavements (thin asphalt rubber friction course over jointed plain concrete pavement [JPCP] and continuously reinforced concrete pavement [CRCP]), JPCP, and HMA overlays of flexible pavement; characterizing materials and subgrades; determining traffic loadings (conducted under Darter et al. 2010); collecting and assembling DARWin-ME input data from 180 Long Term Pavement Performance and pavement management system sections of flexible, rigid, composite, and rehabilitated pavements; calibrating the DARWin-ME distress and International Roughness Index (IRI) prediction models to Arizona conditions; and training ADOT staff. Several biased distress and IRI models were corrected through the local calibration of Arizona pavements. Several key inputs were more accurately defined and Arizona defaults provided (e.g., subgrade resilient modulus). The calibration process improved these models through verification, validation, and calibration with Arizona data. Overall, the inputs and calibrated models will provide more accurate, reliable, and cost-effective pavement designs than designs created with global calibrations.					
17. Key Words Mechanistic-empirical pavement design, AASHTO, calibration, validation, MEPDG, DARWin-ME, Long Term Pavement Performance, LTPP, hot-mix asphalt, concrete, rehabilitation, performance			18. Distribution Statement This document is available to the US public through the National Technical Information Service, Springfield, Virginia, 22161.		23. Registrant's Seal Unclassified.
19. Security Classification Unclassified.	20. Security Classification Unclassified.	21. No. of Pages 208	22. Price		

SI* (MODERN METRIC) CONVERSION FACTORS

APPROXIMATE CONVERSIONS TO SI UNITS

Symbol	When You Know	Multiply By	To Find	Symbol
LENGTH				
in	inches	25.4	millimeters	mm
ft	feet	0.305	meters	m
yd	yards	0.914	meters	m
mi	miles	1.61	kilometers	km
AREA				
in ²	square inches	645.2	square millimeters	mm ²
ft ²	square feet	0.093	square meters	m ²
yd ²	square yard	0.836	square meters	m ²
ac	acres	0.405	hectares	ha
mi ²	square miles	2.59	square kilometers	km ²
VOLUME				
fl oz	fluid ounces	29.57	milliliters	mL
gal	gallons	3.785	liters	L
ft ³	cubic feet	0.028	cubic meters	m ³
yd ³	cubic yards	0.765	cubic meters	m ³
NOTE: volumes greater than 1000 L shall be shown in m ³				
MASS				
oz	ounces	28.35	grams	g
lb	pounds	0.454	kilograms	kg
T	short tons (2000 lb)	0.907	megagrams (or "metric ton")	Mg (or "t")
TEMPERATURE (exact degrees)				
°F	Fahrenheit	5 (F-32)/9 or (F-32)/1.8	Celsius	°C
ILLUMINATION				
fc	foot-candles	10.76	lux	lx
fl	foot-Lamberts	3.426	candela/m ²	cd/m ²
FORCE and PRESSURE or STRESS				
lbf	poundforce	4.45	newtons	N
lbf/in ²	poundforce per square inch	6.89	kilopascals	kPa

APPROXIMATE CONVERSIONS FROM SI UNITS

Symbol	When You Know	Multiply By	To Find	Symbol
LENGTH				
mm	millimeters	0.039	inches	in
m	meters	3.28	feet	ft
m	meters	1.09	yards	yd
km	kilometers	0.621	miles	mi
AREA				
mm ²	square millimeters	0.0016	square inches	in ²
m ²	square meters	10.764	square feet	ft ²
m ²	square meters	1.195	square yards	yd ²
ha	hectares	2.47	acres	ac
km ²	square kilometers	0.386	square miles	mi ²
VOLUME				
mL	milliliters	0.034	fluid ounces	fl oz
L	liters	0.264	gallons	gal
m ³	cubic meters	35.314	cubic feet	ft ³
m ³	cubic meters	1.307	cubic yards	yd ³
MASS				
g	grams	0.035	ounces	oz
kg	kilograms	2.202	pounds	lb
Mg (or "t")	megagrams (or "metric ton")	1.103	short tons (2000 lb)	T
TEMPERATURE (exact degrees)				
°C	Celsius	1.8C+32	Fahrenheit	°F
ILLUMINATION				
lx	lux	0.0929	foot-candles	fc
cd/m ²	candela/m ²	0.2919	foot-Lamberts	fl
FORCE and PRESSURE or STRESS				
N	newtons	0.225	poundforce	lbf
kPa	kilopascals	0.145	poundforce per square inch	lbf/in ²

* SI is the symbol for the International System of Units. Appropriate rounding should be made to comply with Section 4 of ASTM E380. (Revised March 2003)

Contents

Executive Summary	1
Chapter 1. Introduction.....	3
Background	3
Overview of MEPDG Implementation Efforts in Arizona.....	4
Project Objectives.....	4
Report Overview	5
Chapter 2. Framework for MEPDG Performance Model Verification and Local Calibration	7
Step 1: Select Hierarchical input Levels	8
Steps 2 and 3: Determine Experimental Design and Sampling Needs	10
Steps 4 and 5: Select HMA and JPCP Projects to Populate Sampling Template.....	14
Step 6: Conduct Field and Forensic Investigations	50
Steps 7 Through 10: Assess Local Bias and Standard Error of the Estimate from Global Calibration Factors, and Eliminate/Reduce Standard Error of the Estimate and Local Bias of Distress Prediction Models.....	50
Step 11: Interpret Results and Determine Adequacy of ADOT MEPDG Locally Calibrated Models	54
Chapter 3. Verification, Local Recalibration, and Validation of MEPDG Models	57
New HMA and HMA Overlaid HMA Alligator Cracking.....	57
New HMA and HMA Overlaid HMA Rutting	64
Transverse Low-Temperature Cracking.....	69
New HMA and HMA Overlaid HMA Smoothness (IRI).....	74
New and Reconstructed JPCP Transverse Cracking.....	79
New JPCP Transverse Joint Faulting	86
New JPCP Smoothness (IRI)	90
ARFC/JPCP Composite Pavement Models	95
Chapter 4. Sensitivity Analysis	107
New HMA Sensitivity Analysis Results.....	108
New JPCP Sensitivity Analysis Results	125
Chapter 5. Validation of Locally Calibrated DARWin-ME New HMA and JPCP Design Procedures for Arizona	139
New HMA Pavement Design Comparison	139
New JPCP Design Comparison	144
Chapter 6. Practical Methodology to Recalibrate DARWin-ME	149
Step 1: Select Hierarchical input Levels	150
Steps 2 and 3: Develop Experimental Design and Sampling Needs	151
Steps 4 and 5: Select HMA and JPCP Pavement Projects to Populate Sampling Template, and Extract and Evaluate Distress and Project Data.....	153
Step 6: Conduct Field and Forensic Investigations	153
Step 7: Characterize Bias and Goodness of Fit of DARWin-ME Global Models Used Under Arizona Conditions	153

Step 8: Perform Local Calibration to Reduce Bias and Improve Goodness of Fit.....	156
Steps 9 Through 11: Assess and Reduce Standard Error, and Interpret Results and Determine Adequacy of Locally Calibrated DARWin-ME Models	157
Chapter 7. Arizona Input Defaults and Calibration Coefficients for MEPDG	159
Default Level 3 Inputs	159
DARWin-ME Arizona Local Calibration Coefficients	165
Checklist of All Inputs	168
Chapter 8. Summary and Recommendations.....	173
References.....	177
Appendix: DARWin-ME HMA Pavement and JPCP Performance Prediction Models.....	179

List of Figures

Figure 1.	Construction/Rehabilitation Year of Projects Selected for the ADOT MEPDG Calibration/Validation Database	17
Figure 2.	Arizona Locations of Projects Selected for the ADOT MEPDG Calibration/Validation Database	17
Figure 3.	Highway Functional Class of Projects Selected for the ADOT MEPDG Calibration/Validation Database	18
Figure 4.	Volumetric (Not Gravimetric) Binder Content of Projects Selected for the ADOT MEPDG Calibration/Validation Database.....	18
Figure 5.	In-Place Air Voids of Projects Selected for the ADOT MEPDG Calibration/Validation Database	19
Figure 6.	PCC CTE (from LTPP) of Projects Selected for the ADOT MEPDG Calibration/Validation Database	19
Figure 7.	PCC 28-Day Compressive Strength of Projects Selected for the ADOT MEPDG Calibration/Validation Database.....	20
Figure 8.	PCC 28-Day Elastic Modulus of Projects Selected for the ADOT MEPDG Calibration/Validation Database	20
Figure 9.	Aggregate Base and Subgrade Liquid Limit of Projects Selected for the ADOT MEPDG Calibration/Validation Database.....	21
Figure 10.	Aggregate Base and Subgrade Plasticity Index of Projects Selected for the ADOT MEPDG Calibration/Validation Database.....	22
Figure 11.	Aggregate Base and Subgrade Maximum Dry Density of Projects Selected for the ADOT MEPDG Calibration/Validation Database.....	23
Figure 12.	Subgrade Type (Coarse- or Fine-Grained) of Projects Selected for the ADOT MEPDG Calibration/Validation Database.....	23
Figure 13.	New HMA Pavement Thickness of Projects Selected for the ADOT MEPDG Calibration/Validation Database	24
Figure 14.	Existing HMA Thickness for HMA Overlaid HMA Pavement Projects Selected for the ADOT MEPDG Calibration/Validation Database.....	24
Figure 15.	HMA Overlay Thickness of HMA Overlaid HMA Pavement Projects Selected for the ADOT MEPDG Calibration/Validation Database.....	25
Figure 16.	Relationship Between ADOT and LTPP Rutting Measurements.....	27
Figure 17.	Measured Alligator Cracking in LTPP and PMS Sections of New HMA and HMA Overlaid HMA Projects.	29
Figure 18.	Measured HMA Transverse Cracking in LTPP and PMS Sections of New HMA and HMA Overlaid HMA Projects.	29
Figure 19.	Measured Rutting in LTPP and PMS Sections of New HMA and HMA Overlaid HMA Projects	30
Figure 20.	Measured AC IRI in LTPP and PMS Sections of New HMA and HMA Overlaid HMA Projects	30

Figure 21.	Measured JPCP Transverse Cracking in LTPP and PMS Sections of New JPCP Projects	31
Figure 22.	Measured JPCP Transverse Joint Faulting in LTPP and PMS Sections of New JPCP Projects	31
Figure 23.	Measured JPCP IRI of LTPP and PMS Sections of New JPCP Projects.....	32
Figure 24.	Progression of Measured IRI with Age in ADOT PMS 03-31.....	33
Figure 25.	Progression of Measured Rutting with Age in ADOT LTPP 0509.....	33
Figure 26.	Progression of Measured HMA Transverse Cracking with Age in ADOT LTPP 0113	34
Figure 27.	Progression of Measured JPCP Transverse Cracking with Age in ADOT LTPP 0217	34
Figure 28.	Location of Selected New HMA and HMA Overlaid HMA Pavement Projects.....	38
Figure 29.	Location of Selected New Bare JPCP Projects.	39
Figure 30.	Location of Selected New ARFC-surfaced JPCP Composite Projects.....	40
Figure 31.	Initial Verification of the HMA Alligator Fatigue Cracking Models with Global Coefficients Using Arizona Performance Data.	57
Figure 32.	Measured and Predicted Alligator Cracking Versus Cumulated Fatigue Damage for the Locally Calibrated Alligator Cracking Submodels	62
Figure 33.	Predicted and Measured Alligator (Fatigue) Cracking for Arizona I-8 HMA (LTPP 4_0501) Pavement	63
Figure 34.	Predicted and Measured Alligator (Fatigue) Cracking for Arizona I-8 HMA (LTPP 4_050) Overlaid Pavement	63
Figure 35.	Predicted and Total Rutting Using Global Coefficients and Arizona HMA Pavement Performance Data	64
Figure 36.	Measured and Predicted Total Rutting for New HMA and HMA Overlaid HMA Pavements for the Locally Calibrated Rutting Submodels (Using 100 Percent of Projects).....	67
Figure 37.	High Variation of Measured Rutting for LTPP Project 4_0162.....	68
Figure 38.	Measured and Predicted (Global and Arizona Local Calibrated Models) Total Rutting for Arizona LTPP Project 4_0113	68
Figure 39.	Transverse Cracking in Nonfreeze Areas of Phoenix and Tucson	69
Figure 40.	Monthly Temperatures Recorded at the SPS-1 Site Near Kingman, Arizona.....	70
Figure 41.	Measured Transverse Cracking at the SPS-1 Site After 10 Years of Service	70
Figure 42.	Predicted and Measured Transverse Cracking Using Global Coefficients in SPS-1 HMA Pavement Sections	71
Figure 43.	Predicted (Calibration K = 100) Versus Measured Transverse Cracking in SPS-1 HMA Pavement Sections	72
Figure 44.	MEPDG Predicted Transverse Cracking at Various Arizona Locations	74
Figure 45.	Predicted Versus Measured IRI Using Global Coefficients and Arizona HMA Pavement Performance Data	75
Figure 46.	Measured and Predicted HMA IRI for New HMA and HMA Overlaid HMA Pavements for the Locally Calibrated IRI Model (Using 100 Percent of Projects).	77

Figure 47.	Measured and Predicted IRI for HMA LTPP Project 4_0260	78
Figure 48.	Measured and Predicted (Global and Arizona Local Calibrated Models) Total IRI for Arizona LTPP Project 4_0122.....	78
Figure 49.	Predicted Versus Measured Percent Slabs Cracked for Arizona JPCP with Global Calibration Coefficients.....	79
Figure 50.	Arizona JPCP with HMA Base Course Measured and Predicted Percent Slabs Transversely Cracked	81
Figure 51.	Arizona JPCP with Unbound Aggregate Base Course Measured and Predicted Percent Slabs Transversely Cracked	81
Figure 52.	Measured and Predicted JPCP Transverse Cracking Using MEPDG Global Models for JPCP Over Lean Concrete Base	82
Figure 53.	Predicted Versus Measured Percent Slabs Transverse Cracked for Arizona JPCP with All Types of Base Courses	83
Figure 54.	Measured and Predicted JPCP Transverse Cracking Versus Cumulative Fatigue Damage for Local Arizona Calibration Coefficients (Using 100 Percent of Projects).....	84
Figure 55.	Predicted (Using Local Calibration Factors and Input Recommendations) and Measured Transverse Cracking for JPCP 4_0217 (SPS-2) with Lean Concrete Base	85
Figure 56.	Predicted (Using Local Calibration Factors and Input Recommendations) and Measured Transverse Cracking for JPCP 4_0214 (SPS-2) with Untreated Aggregate Base	85
Figure 57.	Predicted (Using Local Calibration Factors and Input Recommendations) and Measured Transverse Cracking for JPCP 4_0224 (SPS-2) with HMA Base.	86
Figure 58.	Predicted Versus Measured Joint Faulting for JPCP with Global Calibration Coefficients	87
Figure 59.	Measured and Predicted Transverse Joint Faulting for Locally Calibrated Faulting Submodels (Using 100 Percent of Projects)	89
Figure 60.	Measured and Predicted Joint Faulting Using the Arizona Calibrated Model for JPCP Section 4_0265 on I-10.....	90
Figure 61.	Predicted JPCP IRI Versus Measured Arizona JPCP with Global Calibration Coefficients	91
Figure 62.	Measured and Predicted JPCP IRI (Using 100 Percent of Projects).....	93
Figure 63.	Predicted and Measured JPCP IRI for Arizona Section 04_0262.....	94
Figure 64.	Predicted and Measured JPCP IRI for Arizona Section 04_0267.....	94
Figure 65.	Measured Rutting of ARFC (0.75-inch) for Arizona Composite Pavements.....	98
Figure 66.	Measured Versus Predicted Rutting for ARFC Surfacing Over JPCP.....	98
Figure 67.	Percentage of Slabs Cracked Versus JPCP Slab Fatigue Damage in JPCP LTPP and PMS Sections and in Composite Pavement.....	101
Figure 68.	MEPDG Predicted Versus Measured IRI for Composite Pavement Project (2 to 16 Years).....	102

Figure 69. CRCP Observed Punchouts Versus Fatigue Damage for All CRCP Used in the 2007 National Calibration.....	105
Figure 70. Effect of AADTT on HMA Alligator Fatigue Cracking	109
Figure 71. Effect of AADTT on HMA Total Rutting	109
Figure 72. Effect of Initial AADTT on HMA IRI	110
Figure 73. Effect of HMA Thickness on HMA Alligator Fatigue Cracking	111
Figure 74. Effect of HMA Thickness on Total Rutting.....	111
Figure 75. Effect of HMA Thickness on IRI	112
Figure 76. Effect of Binder Content on HMA Alligator Cracking	113
Figure 77. Effect of Binder Content on HMA Total Rutting.....	113
Figure 78. Effect of Binder Content on HMA IRI	114
Figure 79. Effect of Air Voids on HMA Alligator Cracking	115
Figure 80. Effect of Air Voids on HMA Total Rutting.....	115
Figure 81. Effect of Air Voids on HMA IRI.....	116
Figure 82. Effect of PG Binder on HMA Alligator Cracking.....	117
Figure 83. Effect of PG Binder on HMA Total Rutting	117
Figure 84. Effect of PG Binder on HMA IRI.....	118
Figure 85. Effect of Subgrade Type on HMA Alligator Cracking.....	119
Figure 86. Effect of Subgrade Type on HMA Total Rutting	119
Figure 87. Effect of Subgrade Type on HMA IRI	120
Figure 88. Effect of Climate on HMA Alligator Cracking.....	121
Figure 89. Effect of Climate on HMA Total Rutting	121
Figure 90. Effect of Climate on HMA IRI.....	122
Figure 91. Effect of Reliability on HMA Alligator Cracking	123
Figure 92. Effect of Reliability on HMA Total Rutting	124
Figure 93. Effect of Reliability on HMA IRI	124
Figure 94. Effect of AADTT on JPCP Transverse Cracking.....	125
Figure 95. Effect of AADTT on JPCP Mean Joint Faulting	126
Figure 96. Effect of Initial AADTT on JPCP IRI.....	126
Figure 97. Effect of PCC Thickness on JPCP Transverse Cracking.....	127
Figure 98. Effect of PCC Thickness on JPCP Mean Joint Faulting	128
Figure 99. Effect of PCC Thickness on JPCP IRI	128
Figure 100. Effect of CTE on JPCP Transverse Cracking.....	129
Figure 101. Effect of CTE on JPCP Mean Joint Faulting	130
Figure 102. Effect of CTE on JPCP IRI.....	130
Figure 103. Effect of Shoulder Type on JPCP Transverse Cracking	131
Figure 104. Effect of Shoulder Type on JPCP Mean Joint Faulting	132
Figure 105. Effect of Shoulder Type on JPCP IRI.....	132
Figure 106. Effect of Subgrade Type on JPCP Transverse Cracking.....	133
Figure 107. Effect of Subgrade Type on JPCP Mean Joint Faulting	134
Figure 108. Effect of Subgrade Type on JPCP IRI.....	134
Figure 109. Effect of Climate on JPCP Transverse Cracking	135

Figure 110. Effect of Climate on JPCP Mean Joint Faulting.....	136
Figure 111. Effect of Climate on JPCP IRI	136
Figure 112. Effect of Reliability on JPCP Transverse Cracking.....	137
Figure 113. Effect of Reliability on JPCP Mean Joint Faulting	138
Figure 114. Effect of Reliability on JPCP IRI	138
Figure 115. New HMA Project Trial Design Structure	140
Figure 116. Predicted Alligator Cracking for the New HMA Trial Design Using DARWin-ME	142
Figure 117. Predicted Rutting for the New HMA Trial Design Using DARWin-ME.....	143
Figure 118. Predicted IRI for the New HMA Trial Design Using DARWin-ME	143
Figure 119. New JPCP Project Trial Design Structure.....	144
Figure 120. Predicted Transverse Cracking for the New JPCP Trial Design Using DARWin-ME	147
Figure 121. Predicted Faulting for the New JPCP Trial Design Using DARWin-ME	148
Figure 122. Predicted IRI for the New JPCP Trial Design Using DARWin-ME	148

List of Tables

Table 1.	Recommended MEPDG Hierarchical Input Levels for New HMA and HMA Overlaid Pavements	9
Table 2.	Recommended MEPDG Hierarchical Input Levels for New JPCP	9
Table 3.	ADOT Pavement Design and Construction Practices	11
Table 4.	Sampling Template for New and Rehabilitated HMA Pavements	12
Table 5.	Sampling Template for New and Rehabilitated JPCP	13
Table 6.	Estimated Number of Pavement Projects Required for MEPDG Validation and Local Calibration	14
Table 7.	Sources for the ADOT MEPDG Calibration and Validation Database	16
Table 8.	Distress and IRI Data Sources for Local Calibration and Validation.	26
Table 9.	Comparison of Distress and IRI Values with Design Criteria or Threshold Values	32
Table 10.	Breakdown of Selected Projects for Validation and Local Calibration	36
Table 11.	Populated Sampling Template for New and Rehabilitated HMA-Surfaced Pavements.....	36
Table 12.	Populated Sampling Template for New and Rehabilitated JPCP	37
Table 13.	LTPP and ADOT PMS Projects Selected for Validation and Local Calibration	41
Table 14.	National Calibration Under NCHRP 1-40D New HMA Pavement and New JPCP Model Statistics	51
Table 15.	Sampling Template for the 10 Percent Validation/90 Percent Calibration Databases for New and Rehabilitated HMA-Surfaced Pavements	55
Table 16.	Simplified Sampling Template for the Validation and Local Calibration of New JPCP	56
Table 17.	MEPDG Global Models Evaluated for Arizona Local Conditions	58
Table 18.	Preliminary Local Calibration Coefficients and Goodness of Fit Statistics for Alligator Cracking Submodels Using 90 Percent of Projects	60
Table 19.	Goodness of Fit Statistics for Validating the Preliminary 90 Percent Locally Calibrated Alligator Cracking Submodels with 10 Percent of Projects.	60
Table 20.	Goodness of Fit and Bias Test Statistics for Final Locally Calibrated Alligator Cracking Model (Based on 100 Percent of All Projects).....	61
Table 21.	Preliminary Local Calibration Coefficients and Goodness of Fit Statistics for Total Rutting Submodels Using 90 Percent of Projects.....	66
Table 22.	Goodness of Fit Statistics for Validating the Preliminary 90 Percent Locally Calibrated Total Rutting Submodels with 10 Percent of Projects.....	66
Table 23.	Goodness of Fit and Bias Test Statistics for Final Locally Calibrated Rutting Model (Based on 100 Percent of All Projects)	67
Table 24.	Measured and Predicted HMA Transverse Cracking at the SPS-1 Site	72
Table 25.	MEPDG Prediction of HMA Transverse Cracking for Arizona Climates (Calibration K = 50)	73
Table 26.	Preliminary Local Calibration Coefficients and Goodness of Fit Statistics for HMA IRI Model Using 90 Percent of Projects.....	76
Table 27.	Goodness of Fit Statistics for Validating the 90 Percent Preliminary Locally Calibrated HMA IRI Model with 10 Percent of Projects.....	76

Table 28.	Goodness of Fit and Bias Test Statistics for Final Locally Calibrated HMA IRI Model (Based on 100 Percent of All Projects)	77
Table 29.	Goodness of Fit and Bias Test Statistics for Globally Calibrated JPCP Transverse Cracking Model (Based on 100 Percent of All Projects)	83
Table 30.	Preliminary Local Calibration Coefficients and Goodness of Fit Statistics for Transverse Joint Faulting Model Using 90 Percent of Projects	88
Table 31.	Goodness of Fit Statistics for Validating the 90 Percent Preliminary Locally Calibrated Transverse Joint Faulting Model with 10 Percent of the Data	88
Table 32.	Goodness of Fit and Bias Test Statistics for Final Locally Calibrated Transverse Joint Faulting Model (Based on 100 Percent of All Projects)	89
Table 33.	Preliminary Local Calibration Coefficients and Goodness of Fit Statistics for JPCP IRI Model Using 90 Percent of Selected Calibration Projects	92
Table 34.	Goodness of Fit Statistics for Validating the 90 Percent Preliminary Locally Calibrated JPCP IRI Model with the 10 Percent Model	92
Table 35.	Goodness of Fit and Bias Test Statistics for Final Arizona Calibrated JPCP IRI Model (Based on 100 Percent of All Projects)	93
Table 36.	Arizona Composite Pavement Rutting and IRI Calibration Data	97
Table 37.	Fatigue Damage and Cracking Analysis for ARFC/JPCP Composite Pavements	99
Table 38.	Measured and Predicted Performance of Loop 101 and I-10 CRCP Sections	104
Table 39.	Key Inputs in New or Reconstructed HMA Pavement Sensitivity Analysis	107
Table 40.	Key Inputs in New or Reconstructed JPCP Sensitivity Analysis	108
Table 41.	Effect of Climate on Predicted Distress and IRI	122
Table 42.	Key Inputs for New HMA Pavement Project Design Comparison	1410
Table 43.	Trial Design Results for New HMA Pavement Projects	1421
Table 44.	Key Inputs for New JPCP Project Design	146
Table 45.	Trial Design Results for New JPCP Project Design	147
Table 46.	Recommended DARWin-ME Hierarchical Input Levels for New HMA and HMA Overlaid Pavements	150
Table 47.	Recommended DARWin-ME Hierarchical Input Levels for New JPCP	151
Table 48.	Sampling Template for New and Rehabilitated HMA Pavements	152
Table 49.	Estimated Number of Pavement Projects Required for Validation and Local Calibration	152
Table 50.	National Calibration under NCHRP 1-40D of New HMA Pavement and New JPCP Model Statistics	155
Table 51.	Default Level 3 Inputs for HMA Materials	159
Table 52.	Default Level 3 PCC Compressive Inputs	160
Table 53.	Default Level 3 PCC Flexural Strength Inputs	160
Table 54.	Default Level 3 PCC Elastic Modulus Inputs	161
Table 55.	Default Level 3 PCC CTE Inputs	161
Table 56.	Default Level 3 PCC Mixture Constituents Inputs	161
Table 57.	Default Level 3 Inputs for Cement Aggregate Mixture Materials	162
Table 58.	Default Level 3 Inputs for Unbound Aggregate Materials	163

Table 59.	Default Level 3 Inputs for Subgrade Materials Mr at Optimum Moisture Content	164
Table 60.	DARWin-ME Local Calibration Coefficients for New HMA and HMA Overlaid HMA Pavement	166
Table 61.	DARWin-ME Local Calibration Coefficients for New JPCP	167
Table 62.	DARWin-ME Local Calibration Coefficients for New CRCP	167
Table 63.	Checklist of Flexible Pavement Inputs	168
Table 64.	Checklist of Rigid Pavement Inputs	170
Table 65.	Comparison of MEPDG Global and Arizona-Specific Model Goodness of Fit Statistics	175
Table 66.	HMA Pavement Local Calibration Coefficients	196
Table 67.	JPCP Local Calibration Coefficients	196

List of Acronyms

AADTT	average annual daily truck traffic
AASHTO	American Association of State Highway and Transportation Officials
AC	asphalt concrete
ADOT	Arizona Department of Transportation
AR	asphalt rubber
ARFC	asphalt rubber friction course
ASU	Arizona State University
CPR	concrete pavement restoration
CRCP	continuously reinforced concrete pavement
CTE	coefficient of thermal expansion
FHWA	Federal Highway Administration
GPS	global positioning system
HMA	hot-mix asphalt
IRI	International Roughness Index
JPCP	jointed plain concrete pavement
JTFP	Joint Task Force on Pavements
LTPP	Long-Term Pavement Performance
MEPDG	<i>Mechanistic Empirical Pavement Design Guide</i>
NCDC	National Climate Data Center
NCHRP	National Cooperative Highway Research Program
NRCS	Natural Resources Conservation Service
PCC	portland cement concrete
PG	performance grade
PMS	Pavement Management Services
QA	quality assurance
SEE	standard error of the estimate
SHA	state highway administration
SPR	State Planning and Research
SPS	specific pavement study
SSURGO	Soil Survey Geographic database
USDA	United States Department of Agriculture

EXECUTIVE SUMMARY

This report documents the efforts of the Arizona Department of Transportation (ADOT) to implement the American Association of State Highway and Transportation Officials (AASHTO) DARWin-ME pavement design and rehabilitation guide. As part of this implementation, the research team also prepared a practical stand-alone user's guide that provides guidance for obtaining inputs, conducting design, and establishing the recommended pavement design.

Adopting AASHTO DARWin-ME will result in more accurate, reliable, and cost-effective ADOT pavement and rehabilitation designs. The objectives of ADOT's implementation efforts were to:

- Ensure that all design inputs were proper and were tailored to Arizona conditions and resources.
- Ensure that the distress and International Roughness Index (IRI) prediction models were unbiased (i.e., did not consistently over- or underpredict).
- Reduce the prediction error of the distress and IRI models. (Each model's error is used in the reliability design and thus affects the resulting design.)
- Provide a user's guide and training for ADOT designers and consultants.

ADOT identified the following desired pavement design applications in DARWin-ME for implementation:

- Flexible (hot-mix asphalt [HMA]) pavements.
- Composite pavements (thin asphalt rubber friction course over jointed plain concrete pavement [JPCP] and continuously reinforced concrete pavement [CRCP]).
- JPCP and CRCP (bare designs).
- HMA overlays of flexible pavement.

To achieve these objectives, the researchers used Microsoft Excel to create an ADOT pavement database that comprised 180 pavement sections and inputs for the DARWin-ME. The database included:

- The four pavement design applications. The project team obtained pavement sections from the Long-Term Pavement Performance (LTPP) experiment, previous field research studies, and other projects included in the pavement management database (SODA).
- Design, materials, and construction inputs for each section, obtained from the LTPP database and ADOT files.
- Past traffic loading information, also obtained from the LTPP database and ADOT files.
- Measured performance data over the life of the pavement, obtained from the LTPP database, ADOT files and videos, and manual field surveys conducted by the research team.

After reviewing and analyzing all DARWin-ME inputs for their importance and sensitivity, the researchers identified several key inputs to more accurately define them and to develop Arizona defaults. These inputs (listed below) were based on data from the ADOT pavement database established for this study:

- Default values for all design, traffic, materials, and construction inputs that are specific to Arizona.
- Subgrade resilient modulus (Arizona-specific soils based on backcalculation).
- Time of full slab and base friction for various base courses.
- Performance criteria and design reliability levels for all classes of highways.
- Traffic inputs (gathered from work accomplished under the ADOT project, *Development of a Traffic Data Input System in Arizona for the MEPDG* (Darter et al. 2010)).
- Weather station data correction.

The researchers then applied a formal verification, calibration, and final validation process of the distress and IRI models to each distress and IRI model in DARWin-ME, using Arizona data from the 180 sections. Verification involved testing the model predictions with global coefficients but using only Arizona performance data. If the model showed bias (over- or underprediction overall), it was identified for recalibration. Recalibration involved deriving new local coefficients for each model using the Arizona performance data that removed the bias and reduced the prediction error. Validation involved a further independent check of the model using 10 percent of the data withheld from the recalibration effort.

This process removed bias (consistent over- or underprediction) and improved accuracy of model prediction. In most cases, this effort improved distress and IRI model accuracy and removed the over- and underprediction of bias. For example, the goodness of fit for the HMA IRI model improved from $R^2 = 30$ percent with global coefficients to 80 percent with Arizona-specific coefficients. The standard error of IRI went from 19 to 8 inch/mi. The improvement in these models was notable, indicating that the Arizona-calibrated models will provide much more accurate, reliable, and cost-effective designs than models using global calibrations.

The researchers also prepared design comparisons and sensitivity studies that helped to establish confidence in the pavement design results from the *Mechanistic-Empirical Pavement Design Guide*.

CHAPTER 1. INTRODUCTION

BACKGROUND

In 1998 the American Association of State Highway and Transportation Officials (AASHTO) Joint Task Force on Pavements (JTFP) initiated National Cooperative Highway Research Program (NCHRP) Project 1-37A, Development of the Guide for Design of New and Rehabilitated Pavement Structures: Phase II, to develop a mechanistic-based design procedure for new and rehabilitated pavement structures. This project resulted in the *Mechanistic-Empirical Pavement Design Guide* (MEPDG) in 2004. The project deliverables consisted of a guide for mechanistic-empirical pavement design and analysis, companion software and a software user's manual, and implementation and training materials.

Following completion of NCHRP Project 1-37A, the AASHTO JTFP developed a plan for state highway agencies (SHAs) to adopt and implement the MEPDG. Key components of the plan, which was implemented under NCHRP Projects 01-40A, 01-40B, 01-40D, and 20-07, included developing guides and software tools such as the AASHTO MEPDG (Interim Edition), AASHTO MEPDG Local Calibration Guide, and DARWin-ME (the professional/commercial-grade software tool based on the MEPDG design and analysis principles). These products collectively allow users to analyze and perform new and rehabilitated pavement design and forensic analysis such as:

- Modeling truck traffic growth, truck class distribution, various volume adjustments, axles per truck type, and axle load distribution.
- Modeling temperature and moisture conditions within the pavement structure and subgrade.
- Characterizing time- and climate-dependent paving materials properties.
- Computing critical pavement responses (such as stresses, strains, and deflections) to applied traffic loads using layer elastic and finite-element-based analysis techniques.
- Predicting pavement damage and distress using transfer models and smoothness.
- Designing a variety of flexible, rigid, and rehabilitated pavement structures to meet selected performance criteria for a specified level of reliability.

The MEPDG distress and smoothness models were calibrated using data from hundreds of flexible, rigid, and rehabilitated pavement projects included in the Federal Highway Administration (FHWA) Long-Term Pavement Performance (LTPP) program as well as additional state and other research sections. These projects were located throughout the United States, including Arizona. Calibration here indicates that various model coefficients were derived so that the cracking, rutting, faulting, and smoothness models predict as closely as possible similar distresses that exist in the field for hundreds of projects.

OVERVIEW OF MEPDG IMPLEMENTATION EFFORTS IN ARIZONA

The Arizona Department of Transportation (ADOT) and other U.S. SHAs initiated efforts to adopt the MEPDG as the standard procedure for designing new and rehabilitated pavements. ADOT's MEPDG implementation plans began in 2008 and have focused on:

- Characterizing asphalt binder, hot-mix asphalt (HMA), granular base course, and subgrade soils to provide inputs to the MEPDG.
- Characterizing traffic loadings, volumes, vehicle distribution, lane distribution, lateral distribution, and other inputs under Darter et al. 2010.
- Identifying the desired MEPDG applications, which included flexible (HMA) pavements, jointed plain concrete pavement (JPCP), composite pavements (thin asphalt rubber friction [ARFC] course over JPCP and continuously reinforced concrete pavement [CRCP]), HMA overlays of flexible pavement, concrete pavement restoration (CPR), and JPCP overlays.
- Collecting and assembling MEPDG input data from 180 LTPP and pavement management system sections of flexible, rigid, composite, and rehabilitated pavements for use in local calibration.
- Calibrating the MEPDG (including the accompanying analysis and design software) for select applications in Arizona conditions (such as highway pavement structures, materials, traffic, and climate).
- Validating the calibrated MEPDG, including the accompanying analysis and design software, for Arizona conditions.

This report provides details of all activities, results, and recommendations needed for ADOT to implement the MEPDG.

PROJECT OBJECTIVES

This project's objectives were to:

- Evaluate the applicability of the MEPDG for Arizona conditions.
- Calibrate the MEPDG, including the accompanying analysis and design software, for Arizona conditions such as highway pavement structures, materials, traffic, and climate.
- Validate the calibrated MEPDG, including the accompanying analysis and design software, for Arizona conditions.
- Finalize a comprehensive MEPDG and associated analysis and design software user or practice manual for Arizona.

- Develop a practical methodology and tools for use in periodically recalibrating the Arizona-calibrated MEPDG.
- Deliver a populated and implementable calibrated Arizona *MEPDG* along with associated software based on this work, including all material types and pavement structures commonly used in Arizona.
- Deliver an ADOT MEPDG user's manual.
- Train select ADOT staff in the use and structure of the Arizona MEPDG.

REPORT OVERVIEW

The remainder of this report is organized into eight chapters. Chapter 2 provides the overall framework for calibrating the MEPDG models for local Arizona conditions and practices. Chapter 3 describes efforts to verify, calibrate, and validate the MEPDG performance models and design procedure for Arizona. Chapter 4 includes a comprehensive sensitivity analysis performed to verify reasonableness of the ADOT locally calibrated MEPDG models and design procedure. Chapter 5 presents comparisons of new flexible and rigid pavement designs using current empirical ADOT pavement design procedures and the ADOT locally calibrated MEPDG. Chapter 6 describes the procedure and methodology for future recalibration of the MEPDG performance models and design procedure. Chapter 7 describes the default traffic and materials data used in Arizona pavement designs as well as the locally calibrated performance model coefficients for the MEPDG. Chapter 7 also provides input defaults and Arizona calibration coefficients. Chapter 8 summarizes this study's findings and provides recommendations for future improvement.

CHAPTER 2. FRAMEWORK FOR MEPDG PERFORMANCE MODEL VERIFICATION AND LOCAL CALIBRATION

The AASHTO *Guide for the Local Calibration of the Mechanistic-Empirical Pavement Design Guide* (2010), developed under NCHRP Project 1-40B, provides an 11-step roadmap for calibrating the MEPDG software to local conditions, policies, and materials (AASHTO 2010):

- Step 1—Select hierarchical input levels.
- Step 2—Develop experimental factorial design and matrix or sampling template.
- Step 3—Estimate minimum sample size (number of pavement projects) required for each distress/International Roughness Index (IRI) prediction model validation and local calibration.
- Steps 4—Select projects to populate sampling template.
- Step 5—Extract and assess distress and project data.
- Step 6—Conduct field and forensic investigations.
- Step 7—Assess local bias: validation of global calibration values to local conditions, policies, and materials.
- Step 8—Eliminate local bias of distress and IRI prediction models.
- Step 9—Assess the standard error of the estimate.
- Step 10—Reduce standard error of the estimate.
- Step 11—Interpret results and determine adequacy of ADOT MEPDG locally calibrated models.

This process was adopted with modifications for calibrating the MEPDG for ADOT. This chapter describes the local calibration framework and evaluates its suitability for local Arizona conditions.

STEP 1: SELECT HIERARCHICAL INPUT LEVELS

In the MEPDG, pavement design inputs such as traffic, materials, climate, and rehabilitation are available at three hierarchical levels (AASHTO 2008):

- **Level 1:** Material input requires laboratory or field testing such as the dynamic modulus (E^*) testing of HMA concrete, coefficient of thermal expansion (CTE) of concrete, or falling weight deflectometer (FWD) deflection testing. Level 1 inputs for traffic require on-site measurement of axle load distribution, truck lane usage, and truck classification. Obtaining Level 1 inputs requires more resources and time than other levels. Level 1 inputs are typically used for designing heavily trafficked pavements or wherever there is dire safety or economic consequences of early failure.
- **Level 2:** Inputs are user-selected (possibly from an agency database), can be derived from a limited testing program, or can be estimated through correlations of simpler tests with the more complicated inputs for the DARWin-ME. Examples include estimating HMA dynamic modulus (E^*) from binder, aggregate, and mix properties; estimating portland cement concrete (PCC) elastic moduli from compressive strength tests; or using traffic classification data based on functional class of highway in the state. This level is used when resources or testing equipment are not available for tests required for Level 1.
- **Level 3:** Inputs are user-selected values or typical averages for the region. Examples include Arizona default unbound materials' resilient modulus values or default PCC CTE for a given coarse aggregate type. This level might be used for design where there are minimal consequences of early needed rehabilitation such as lower volume roads.

The Guide for the Local Calibration of the Mechanistic-Empirical Pavement Design Guide (2010) recommends selecting an appropriate hierarchical input level (1, 2, or 3) that is consistent with the highway agency's day-to-day practices for characterizing pavement inputs for design. Another consideration for selecting input level is how sensitive the given input is to predicted performance and thus designs.

Tables 1 and 2 summarize the hierarchical levels for flexible and rigid pavement design inputs. The recommended level is derived from both sensitivity analysis outcomes and ADOT practices for characterizing pavement materials properties, subgrade properties, and traffic.

Table 1. Recommended MEPDG Hierarchical Input Levels for New HMA and HMA Overlaid Pavements

MEPDG Input Variable	Sensitivity to Predicted Distress/Smoothness				Recommended Hierarchical Input Level
	Alligator Cracking	Rutting	Transverse Cracking	IRI	
HMA thickness	XXX	XX	X	XX	Level 1
HMA coefficient of thermal contraction			XX		Levels 2 and 3
HMA dynamic modulus	XX	XXX			Level 2
HMA air voids in situ (at placement)	XXX	XXX	XX		Level 3
Effective HMA binder content	XXX	XX	XX	X	Level 3
HMA creep compliance	XX	XXX	XXX		Level 1
HMA tensile strength			XXX		Level 3
Base type/modulus	XXX	XX			Level 2
Base thickness	X				Level 1
Subgrade type/modulus	XX	XX			Level 1
Groundwater table	X	X			Level 3
Climate	XX	XX	XXX	X	Level 2
Truck volume	XXX	XXX			Level 2
Truck axle load distribution	X	X			Level 2
Tire load, contact area, and pressures	XX	XXX			Level 3
Truck speed	XX	XXX			Level 3
Truck wander	XX	XX			Level 3
Initial IRI				XXX	Level 2

X = Small effect on distress/IRI. XX = Moderate effect on distress/IRI. XXX = Large effect on distress/IRI.

Table 2. Recommended MEPDG Hierarchical Input Levels for New JPCP

MEPDG Input Variable	Sensitivity to Predicted Distress/Smoothness			Recommended Hierarchical Input Level
	Faulting	Transverse Cracking	IRI	
PCC thickness	XX	XXX	XX	Level 1
PCC modulus of rupture and elasticity		XXX	X	Levels 2 and 3
PCC CTE	XXX	XXX	XXX	Levels 1 and 2 (current data available)
Joint spacing	XX	XXX	XX	Level 1
Lane to PCC shoulder long-term load transfer efficiency	XXX		XXX	Level 3
Edge support	XX	XXX	XX	Level 1
Permanent curl/warp	XXX	XXX	XXX	Level 3
Base type	XXX	XXX	X	Level 1
Climate	XXX	XXX	XXX	Level 2
Subgrade type/modulus	X	XX	X	Level 1
Truck axle load distribution	X	XXX	X	Level 1
Truck volume	XXX	XXX	XXX	Level 1
Tire pressure		X		Level 3
Truck lateral offset	XX	XXX	XX	Level 3
Truck wander		XX		Level 3
Initial IRI			XXX	Level 1 or 2

X = Small effect on distress/IRI. XX = Moderate effect on distress/IRI. XXX = Large effect on distress/IRI.

STEPS 2 AND 3: DETERMINE EXPERIMENTAL DESIGN AND SAMPLING NEEDS

Experimental Design

In Step 2 of the local calibration effort, the researchers developed a statistical experiment to verify that the MEPDG global models and procedure were adequate for Arizona local conditions and practices, and to calibrate the global models if they were inadequate. Meeting these objectives involved defining the population, determining sampling needs and extent, and establishing the experimental design.

Defining the pavement population required a thorough review of past and current ADOT pavement design and construction practices and planned innovation regarding future ADOT pavement design and construction. Issues identified from this review follow:

- Past and current ADOT design and construction practices:
 - Pavement types (new and rehabilitation).
 - Material types.
 - Site properties (subgrade, climate, and traffic).
 - Design features.
 - Types of rehabilitation practices employed.
 - Construction practices.
- Future ADOT design and construction practices:
 - New materials (e.g., warm mix asphalt and polymer modified asphalt).
 - Incentive-based construction (e.g., warranties, design build, and performance-related specifications).
 - New construction techniques and equipment (e.g., intelligent compaction).

Table 3 summarizes the information gathered about these issues.

Table 3. ADOT Pavement Design and Construction Practices

Design/Construction Issues	Current/Past ADOT Practices	Future ADOT Practices
Pavement types (new and rehabilitation)	<ul style="list-style-type: none"> • New flexible (asphalt concrete [AC] over granular base). • New JPCP over granular base. • Composite thin AC over JPCP. 	Same. No significant change in pavement design types anticipated.
Material types	<ul style="list-style-type: none"> • AC (conventional and Superpave mixes). • Granular (base) materials (typically AASHTO Class A-1 and A-2). • PCC (typical 28-day compressive strength of 5000 psi and CTE of 4.7 inch/° F). 	Same. No significant change anticipated.
Site properties	<ul style="list-style-type: none"> • Subgrade (mostly coarse grained). Pockets of fine-grained soils present. 	Same. No significant change anticipated.
	<ul style="list-style-type: none"> • Climate (primarily change in elevation). 	Same. No significant change anticipated.
	<ul style="list-style-type: none"> • Traffic (three main vehicle class distributions). 	Same. No significant change anticipated.
Design features	<ul style="list-style-type: none"> • JPCP (only): <ul style="list-style-type: none"> ○ Joint spacing. ○ Shoulder type. ○ Slab width. ○ Load transfer mechanism. 	Same. No significant change anticipated.
Rehabilitation practices	<ul style="list-style-type: none"> • Existing AC pavements (thin/thick AC overlays and mill and fill). • Existing JPCP (thin AC overlays). 	Same. No significant change anticipated.
Construction practices	<ul style="list-style-type: none"> • Performance targets (e.g., initial smoothness, PCC compressive strength, AC air voids, and AC Marshall strength) deployed. 	Incentive based construction a possibility.

Based on this information, the researchers defined the pavement population and properties to include current and past ADOT practices:

- New pavement types (AC/granular, JPCP/granular, thin AC/JPCP).
- Rehabilitated pavement types (AC/AC, AC/JPCP).
- Materials:
 - AC (conventional and Superpave mixes).
 - Granular (base) materials (typically A-1 and A-2).
 - PCC (typical 28-day compressive strength of 5000 psi and CTE of 4.7 inch/° F).

- Subgrade (mostly coarse-grained material).
- Climate (northern, central, and southern regions of state; low and high elevations).
- Traffic (three vehicle class distribution representative of the entire state).
- Design features:
 - Joint spacing (mostly 15 ft).
 - Shoulder type (mostly tied PCC).
 - Slab width (12 ft).
 - Load transfer mechanism (mostly doweled).

Sampling

Creating a Sampling Template

To collect data required for this analysis, the researchers developed a sampling template representing key aspects of the ADOT pavement population: current and future ADOT pavement design features, material types, site conditions, and construction practices. Table 4 shows the sampling template for flexible pavements, which contained eight cells, while Table 5 indicates 64 cells for JPCP. Note that not all cells represent current or future ADOT design and construction practices.

Table 4. Sampling Template for New and Rehabilitated HMA Pavements

HMA Thickness (inches)	Granular Base Thickness (inches)*	Subgrade Type	
		Coarse-Grained Soils (AASHTO Class A-1 through A-3)	Fine-Grained Soils (AASHTO Class A-4 through A-7)
<8	<6	1	2
	≥6	3	4
≥8	<6	5	6
	≥6	7	8

*All projects had granular base. Note: An equivalent dense-graded aggregate base was assumed for permeable asphalt-treated bases (PATBs).

Table 5. Sampling Template for New and Rehabilitated JPCP

PCC Thickness (inches)	Dowel Diameter (inches)	Edge Support*	Subgrade and Base Type			
			Coarse-Grained Subgrade Soils (AASHTO Class A-1 through A-3)		Fine-Grained Subgrade Soils (AASHTO Class A-4 through A-7)	
			Lean Concrete Base	Granular or Asphalt-Treated Base	Lean Concrete Base	Granular or Asphalt-Treated Base
≤ 10	No dowels	None	1	2	3	4
		Yes	5	6	7	8
	Doweled	None	9	10	11	12
		Yes	13	14	15	16
> 10	No dowels	None	17	18	19	20
		Yes	21	22	23	24
	Doweled	None	25	26	27	28
		Yes	29	30	31	32

*Tied PCC and or widened lanes.

Minimum Sample Size Required for Each Distress/IRI Prediction Model Validation and Local Calibration

Under this step, the project team estimated the minimum number of projects required for MEPDG distress/IRI model validation and local calibration. Information required for this task included model error (i.e., standard error estimate [SEE]); confidence interval for statistical analysis; and performance indicators’ threshold value at typical agency design reliability level.

Table 6 summarizes the results from this analysis. The researchers assumed the following parameters for estimating the minimum number of projects (18 flexible and 21 JPCP):

- Design reliability level: 90 percent.
- Confidence interval: 90 percent.
- SEE for the global MEPDG models as presented in Table 6.
- ADOT distress/IRI threshold value as presented in Table 6.

**Table 6. Estimated Number of Pavement Projects Required for
MEPDG Validation and Local Calibration**

Pavement Type	Distress/IRI	Distress/IRI Threshold (at 90% Reliability)	SEE	Minimum Number of Projects Required for Validation and Local Calibration	Minimum Number of Projects Required for Each Pavement Type (n)*
New HMA and HMA overlaid HMA	Alligator cracking	20% lane area	5.01%	16	18
	Transverse thermal cracking	Crack spacing >100 ft of 630 ft/mi	150 ft/mi**	18	
	Rutting	0.4 inch	0.107 inch	14	
	IRI	169 inch/mi	18.9 inch/mi	80	
New JPCP	Faulting	<0.15 inch	0.033 inch	21	21
	Transverse cracking	<10% slabs	4.52%	5	
	IRI	169 inch/mi	17.1 inch/mi	98	

* $n = \left(\frac{Z_{\alpha/2} \sigma}{E} \right)^2$, where $Z_{\alpha/2} = 1.601$ (for a 90 percent confidence interval), α = performance indicator threshold

(design criteria), and E = tolerable bias at 90 percent reliability (1.601*SEE).

**Estimated from other MEPDG implementation projects.

Note: In selecting the overall minimum number of required pavement HMA and JPCP projects, the performance indicator IRI was excluded because the accuracy of the IRI models depends very much on the accuracy of other pavement distress predictions. Sampling a vast number of projects to validate the IRI models is therefore unnecessary if the individual distress prediction models are considered accurate and reasonable.

STEPS 4 AND 5: SELECT HMA AND JPCP PROJECTS TO POPULATE SAMPLING TEMPLATE

Identifying Projects for an ADOT MEPDG Local Calibration/Validation Database

To populate the sampling templates developed in Step 3, the research team selected projects based on recommendations from the *Guide for the Local Calibration of the Mechanistic-Empirical Pavement Design Guide* (2010):

- Projects should be representative of Arizona pavement design and construction practices.
- Projects should be representative of typical pavement condition (i.e., poor, moderate, and good).
- Project age should span the range typical of Arizona practice (i.e., newly constructed, older existing, and rehabilitated).
- Projects must be located throughout the state.

First, the researchers identified potential projects that met these recommendations. The main sources of these projects were the LTPP (specifically, LTPP projects located in Arizona); research and forensic reports containing detailed descriptions of in-service pavements; and ADOT pavement management system (PMS) databases. The pavement types in these projects were new HMA pavements (including HMA pavements subjected to routine or preventive maintenance); HMA overlaid existing HMA pavement; new JPCP (including JPCP over existing aggregate, asphalt-treated, and cement-treated bases); and composite ARFC-surfaced new JPCP.

Selecting Projects to Populate the Sampling Template

Next, the project team reviewed the identified projects to determine the availability of sufficiently detailed input data (such as traffic, materials, and construction) and distress/IRI data in MEPDG-required formats. Once these projects were identified, the team:

- Extracted and reviewed key MEPDG input data to identify and correct or eliminate anomalies and outliers.
- Extracted and reviewed distress/IRI data to identify and correct or eliminate anomalies and outliers.
- Compared distress/IRI magnitudes to the design threshold values (Table 6).
- Assembled the ADOT MEPDG calibration and validation database.

Extract and Review Key MEPDG Input Data for Selected Projects

As shown in Tables 1 and 2, the MEPDG requires several categories of input data. For this implementation project, pavement data were primarily obtained from the LTPP; ADOT PMS traffic and inventory data tables; ADOT design and construction reports, and construction quality assurance (QA) testing databases; and pavement research and forensic examination reports. The researchers obtained additional data as needed from national pavement, climate, and soils databases, including MEPDG default pavement-related data; the National Climatic Data Center (NCDC) database; and the U.S. Department of Agriculture (USDA) Natural Resources Conservation Service (NRCS) Soil Survey Geographic (SSURGO) database. Table 7 presents the data sources; Figures 1 through 15 summarize the data that were extracted and reviewed.

Table 7. Sources for the ADOT MEPDG Calibration and Validation Database

Data Type	Project Source		
	LTPP	Research/Forensic	ADOT Pavement Mgt Services (PMS)
Inventory	INV_GENERAL INV_AGE INV_ID SPS_GENERAL SPS_ID	Smith et al. 1991 Western Research Institute (WRI) reports	dbo_SODAMASTER
Traffic		Darter et al. 2010 Smith et al. 1991 WRI research reports dbo_SODAMASTER	dbo_SODAMASTER SHSkdtFactors2007-2008ver4 SHS2028AADTForecastsver2 SHStrafficeProjectionsDataDictionary Mar2010
Materials	INV_PCC_MIXTURE INV_PMA_ASPHALT TST_L05B TST_PC01 TST_PC02 TST_PC03 TST_PC04 TST_PC08 TST_PC09 TST_SS01_UG01_UG02 TST_SS14_UG14 TST_UG04_SS03	Smith et al. 1991 WRI research reports	Soil Aggregate Tabulation (Subgrade 12-06-10) Soil Aggregate Tabulation (Aggregate 12-06-10) Soil Aggregate Tabulation (Aggregate Base 12-06-10) Soil Aggregate Tabulation (Aggregate Subbase 12-06-10) Soil Aggregate Tabulation (Embankment 12-06-10) Soil Aggregate Tabulation (Borrow 12-06-10) Soil Aggregate Tabulation (ARACFC 12-06-10) ADOT Materials Specifications
Climate	MEPDG NCDC database	MEPDG NCDC database	MEPDG NCDC database
Design	INV_PCC_JOINT SPS-1, -2, -5, -6 construction reports	Smith et al. 1991 WRI research reports	ADOT pavement design manual ADOT projects materials/design reports
Construction	SPS-1, -2, -3, -5, -6, -9 construction reports	Smith et al. 1991 WRI research reports	ADOT projects materials/design reports

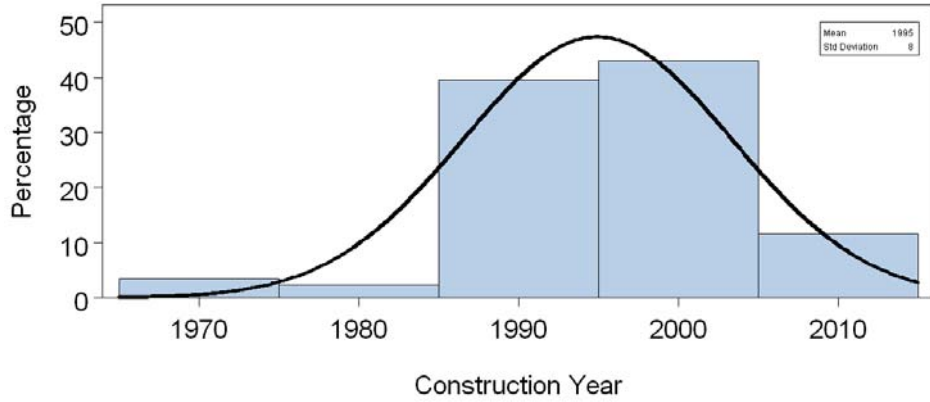


Figure 1. Construction/Rehabilitation Year of Projects Selected for the ADOT MEPDG Calibration/Validation Database

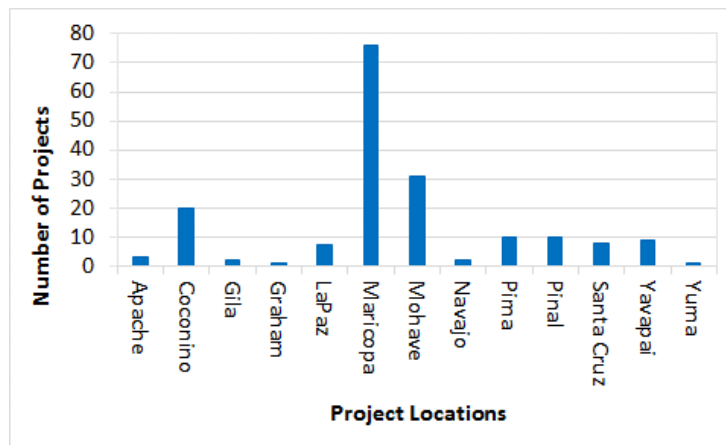


Figure 2. Arizona Locations of Projects Selected for the ADOT MEPDG Calibration/Validation Database

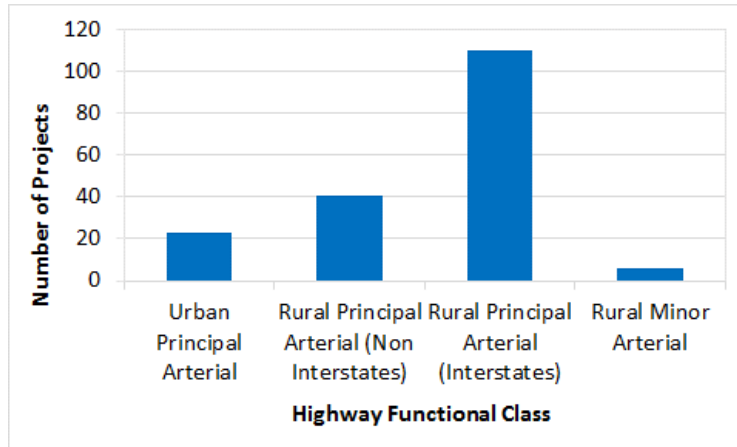


Figure 3. Highway Functional Class of Projects Selected for the ADOT MEPDG Calibration/Validation Database

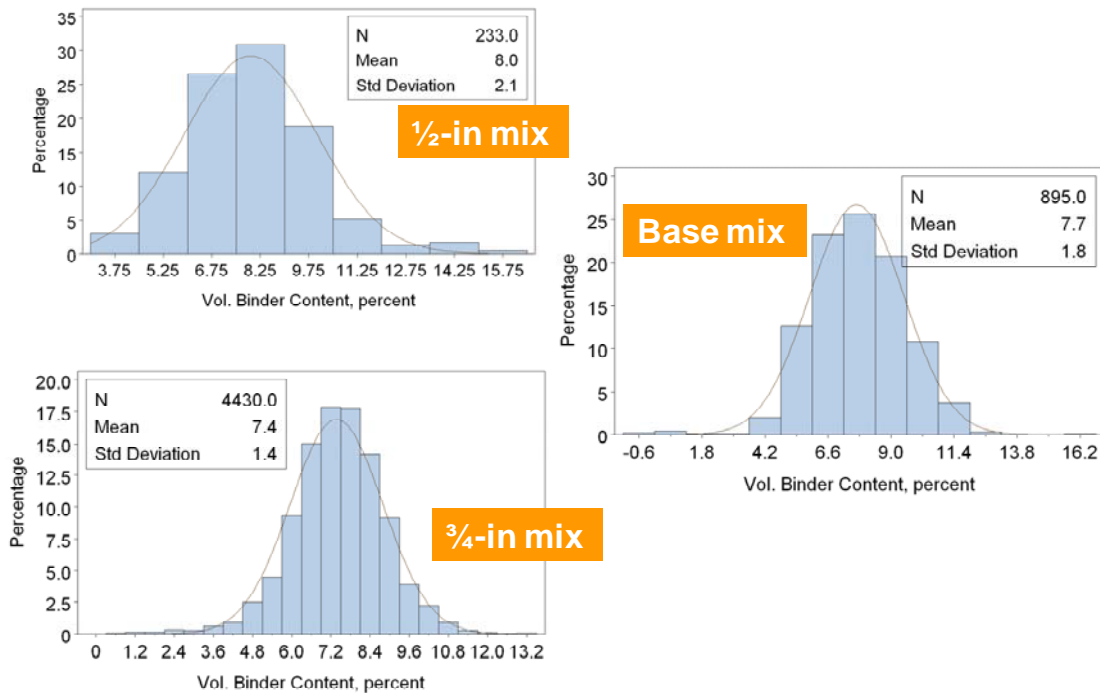


Figure 4. Volumetric (Not Gravimetric) Binder Content of Projects Selected for the ADOT MEPDG Calibration/Validation Database

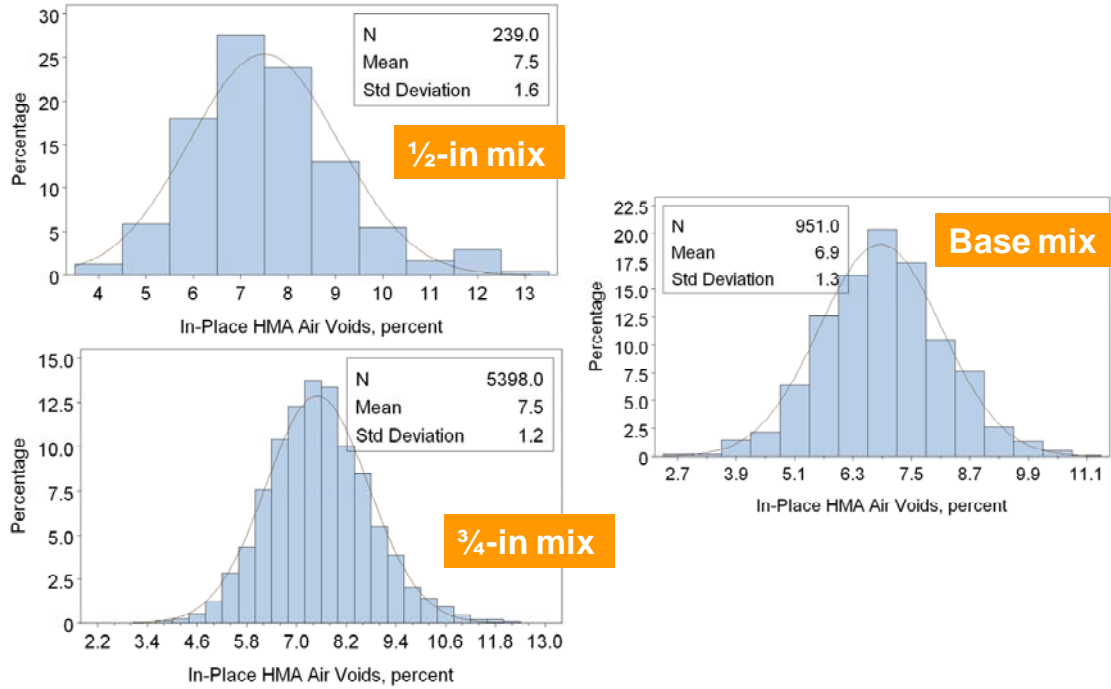


Figure 5. In-Place Air Voids of Projects Selected for the ADOT MEPDG Calibration/Validation Database

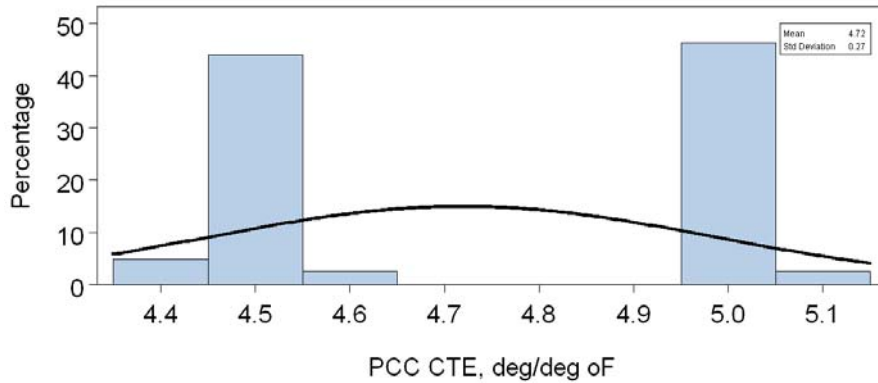


Figure 6. PCC CTE (from LTPP) of Projects Selected for the ADOT MEPDG Calibration/Validation Database

(Note that the concrete CTE values used for all calibration work were those corrected values obtained from the FHWA/LTPP lab testing.)

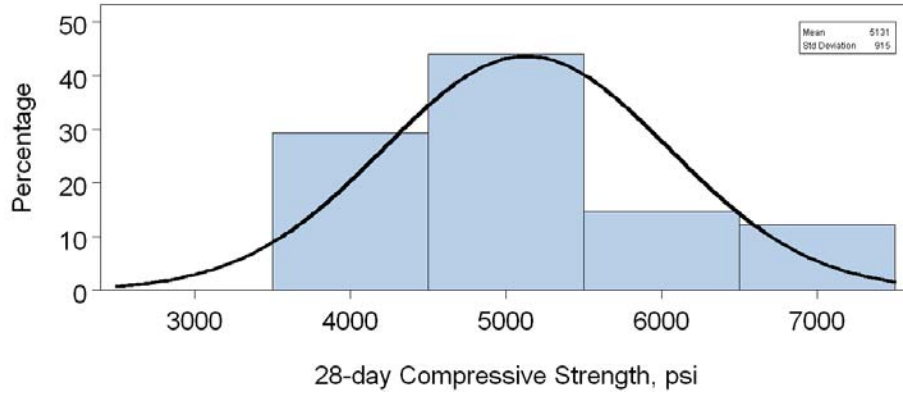


Figure 7. PCC 28-Day Compressive Strength of Projects Selected for the ADOT MEPDG Calibration/Validation Database

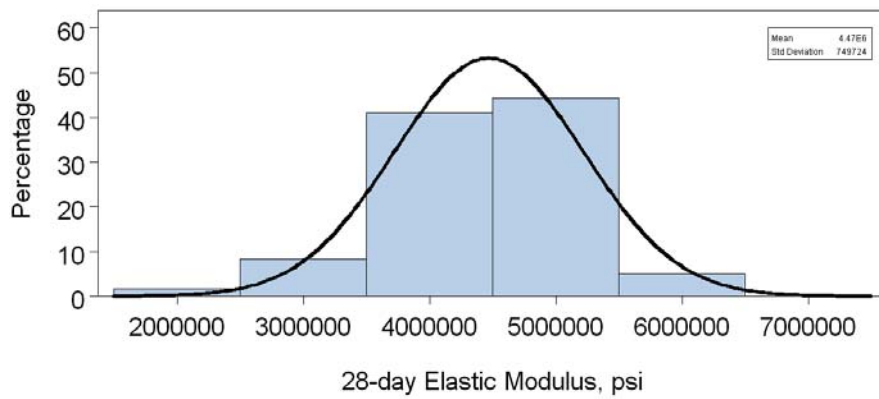


Figure 8. PCC 28-Day Elastic Modulus of Projects Selected for the ADOT MEPDG Calibration/Validation Database

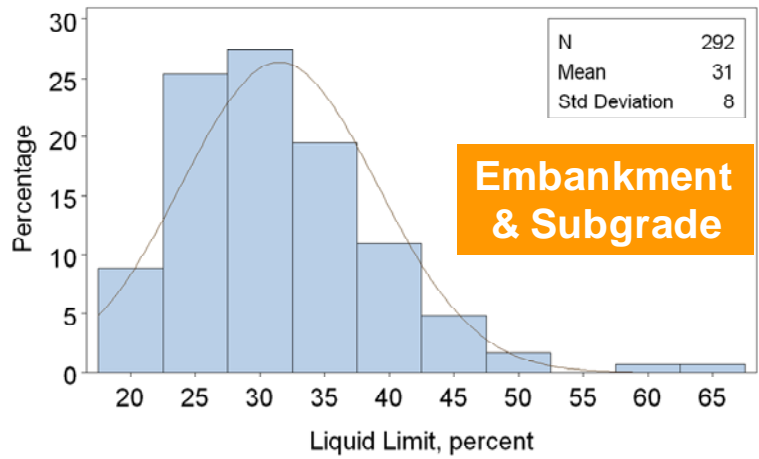
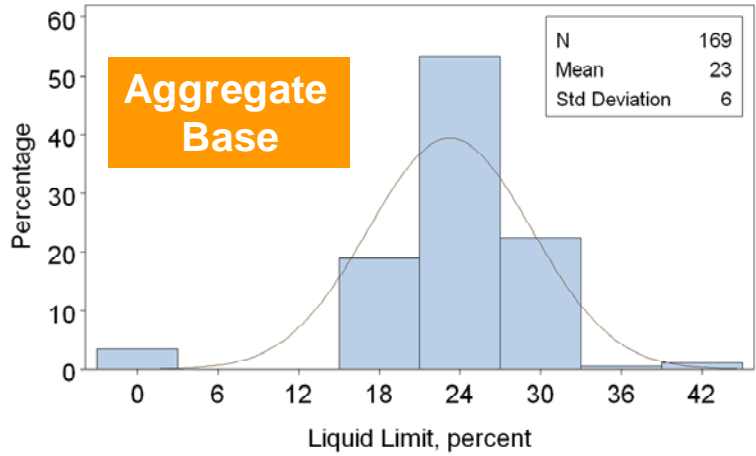


Figure 9. Aggregate Base and Subgrade Liquid Limit of Projects Selected for the ADOT MEPDG Calibration/Validation Database

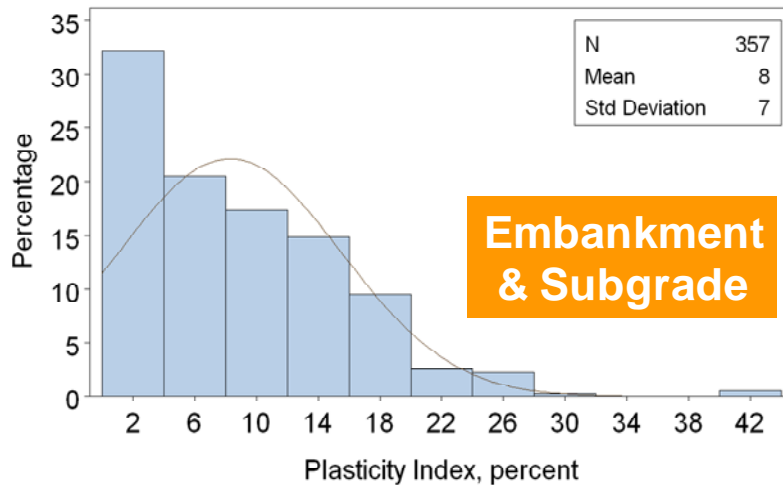
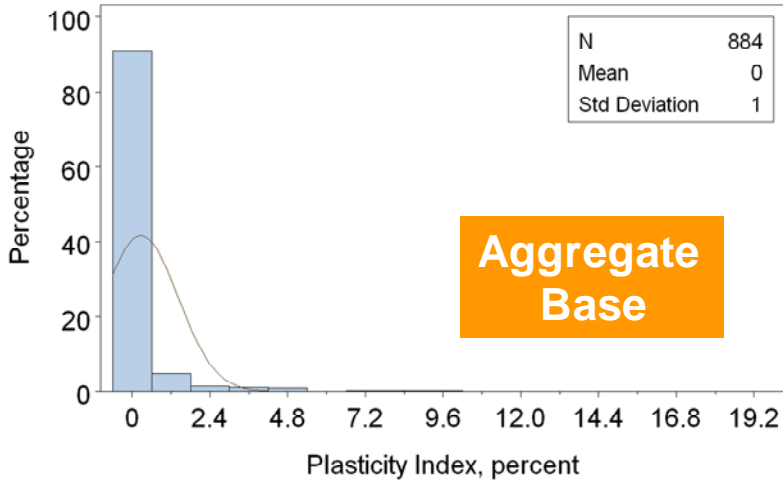


Figure 10. Aggregate Base and Subgrade Plasticity Index of Projects Selected for the ADOT MEPDG Calibration/Validation Database

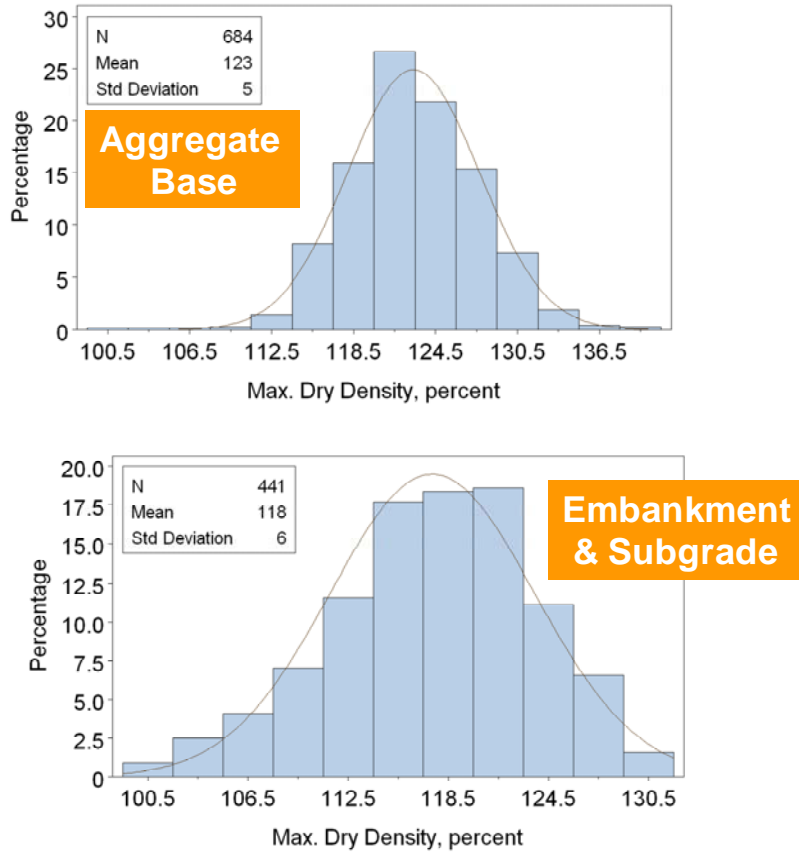


Figure 11. Aggregate Base and Subgrade Maximum Dry Density of Projects Selected for the ADOT MEPDG Calibration/Validation Database

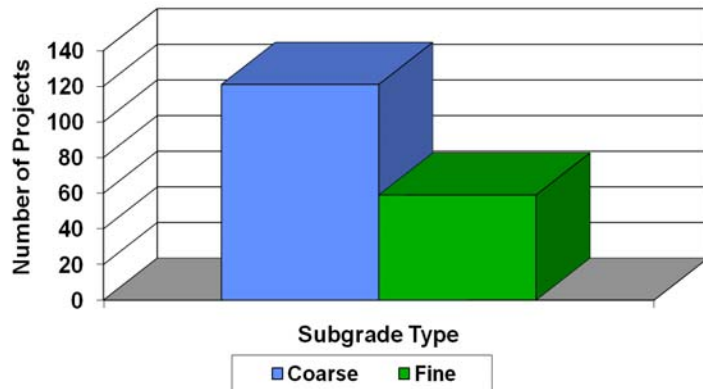


Figure 12. Subgrade Type (Coarse- or Fine-Grained) of Projects Selected for the ADOT MEPDG Calibration/Validation Database

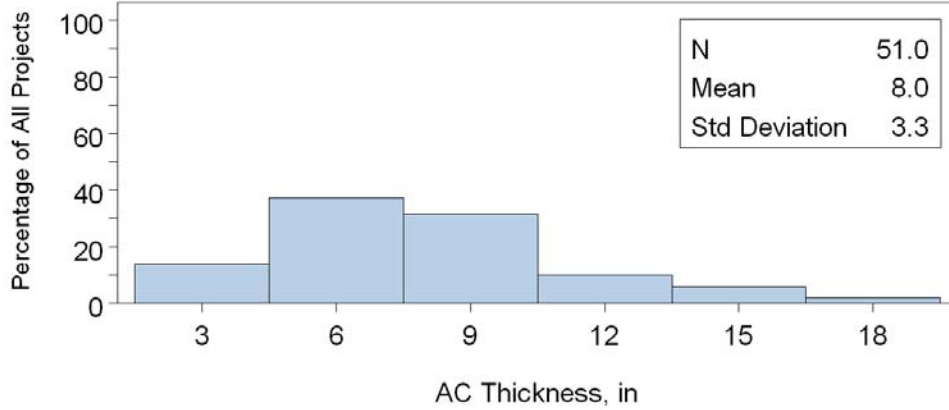


Figure 13. New HMA Pavement Thickness of Projects Selected for the ADOT MEPDG Calibration/Validation Database

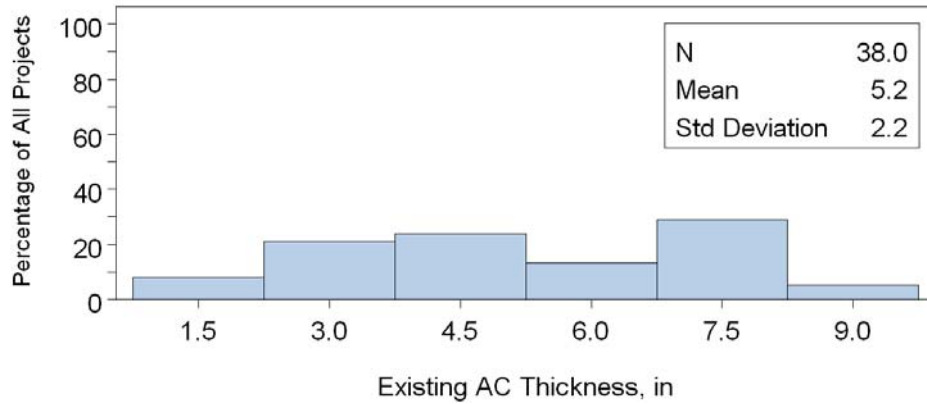


Figure 14. Existing HMA Thickness for HMA Overlaid HMA Pavement Projects Selected for the ADOT MEPDG Calibration/Validation Database

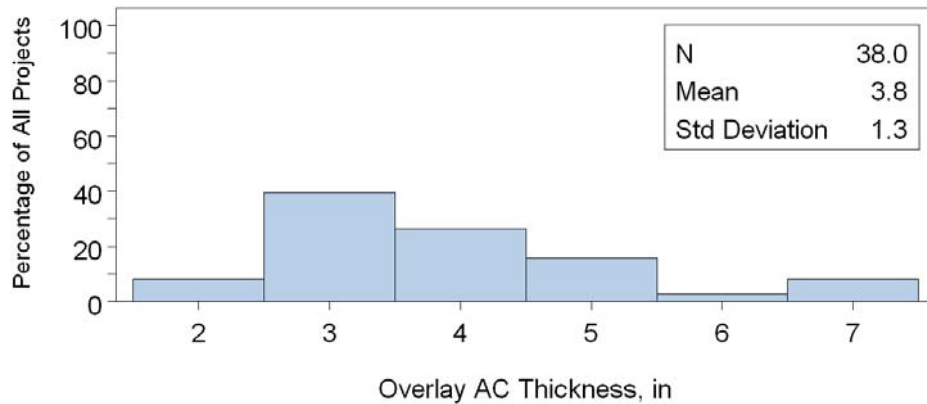


Figure 15. HMA Overlay Thickness of HMA Overlaid HMA Pavement Projects Selected for the ADOT MEPDG Calibration/Validation Database

Once assembled, the key inventory, traffic, materials, climate, design, and construction data were reviewed to identify and correct missing data, outliers, and errors:

- The project team removed questionable data and replaced the information with typical values or with project-specific information from other sources.
- Team members used assembled historical traffic volume data to compute initial truck traffic volume and future traffic growth rates.
- They also used Level 3 typical values developed from ADOT materials and traffic databases for ADOT and research and forensic projects with inadequate amounts of project-specific traffic and materials data.

After the data review, the researchers revised the project database and included only data that were considered reasonable based on engineering judgment. Information presented in Figures 1 through 15 shows that the selected projects represented typical Arizona pavement designs, construction practices, and site conditions.

Extract and Review Distress and IRI Data for Each Selected Project

Table 8 presents the distress and IRI data obtained from LTPP, ADOT PMS, and ADOT research projects. The ADOT PMS data were augmented by distress information obtained through a review of ADOT distress videos archived since the late 1990s and field distress surveys conducted by Applied Research Associates, Inc. (ARA) staff. Distress and IRI data from the research projects were obtained from surveys conducted as part of this project. Researchers reviewed all distress and IRI data for accuracy,

reasonableness, and consistency. A key consideration was whether the raw data as measured and reported could be converted into the MEPDG reporting units for each performance indicator.

Data Collection and Reporting

Since MEPDG performance indicators' measuring units were consistent with LTPP distress and IRI data collection protocols, by default all LTPP projects reported distress and IRI data that could easily be converted into MEPDG-compatible units.

Table 8. Distress and IRI Data Sources for Local Calibration and Validation

Pavement Type	Distress/IRI	Distress and IRI Data Source		
		LTPP Projects**	ADOT PMS Projects	ADOT Research Projects
New HMA and HMA overlaid HMA	Alligator cracking*	MON_DIS_AC_REV	Distress video and field survey	ADOT/WRI
	Transverse cracking*	MON_DIS_AC_REV	Distress video and field survey	ADOT/WRI
	Rutting		dbo_SodaMaster	ADOT/WRI
	IRI	MON_PROFILE_MASTER	dbo_SodaMaster	ADOT/WRI
New JPCP	Transverse cracking	MON_DIS_JPCC_REV	Distress video and field survey	ADOT SPR 264
	Transverse joint faulting	MON_DIS_JPCC_FAULT_SECT	NA	ADOT SPR 264
	IRI	MON_PROFILE_MASTER	dbo_SodaMaster	ADOT SPR 264
Composite (ARFC overlaid JPCP)	Alligator cracking	MON_DIS_AC_REV	Distress video and field survey	N/A
	Transverse cracking*	MON_DIS_AC_REV	Distress video and field survey	N/A
	Rutting	MON_T_PROF_INDEX_SECTION	dbo_SodaMaster	N/A
	IRI	MON_PROFILE_MASTER	dbo_SodaMaster	N/A

N/A = not available.

*Includes reflection cracking.

**Data tables listed were obtained from the LTPP database, version 25 (January 2011).

Results of the ADOT measured distress and IRI data review follow:

- HMA-surfaced pavements:
 - **Alligator cracking.** Data were not available in the ADOT PMS dbo_SodaMaster data table in a format that could be used for analysis. Alligator cracking distress data were obtained by viewing archived ADOT PMS distress survey videos and conducting windshield surveys.
 - **Transverse cracking.** Data were not available in the ADOT PMS dbo_SodaMaster data table in a format that could be used for analysis. Transverse cracking data were also obtained by viewing archived ADOT PMS distress survey videos and conducting windshield surveys.
 - **Rutting.** Although data were available in the ADOT dbo_SodaMaster data table, measurements were made using three-point laser equipment, which is different from LTPP wire or straight-edge measurements. After comparing the ADOT and LTPP rutting measurements to determine if they were compatible, the researchers found that LTPP rutting measurements were approximately 28 percent higher than ADOT rutting measurements (Figure 16). ADOT rutting measurements were corrected to make them more comparable to LTPP.
 - **IRI.** ADOT reported smoothness in terms of IRI.

Much of the recent years' ride measurement has been in terms of IRI, as defined by LTPP, so these values were used directly.

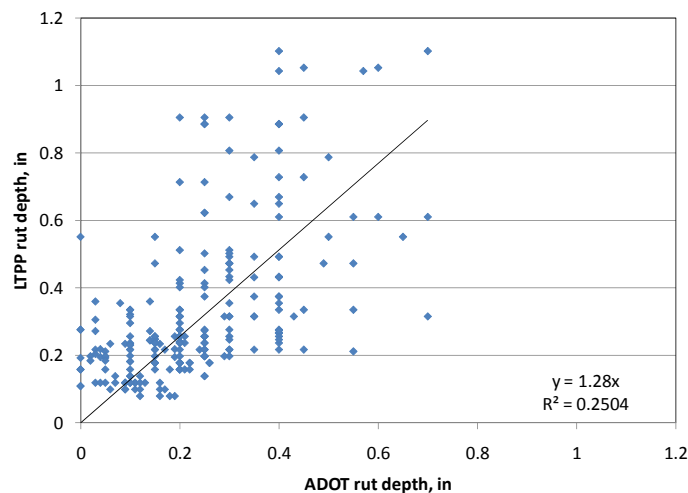


Figure 16. Relationship Between ADOT and LTPP Rutting Measurements

- JPCP:
 - **Transverse cracking.** Data were not available in the ADOT PMS dbo_SodaMaster data table in a format that could be used for analysis. Transverse cracking distress data were obtained by viewing archived ADOT PMS distress survey videos and conducting windshield surveys.
 - **Transverse joint faulting.** Data were not available in the ADOT PMS dbo_SodaMaster data table in a format that could be used for analysis.
 - **IRI.** ADOT reported smoothness in terms of IRI.
- Composite (ARFC overlaid JPCP) pavements:
 - **Alligator cracking.** None was identified in windshield surveys or from ADOT videos.
 - **Transverse cracking.** Primarily Data suggest that transverse cracking occurred primarily as transverse joint reflection cracking. No transverse midpanel cracks were identified.
 - **Rutting.** Like HMA pavements, LTPP rutting measurements in composite pavements were approximately 28 percent higher than ADOT rutting measurements. ADOT rutting measurements were corrected to make them more comparable to LTPP.
 - **IRI.** ADOT reported smoothness in terms of IRI.

Comparison of Performance Indicator Magnitudes to the Design Threshold (Trigger) Values

The researchers compared the magnitudes of time-series distress and IRI data from the identified LTPP, ADOT PMS, and Arizona research projects with design threshold values for each distress type and IRI to determine whether distress and IRI from the identified projects were typical for Arizona. Results of the comparison follow:

- Average maximum distress and IRI for the projects selected ranged from 10 to 77 percent, which suggests that for both HMA- and JPC-surfaced pavements, most pavements were in relatively better condition than the design threshold values. This is typical for in-service pavements, as moderately to badly deteriorated pavements are rehabilitated as soon as possible.
- Some of the projects selected, however, exhibited distress and IRI values that were significantly higher than the threshold values, as shown in Figures 17 through 23.
- For all the distress types and IRI, the maximum distress and IRI values were greater than the design threshold values. Thus, the range of distress and IRI values from the identified projects covered ADOT design threshold values.

Table 9 and Figures 17 through 23 summarize the results of the comparison.

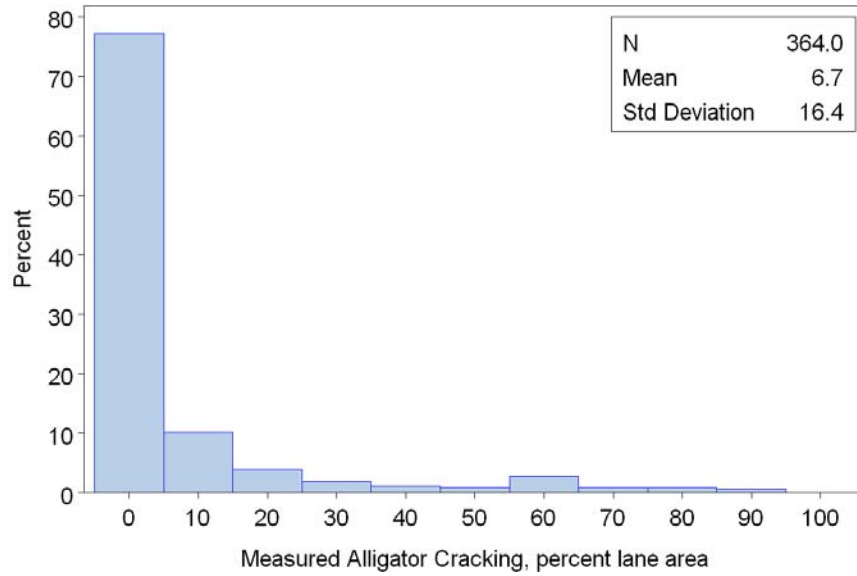


Figure 17. Measured Alligator Cracking in LTPP and PMS Sections of New HMA and HMA Overlaid HMA Projects

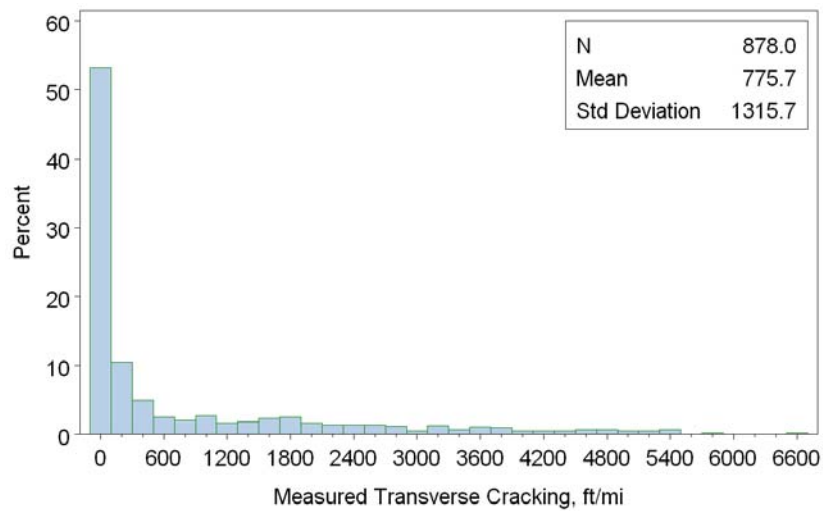


Figure 18. Measured HMA Transverse Cracking in LTPP and PMS Sections of New HMA and HMA Overlaid HMA Projects

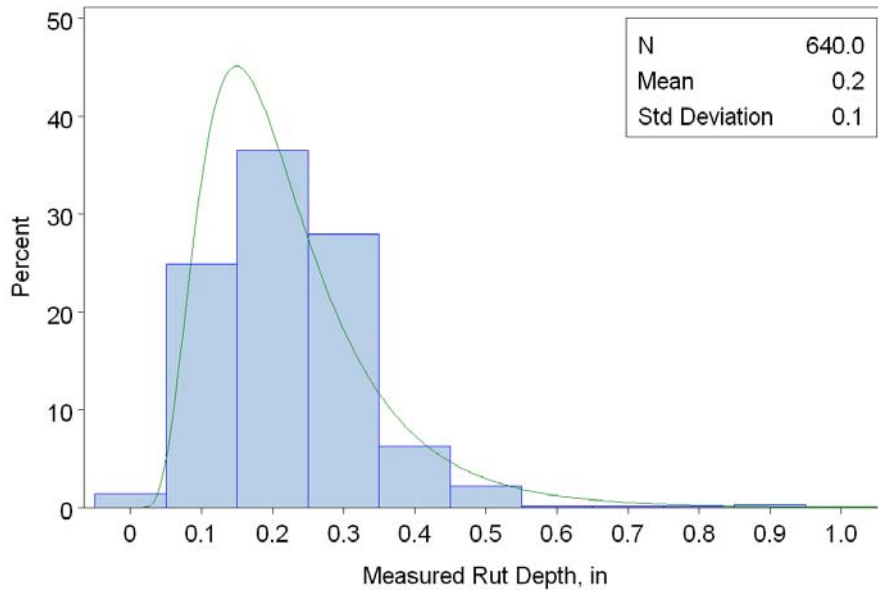


Figure 19. Measured Rutting in LTPP and PMS Sections of New HMA and HMA Overlaid HMA Projects

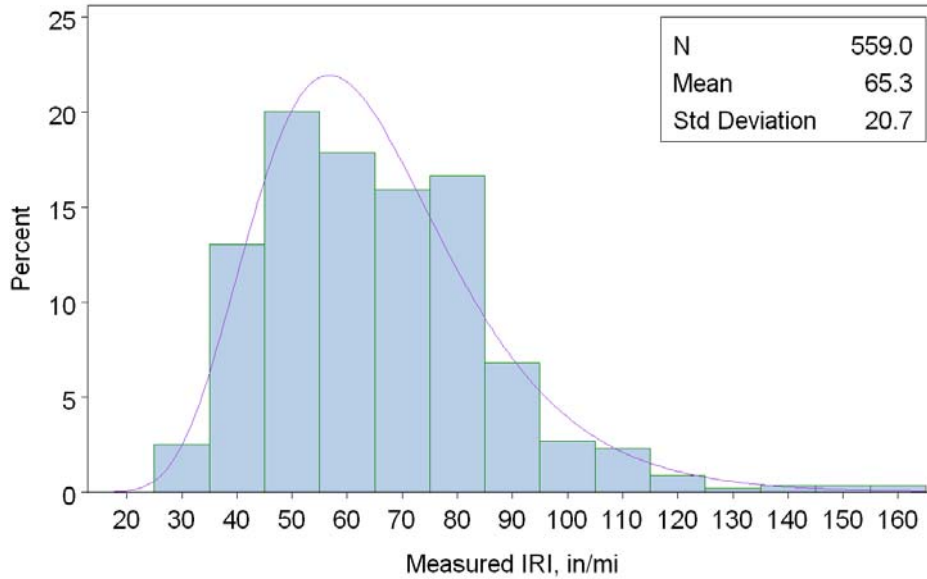


Figure 20. Measured AC IRI in LTPP and PMS Sections of New HMA and HMA Overlaid HMA Projects

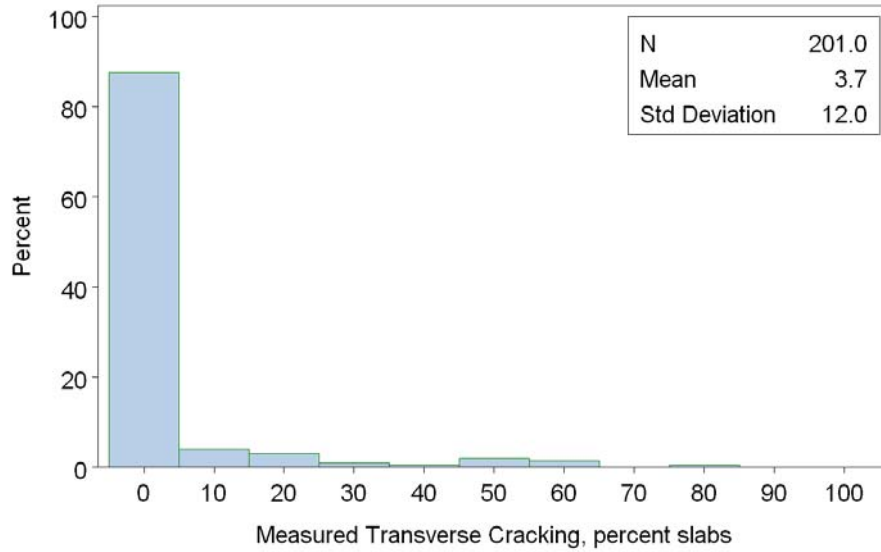


Figure 21. Measured JPCP Transverse Cracking in LTPP and PMS Sections of New JPCP Projects

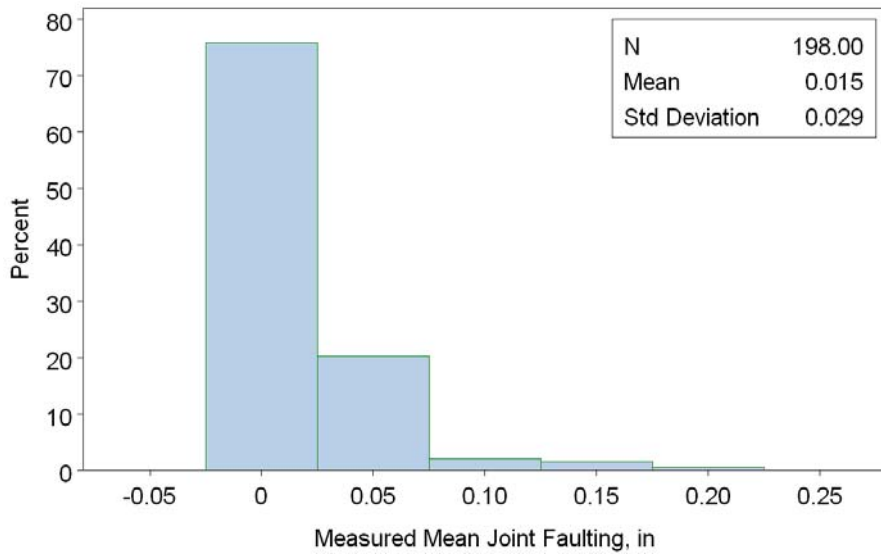


Figure 22. Measured JPCP Transverse Joint Faulting in LTPP and PMS Sections of New JPCP Projects

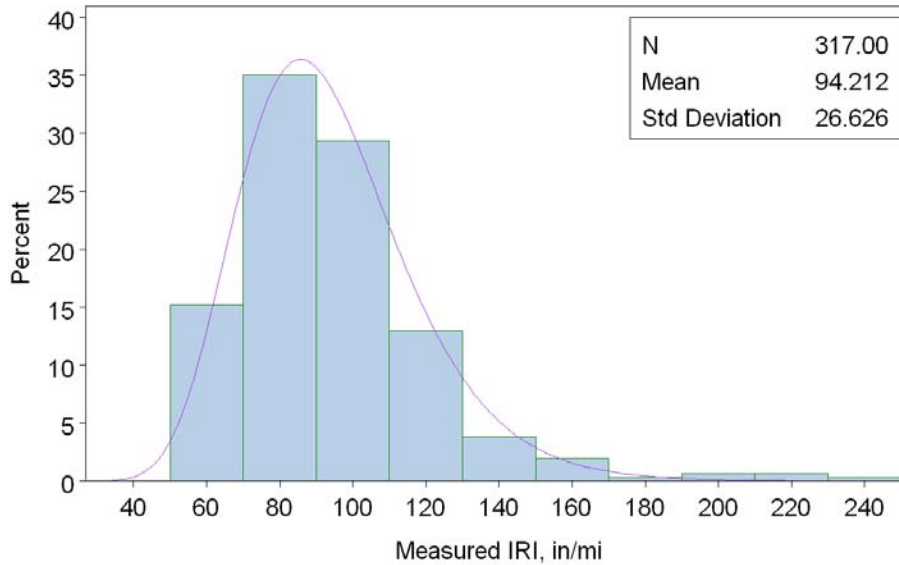


Figure 23. Measured JPCP IRI of LTPP and PMS Sections of New JPCP Projects

Table 9. Comparison of Distress and IRI Values with Design Criteria or Threshold Values

Pavement Type	Distress or Performance Indicator	Design Criteria	Maximum Value Statistics for All Projects	
			Average Value	Percentage of Design Criteria (%)
HMA and HMA overlaid HMA	Alligator cracking (percent lane area)	10	6.7	67.0
	Transverse thermal cracking (ft/mi)	1000	775.7	77.6
	Rutting (inch)	0.4	0.2	50.0
	IRI (inch/mi)	169	65.3	38.6
JPCP	Transverse cracking (percent slabs cracked)	10	3.7	37.0
	Transverse joint faulting (inch)	0.15	0.015	10.0
	IRI (inch/mi)	169	94.212	55.6

Evaluating Distress/IRI Data to Identify Anomalies and Outliers

Before determining MEPDG inputs, the research team visually inspected time series plots of distress and IRI data for each LTPP and ADOT PMS project to determine if observed trends in distress and IRI progression were reasonable and to identify potential anomalies (e.g., significant decrease in distress

and IRI magnitude, indicating an occurrence of significant rehabilitation or maintenance event) and outliers. Figures 24 through 27 are examples of these plots.

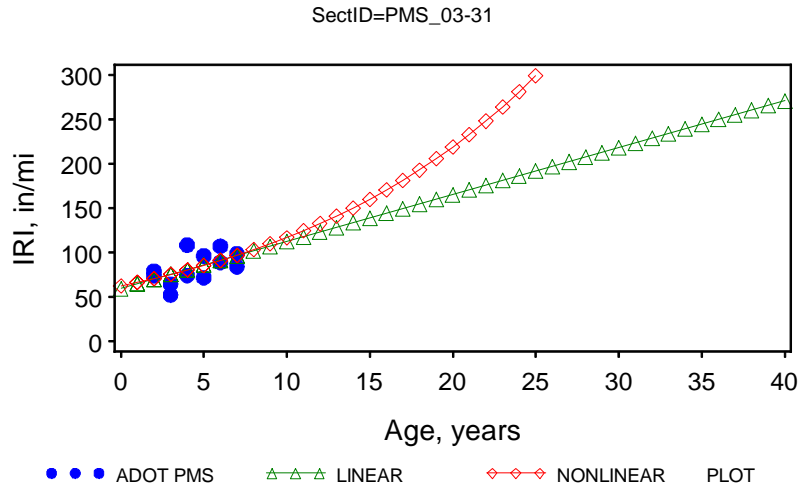


Figure 24. Progression of Measured IRI with Age in ADOT PMS 03-31

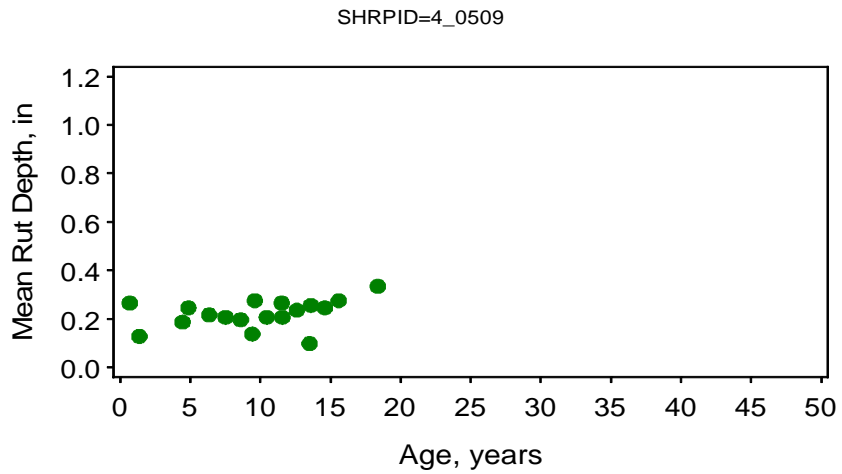


Figure 25. Progression of Measured Rutting with Age in ADOT LTPP 0509

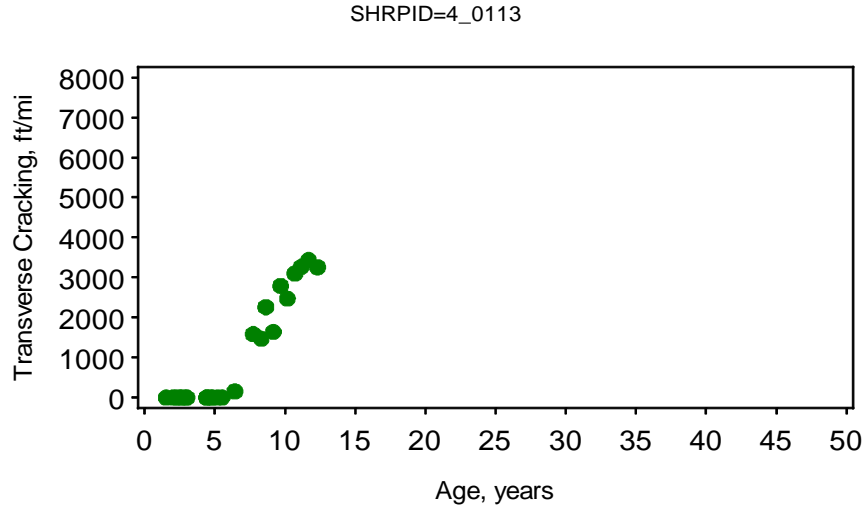


Figure 26. Progression of Measured HMA Transverse Cracking with Age in ADOT LTPP 0113



Figure 27. Progression of Measured JPCP Transverse Cracking with Age in ADOT LTPP 0217

The results of this exercise follow:

- Projects exhibiting unreasonable trends in distress and IRI progression were removed and not used in the analysis. Each distress type and IRI were treated separately, and thus removing a project from the HMA rutting database, for example, does not imply that it was also removed from the HMA transverse cracking database.
- Individual distress and IRI data (from several years of data for a given project) identified as outliers and erroneous were removed. Examples include zero measurements that could represent nonentry values, and significantly high or low distress and IRI values that were considered unreasonable and not in agreement with observed trends from previous and subsequent years.
- Individual distress and IRI data points measured after the performance of a significant maintenance or rehabilitation event that significantly altered the pavement design were removed. Distress and IRI data prior to that point were retained.
- Reasonable variability from year to year in distress and IRI measurements was considered acceptable. This variability is caused by many factors and ultimately contributes to the SEEs used in defining reliability in predicted distress and IRI.

While initial IRI values (defined as IRI measured within a year of construction or rehabilitation) were available for some of the projects, other initial IRI values were estimated by extrapolating historical measurements of IRI back to the construction or overlay completion date.

Final Projects Selection

Following data assembly, review, and cleanup, the researchers selected projects with adequate detailed information for model verification and local calibration (Table 10). The populated sampling templates for the new and rehabilitated HMA and JPCP pavements are presented in Tables 11 and 12, respectively.

The number of selected flexible (new HMA and HMA overlaid HMA) pavements and new JPCP projects exceeded the 18 flexible and 21 JPCP projects required. (See Table 6.) The maps in Figures 28 through 30 show the locations of the identified projects; Table 13 presents a detailed description of these projects.

Table 10. Breakdown of Selected Projects for Validation and Local Calibration

Pavement Type	LTPP Projects	PMS/Research Projects	Total
New HMA pavement	42	16	58*
AC overlay over existing AC pavement	34	8	42*
New JPCP (bare and CPR)	26	22	48*
CRCP (new)	1	1	2
New composite (AC overlaid JPCP)	1	15	16*
AC overlay (old, intact JPCP and fractured JPCP)	15	0	15*

*Conforms to ADOT pavement design and construction practices.

Table 11. Populated Sampling Template for New and Rehabilitated HMA-Surfaced Pavements

HMA Thickness (inches)	Granular Base Thickness* (inches)	Subgrade Type	
		Coarse-Grained Soils (AASHTO Class A-1 through A-3)	Fine-Grained Soils (AASHTO Class A-4 through A-7)
<8	<6	161, 902, 903, A901, A902, A903, PMS_98-115	
	≥6	113, 114, 119, 120, 121, 501, 502, 509, 559, 560, 1007_1, 1021_1, 1034_1, 1034_5, 1036_1, 1037_1, 6053_1, 6055_1, 6055_3, 6060_1, PMS_03-07, PMS_03-15, PMS_03-52, PMS_03-59, PMS_03-71	AZ1-WRI, AZ2-WRI, AZ3-WRI, AZ4-WRI, 505, PMS_03-12
≥8	<6	115, 116, 117, 118, 123, 124, 162, 260, 261, 1001, 1002_1, 1002_3	PMS_03-21_1, PMS_03-21_2, PMS_03-31_1, PMS_03-31_2
	≥6	122, 503, 504, 506, 507, 508, 1003_1, 1003_3, 1006_1, 1006_2, 1007_4, 1015_1, 1015_2, 1016_1, 1016_3, 1017_1, 1017_3, 1021_5, 1022_1, 1022_3, 1024_1, 1024_7, 6054_1, B901, B902, B903, B959, B960, B961, B964, 6060_5, PMS_03-28	1018_1, 1018_4, PMS_03-60

*All projects had a granular base. An equivalent, dense-graded aggregate base was assumed for PATBs.

Table 12. Populated Sampling Template for New and Rehabilitated JPCP

PCC Thickness (inches)	Dowel Diameter	Edge Support*	Subgrade and Base Type			
			Coarse-Grained Subgrade Soils (AASHTO Class A-1 through A-3)		Fine-Grained Subgrade Soils (AASHTO Class A-4 through A-7)	
			Lean Concrete Base	Granular- or Asphalt-Treated Base	Lean Concrete Base	Granular- or Asphalt-Treated Base
≤10	No dowels	None			ERES_AZ1-1, ERES_AZ1-6, ERES_AZ1-7, ERES_AZ 360-01, ERES_AZ 360-02, ERES_AZ 360-03	0601, 0602
		Yes		262, 263		
	Doweled	None	218, 7614	214, 222	ERES_AZ-2, ERES_AZ 10-04, ERES_AZ 10-05, ERES_AZ 10-06, ERES_AZ 10-07	
		Yes	217	213, 221, 268		
>10	No dowels	None				ERES_AZ1-2, ERES_AZ1-5, PMS_04-39
		Yes		264, 265, 7613,		
	Doweled	None	219	160, 215, 223		
		Yes	220	216, 266, 267		224, PMS_88-68

*Tied PCC and or widened lanes.

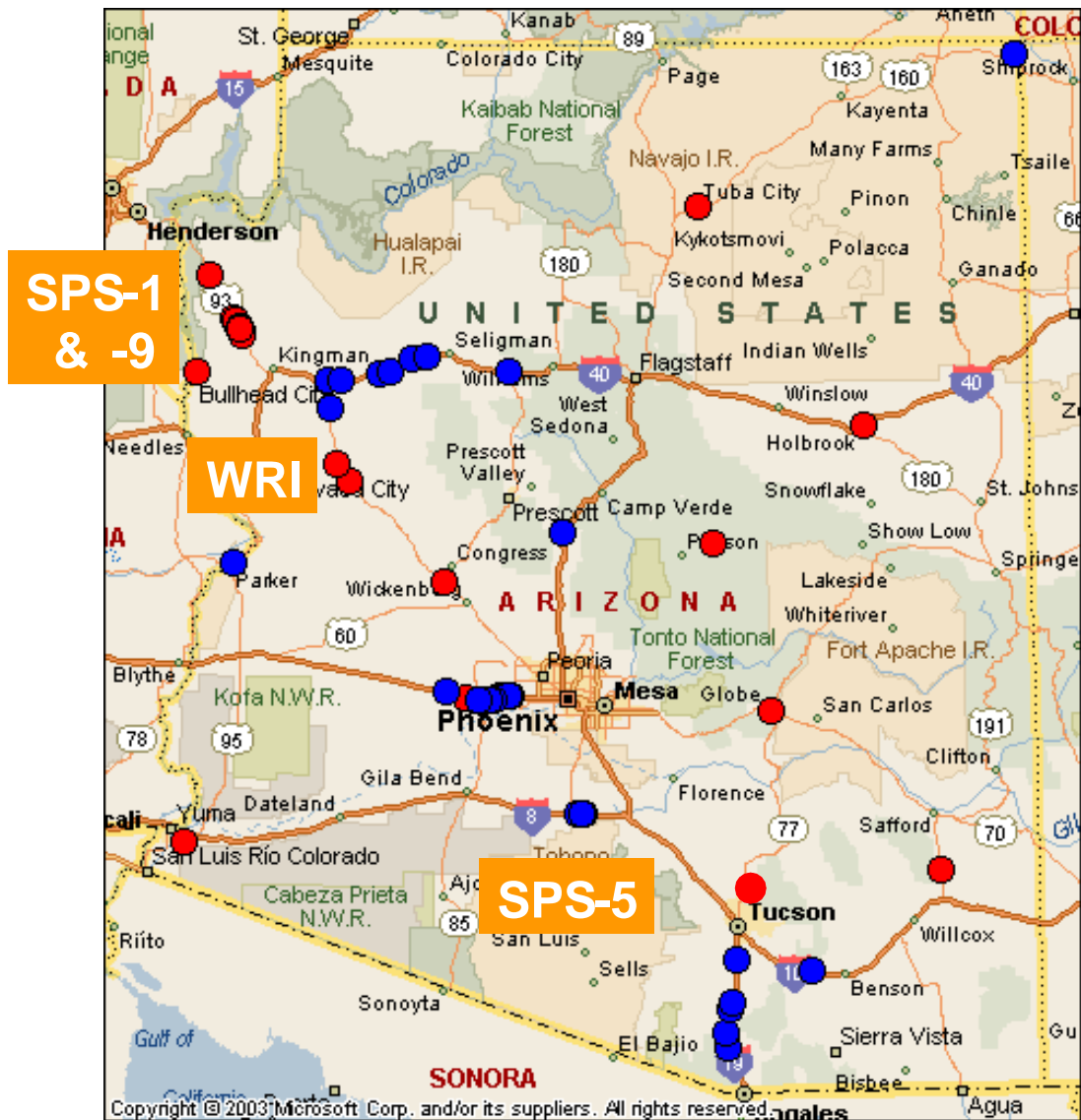


Figure 28. Location of Selected New HMA and HMA Overlaid HMA Pavement Projects
(LTTP = blue; PMS = red)

(base maps product of Microsoft Corporation, copyright 2003)



Figure 29. Location of Selected New Bare JPCP Projects
 (base maps product of Microsoft Corporation, copyright 2003)

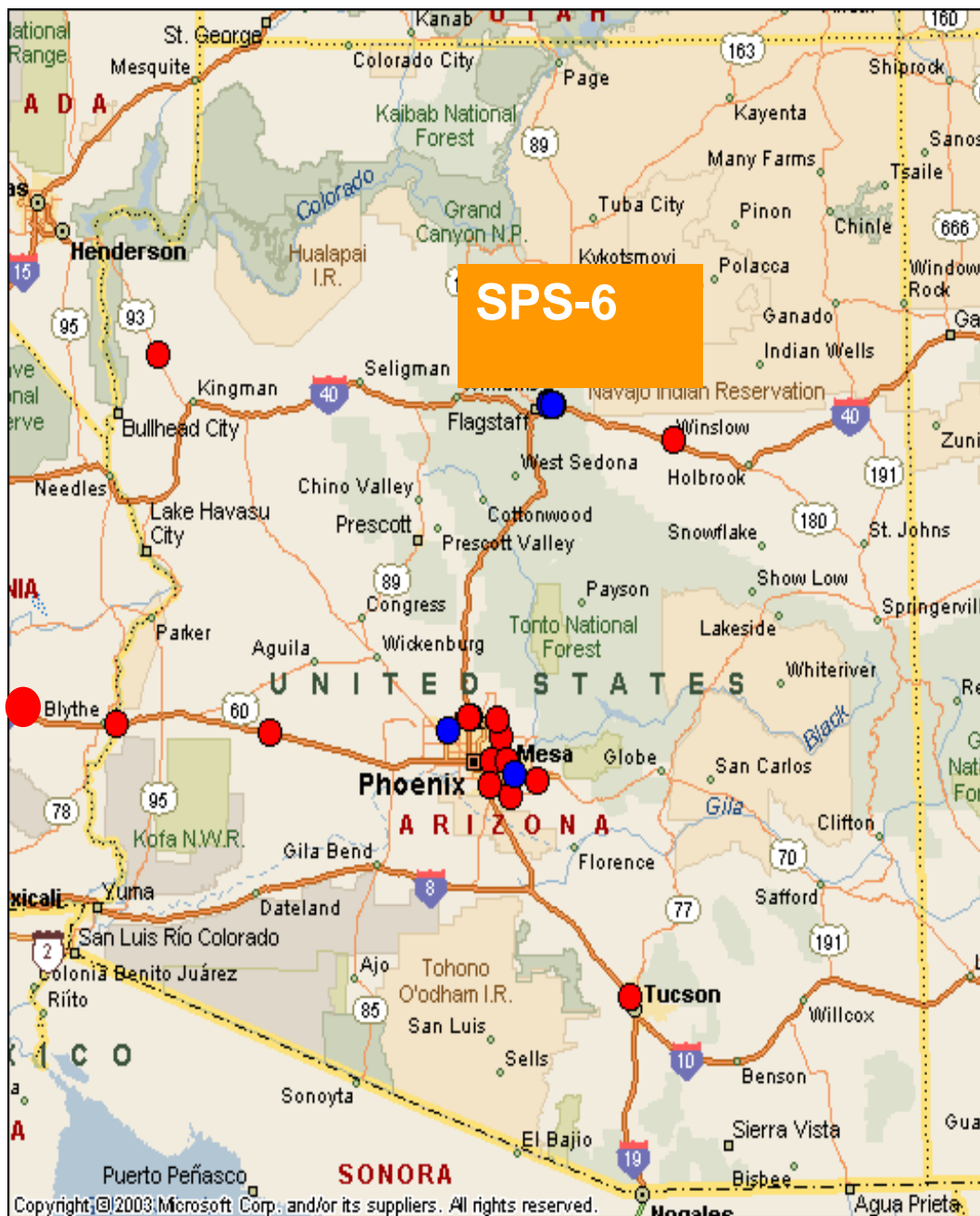


Figure 30. Location of Selected New ARFC-Surfaced JPCP Composite Projects

(LTPP = blue; PMS = red)

(base map product of Microsoft Corporation, copyright 2003)

Table 13. LTPP and ADOT PMS Projects Selected for Validation and Local Calibration

(GB = granular base; LCB = lean concrete base; ATB = asphalt-treated base)

Source	Pavement Type	ARA ID	Construction or Rehab Year	Original Construction Year	County	Route Signing	Route No.	Milepost
Smith et al. 1991	New JPCP over GB	AZ-10-01	N/A	1968	Maricopa	Interstate	10	154.05
Ibid.	New JPCP over GB	AZ-10-02	N/A	1968	Maricopa	Interstate	10	154.4
Ibid.	New JPCP over GB	AZ-10-03	N/A	1968	Maricopa	Interstate	10	153.87
Ibid.	New JPCP over LCB	AZ-10-04	N/A	1986	Maricopa	Interstate	10	140.67
Ibid.	New JPCP over LCB	AZ-10-05	N/A	1985	Maricopa	Interstate	10	136.68
Ibid.	New JPCP over LCB	AZ-10-06	N/A	1984	Maricopa	Interstate	10	130.88
Ibid.	New JPCP over LCB	AZ-10-07	N/A	1984	Maricopa	Interstate	10	130.5
Ibid.	New JPCP over CTB	AZ1-1	N/A	1972	Maricopa	State (U.S.)	360 (60)	172
Ibid.	New JPCP over subgrade	AZ1-2	N/A	1975	Maricopa	State (U.S.)	360 (60)	174.3
Ibid.	New JPCP over subgrade	AZ1-5	N/A	1979	Maricopa	State (U.S.)	360 (60)	177.5
Ibid.	New JPCP over LCB	AZ1-6	N/A	1981	Maricopa	State (U.S.)	360 (60)	179.5
Ibid.	New JPCP over LCB	AZ1-7	N/A	1981	Maricopa	State (U.S.)	360 (60)	181.3
Ibid.	New JPCP over GB	AZ-17-01	N/A	1961	Maricopa	Interstate	17	203.5
Ibid.	New JPCP over GB	AZ-17-03	N/A	1965	Maricopa	Interstate	17	211.89
Ibid.	New JPCP over GB	AZ-17-04	N/A	1965	Maricopa	Interstate	17	208.2
Ibid.	New JPCP over GB	AZ-17-11	N/A	1965	Maricopa	Interstate	17	208.7
Ibid.	New JPCP over LCB	AZ-2	N/A	1985	Maricopa	Interstate	10	141.19
Ibid.	New JPCP over LCB	AZ-360-01	N/A	1985	Maricopa	State (U.S.)	360 (60)	186.3
Ibid.	New JPCP over LCB	AZ-360-02	N/A	1985	Maricopa	State (U.S.)	360 (60)	185.3
Ibid.	New JPCP over LCB	AZ-360-03	N/A	1983	Maricopa	State (U.S.)	360 (60)	183.3
LTPP	New AC over GB	0113	N/A	1993	Mohave	U.S.	93	52.62
LTPP	New AC over GB	0114	N/A	1993	Mohave	U.S.	93	52.62
LTPP	New AC over ATB	0115	N/A	1993	Mohave	U.S.	93	52.62
LTPP	New AC over ATB	0116	N/A	1993	Mohave	U.S.	93	52.62

Table 13. LTPP and ADOT PMS Projects Selected for Validation and Local Calibration (Continued)

(GB = granular base; LCB = lean concrete base; ATB = asphalt-treated base)

Source	Pavement Type	ARA ID	Construction or Rehab Year	Original Construction Year	County	Route Signing	Route No.	Milepost
LTPP	New AC over ATB	0117	N/A	1993	Mohave	U.S.	93	52.62
LTPP	New AC over ATB	0118	N/A	1993	Mohave	U.S.	93	52.62
LTPP	New AC over ATB	0119	N/A	1993	Mohave	U.S.	93	52.62
LTPP	New AC over ATB	0120	N/A	1993	Mohave	U.S.	93	52.62
LTPP	New AC over ATB	0121	N/A	1993	Mohave	U.S.	93	52.62
LTPP	New AC over ATB	0122	N/A	1993	Mohave	U.S.	93	52.62
LTPP	New AC over ATB	0123	N/A	1993	Mohave	U.S.	93	52.62
LTPP	New AC over ATB	0124	N/A	1993	Mohave	U.S.	93	52.62
LTPP	New JPCP over GB	0160	N/A	1993	Mohave	U.S.	93	52.62
LTPP	New AC over GB	0161	N/A	1993	Mohave	U.S.	93	52.62
LTPP	New AC over GB	0162	N/A	1993	Mohave	U.S.	93	52.62
LTPP	New composite (AC/RCC)	0163	N/A	1993	Mohave	U.S.	93	52.62
LTPP	New JPCP over GB	0213	N/A	1993	Maricopa	Interstate	10	109
LTPP	New JPCP over GB	0214	N/A	1993	Maricopa	Interstate	10	109
LTPP	New JPCP over GB	0215	N/A	1993	Maricopa	Interstate	10	109
LTPP	New JPCP over GB	0216	N/A	1993	Maricopa	Interstate	10	109
LTPP	New JPCP over LCB	0217	N/A	1993	Maricopa	Interstate	10	109
LTPP	New JPCP over LCB	0218	N/A	1993	Maricopa	Interstate	10	109
LTPP	New JPCP over LCB	0219	N/A	1993	Maricopa	Interstate	10	109
LTPP	New JPCP over LCB	0220	N/A	1993	Maricopa	Interstate	10	109
LTPP	New JPCP over PATB	0221	N/A	1993	Maricopa	Interstate	10	109
LTPP	New JPCP over PATB	0222	N/A	1993	Maricopa	Interstate	10	109
LTPP	New JPCP over PATB	0223	N/A	1993	Maricopa	Interstate	10	109
LTPP	New JPCP over PATB	0224	N/A	1993	Maricopa	Interstate	10	109

Table 13. LTPP and ADOT PMS Projects Selected for Validation and Local Calibration (Continued)

(GB = granular base; LCB = lean concrete base; ATB = asphalt-treated base)

Source	Pavement Type	ARA ID	Construction or Rehab Year	Original Construction Year	County	Route Signing	Route No.	Milepost
LTPP	New AC over GB	0260	N/A	1993	Maricopa	Interstate	10	109
LTPP	New AC over GB	0261	N/A	1993	Maricopa	Interstate	10	109
LTPP	New JPCP over GB	0262	N/A	1993	Maricopa	Interstate	10	109
LTPP	New JPCP over PATB	0263	N/A	1993	Maricopa	Interstate	10	109
LTPP	New JPCP over PATB	0264	N/A	1993	Maricopa	Interstate	10	109
LTPP	New JPCP over GB	0265	N/A	1993	Maricopa	Interstate	10	109
LTPP	New JPCP over ATB	0266	N/A	1993	Maricopa	Interstate	10	109
LTPP	New JPCP over ATB	0267	N/A	1993	Maricopa	Interstate	10	109
LTPP	New JPCP over ATB	0268	N/A	1993	Maricopa	Interstate	10	109
LTPP	New AC over GB	0501	N/A	1968	Pinal	Interstate	8	159.01
LTPP	Mill and overlay AC	0502	1990	1968	Pinal	Interstate	8	159.01
LTPP	Mill and overlay AC	0503	1990	1968	Pinal	Interstate	8	159.01
LTPP	Mill and overlay AC	0504	1990	1968	Pinal	Interstate	8	159.01
LTPP	Mill and overlay AC	0505	1990	1968	Pinal	Interstate	8	159.01
LTPP	Mill and overlay AC	0506	1990	1968	Pinal	Interstate	8	159.01
LTPP	Mill and overlay AC	0507	1990	1968	Pinal	Interstate	8	159.01
LTPP	Mill and overlay AC	0508	1990	1968	Pinal	Interstate	8	159.01
LTPP	Mill and overlay AC	0509	1990	1968	Pinal	Interstate	8	159.01
LTPP	Mill and overlay AC	0559	1990	1968	Pinal	Interstate	8	159.01
LTPP	Mill and overlay AC	0560	1990	1968	Pinal	Interstate	8	159.01
LTPP	New JPCP	0601	1991	1967	Coconino	Interstate	40	202.16
LTPP	New JPCP	0602	1990	1967	Coconino	Interstate	40	202.16
LTPP	AC overlay of intact PCC	0603	1990	1967	Coconino	Interstate	40	202.16
LTPP	AC overlay of intact PCC	0604	1990	1967	Coconino	Interstate	40	202.16

Table 13. LTPP and ADOT PMS Projects Selected for Validation and Local Calibration (Continued)

(GB = granular base; LCB = lean concrete base; ATB = asphalt-treated base)

Source	Pavement Type	ARA ID	Construction or Rehab Year	Original Construction Year	County	Route Signing	Route No.	Milepost
LTPP	CPR	0605	1990	1967	Coconino	Interstate	40	202.16
LTPP	AC overlay of intact PCC	0606	1990	1967	Coconino	Interstate	40	202.16
LTPP	AC overlay of crack and seat PCC	0607	1990	1967	Coconino	Interstate	40	202.16
LTPP	AC overlay of crack and seat PCC	0608	1990	1967	Coconino	Interstate	40	202.16
LTPP	AC overlay of rubblized PCC	0659	1990	1967	Coconino	Interstate	40	202.16
LTPP	AC overlay of crack and seat PCC	0660	1990	1967	Coconino	Interstate	40	202.16
LTPP	AC overlay of crack and seat PCC	0661	1990	1967	Coconino	Interstate	40	202.16
LTPP	AC overlay of crack and seat PCC	0662	1990	1967	Coconino	Interstate	40	202.16
LTPP	PCC overlay of crack and seat PCC (2-inch AC interlayer)	0663	1990	1967	Coconino	Interstate	40	202.16
LTPP	AC overlay of intact PCC	0664	1990	1967	Coconino	Interstate	40	202.16
LTPP	AC overlay of crack and seat PCC	0665	1990	1967	Coconino	Interstate	40	202.16
LTPP	AC overlay of rubblized PCC	0666	1990	1967	Coconino	Interstate	40	202.16
LTPP	AC overlay of crack and seat PCC	0667	1990	1967	Coconino	Interstate	40	202.16

Table 13. LTPP and ADOT PMS Projects Selected for Validation and Local Calibration (Continued)

(GB = granular base; LCB = lean concrete base; ATB = asphalt-treated base)

Source	Pavement Type	ARA ID	Construction or Rehab Year	Original Construction Year	County	Route Signing	Route No.	Milepost
LTPP	AC overlay of intact PCC	0668	1990	1967	Coconino	Interstate	40	202.16
LTPP	AC overlay of rubblized PCC	0669	1990	1967	Coconino	Interstate	40	122.29
LTPP	New AC over GB	0902	N/A	1993	Mohave	U.S.	93	60.14
LTPP	New AC over GB	0903	N/A	1993	Mohave	U.S.	93	60.14
LTPP	New AC over GB	1001	N/A	1978	Maricopa	Interstate	10	123.34
LTPP	Mill and overlay AC	1002B	1996	1980	Yavapai	Interstate	40	145.37
LTPP	New AC over GB	1002A	N/A	1980	Yavapai	Interstate	40	145.37
LTPP	Mill and overlay AC	1003	1993	1975	Maricopa	Interstate	10	98.53
LTPP	New AC over GB	1003	N/A	1975	Maricopa	Interstate	10	98.53
LTPP	Mill and overlay AC	1006	1993	1976	Maricopa	Interstate	10	110.65
LTPP	New AC over GB	1006	N/A	1976	Maricopa	Interstate	10	110.65
LTPP	Mill and overlay AC	1007	1995	1978	Maricopa	Interstate	10	115.43
LTPP	New AC over GB	1007	N/A	1978	Maricopa	Interstate	10	115.43
LTPP	Mill and overlay AC	1015	1998	1979	Santa Cruz	Interstate	19	18.33
LTPP	New AC over GB	1015	N/A	1979	Santa Cruz	Interstate	19	18.33
LTPP	Mill and overlay AC	1016	1997	1979	Santa Cruz	Interstate	19	24.17
LTPP	New AC over GB	1016	N/A	1979	Santa Cruz	Interstate	19	24.17
LTPP	Mill and overlay AC	1017	1997	1976	Pima	Interstate	19	32.98
LTPP	New AC over GB	1017	N/A	1976	Pima	Interstate	19	32.98
LTPP	Mill and overlay AC	1018	1997	1976	Pima	Interstate	19	36.2
LTPP	New AC over GB	1018	N/A	1976	Pima	Interstate	19	36.2
LTPP	Mill and overlay AC	1021	1997	1978	Mohave	Interstate	40	72.87
LTPP	New AC over GB	1021	N/A	1978	Mohave	Interstate	40	72.87
LTPP	Mill and overlay AC	1022	1996	1977	Mohave	Interstate	40	77.69

Table 13. LTPP and ADOT PMS Projects Selected for Validation and Local Calibration (Continued)

(GB = granular base; LCB = lean concrete base; ATB = asphalt-treated base)

Source	Pavement Type	ARA ID	Construction or Rehab Year	Original Construction Year	County	Route Signing	Route No.	Milepost
LTPP	New AC over GB	1022	N/A	1977	Mohave	Interstate	40	77.69
LTPP	Mill and overlay AC	1024B	1999	1977	Yavapai	Interstate	40	106.95
LTPP	New AC over GB	1024A	N/A	1977	Yavapai	Interstate	40	106.95
LTPP	Mill and overlay AC	1025B	1999	1978	Yavapai	Interstate	40	113.03
LTPP	New AC over GB	1025A	N/A	1978	Yavapai	Interstate	40	113.03
LTPP	AC over existing AC	1034	2001	1975	La Paz	State	95	145.25
LTPP	New AC over GB	1034	N/A	1975	La Paz	State	95	145.25
LTPP	New AC over GB	1036	N/A	1983	Mohave	U.S.	93	27.64
LTPP	New AC over GB	1037	N/A	1985	Mohave	State	68	1.4
LTPP	AC over existing AC	1062	1999	1977	Mohave	Interstate	40	92.75
LTPP	AC over existing AC	1065	1999	1977	Yavapai	Interstate	40	97.72
LTPP	AC over existing AC	6053	1968	N/A	Pima	Interstate	10	292.89
LTPP	AC over existing AC	6054	1969	N/A	Santa Cruz	Interstate	19	52.25
LTPP	AC over existing AC	6055	1975	N/A	Maricopa	State	85	141.84
LTPP	Mill and overlay AC	6055	1999	1975	Maricopa	State	85	141.84
LTPP	AC over existing AC	6060	1967	N/A	Santa Cruz	Interstate	19	14.88
LTPP	Mill and overlay AC	6060	1998	1967	Santa Cruz	Interstate	19	14.88
LTPP	New CRCP over ATB	7079	N/A	1989	Maricopa	Other	101	11.9
LTPP	New JPCP over subgrade	7613	N/A	1979	Maricopa	State (U.S.)	360 (60)	180
LTPP	New JPCP over CTB	7614	N/A	1984	Maricopa	Interstate	10	130.5
LTPP	New AC over GB	A901	N/A	1993	Mohave	U.S.	93	60.14
LTPP	New AC over GB	A902	N/A	1993	Mohave	U.S.	93	60.14
LTPP	New AC over GB	A903	N/A	1993	Mohave	U.S.	93	60.14
LTPP	Mill and overlay AC	B901	1995	1978	Maricopa	Interstate	10	122.29

Table 13. LTPP and ADOT PMS Projects Selected for Validation and Local Calibration (Continued)

(GB = granular base; LCB = lean concrete base; ATB = asphalt-treated base)

Source	Pavement Type	ARA ID	Construction or Rehab Year	Original Construction Year	County	Route Signing	Route No.	Milepost
LTPP	Mill and overlay AC	B902	1995	1978	Maricopa	Interstate	10	122.29
LTPP	Mill and overlay AC	B903	1995	1978	Maricopa	Interstate	10	122.29
LTPP	Mill and overlay AC	B959	1995	1978	Maricopa	Interstate	10	122.29
LTPP	Mill and overlay AC	B960	1995	1978	Maricopa	Interstate	10	122.29
LTPP	Mill and overlay AC	B961	1995	1978	Maricopa	Interstate	10	122.29
LTPP	Mill and overlay AC	B964	1995	1978	Maricopa	Interstate	10	122.29
PMS	New composite (ARFC/JPCP)	95-22	2004	1997	Maricopa	State	202	13.23
PMS	New composite (ARFC/JPCP)	92-39	1994	1994	La Paz	Interstate	10	62
PMS	New composite (ARFC/CRCP)	92-39	1994	1994	La Paz	Interstate	10	70.66
PMS	New composite (ARFC/JPCP)	95-49	2004	2001	Maricopa	State	101	34.5
PMS	New composite (ARFC/JPCP)	96-36	2003	1999	Maricopa	State	101	41
PMS	New AC over CTB	00-78	N/A	2001	Gila	State	260	266
PMS	New composite (ARFC/JPCP)	04-68	2007	2007	Navajo	Interstate	40	253.2
PMS	New AC over AB	03-02	2007	2007	Coconino	U.S.	160	319.7
PMS	New AC over AB	03-02	2007	2007	Coconino	U.S.	160	319.7
PMS	AC over existing AC	98-115	1999	N/A	Apache	U.S.	160	465.3
PMS	New composite (ARFC/JPCP)	97-68	2003	1999	Maricopa	State	101	22.69
PMS	New composite (ARFC/JPCP)	99-13	2003	2001	Maricopa	State	101	24.5

Table 13. LTPP and ADOT PMS Projects Selected for Validation and Local Calibration (Continued)

(GB = granular base; LCB = lean concrete base; ATB = asphalt-treated base)

Source	Pavement Type	ARA ID	Construction or Rehab Year	Original Construction Year	County	Route Signing	Route No.	Milepost
PMS	New composite (ARFC/JPCP)	98-159	2003	2001	Maricopa	State	101	28
PMS	New AC over GB	03-28	N/A	2005	Graham	U.S.	191	97.6
PMS	Mill and overlay AC	02-55	2006	2006	La Paz	State	95	143.0
PMS	Mill and overlay AC	03-31	2002	1988	Pima	State	77	72.5
PMS	Mill and overlay AC	03-31	2002	1988	Pima	State	77	72.95
PMS	New composite (ARFC/JPCP)	02-63	2005	2005	Maricopa	State	202	44.6
PMS	New AC over GB	03-71	N/A	2008	Mohave	U.S.	93	156.5
PMS	New AC over GB	03-52	N/A	2005	Mohave	U.S.	93	122.96
PMS	New composite (ARFC/JPCP)	02-79	2004	1997	Maricopa	Interstate	10	157.7
PMS	New AC over GB	03-59	N/A	2008	Yuma	State	195	9.1
PMS	New composite (ARFC/JPCP)	01-86	2008	2007	Pima	Interstate	10	255
PMS	New AC over GB	03-60	N/A	2006	Navajo	Interstate	40	287.6
PMS	Mill and overlay AC	03-12	2006	2006	Yavapai	Interstate	17	263
PMS	AC over existing AC	03-15	2006	N/A	Mohave	U.S.	93	95.1
PMS	Mill and overlay AC	03-21	2005	2005	Apache	U.S.	180	416.31
PMS	Mill and overlay AC	03-21	2005	2005	Apache	U.S.	180	416.31
PMS	New composite (ARFC/JPCP)	03-06	2005	2005	Maricopa	State	202	31
PMS	New AC over GB	03-07	N/A	2004	Gila	U.S.	70	252.14
PMS	AC over existing AC	03-31	2009	2002	Pima	State	77	72.95

48 #

Table 13. LTPP and ADOT PMS Projects Selected for Validation and Local Calibration (Continued)

(GB = granular base; LCB = lean concrete base; ATB = asphalt-treated base)

Source	Pavement Type	ARA ID	Construction or Rehab Year	Original Construction Year	County	Route Signing	Route No.	Milepost
PMS	New composite (ARFC/JPCP)	02-24	N/A	2004	La Paz	Interstate	10	1.8
PMS	New JPCP over AB	04-39	N/A	2006	Mohave	State	66	56.56
PMS	New JPCP over ATB	88-68	N/A	1993	Pima	Interstate	10	260.4
PMS	ARFC surfacing of CRCP	PMS7079	2005	1989	Maricopa	State	101	11.9
WRI	New AC over GB	AZ1-1 WRI	N/A	2001	Maricopa	U.S.	93	145.45
WRI	New AC over GB	AZ1-2 WRI	N/A	2001	Maricopa	U.S.	93	146.47
WRI	New AC over GB	AZ1-3 WRI	N/A	2001	Maricopa	U.S.	93	147.13
WRI	New AC over GB	AZ1-4 WRI	N/A	2001	Maricopa	U.S.	93	147.83

Extract and Review Key MEPDG Input Data for Rehabilitated Projects

Specifically, for AC overlaid existing HMA and ARFC over JPCP projects, the distress condition of the existing pavement before overlay and repair work performed as part of rehabilitation is a key input for modeling future performance. The following information is required for existing new HMA pavements and existing JPCP:

- Existing HMA pavements:
 - Alligator cracking.
 - Rutting (in all layers of relevance).
 - Repair work done (full-depth patching and milling depth).
- Existing JPCP:
 - Transverse cracking.
 - Slab replacement.

Before overlay placement, the researchers used this information to characterize pavement condition. The distress and IRI data were obtained as described previously.

STEP 6: CONDUCT FIELD AND FORENSIC INVESTIGATIONS

Forensic investigations were limited to ADOT PMS projects and were composed of either a windshield distress survey, FWD testing, or both. As noted, the researchers conducted windshield distress surveys on many ADOT PMS projects with insufficient distress data to update condition information or to characterize the condition entirely. The researchers also completed FWD testing and backcalculation of subgrade elastic/resilient modulus for ADOT PMS sections with no foundation support data.

STEPS 7 THROUGH 10: ASSESS LOCAL BIAS AND STANDARD ERROR OF THE ESTIMATE FROM GLOBAL CALIBRATION FACTORS, AND ELIMINATE/REDUCE STANDARD ERROR OF THE ESTIMATE AND LOCAL BIAS OF DISTRESS PREDICTION MODELS

Several methods were used singly or in combination to verify the MEPDG global models for Arizona local conditions. Statistical methods were used when there was a good distribution of measured distress and IRI; when measured distress was mostly zero, a nonstatistical approach to model validation was used. Model validation consisted of the following steps:

1. Execute the MEPDG for each selected LTPP, ADOT PMS, and ADOT research project (see Table 13) and predict pavement distresses and IRI over a reasonable time period (typically 10 to 40 years).

2. Extract predicted distress and IRI data from the MEPDG outputs that match the age of measured distress and IRI.
3. Perform statistical or nonstatistical analysis as appropriate to characterize bias and prediction capacity.
4. Determine suitability of the MEPDG global models for Arizona local conditions.

Details of the statistical or nonstatistical analysis used to verify model suitability are presented in the following sections.

Evaluate Model Prediction Capacity (Goodness of Fit)

To assess the goodness of fit of a given MEPDG distress and IRI prediction model, the researchers determined the coefficient of determination (R^2) and SEE using measured Arizona and MEPDG predicted distress and IRI data. Reasonableness of both diagnostic statistics was determined by comparing the Arizona diagnostic statistics with those obtained for the MEPDG global models under NCHRP 1-40D (see Table 14). Engineering judgment was then used to determine the reasonableness of Arizona diagnostic statistics.

Models exhibiting a poor R^2 (i.e., R^2 significantly less than the values presented in Table 14) or excessive SEE (significantly higher than the values presented in Table 14) were considered inadequate for Arizona conditions.

Table 14. National Calibration Under NCHRP 1-40D New HMA Pavement and New JPCP Model Statistics

Pavement Type	Performance Model	Model Statistics		
		R^2	SEE	Number of Data Points (N)
New HMA	Alligator cracking	0.275	5.01%	405
	Transverse thermal cracking	Level 1*: 0.344 Level 2*: 0.218 Level 3*: 0.057	—	—
	Rutting	0.58	0.107 inch	334
	IRI	0.56	18.9 inch/mi	1926
New JPCP	Transverse slab cracking	0.85	4.52%	1505
	Transverse joint faulting	0.58	0.033 inch	1239
	IRI	0.60	17.1 inch/mi	163

*Level of inputs used for calibration.

Evaluate Model Bias

Bias was defined as the consistent under- or overprediction of distress and IRI. The researchers determined bias by performing linear regression using Arizona measured and MEPDG predicted distress and IRI, and performing the following two hypothesis tests. A significance level, α , of 0.05 or 5 percent was assumed for all hypothesis testing.

- **Hypothesis 1: Paired t-test.** This test determined whether the Arizona measured and MEPDG predicted distress and IRI represented the same population. The paired t-test consisted of the following steps:
 - Assume the following null and alternative hypothesis:
 - a. H_0 : mean measured distress/IRI = mean predicted distress/IRI.
 - b. H_A : mean measured distress/IRI \neq mean predicted distress/IRI.
 - Compute test p-value using SAS Institute Inc. (SAS) statistical software.
 - Compare computed p-value to predetermined level of significance for this test.
(Note: A significance level of 5 percent was adopted for this analysis.)

The null hypothesis H_0 was rejected if the p-value was less than 0.05. Rejecting H_0 implied that the Arizona measured and MEPDG predicted distress and IRI were essentially from different populations at the 5 percent significance level. Belonging to different populations indicates a potential bias in the MEPDG predicted distress and IRI since the measured distress and IRI are considered to represent the ground truth for this test analysis.

- **Hypothesis 2.** This paired t-test (which is only meaningful if hypothesis 1 was accepted) determined whether a linear regression model (predicted distress/IRI = α *measured distress/IRI) has a slope (α) of 1.0 at the 5 percent significance level. The test consisted of the following steps:
 - Using the results of the linear regression analysis, test the following null and alternative hypotheses to determine if the linear regression model slope is 1.0:
 - a. H_0 : model slope (α) = 1.0.
 - b. H_A : model slope (α) \neq 1.0.
 - Compute test p-value using SAS.
 - Compare computed p-value to predetermined level of significance for this test.
(Note: A significance level of 5 percent was adopted for this analysis.)

The null hypothesis H_0 was rejected if p-value was less than 0.05. Rejecting H_0 implied that the linear model has a slope significantly different from 1.0 at the 5 percent significance level, which indicates that using the MEPDG global models outside of the range of Arizona measured distress and IRI will produce biased predictions.

The presence of bias did not necessarily imply that the MEPDG global models were defective. It simply means that there is some bias in predicted distress and IRI values when the MEPDG is used under Arizona conditions.

The global MEPDG models that were considered biased or had an inadequate prediction capacity or goodness of fit needed local calibration.

Calibrate MEPDG Models for Arizona Local Conditions

The researchers used both linear and nonlinear regression procedures from the SAS statistical software to calibrate MEPDG models for local conditions:

1. Split the assembled LTPP and ADOT projects data into two separate databases for calibration and validation. For this study, a 90/10 percent split was adopted. Thus, approximately 90 percent of all projects were used to create a local calibration database while the remaining 10 percent of projects were used to create a validation database. While projects were selected at random, the researchers ensured the projects represented a balance in pavement type, design features, material properties, traffic, construction year, location and climate, and other parameters. In essence, the 10 percent validation database had the same distributions and key statistics such as the range of AC or PCC thickness and mean values of such key inputs. After the preliminary or tentative locally calibrated MEPDG models were developed and validated using the 90 percent local calibration and 10 percent validation databases, respectively, the final locally calibrated MEPDG models were developed using all projects. Tables 15 and 16 present the projects selected for the databases.
2. Perform local calibration:
 - a. Run the MEPDG for all projects in the 90 percent local calibration database.
 - b. Assemble critical MEPDG inputs (HMA thickness); MEPDG outputs (predicted damage, distress, and IRI); and measured distress and IRI required for local calibration in an optimization database.
 - c. Determine MEPDG models calibration coefficients that can be modified as part of local calibration (see Chapter 2).
 - d. Perform optimization using linear and nonlinear regression techniques to select local calibration coefficients that maximizes R^2 , minimizes SEE, and eliminates bias.

3. Validate the tentative locally calibrated MEPDG models:
 - a. Run the MEPDG for all projects in the 10 percent validation database using the local calibration coefficients previously determined.
 - b. Assemble critical MEPDG inputs (HMA thickness); MEPDG outputs (predicted damage, distress, and IRI); and measured distress and IRI required for local calibration in an optimization database.
 - c. Determine goodness of fit and presence or absence of bias.
4. Modify the tentative locally calibrated MEPDG models as needed until an adequate model or solution is obtained (i.e., reasonable goodness of fit and no bias).
5. Develop final locally calibrated MEPDG models using 100 percent of all projects.

Chapter 3 of this report provides a detailed description of Steps 7 through 10.

STEP 11: INTERPRET RESULTS AND DETERMINE ADEQUACY OF ADOT MEPDG LOCALLY CALIBRATED MODELS

Under this step, the project team developed pavement designs for selected typical ADOT projects using the final locally calibrated MEPDG models. The new designs were then evaluated for reasonableness using the following criteria:

- Selected in-service pavements that have performed adequately (i.e., presence of little or no distress over 15 to 30 years): The new designs are expected to be comparable to the existing pavement design.
- Selected in-service pavements that have exhibited early failures (i.e., presence of high levels of distress within 10 to 15 years of a 20- to 30-year design): The new designs are expected to be an improvement (e.g., thicker HMA and PCC layers) of the existing pavement designs.

These results are presented in Chapter 3.

Table 15. Sampling Template for the 10 Percent Validation/90 Percent Calibration Databases for New and Rehabilitated HMA-Surfaced Pavements

HMA Thickness (inches)	Base Thickness (inches)	Projects for Validation and Calibration Databases	Subgrade Type	
			Coarse (AASHTO Class A-1 through A-3)	Fine (AASHTO Class A-4 through A-7)
4 to 8	<6	10% validation		
		90% calibration	161, A901, A902, A903, PMS_98-115	
	≥6	10% validation	560, 1007_1, 1021_1, 6055_1	AZ1-WRI
		90% calibration	113, 114, 119, 120, 121, 501, 502, 509, 559, 1034_1, 1034_5, 1036_1, 1037_1, 6053_1, 6055_3, 6060_1, PMS_03-07, PMS_03-15, PMS_03-52, PMS_03-59, PMS_03-71	AZ2-WRI, AZ3-WRI, AZ4-WRI, 505
>8	<6	10% validation	115	PMS_03-21_1
		90% calibration	116, 117, 118,123,124, 162, 260, 261, 1001, 1002_1, 1002_3	PMS_03-21_2, PMS_03-31_1, PMS_03-31_2
	≥6	10% validation	1017_3, B901	
		90% calibration	122, 503, 504, 506, 507, 508, 1003_1, 1003_3, 1006_1, 1006_2, 1007_4, 1015_1, 1015_2, 1016_1, 1016_3, 1017_1 1021_5, 1022_1, 1022_3, 1024_1, 1024_7, 6054_1, B902, B903, B959, B960, B961, B964, 6060_5, PMS_03-28	1018_1, 1018_4, PMS_03-60

Note: Nine of 85 new HMA and HMA overlaid HMA pavements were selected for the 10 percent validation database.

Table 16. Simplified Sampling Template for the Validation and Local Calibration of New JPCP

PCC Thickness (inches)	Dowels	Edge Support	Projects for Validation and Calibration Databases	Subgrade Type				
				Coarse (AASHTO Class A-1 through A-3)		Fine (AASHTO Class A-4 through A-7)		
				Base Type				
				Lean Concrete Base	Granular and Asphalt-Treated Base/AC	Lean Concrete Base	Granular and Asphalt-Treated Base/AC	
≤10	No dowels	None	10% validation			ERES_AZ1-1		
			90% calibration			ERES_AZ1-6, ERES_AZ1-7, ERES_AZ 360-01, ERES_AZ 360-02, ERES_AZ 360-03		
		Tied PCC and or widened lanes	10% validation					
			90% calibration		262,263			
	Doweled	None	10% validation			ERES_AZ-2		
			90% calibration	218, 7614	214,222	ERES_AZ 10-04, ERES_AZ 10-05, ERES_AZ 10-06, ERES_AZ 10-07		
		Tied PCC and or widened lanes	10% validation					
			90% calibration	217	213,221, 268			
	>10	No dowels	None	10% validation				
				90% calibration			ERES_AZ1-2, ERES_AZ1-5, PMS_04-39	
Tied PCC and or widened lanes			10% validation					
			90% calibration		264,265, 7613			
Doweled		None	10% validation		160			
			90% calibration	219	215,223			
		Tied PCC and or widened lanes	10% validation				224	
			90% calibration	220	216,266, 267		PMS_88-68	

Note: Four of 37 new JPCP were selected for the 10 percent validation database.

CHAPTER 3. VERIFICATION, LOCAL RECALIBRATION, AND VALIDATION OF MEPDG MODELS

Verification of the MEPDG nationally calibrated global models and local calibration and validation results are presented in this chapter. Table 17 lists the models evaluated as part of Arizona's MEPDG implementation. The appendix presents detailed descriptions of these models.

NEW HMA AND HMA OVERLAID HMA ALLIGATOR CRACKING

Verification

To verify the MEPDG global alligator cracking models for Arizona conditions, the researchers ran the MEPDG with the global coefficients for all projects and evaluated goodness of fit and bias. Figure 31 plots the cumulative fatigue damage versus alligator cracking for all Arizona HMA sections. The goodness of fit statistics shown in this figure are very poor ($R^2 = 8.2\%$, $SEE = 14.3\%$ lane area), and the model predictions are obviously biased. (Under prediction, the curve represents the global calibration model.) Thus, local calibration of this very important model was necessary.

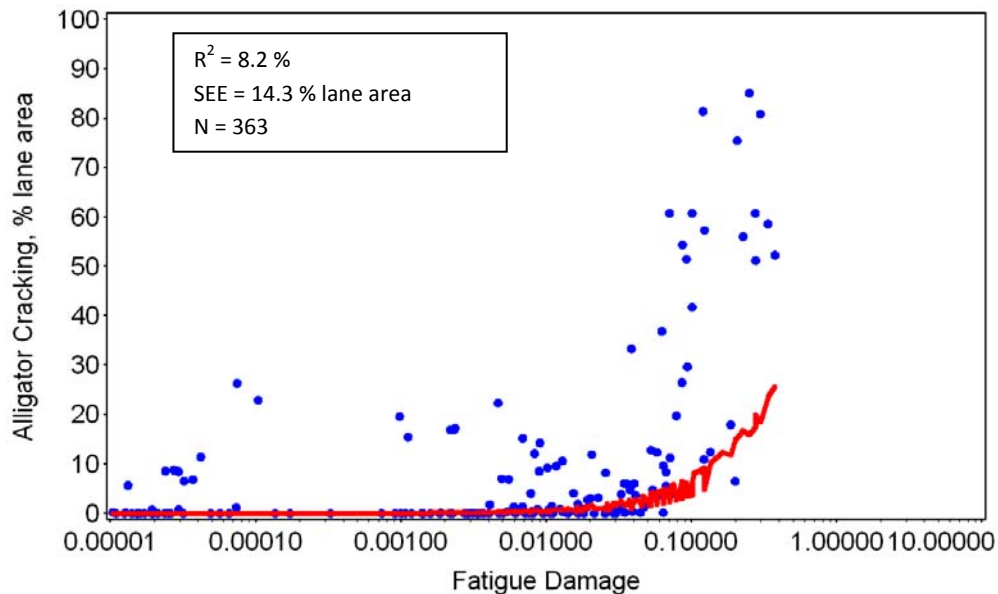


Figure 31. Initial Verification of the HMA Alligator Fatigue Cracking Models with Global Coefficients Using Arizona Performance Data

Table 17. MEPDG Global Models Evaluated for Arizona Local Conditions

Pavement Type	MEPDG Global Models Evaluated												
	HMA Alligator Cracking	HMA Transverse Cracking	Total Rutting (3 Submodels)	New HMA and HMA/HMA IRI	JPCP Transverse Cracking	JPCP Transverse Joint Faulting	New JPCP IRI	CRCP Punchouts	CRCP IRI	HMA/HMA Reflected Alligator Cracking	HMA/JPCP Reflected Transverse Cracking	HMA/JPCP Reflected IRI	HMA/CRCP Reflected IRI
New HMA	✓	✓	✓	✓									
HMA/HMA	✓	✓	✓	✓						✓			
JPCP/HMA													
CRCP/HMA													
New JPCP					✓	✓	✓						
HMA/JPCP					✓						✓	✓	
PCC/JPCP (bonded)													
JPCP/JPCP (unbonded)													
New CRCP								✓*	✓*				
HMA/CRCP													
PCC/CRCP (bonded)													
CRCP/CRCP (unbonded)													

*Limited checks and evaluation.

Local Calibration

Local calibration involves investigating the causes of poor goodness of fit and bias in MEPDG nationally calibrated models, and modifying the calibration coefficients of the HMA fatigue model and the alligator cracking model (see Chapter 2) as needed based on information derived from Eq. 1 to improve goodness of fit and reduce or eliminate bias. Specifically, the coefficients k_1 , k_2 , and k_3 for the HMA fatigue model and C_1 , C_2 , and C_4 of the alligator cracking model were modified during the analysis to improve prediction. In HMA overlays of HMA pavements, the reflection cracking model was also calibrated during the analysis. This model predicts total alligator cracking at the surface composed of alligator cracking initiating at the bottom of the HMA overlay and reflected through from the underlying existing HMA layer.

Investigation of Causes of Poor Goodness of Fit and Bias

There were no obvious causes for poor goodness of fit and bias in the global cracking model.

Local Calibration of Alligator Cracking Models

The researchers computed model local coefficients through optimization using SAS statistical software for the HMA load applications to cracking model:

$$N_{f-HMA} = k_{f1}(C)(C_H)\beta_{f1}(\epsilon_t)^{k_{f2}\beta_{f2}}(E_{HMA})^{k_{f3}\beta_{f3}} \quad (\text{Eq. 1})$$

They also computed model local coefficients for the alligator cracking fatigue damage model (S-shaped curve):

$$FC_{Bottom} = \left(\frac{1}{60} \right) \left(\frac{C_4}{1 + e^{(C_1 C_1^* + C_2 C_2^* \text{Log}(DI_{Bottom}))}} \right) \quad (\text{Eq. 2})$$

For HMA overlays, they analyzed the percentage of reflected cracks model from the existing HMA pavement and optimized coefficients determined:

$$RC = \frac{100}{1 + e^{ac+bd}} \quad (\text{Eq. 3})$$

Where

RC = alligator cracks from existing HMA layer reflected, percent reflected through overlay (0 to 100)

t = age (in years)

a, b, c, d = model coefficients

Table 18 provides the preliminary local calibration coefficients and goodness of fit statistics developed using 90 percent of projects. The results indicate an adequate goodness of fit; several of the global models coefficients changed.

The preliminary locally calibrated alligator cracking model was then independently validated using the 10 percent of projects set aside for validation. The results, presented in Table 19, show an equally good fit to the measured alligator cracking model. For the validation, however, SEE was significantly higher.

Table 18. Preliminary Local Calibration Coefficients and Goodness of Fit Statistics for Alligator Cracking Submodels Using 90 Percent of Projects

Model or Submodel Type	Goodness of Fit	Model Coefficients	ADOT Local Calibration (Using 90% of Projects)
Fatigue damage model	R ² = 55.1% SEE = 12.6% lane area N = 332	k1	1.884
		k2	3.9492
		k3	1.58
Alligator cracking model		C1	0.75
		C2	4.5
		C4	6000
Reflection cracking model		a	3.5+0.75heff
		b	-0.688584-3.37302*heff 0.915469
		c	2.7 if heff < 3-in 4.0 if heff ≥ 3-in
		d	1

Table 19. Goodness of Fit Statistics for Validating the Preliminary 90 Percent Locally Calibrated Alligator Cracking Submodels with 10 Percent of Projects

Model or Submodel Type	Goodness of Fit Based on 90% of Selected Calibration Projects	Goodness of Fit Based on 10% of Selected Validation Projects
Fatigue damage model	R ² = 55.1% SEE = 12.6% lane area N = 332	R ² = 64.9% SEE = 21.2% lane area N = 30
Alligator cracking model		
Reflection cracking model		

Given this validation check, the researchers combined the databases and developed the final locally calibrated alligator cracking models. The models coefficients did not change and goodness of fit was adequate, as shown in Table 20. The final locally calibrated alligator cracking model was evaluated for bias. The results, presented in Figure 32, showed the model has no significant bias.

Table 20. Goodness of Fit and Bias Test Statistics for Final Locally Calibrated Alligator Cracking Model (Based on 100 Percent of All Projects)

Model	Goodness of Fit and Bias Statistics	Model Coefficients	ADOT Local Calibration (Using 100% of Projects)	Change from NCHRP 1-40D Global Models
Fatigue damage model	<u>Goodness of Fit</u> $R^2 = 50\%$ SEE = 14.8% lane area N = 419	k1	0.007566	Yes
		k2	3.9492	No
		K3	1.281	Yes
		BF1	249.0087	Yes
		BF2	1.00	No
		BF3	1.2334	Yes
Alligator cracking model	<u>Bias Test</u> H_0 : Slope = 1.0 (p-value = 0.9897)	C1	1.00	No
		C2	4.50	Yes
		C4	6000	No
Reflection cracking model	H_0 : Predicted and measured cracking from the same population (paired t test) (p-value = 0.0837)	a	$3.5+0.75heff$	No
		b	$-0.688584-3.37302*heff$ 0.915469	No
		c	2.55	Yes
		d	1.23	Yes

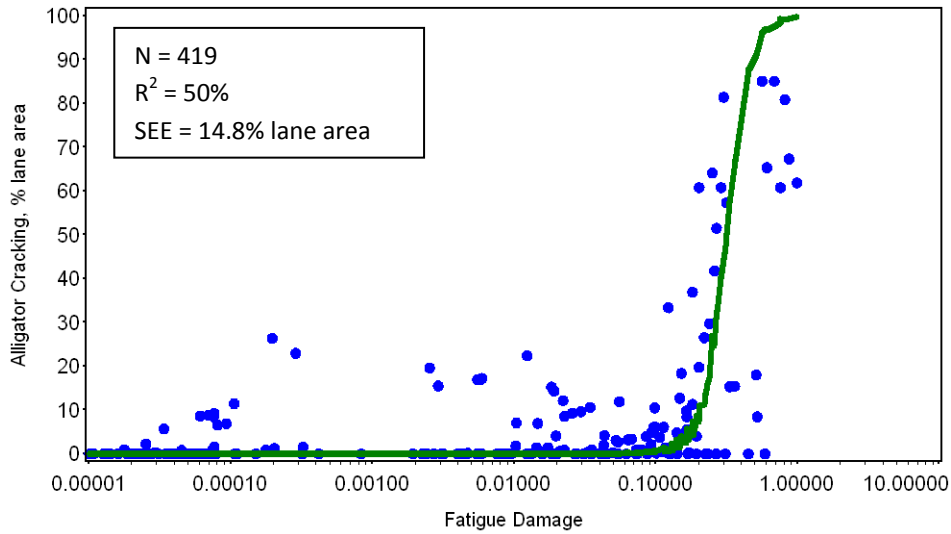


Figure 32. Measured and Predicted Alligator Cracking Versus Cumulated Fatigue Damage for the Locally Calibrated Alligator Cracking Submodels

Figure 33 illustrates the model prediction for a new HMA pavement and Figure 34 shows the model prediction for an overlaid pavement. The impact of local calibration of the HMA pavement alligator fatigue cracking model is most significant after removing the bias (underprediction) of prediction, as can be seen when comparing the global coefficients of Figure 31 and the local coefficients in Figure 32. The goodness of fit increased from 8 percent to 50 percent while the SEE increased slightly—from 14.3 to 14.8. These combined effects will increase the accuracy and eliminate the bias of the alligator fatigue cracking model. HMA pavement designs based in part on HMA fatigue cracking in Arizona will be more accurate and optimum (lower cost) at the selected level of design reliability.

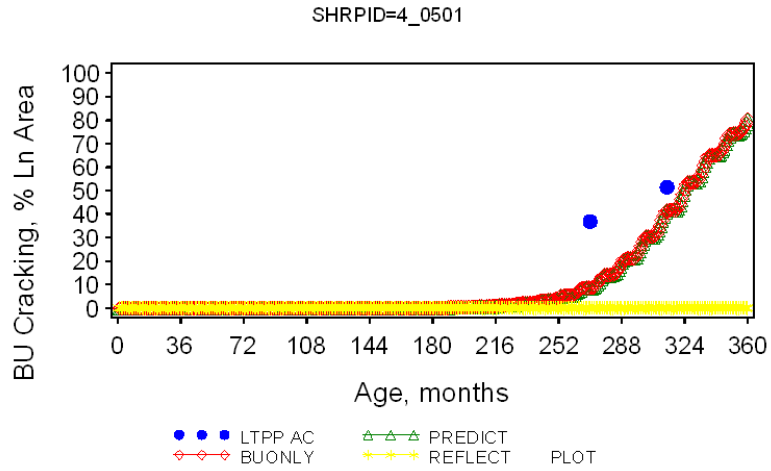


Figure 33. Predicted and Measured Alligator (Fatigue) Cracking for Arizona I-8 HMA (LTPP 4_0501) Pavement

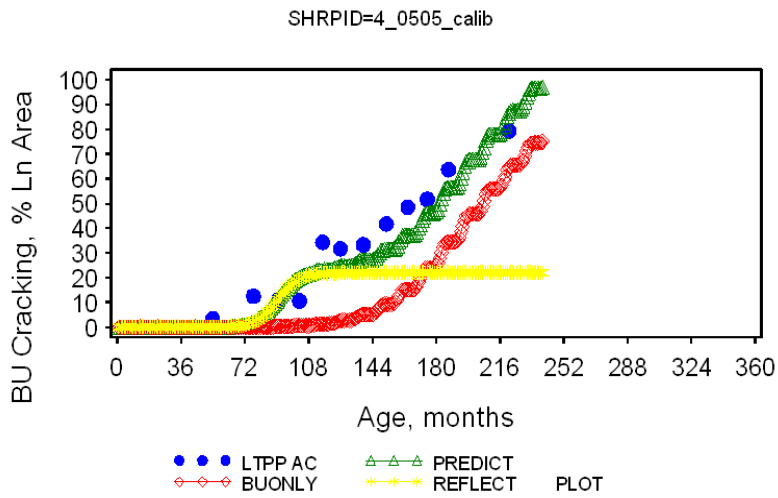


Figure 34. Predicted and Measured Alligator (Fatigue) Cracking for Arizona I-8 HMA (LTPP 4_0505) Overlaid Pavement

NEW HMA AND HMA OVERLAID HMA RUTTING

Verification

To verify the MEPDG global permanent deformation or rutting models for Arizona conditions, researchers ran the MEPDG with the global coefficients for all projects and then evaluated goodness of fit and bias. Figure 35 plots predicted versus measured total rutting for all Arizona HMA sections. The goodness of fit statistics are very poor ($R^2 = 4.6\%$, $SEE = 0.31$ inch), and the model predictions are obviously biased (large overprediction using the global calibration model). Thus, local calibration of this very important model was necessary.

Local Calibration

To calibrate the model, researchers investigated the causes of poor goodness of fit and bias of the MEPDG nationally calibrated models and modified the local calibration coefficients of the fatigue damage and alligator cracking submodels as needed based on information derived from Eq. 1. Specifically, the coefficients k_1 , k_2 , and k_3 for the HMA pavement rutting submodels and k_1 (aggregate base) and k_1 (subgrade) for the aggregate base and subgrade submodels were modified to improve total rutting prediction.

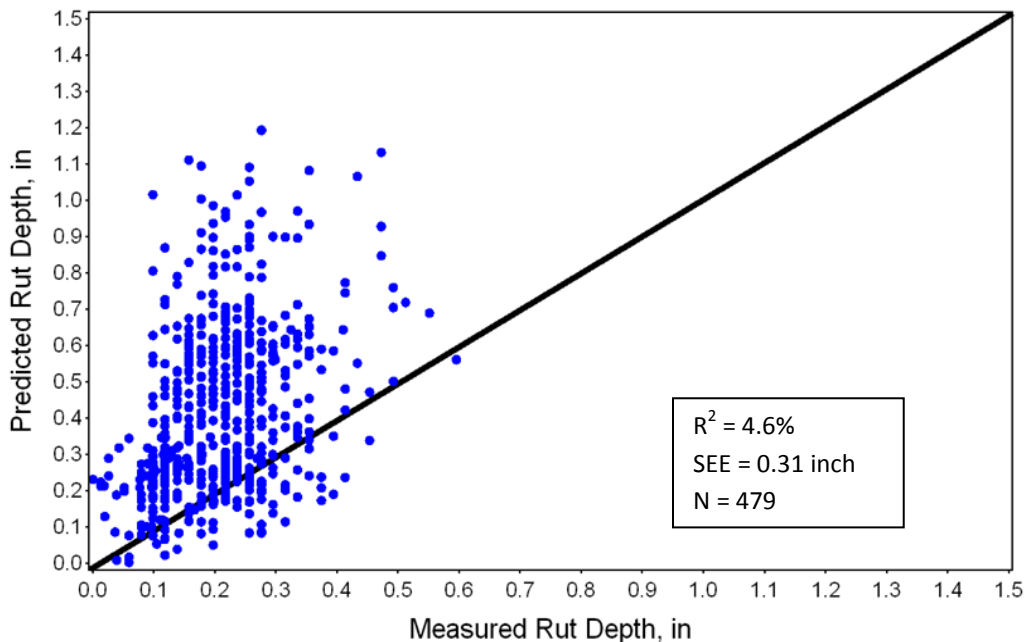


Figure 35. Predicted and Total Rutting Using Global Coefficients and Arizona HMA Pavement Performance Data

Investigation of Causes of Poor Goodness of Fit and Bias

Although there were no obvious causes for poor goodness of fit and bias in the global model rutting predictions in Arizona, the following was observed:

- For new HMA pavement LTPP GPS projects (constructed mostly in the late 1970s and early 1980s), the global models underestimated total measured rutting.
- For new HMA pavement LTPP SPS projects (constructed mostly in the 1990s), the global models predicted total rutting reasonably well.
- For HMA overlaid HMA pavements, the global models predicted very little rutting in the existing pavement layers and underestimated predicted total rutting, which consisted almost entirely of rutting in the HMA overlay.
- Goodness of fit was very poor due mostly to the magnitude of variability in year-to-year measurements for individual projects.

Local Calibration of Rutting Submodels

Model local coefficients were determined through optimization using SAS statistical software for the following model (note that the three main terms in this model are HMA, unbound aggregate base, and subgrade):

$$\Delta_{p(total)} = \beta_{1r} k_z \varepsilon_r(HMA) 10^{k_{1r}} n^{k_{2r} \beta_{2r}} T^{k_{3r} \beta_{3r}} + \beta_{B1} k_{B1} \varepsilon_{vbase} h_{base} \left(\frac{\varepsilon_o}{\varepsilon_r} \right) e^{-\left(\frac{\rho}{n} \right)^\beta} + \beta_{s1} k_{s1} \varepsilon_{vsubgrade} h_{subgrade} \left(\frac{\varepsilon_o}{\varepsilon_r} \right) e^{-\left(\frac{\rho}{n} \right)^\beta} \quad (\text{Eq. 4})$$

All inputs are defined in the appendix.

Table 21 presents the preliminary local calibration coefficients and goodness of fit statistics developed using 90 percent of projects. These results indicate a large improvement in the goodness of fit between the global models and the Arizona calibrated models as the R² is now 18 percent compared to 5 percent, and the SEE is 0.12 inch compared to 0.31 inch. This is still a fairly poor goodness of fit for the preliminary locally calibrated rutting models. Rutting data only shows excessive variability for many projects over time. This variability, which is caused by equipment changes or problems from year to year, contributes to poor goodness of fit and high standard error.

The preliminary locally calibrated rutting model was then independently validated using the 10 percent of projects set aside for validation. The 10 percent sample randomly selected

demonstrated much better fit to the measured rutting model, which indicates that it would be best to combine all of the data into a 100 percent database for a final calibration (Table 22).

Given this result, the databases were combined to obtain a final locally calibrated rutting model. For this final calibration, the model coefficients did not change much and goodness of fit was still poor, as shown in Table 23. The final locally calibrated rutting model was evaluated for bias. Figure 36 presents the results, which show that the overprediction bias has been removed.

Table 21. Preliminary Local Calibration Coefficients and Goodness of Fit Statistics for Total Rutting Submodels Using 90 Percent of Projects

Model or Submodel Type	Goodness of Fit	Model Coefficients	ADOT Local Calibration (Using 90% of Projects)
AC rutting	R ² = 18.1% SEE = 0.123 inch N = 616	k1	-3.491598051 (new HMA) -3.190568055 (HMA over HMA)
		k2	1.5606
		k3	0.235
Base rutting		k1 (base)	0.7905
Subgrade rutting		k1 (subgrade)	1.116

Table 22. Goodness of Fit Statistics for Validating the Preliminary 90 Percent Locally Calibrated Total Rutting Submodels with 10 Percent of Projects

Model or Submodel Type	Goodness of Fit Based on 90% of Selected Calibration Projects	Goodness of Fit Based on 10% of Selected Validation Projects
AC rutting	R ² = 18.1% SEE = 0.123 inch N = 616	R ² = 49.4% SEE = 0.107 inch N = 58
Base rutting		
Subgrade rutting		

Table 23. Goodness of Fit and Bias Test Statistics for Final Locally Calibrated Rutting Model (Based on 100 Percent of All Projects)

Model or Submodel Type	Goodness of Fit and Bias Statistics	Model Coefficients	ADOT Local Calibration (Using 100% of Projects)	Change from NCHRP 1-40D Global Models
AC rutting	<u>Goodness of Fit</u> $R^2 = 16.5\%$ SEE = 0.11 inch N = 497 <u>Bias Test</u> H_0 : Slope = 1.0 (p-value = 0.0521)	K1	-3.3541	No
		K2	1.5606	No
		K3	0.4791	No
		BR1	0.69	Yes
		BR2	1	No
		BR3	1	Yes
Base rutting	H_0 : Predicted and measured cracking from the same population (paired t test) (p-value = 0.0568)	K1 (base)	2.03	No
		BS1 (base)	0.14	Yes
Subgrade rutting		K1 (subgrade)	1.35	No
		BS1 (subgrade)	0.37	Yes

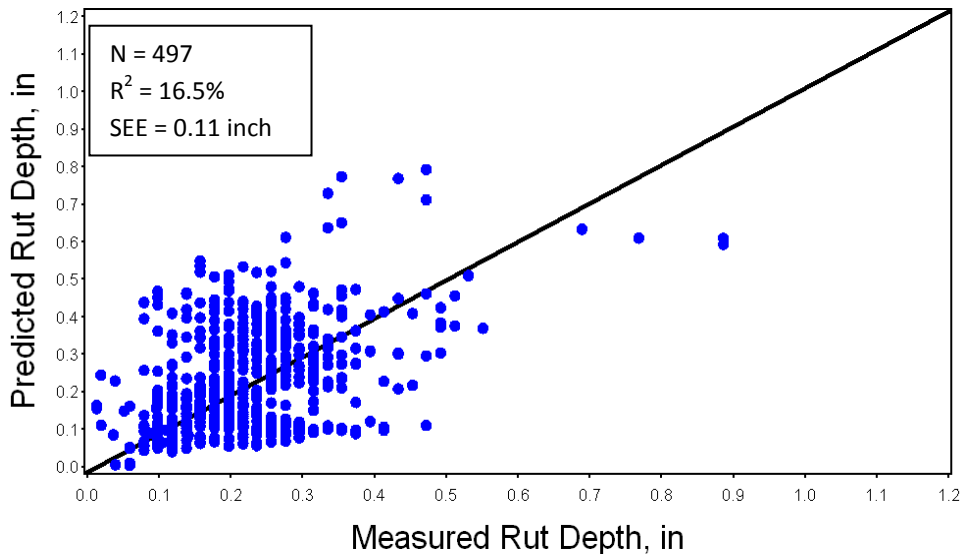


Figure 36. Measured and Predicted Total Rutting for New HMA and HMA Overlaid HMA Pavements for the Locally Calibrated Rutting Submodels (Using 100 Percent of Projects)

The poor goodness of fit was due to excessive variability in measured year-to-year rutting data used for the analysis, not because of a major weakness in the models. An example of excessive variability in rutting measurements over time for one section is shown in Figure 37.

Figure 38 illustrates the model prediction for a typical HMA pavement. The impact of local calibration of the HMA pavement rutting models is most significant after removing the large overprediction bias, as can be seen when comparing the global coefficients in Figure 35 and the local coefficients in Figure 36. The goodness of fit increased from 5 percent to 17 percent. The SEE reduced significantly, from 0.31 inch to 0.11 inch. HMA pavement designs based in part on HMA pavement rutting in Arizona will be much more accurate and optimum (lower cost) at the selected level of design reliability.

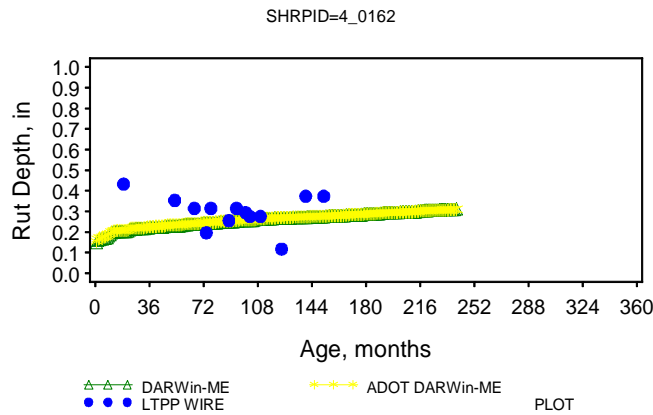


Figure 37. High Variation of Measured Rutting for LTPP Project 4_0162

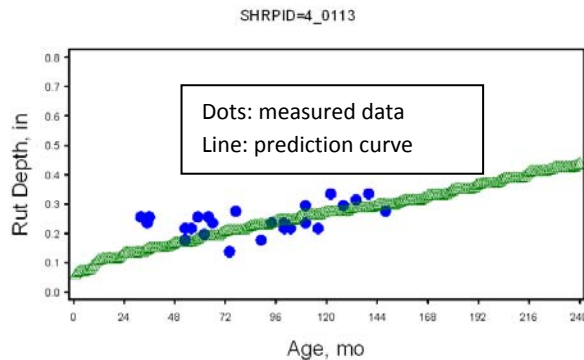


Figure 38. Measured and Predicted (Global and Arizona Local Calibrated Models) Total Rutting for Arizona LTPP Project 4_0113

TRANSVERSE LOW-TEMPERATURE CRACKING

The MEPDG’s HMA pavement transverse cracking models are based on low-temperature contraction of asphalt binders that leads to tensile stresses and transverse cracks. However, much of Arizona is not subjected to such low temperatures. Yet the researchers found transverse cracking at approximately 50- to 200-ft intervals on many LTPP and PMS sections in nonfrost areas such as the Phoenix and Tucson valleys. Figure 39 shows two LTPP examples—one in the nonfreeze Phoenix area and the other in the nonfreeze Tucson area—that have developed extensive transverse cracking over 10 to 15 years. These sections exhibit on the order of 2000 ft/mi in the time frame, which corresponds roughly to a spacing of 30 ft down the highway—a significant number of transverse cracks that as they open and deteriorate cause pavement roughness.

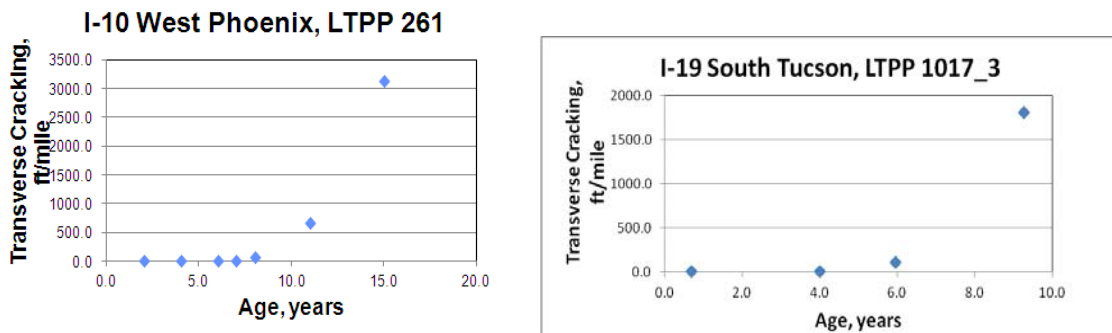


Figure 39. Transverse Cracking in Nonfreeze Areas of Phoenix and Tucson

Sections in cold freeze areas also exhibited transverse cracks with similar spacings. Thus, it became apparent that more than the traditional low-temperature transverse cracking mechanism was occurring in Arizona. Many of the cracks in warm areas were up to 1 inch wide, causing speculation that significant shrinkage of the HMA mixture, possibly from binder absorbing into the aggregate, was another mechanism. Of course, the MEPDG cannot handle this type of mechanism and would therefore underpredict transverse cracking in Arizona’s nonfreeze areas.

Verification

To verify the MEPDG global transverse cracking model for Arizona HMA conditions, researchers ran the MEPDG with the global coefficients for the SPS-1 experimental sections on U.S. 93 and evaluated goodness of fit and bias. The SPS-1 site is northwest of Kingman, Arizona, in a

moderate temperature zone with 57 air temperature freezing cycles per year and a freezing index of 249 degree-days. Figure 40 shows the minimum monthly temperature over the past 10 years at the Kingman airport, which is near the SPS-1 site. Measured transverse cracking on all of the SPS-1 HMA sections after 10 years is shown in Figure 41. The measured transverse cracking ranges widely from 0 to more than 5000 ft/mi (which is 13-ft spacing) after 10 years.

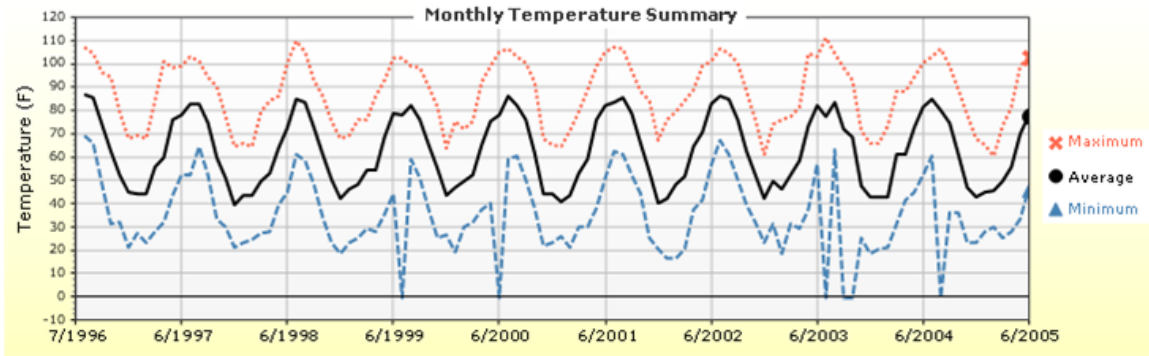


Figure 40. Monthly Temperatures Recorded at the SPS-1 Site Near Kingman, Arizona

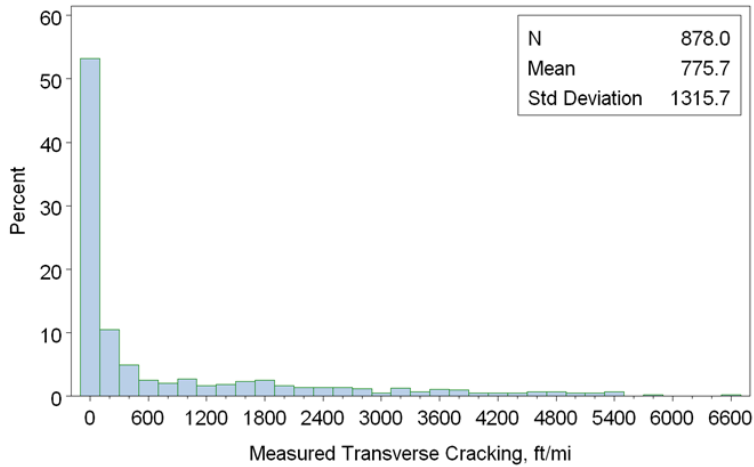


Figure 41. Measured Transverse Cracking at the SPS-1 Site After 10 Years of Service

The MEPDG was then run for all of the HMA sections at the SPS-1 site using the global calibration coefficients for Level 3 (e.g., $K = 1.5$). The results, shown in Figure 42, indicate that using the global calibration coefficients for Arizona led to an underprediction of transverse cracking for a range of HMA sections at this site. The model predictions may be biased (underprediction using the global calibration model with $K = 1.5$). Thus, local calibration of this important model was necessary.

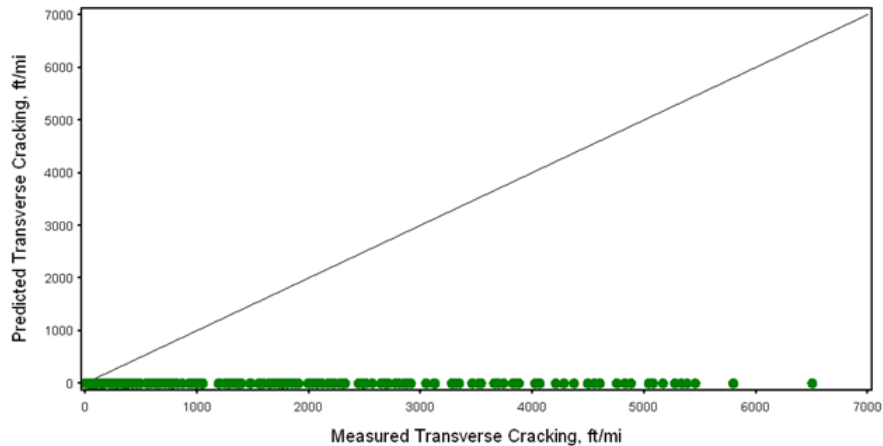


Figure 42. Predicted and Measured Transverse Cracking Using Global Coefficients in SPS-1 HMA Pavement Sections

Local Calibration

The calibration parameter for Level 3 is K . (See appendix.) This value was varied for the SPS-1 site until the predicted transverse cracking matched the measured on average. Obtaining a value of $K = 100$ provided some match at the upper end of cracking but overpredicted at the lower end, as shown in Table 24. Figure 43 illustrates predicted versus measured transverse cracking for all sections over time. These results suggest that while there is obviously little correlation between measured and predicted transverse cracking at the SPS-1 site, there is at least some MEPDG predicted values greater than for a Level 3 coefficient ($K = 100$). This level of K appears to be overpredicting at this site.

Table 24. Measured and Predicted HMA Transverse Cracking at the SPS-1 Site (Calibration K = 100)

LTPP Project ID	Survey Date	LTPP Transverse Cracking (ft/mi)	MEPDG Transverse Cracking (ft/mi [kt = 100])
0113	April 12, 2005	3257	1843
0114	Nov. 28, 2005	1705	1654
0118	Nov. 28, 2005	124	1295
0122	Dec. 1, 2005	255	1499
0124	Nov. 28, 2005	695	934

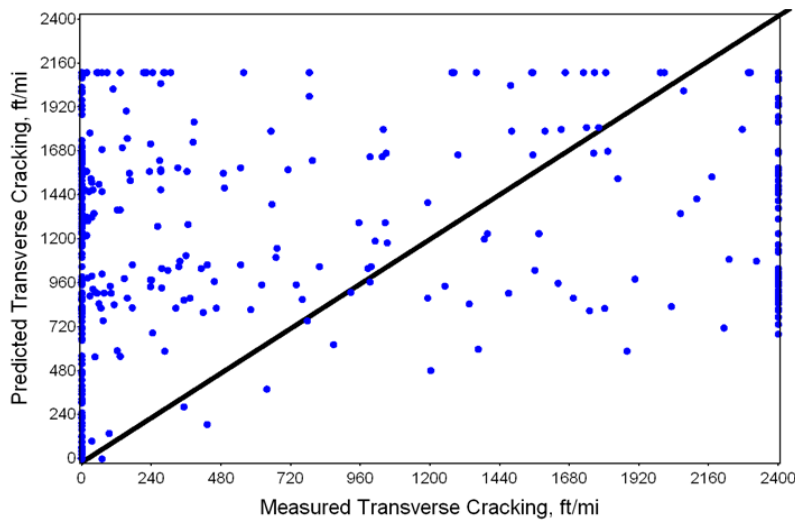


Figure 43. Predicted (Calibration K = 100) Versus Measured Transverse Cracking in SPS-1 HMA Pavement Sections

To determine the effect of a lower K (e.g., 50), the researchers ran the MEPDG for a variety of weather station locations, ranging from low elevation hot desert to very cold high elevation mountain sites, for a typical HMA pavement section (6-inch HMA with PG 64-22 and PG 76-16, 12-inch aggregate base, and A-2-4 coarse-grained subgrade). Key findings of this effort, summarized in Table 25, follow:

- Predicted low-temperature transverse cracking varies from 0 to more than 2000 ft/mi over 10 years for this wide range of climates. Transverse cracking varies directly with elevation (as shown in Figure 44).

- Warm nonfreeze climates of Phoenix and Scottsdale with 0 to 1 air freeze-thaw cycles per year predict no transverse cracking.
- Tucson’s slightly cooler climate, with nine air freeze-thaw cycles per year, predicts transverse crack spacing of about 737 ft/mi or 75-ft spacing. Many local streets in Tucson have transverse crack spacings in this range.
- Colder climates of Safford, Kingman, Nogales, and Bisbee, with 32 to 57 air freeze-thaw cycles per year, predict 1831 to 1966 ft/mi or 31- to 35-ft transverse crack spacing.
- Very cold climates of Winslow, St. Johns, and Window Rock, with 119 to 173 air freeze-thaw cycles per year, all predict transverse crack spacing of 2112 ft/mi or 30-ft crack spacing.

Table 25. MEPDG Prediction of HMA Transverse Cracking for Arizona Climates (Calibration K = 50)

Site Location	Elevation (ft)	Air Freeze-Thaw Cycles/Year	Freezing Index (inches)	Predicted Transverse Cracks (ft/mi, PG 76-16/ PG 64-22)	Predicted Transverse Crack Space (ft, PG 76-16/ PG 64-22)
Phoenix	1105	0	0	0/4	None/None
Scottsdale	1473	1	1	23/29	2754/2182
Tucson	2549	9	21	843/737	75/86
Safford	3170	32	166	1955/1882	32/34
Kingman	3420	57	249	2028/1831	31/35
Nogales	3908	35	174	1847/1872	34/34
Bisbee	4105	55	324	2055/1966	31/32
Winslow	4886	119	1144	2112/2112	30
St. Johns	5722	115	1181	2112/2112	30
Window Rock	6733	173	2157	2112/2112	30

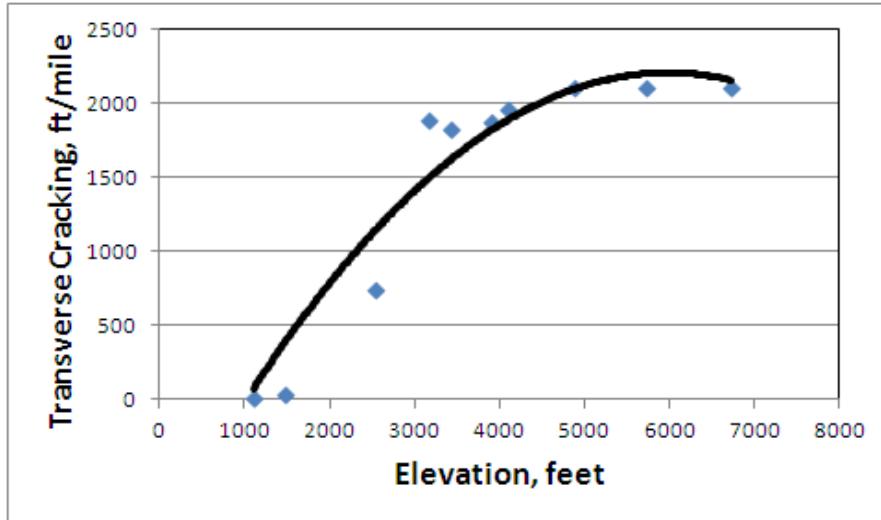


Figure 44. MEPDG Predicted Transverse Cracking at Various Arizona Locations (Calibration K = 50)

These results show that the MEPDG can predict reasonable results for low-temperature cracking, at least for areas with cold temperatures and elevations of 3000 ft and higher. In areas like the Phoenix valley and Tucson valley, where transverse cracking exists on some HMA pavements, another mechanism such as HMA shrinkage may well be causing transverse cracks to develop and widen over time.

At this time, it is not recommended to use the MEPDG predicted transverse cracking as a design performance criteria, similar to alligator cracking or rutting. A calibration coefficient of K ranging from 7.5 to 50 appears reasonable. Transverse cracking should be observed and perhaps the PG grade of the binder and other HMA mix properties modified to minimize the potential development of transverse cracking. Additional research is needed to provide much stronger verification of the HMA transverse cracking model in Arizona.

NEW HMA AND HMA OVERLAID HMA SMOOTHNESS (IRI)

Verification

To verify the MEPDG global IRI model for Arizona HMA conditions, the researchers ran the MEPDG with the global coefficients for all projects and evaluated goodness of fit and bias. Figure 45 plots the predicted versus measured IRI for all Arizona HMA sections. The goodness of fit statistics shown in Figure 45 is poor ($R^2 = 30\%$, $SEE = 18.7$ inch/mi), and the model predictions are obviously biased (large overprediction using the global calibration model for lower IRI and underprediction for higher IRI). Thus, local calibration of this very important model was necessary. Details of this analysis are provided in the appendix.

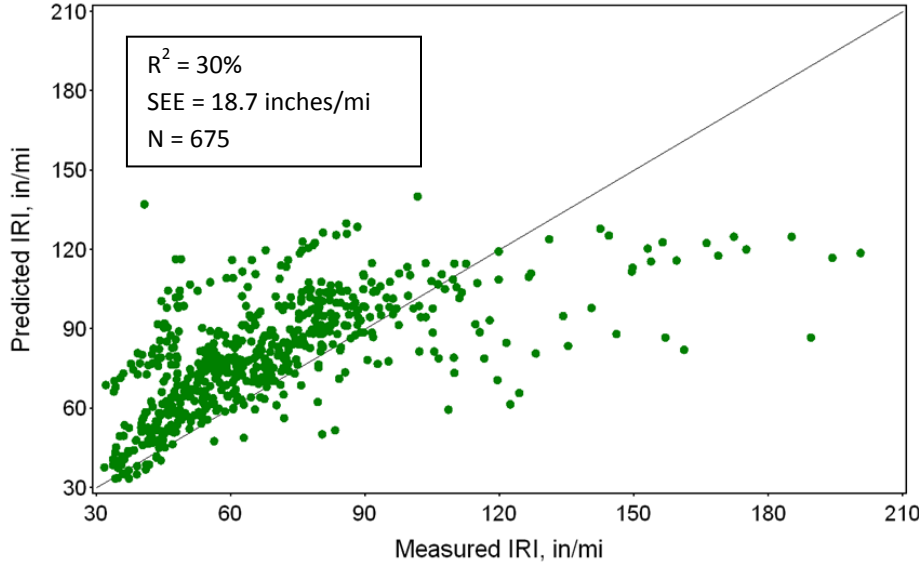


Figure 45. Predicted Versus Measured IRI Using Global Coefficients and Arizona HMA Pavement Performance Data

Local Calibration

To calibrate the model, researchers investigated the causes of poor goodness of fit and bias of the MEPDG nationally calibrated models and modified the local calibration coefficients of the IRI model as needed based on information derived from Eq. 1. Specifically, the coefficients of the distress inputs and site factor (SF) were modified as needed to improve the HMA IRI prediction.

Investigation of Causes of Poor Goodness of Fit and Bias

There were no obvious causes for poor goodness of fit and bias in the global model.

Local Calibration of HMA IRI Model

Model local coefficients were determined through optimization using SAS statistical software for the HMA IRI model:

$$IRI = IRI_o + C1(SF) + C2(FC_{Total}) + C3(TC) + C4(RD) \quad (\text{Eq. 5})$$

where all inputs are as already defined.

Table 26 provides the preliminary local calibration coefficients and goodness of fit statistics developed using 90 percent of projects. The results indicate a large improvement in the

goodness of fit between the global models and the Arizona calibrated models as the R^2 is now 81 percent compared to 30 percent, and the SEE is 8 inches/mi compared to 18.7 inches/mi. This is a very good goodness of fit for the preliminary locally calibrated HMA IRI model. IRI seems to be more consistently measured year after year as opposed to the high variability of rutting from year to year.

The preliminary locally calibrated IRI model was then validated using the 10 percent of projects set aside for validation. The results in Table 27 show a similar fit to the measured rutting model, validating the 90 percent model as reasonable.

Given this successful validation check, the databases were combined to obtain a final locally calibrated rutting model. For this final calibration, the model coefficients did not change much and goodness of fit was still very good, as shown in Table 28. The final locally calibrated HMA pavement IRI model was evaluated for bias. The results, presented in Figure 46, show that the overprediction bias has been removed.

Table 26. Preliminary Local Calibration Coefficients and Goodness of Fit Statistics for HMA IRI Model Using 90 Percent of Projects

Model or Submodel Type	Goodness of Fit	Model Coefficients	ADOT Local Calibration (Using 100% of Projects)
HMA IRI model	$R^2 = 81.4\%$ SEE = 8.1 inch/mi N = 487	C1	0.0202
		C2	0.0400
		C3	0.008
		C4	25.0

Table 27. Goodness of Fit Statistics for Validating the 90 Percent Preliminary Locally Calibrated HMA IRI Model with 10 Percent of Projects

Model or Submodel Type	Goodness of Fit Based on 90% of Selected Calibration Projects	Goodness of Fit Based on 10% of Selected Validation Projects
HMA IRI model	$R^2 = 81.4\%$ SEE = 8.1 inch/mi N = 487	$R^2 = 81.7\%$ SEE = 6.1 inch/mi N = 70

Table 28. Goodness of Fit and Bias Test Statistics for Final Locally Calibrated HMA IRI Model (Based on 100 Percent of All Projects)

Model or Submodel Type	Goodness of Fit and Bias Statistics	Model Coefficients	ADOT Local Calibration	Change from NCHRP 1-40D Global Models
HMA IRI model	<u>Goodness of Fit</u> $R^2 = 82.2\%$ SEE = 8.7 inch/mi N = 559	C1 (for rutting)	1.2281	Yes
		C2 (for fatigue)	0.1175	Yes
		C3 (for transverse cracking)	0.0080	No
	<u>Bias Test</u> H_0 : Slope = 1.0 (p-value = 0.7705) H_0 : Predicted and measured cracking from the same population (paired <i>t</i> test) (p-value = 0.1419)	C4 (for SF)	0.0280	Yes

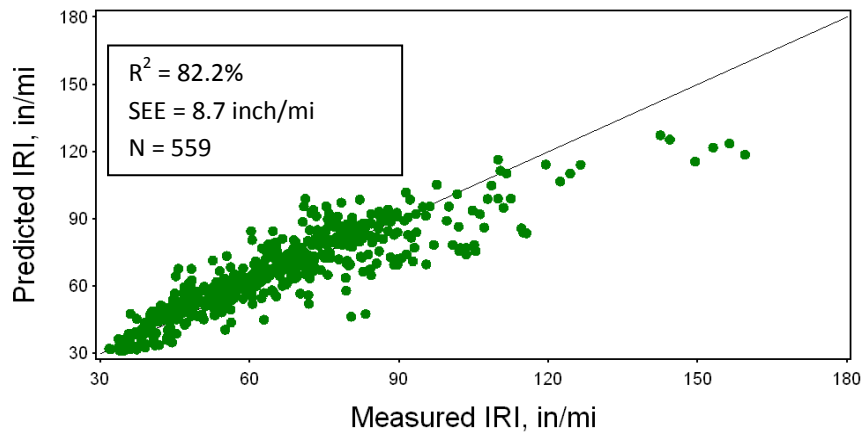


Figure 46. Measured and Predicted HMA IRI for New HMA and HMA Overlaid HMA Pavements for the Locally Calibrated IRI Model (Using 100 Percent of Projects)

Model IRI predictions for typical HMA pavements are shown in Figures 47 and 48. The impact of local calibration of the HMA pavement IRI model is most significant in removing the large overprediction bias, as can be seen when comparing the global coefficients in Figure 45 and the local coefficients in Figure 46. The goodness of fit increased from 30 percent to 82 percent. The SEE reduced significantly from 18.7 inches/mi to 9 inches/mi. HMA pavement designs based in part on HMA pavement IRI in Arizona will be much more accurate and optimum (lower cost) at the selected level of design reliability.

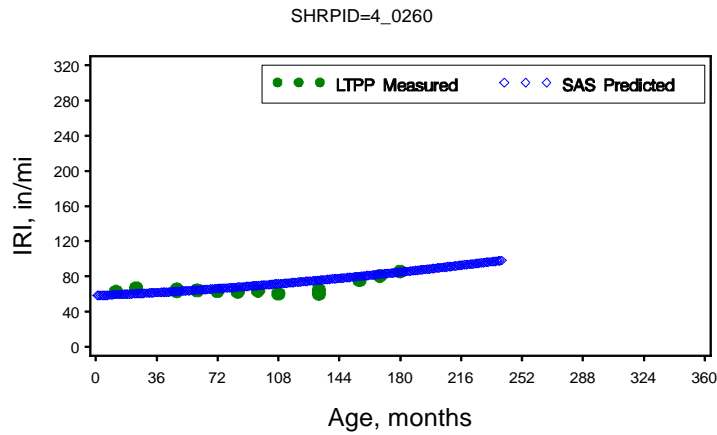


Figure 47. Measured and Predicted IRI for HMA LTPP Project 4_0260

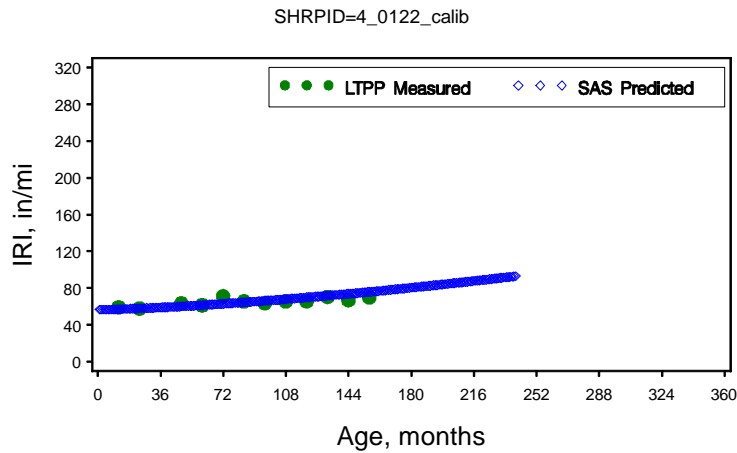


Figure 48. Measured and Predicted (Global and Arizona Local Calibrated Models) Total IRI for Arizona LTPP Project 4_0122

NEW AND RECONSTRUCTED JPCP TRANSVERSE CRACKING

Verification

To verify the MEPDG global JPCP transverse cracking for Arizona conditions, the researchers ran the MEPDG with the global coefficients for all projects and evaluated goodness of fit and bias. Note that for JPCP projects, the global model coefficients developed under the recently completed NCHRP project 20-07 to reflect corrections in concrete CTE values. The corrected CTE values were also used in the Arizona model calibration.

The analysis first used the Arizona database to establish the goodness of fit and bias in the MEPDG transverse cracking models. In Figure 49, the predicted versus measured slab cracking for the global calibration coefficients shows poor goodness of fit along with bias in underprediction of cracking.

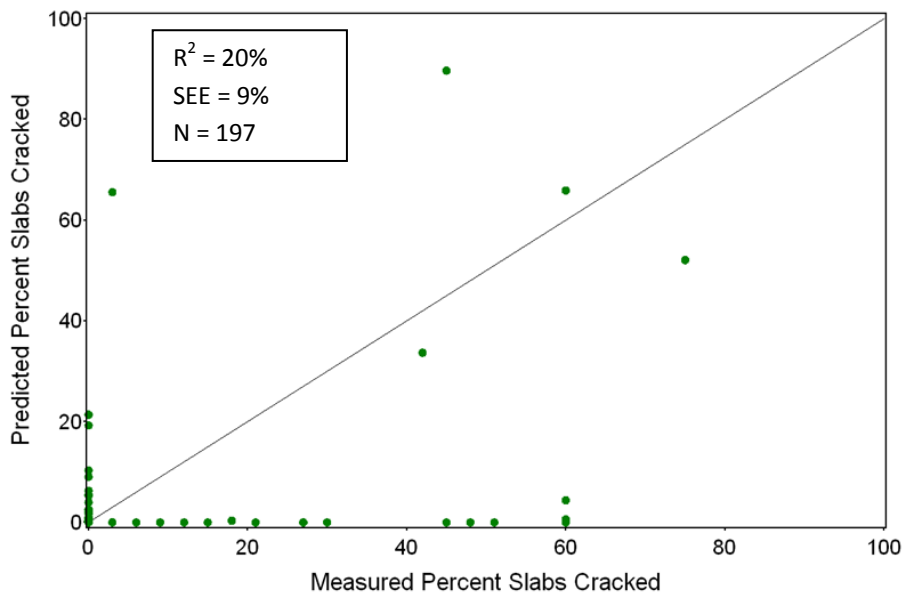


Figure 49. Predicted Versus Measured Percent Slabs Cracked for Arizona JPCP with Global Calibration Coefficients

Local Calibration

To calibrate the model, researchers investigated the causes of poor goodness of fit and bias of the MEPDG nationally calibrated models and modified the local calibration coefficients of the transverse fatigue cracking models as needed based on information derived from Eq. 1. Two key models are involved with the calibration of transverse slab cracking: Eq. 6 estimates the fatigue life (N) of PCC when subjected to repeated stress for a given flexural strength. Calibration factors C1 and C2 could be modified but since this is based on substantial field testing data, changing these coefficients is not recommended.

$$\log(N_{i,j,k,l,m,n}) = C_1 \cdot \left(\frac{MR_i}{\sigma_{i,j,k,l,m,n}} \right)^{C_2} \quad (\text{Eq. 6})$$

The most likely model with appropriate coefficients is the S-shaped curve giving the relationship between field measured cracking and accumulated fatigue damage at the top and bottom of the JPCP slabs. Parameters C4 and C5 are the prime candidates to adjust to remove bias and improve goodness of fit with field data.

$$CRK = \frac{1}{1 + C4(DI_F)^{C5}} \quad (\text{Eq. 7})$$

Investigation of Causes of Poor Goodness of Fit and Bias

JPCPs with asphalt-treated or aggregate bases were found to predict transverse cracking reasonably well (Figures 50 and 51, respectively). There is little cracking measured and the predictions show a similar amount. The main cause of poor goodness of fit and bias in the global model was poor prediction of JPCPs constructed over lean concrete bases for a specific section (Figure 52). The measured fatigue transverse cracking develops far earlier than the MEPDG predicted models using global coefficients.

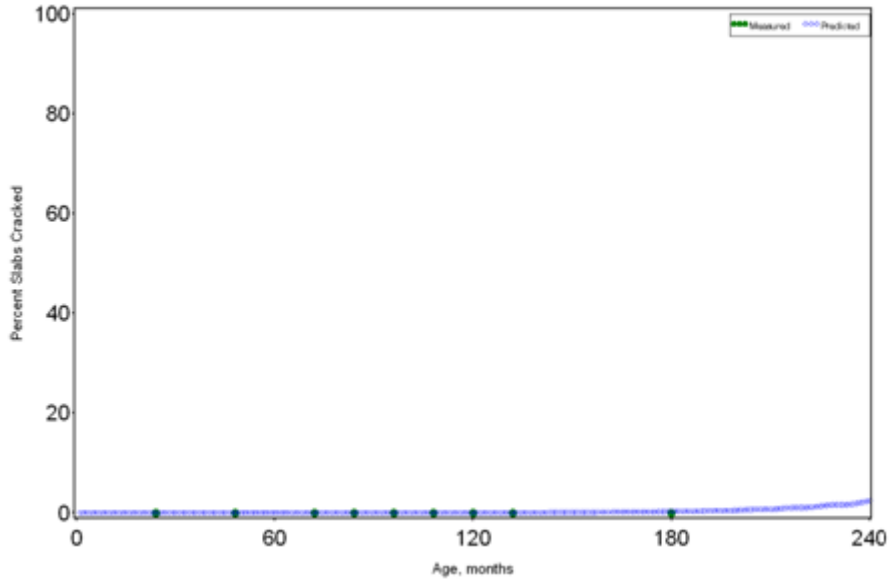


Figure 50. Arizona JPCP with HMA Base Course Measured and Predicted Percent Slabs Transversely Cracked

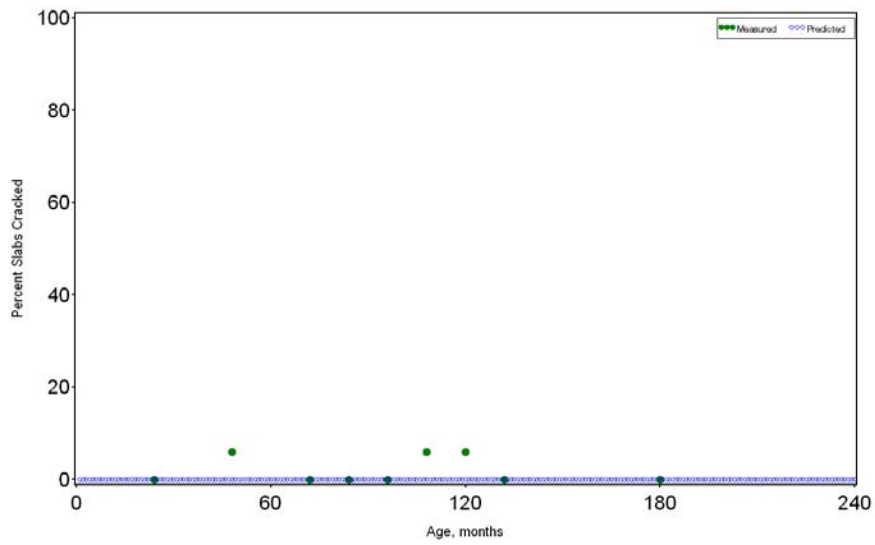


Figure 51. Arizona JPCP with Unbound Aggregate Base Course Measured and Predicted Percent Slabs Transversely Cracked

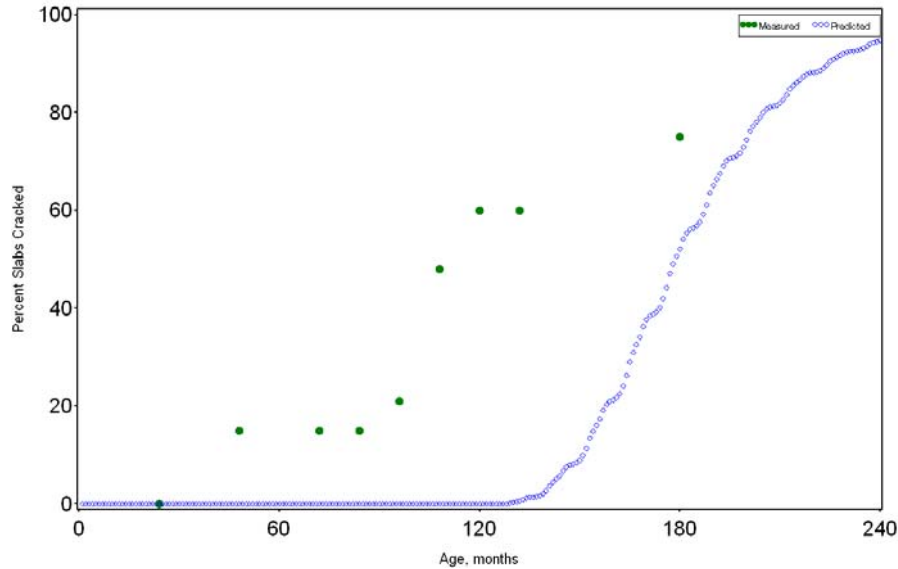


Figure 52. Measured and Predicted JPCP Transverse Cracking Using MEPDG Global Models for JPCP Over Lean Concrete Base

(The slab/base friction was released at 11 years according to DARWin-ME guidelines, but Arizona PCC/ lean concrete base construction indicates friction is lost almost immediately after opening to traffic, which moves the predicted curve back through the data points.)

A close examination of the JPCPs constructed over lean concrete bases transverse cracking prediction indicated that the global-derived typical loss of bonding between the PCC and underlying cement-treated base/lean concrete base age of 10.6 years was unsuitable for Arizona. The lean concrete base construction of these sections from SPS-2 required a smoothed surface sprayed with wax curing compound and then another spraying just before paving. Thus, the slab and lean concrete base lost bond and friction very quickly, and the rapid fatigue damage and transverse cracking process began. Based on the actual trends observed, a loss of bond age of 0 years was adopted assuming that the PCC and underlying cement-treated base/lean concrete base never really bonded.

Local Calibration of Transverse Cracking Model

The Arizona JPCP sections with lean concrete base or cement-treated bases were modified for loss of friction age of 0 and all sections rerun. The other base types were all set at full friction over their service life as before.

Model local coefficients were determined through optimization using SAS statistical software for the JPCP faulting model. The results showed a very significant improved model goodness of fit and no bias in the predictions for JPCP with any type of base course, as summarized in Table 29

and plotted in Figure 53. Figure 54 shows the computed cumulated PCC fatigue damage and measured fatigue transverse cracking (percent slabs). As fatigue damage increases measured cracking doesn't increase until it reaches a very critical point where fatigue cracking rapidly increases. These results are similar to the HMA fatigue cracking curve.

Table 29. Goodness of Fit and Bias Test Statistics for Globally Calibrated JPCP Transverse Cracking Model (Based on 100 Percent of All Projects)

Model Types	Goodness of Fit and Bias Statistics	Model Coefficients	NCHRP 20-07 Global Model (Using 100% of Projects)
PCC fatigue allowable N model	<u>Goodness of Fit</u> $R^2 = 72.8\%$ $SEE = 7.25\%$ $N = 198$	C1	2
		C2	1.22
		C4	0.19
JPCP transverse cracking model	<u>Bias Test</u> H_0 : Slope = 1.0 (p-value = 0.8840) H_0 : Predicted and measured cracking from the same population (paired t test) (p-value = 0.0504)	C5	-2.067

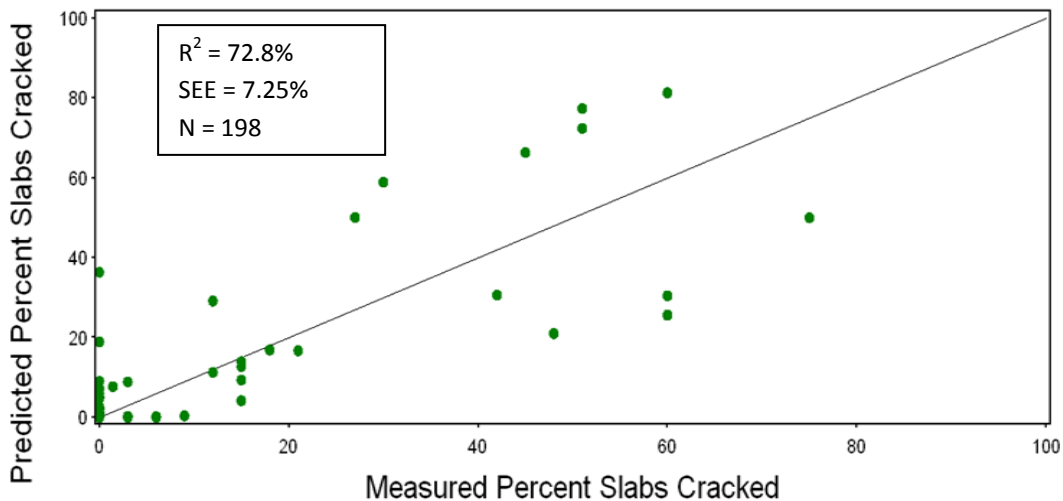


Figure 53. Predicted Versus Measured Percent Slabs Transverse Cracked for Arizona JPCP with All Types of Base Courses

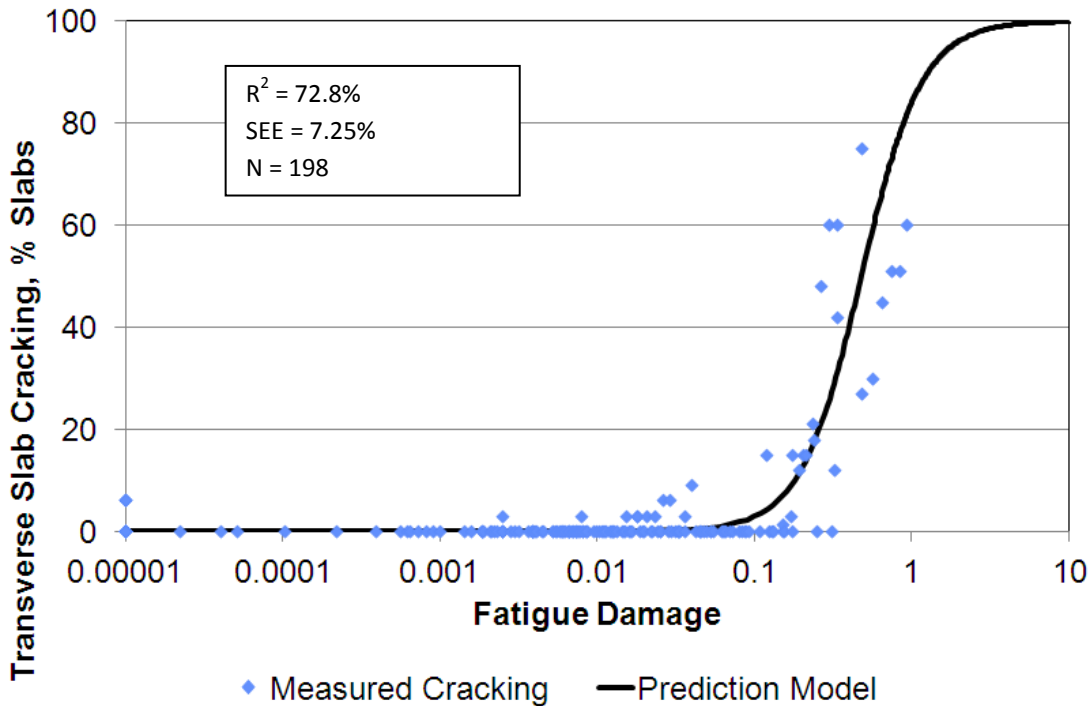


Figure 54. Measured and Predicted JPCP Transverse Cracking Versus Cumulative Fatigue Damage for Local Arizona Calibration Coefficients (Using 100 Percent of Projects)

Transverse fatigue cracking model predictions are shown in Figure 55 (lean concrete base), Figure 56 (untreated aggregate base), and Figure 57 (HMA base). All show good fit to the MEPDG calibrated models.

The impact of local calibration of the JPCP cracking model is most significant in removing the large bias that existed with the lean concrete base. The goodness of fit increased from 20 percent to 73 percent. The SEE reduced significantly from 9 percent to 7 percent. JPCP designs based in part on transverse cracking in Arizona will be much more accurate and optimum (lower cost) at the selected level of design reliability.

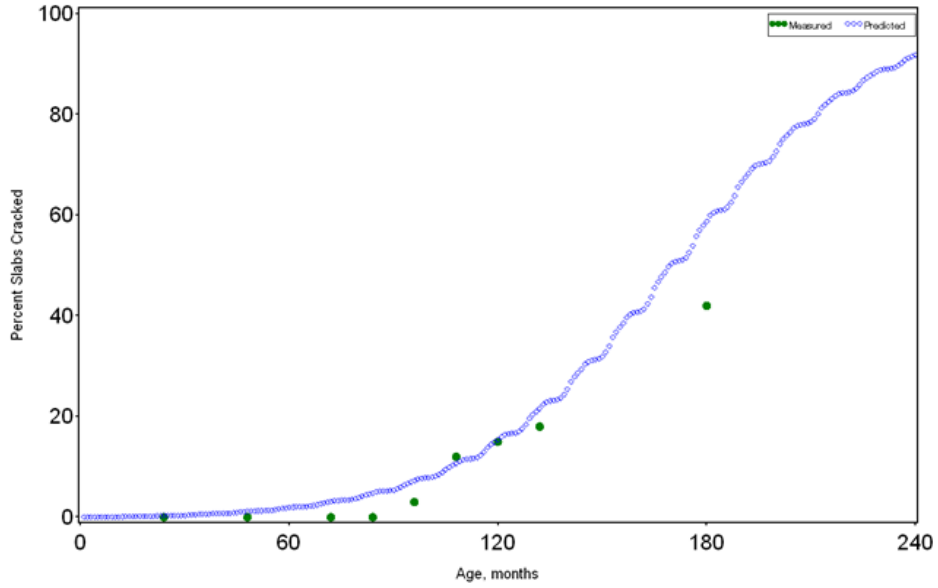


Figure 55. Predicted (Using Local Calibration Factors and Input Recommendations) and Measured Transverse Cracking for JPCP 4_0217 (SPS-2) with Lean Concrete Base (Slab/base friction was released at time 0 opening to traffic for this prediction curve.)

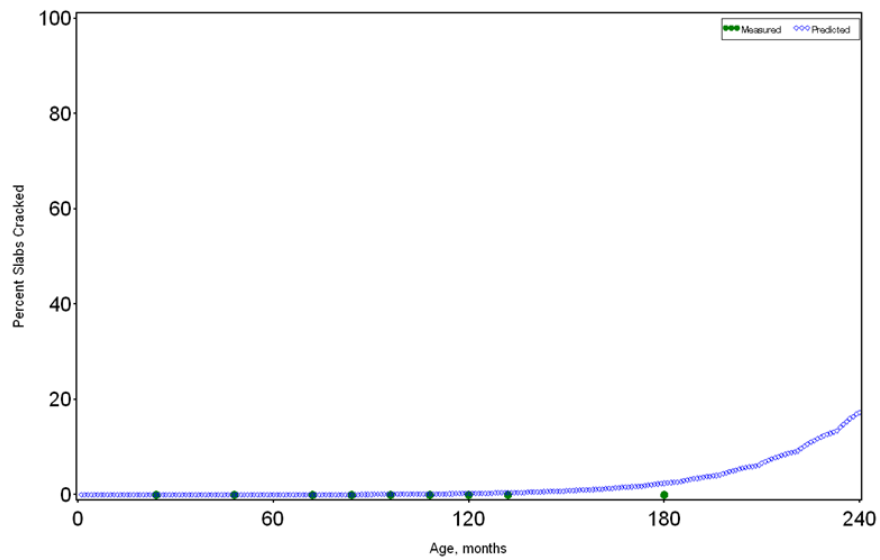


Figure 56. Predicted (Using Local Calibration Factors and Input Recommendations) and Measured Transverse Cracking for JPCP 4_0214 (SPS-2) with Untreated Aggregate Base (Slab/aggregate base friction is full over entire period.)

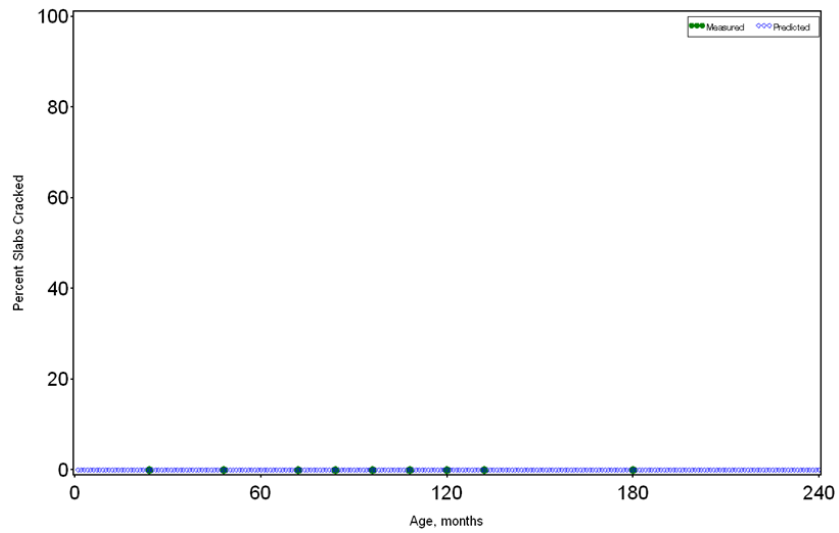


Figure 57. Predicted (Using Local Calibration Factors and Input Recommendations) and Measured Transverse Cracking for JPCP 4_0224 (SPS-2) with HMA Base
(Slab/HMA base friction is full over entire period.)

NEW JPCP TRANSVERSE JOINT FAULTING

Verification

To verify the MEPDG global JPCP transverse joint faulting for Arizona conditions, the researchers ran the MEPDG with the global transverse joint faulting model for all projects and then evaluated goodness of fit and bias. Results in Figure 58 show that goodness of fit was fair along with the SEE but that the model predictions were biased (overprediction).

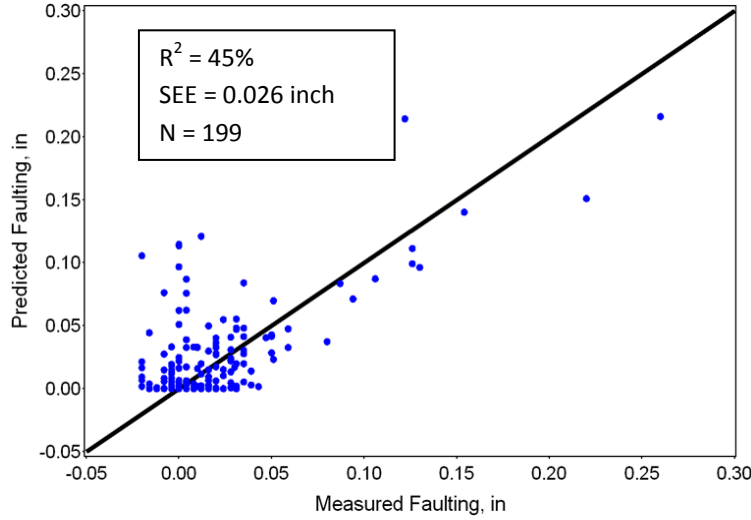


Figure 58. Predicted Versus Measured Joint Faulting for JPCP with Global Calibration Coefficients

Local Calibration

To calibrate the model, researchers investigated the causes of poor goodness of fit and bias of the MEPDG nationally calibrated models and modified the local calibration coefficients of the joint faulting models as needed based on information derived from Eq. 1.

Investigation of Causes of Poor Goodness of Fit and Bias

There were no obvious causes for poor goodness of fit and bias in the global faulting model.

Local Calibration of Transverse Joint Faulting Model

Model local coefficients were determined through optimization using SAS statistical software for the JPCP faulting model:

$$Fault_m = \sum_{i=1}^m \Delta Fault_i \quad (\text{Eq. 8})$$

$$\Delta Fault_i = C_{34} * (FAULTMAX_{i-1} - Fault_{i-1})^2 * DE_i \quad (\text{Eq. 9})$$

$$FAULTMAX_i = FAULTMAX_0 + C_7 * \sum_{j=1}^m DE_j * \text{Log}(1 + C_5 * 5.0^{EROD})^{C_6} \quad (\text{Eq. 10})$$

$$FAULTMAX_0 = C_{12} * \delta_{\text{curling}} * \left[\text{Log}(1 + C_5 * 5.0^{EROD}) * \text{Log}\left(\frac{P_{200} * \text{WetDays}}{P_s}\right) \right]^{C_6} \quad (\text{Eq. 11})$$

where all inputs are as defined in the appendix.

Table 30 provides the preliminary local calibration coefficients and goodness of fit statistics developed using 90 percent of projects. The results indicate a reasonably good goodness of fit; most calibration coefficients were changed. SEE was 0.0284 inches and considered adequate.

The preliminary locally calibrated JPCP faulting model was then independently validated using the 10 percent of projects set aside for validation. Results in Table 31 show a very good correlation coefficient between the measured and predicted JPCP faulting, and SEE was also lower.

With the successful validation of the preliminary Arizona calibrated JPCP faulting model, the researchers developed a final locally calibrated total rutting prediction model using the entire database of projects. Results in Table 32 show that the model's coefficients did not change, and goodness of fit remained essentially the same. The final Arizona calibrated JPCP faulting model was evaluated for bias and the results indicated it has no significant bias.

Figure 59 shows the direct comparison of predicted and measured joint faulting for 100 percent of the data.

Table 30. Preliminary Local Calibration Coefficients and Goodness of Fit Statistics for Transverse Joint Faulting Model Using 90 Percent of Projects

Model and Submodel Types	Goodness of Fit	Model Coefficients	ADOT Local Calibration (Using 90% of Projects)
All faulting submodels	<u>Goodness of Fit</u> $R^2 = 53.8\%$ SEE = 0.0284 inch N = 177	C1	0.0355
		C2	0.1147
		C3	0.00436
		C4	1.1E-07
		C5	20000
		C6	2.0389
		C7	0.1890
		C8	400

Table 31. Goodness of Fit Statistics for Validating the 90 Percent Preliminary Locally Calibrated Transverse Joint Faulting Model with 10 Percent of the Data

Model and Submodel Types	Goodness of Fit Based on 90% of Selected Calibration Projects	Goodness of Fit Based on 10% of Selected Validation Projects
All faulting submodels	$R^2 = 53.8\%$ SEE = 0.0284 inch N = 177	$R^2 = 73.4\%$ SEE = 0.002 inch N = 19

Table 32. Goodness of Fit and Bias Test Statistics for Final Locally Calibrated Transverse Joint Faulting Model (Based on 100 Percent of All Projects)

Model and Submodel Types	Goodness of Fit and Bias Statistics	Model Coefficients	ADOT Local Calibration (Using 100% of Projects)
All faulting submodels	<u>Goodness of Fit</u> $R^2 = 51.6\%$ SEE = 0.0225 inch N = 197 <u>Bias Test</u> H ₀ : Slope = 1.0 (p-value = 0.0632) H ₀ : Predicted and measured cracking from the same population (paired <i>t</i> test, difference = 0, p-value = 0.0221; paired <i>t</i> test, difference = 0.001, p-value = 0.1045)	C1	0.0355
		C2	0.1147
		C3	0.00436
		C4	1.1E-07
		C5	20000
		C6	2.0389
		C7	0.1890
		C8	400

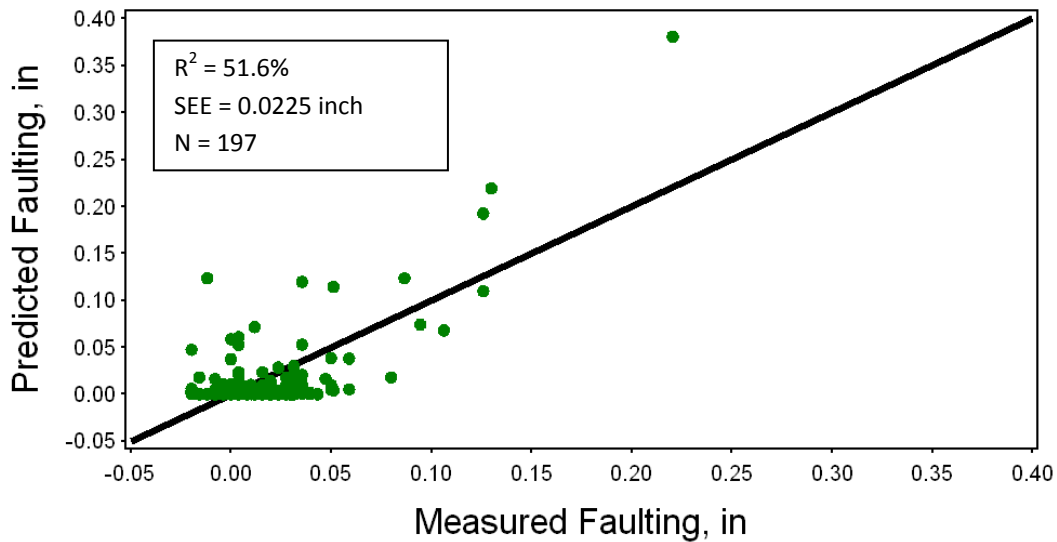


Figure 59. Measured and Predicted Transverse Joint Faulting for Locally Calibrated Faulting Submodels (Using 100 Percent of Projects)

Figure 60 shows the transverse joint faulting model prediction for a JPCP located on Interstate 10 (I-10) west of Phoenix under very heavy traffic. The prediction shows good fit to the MEPDG Arizona calibrated model for transverse joint faulting.

The greatest impact of the Arizona calibration of the JPCP joint faulting model is in removing the overprediction bias that existed. The goodness of fit increased from 45 to 52 percent, and the SEE remained about the same. JPCP designs based in part on transverse joint faulting in Arizona will be more accurate and optimum (lower cost) at the selected level of design reliability.

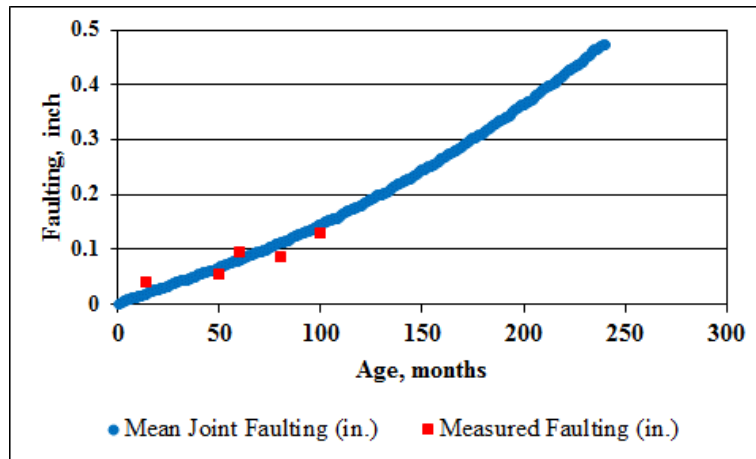


Figure 60. Measured and Predicted Joint Faulting Using the Arizona Calibrated Model for JPCP Section 4_0265 on I-10

NEW JPCP SMOOTHNESS (IRI)

Verification

To verify the MEPDG global JPCP IRI for Arizona conditions, researchers ran the MEPDG with the global JPCP IRI for all projects and then evaluated goodness of fit and bias. Figure 61 plots predicted versus measured IRI using the Arizona database; full details of the verification effort are presented in the appendix. These results indicate that goodness of fit was poor and the model predictions were biased (overprediction for higher IRI). Thus, local calibration with Arizona data was required.

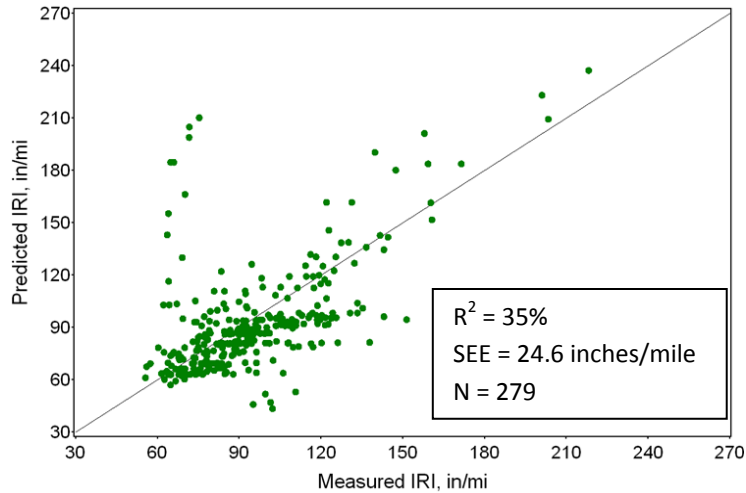


Figure 61. Predicted JPCP IRI Versus Measured Arizona JPCP with Global Calibration Coefficients

Local Calibration

To calibrate the model, researchers investigated the causes of poor goodness of fit and bias of the MEPDG nationally calibrated models and modified the local calibration coefficients of the JPCP IRI submodels as needed based on information derived from Eq. 1. Specifically, the distress inputs and SF coefficients were modified as needed to improve predicted JPCP IRI.

Investigation of Causes of Poor Goodness of Fit and Bias

There were no obvious causes for poor goodness of fit and bias in the global model.

Local Calibration of JPCP IRI Model

Arizona-specific model coefficients were determined through optimization using SAS statistical software for the JPCP IRI model:

$$IRI = IRI_i + J1*CRK + J2*SPALL + J3*TFAULT + J4*SF \quad (\text{Eq. 12})$$

where all inputs are as already defined.

The results presented in Table 33 indicate a reasonably good goodness of fit for the preliminary locally calibrated JPCP IRI model developed using 90 percent of the projects. Note that all of the global models coefficients were changed. The SEE of 19 inches/mi was lower than the 25 inches/mi of the global model.

This model was then independently validated using the 10 percent of projects set aside for validation. The results, presented in Table 34, show a very good correlation coefficient between the measured and predicted JPCP IRI data and much lower SEE, which indicates that the model is predicting the 10 percent independent Arizona data very well.

Table 33. Preliminary Local Calibration Coefficients and Goodness of Fit Statistics for JPCP IRI Model Using 90 Percent of Selected Calibration Projects

Model and Submodel Types	Goodness of Fit	Model Coefficients	ADOT Local Calibration (Using 100% of Projects)
JPCP IRI model	R ² = 57.6% SEE = 19.1 inches/mi N = 282	J1 (CRK)	0.60
		J2 (SPALL)	3.48
		J3 (FLT)	1.22
		J4 (SF)	45.20

Table 34. Goodness of Fit Statistics for Validating the 90 Percent Preliminary Locally Calibrated JPCP IRI Model with the 10 Percent Model

Model and Submodel Types	Goodness of Fit Based on 90% of Selected Calibration Projects	Goodness of Fit Based on 10% of Selected Validation Projects
JPCP IRI model	R ² = 57.6% SEE = 19.1 inches/mi N = 282	R ² = 70.6% SEE = 9.6 inches/mi N = 28

With the successful validation, the researchers developed a final Arizona-calibrated JPCP IRI prediction model using the entire database of projects. For this final calibration, the models coefficients did not change and goodness of fit remained essentially the same. The final Arizona-calibrated JPCP IRI model was evaluated for bias. The results, presented in Table 35, also show no significant bias.

Predicted versus measured JPCP IRI is shown in Figure 62 for 100 percent of the database.

Table 35. Goodness of Fit and Bias Test Statistics for Final Arizona Calibrated JPCP IRI Model (Based on 100 Percent of All Projects)

Model and Submodel Types	Goodness of Fit and Bias Statistics	Model Coefficients	ADOT Local Calibration (Using 100% of Projects)
JPCP IRI model	<u>Goodness of Fit</u> $R^2 = 80.9\%$ SEE = 9.85 inches/mi N = 279 <u>Bias Test</u> H_0 : Slope = 1.0 (p-value = 0.6458) H_0 : Predicted and measured cracking from the same population (paired t test) (p-value = 0.2760)	J1 (CRK)	0.60
		J2 (SPALL)	3.48
		J3 (FLT)	1.22
		J4 (SF)	45.20

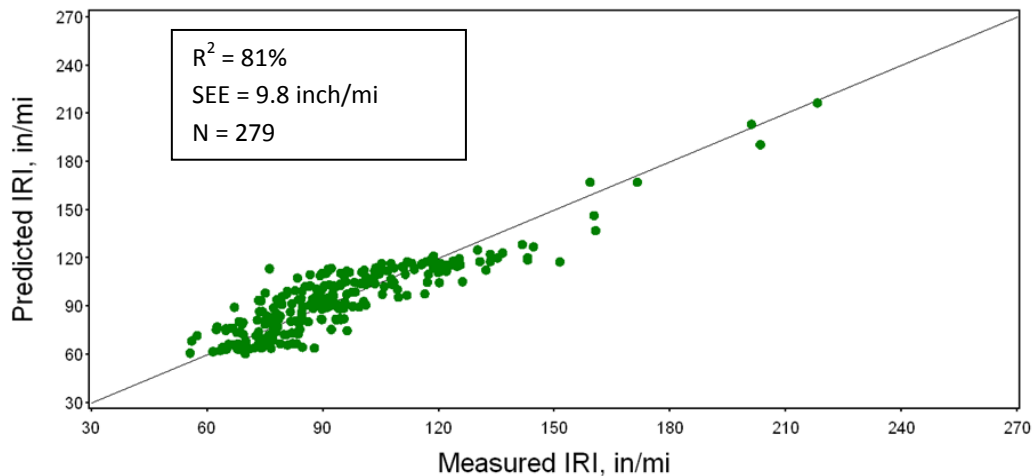


Figure 62. Measured and Predicted JPCP IRI (Using 100 Percent of Projects)

Figures 63 and 64 illustrate the JPCP IRI model predictions for various Arizona JPCP sections over time, showing a good fit to the MEPDG Arizona-calibrated model for IRI of JPCP pavements.

The Arizona calibration affected the JPCP IRI model by removing the bias and improving the goodness of fit statistics. Goodness of fit increased from 35 to 81 percent, and the SEE decreased from 25 inches/mi to 10 inches/mi for the global model. JPCP designs based in part on IRI in Arizona will be more accurate and optimum (lower cost) at the selected level of design reliability.

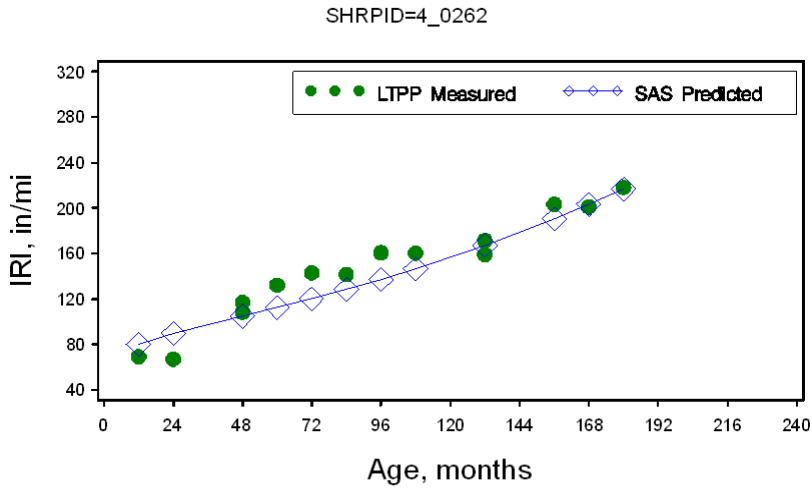


Figure 63. Predicted and Measured JPCP IRI for Arizona Section 04_0262

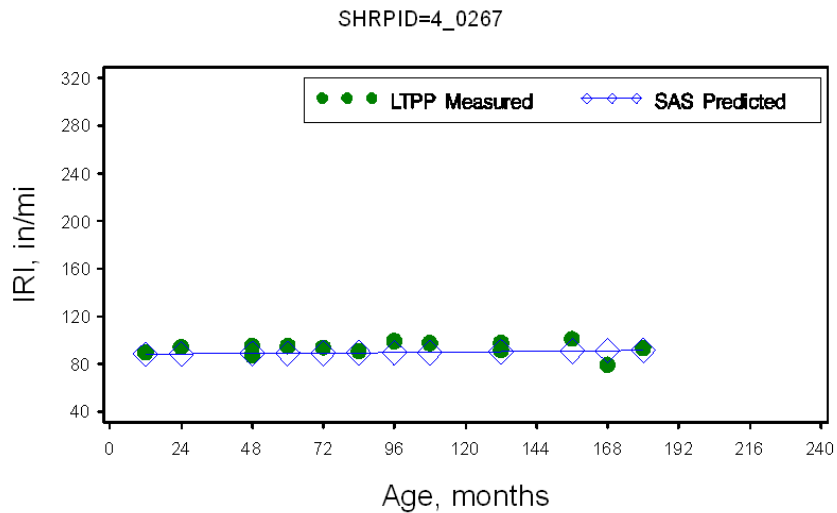


Figure 64. Predicted and Measured JPCP IRI for Arizona Section 04_0267

ARFC/JPCP COMPOSITE PAVEMENT MODELS

The MEPDG uses new HMA and new JPCP models for composite pavement design. This section addresses verification and validation of the various HMA and JPCP models applied to thin ARFC over JPCP.

Definition of Composite Pavement

Arizona has constructed many new composite pavement sections with a thin ARFC on a JPCP. The ARFC is currently 1 inch thick (unlike some older courses that are 0.75 inch thick), ground tire rubber modified asphalt binder, and gap graded with about 20 percent air voids. Many of these ARFC have been placed within a few months after the concrete slab construction, but some were placed after a few years of construction. The ARFC is placed primarily to reduce pavement and tire noise levels, but it also provides reduced splash and spray during rainstorms, high friction, and a very smooth surface. The ARFC can also be removed and replaced rapidly when needed.

The JPCP typically ranges from 11 to 14 inches thick and was designed without consideration of the ARFC surface. JPCP is doweled with perpendicular joints on the heavier trafficked I-10 and Interstate 40 (I-40) routes and nondoweled on the lower truck trafficked urban Loop 101 and 202 freeways in the Phoenix area, and random skewed joints (at 13-, 15-, and 17-ft intervals). The base course has been both unbound granular material and HMA mixture.

The oldest composite section included in the Arizona MEPDG calibration database was constructed on I-10 west of Phoenix in 1994. The section is still in service with the original ARFC intact and zero transverse fatigue cracks performing very well. This good performance exists on several other sections along I-10 from the California state line to Tucson. The youngest was built on Loop 202 in 2007 and is also performing very well. The entire Loop 101 and Loop 202 in the Phoenix metropolitan area were also constructed as bare JPCP, and ARFC surfaces were placed one to seven years later.

Design of Composite Pavements Using MEPDG

The MEPDG software does not directly consider a composite pavement for new design. It must be designed as an HMA overlay over an existing JPCP or CRCP. The time between placement of the JPCP or CRCP can be as short as one month or as late as several years. A future version of MEPDG will likely be modified to directly consider composite pavement as an original new design alternative. For now, the user must select HMA overlay of JPCP or CRCP to design a new composite pavement and specify the dates for construction of the concrete slab and HMA overlay as close as one month apart.

Validation of Distress/IRI Models for Composite Pavements

The key distress models for ARFC over JPCP that are output by DARWin ME include:

- ARFC rutting.
- Transverse fatigue cracking of the JPCP slabs, similar to bare JPCP.
- Smoothness through IRI.
- Reflection cracking of the transverse joints.

Some of these distresses and IRI are measured in the LTPP program and in the ADOT PMS, including rutting and IRI. Transverse slab fatigue cracking and transverse joint reflection cracking were measured in the field for all of the composite pavement sections.

Because the composite pavements built in Arizona have relatively thin asphaltic surface layers, the researchers expected that the thin (0.75 to 1 inch) ARFC layer would not affect performance dramatically, at least the fatigue life of the JPCP. However, the ARFC does alter the temperature and moisture gradients in the slab, making them less significant on fatigue life and transverse cracking. Thus, the verification effort focused on validating the development of transverse fatigue cracks that reflect through the ARFC surface, and verifying the rutting in ARFC, IRI, and reflection joint cracks.

Rutting of the ARFC

The thin ARFC layer did not show much rutting in the field, even under very heavy truck traffic and hot temperatures over a concrete slab. The DARWin ME inputs for this layer include the following for Levels 2 and 3:

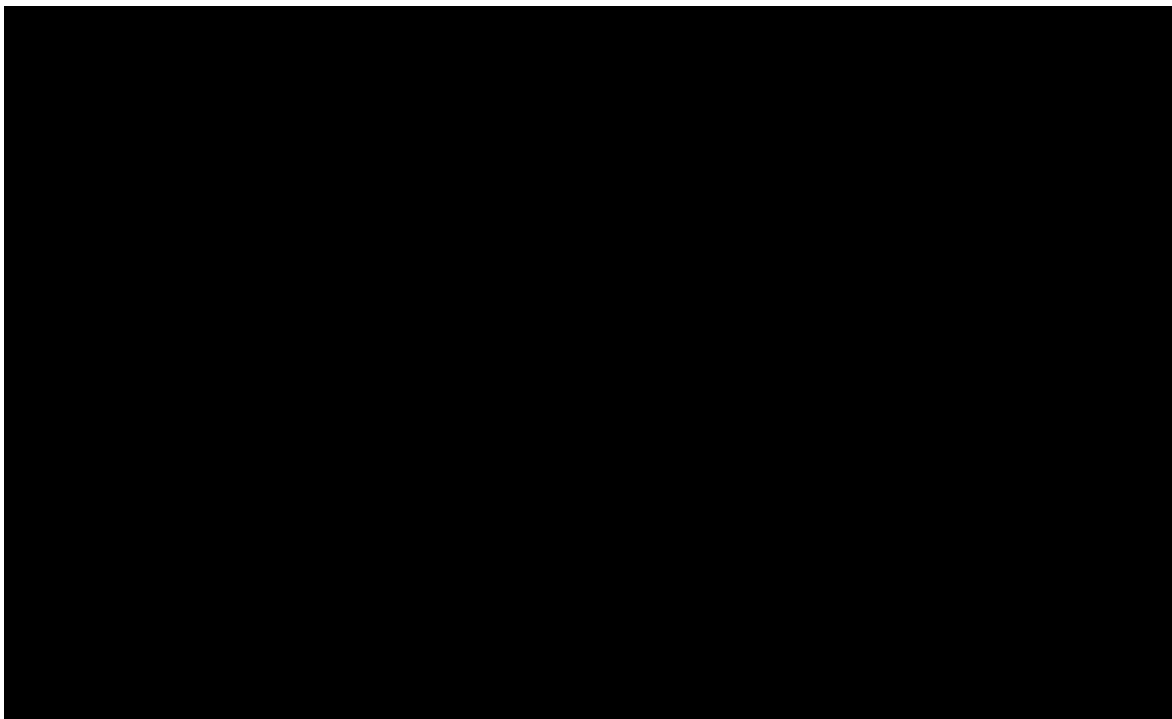
- **Thickness of the layer.** The layers ranged from 0.5 to 1 inch. The MEPDG minimum layer thickness is 1 inch and thus this was used for all cases.
- **Gradation of the aggregate.** A gap gradation was used that approximately corresponded to the following: -3/4-inch = 100 percent; -3/8 = 99 percent; -#4 = 37.7 percent; -#200 = 1.4 percent.
- **Unit weight.** 135 pcf.
- **Binder grade.** The actual binder grade used was PG 64-16 as is stated in most design reports. The rubber asphalt binder is crumb rubber from tires introduced into the asphalt binder in order to enhance its material properties. The researchers used the recommendation from both early testing and empirical observation to select the proper asphalt rubber binder grade to enter into the DARWin ME—a PG grading that best

matched the binder viscosity-temperature relationship coefficients (A_i and VTS_i) for asphalt rubber binders. PG 70-40, which best matched the PG 64-16 asphalt rubber binder, was used for all sections based on initial recommendations.

- **Air voids.** Actual voids reportedly are about 20 percent; however, the MEPDG cannot practically use this high void content. A value of 12 percent was used for all ARFC over the concrete slab, which provided reasonable predictions of actual rutting.
- **Binder content (volumetric basis).** 11 percent.
- **Poisson's ratio.** This input was calculated based on mixture properties and temperature.

Seventeen ARFC/JPCP or CRCP composite sections were used in the rutting validation. Measured rutting was obtained from the ADOT PMS database (SODA) for all of the projects. Table 36 shows the information used to compare measured rutting with DARWin ME predicted rutting. The researchers conducted the validation analysis by first observing the relationship between the numbers of heavy trucks and measured rutting of the ARFC, which is plotted in Figure 65. The graph shows that rutting increases rapidly within the first year but levels out with very little change over many millions of trucks and years. The magnitude of rutting is also very low. Rutting is not a significant problem with the 0.75-inch thick ARFC in Arizona.

Table 36. Arizona Composite Pavement Rutting and IRI Calibration Data



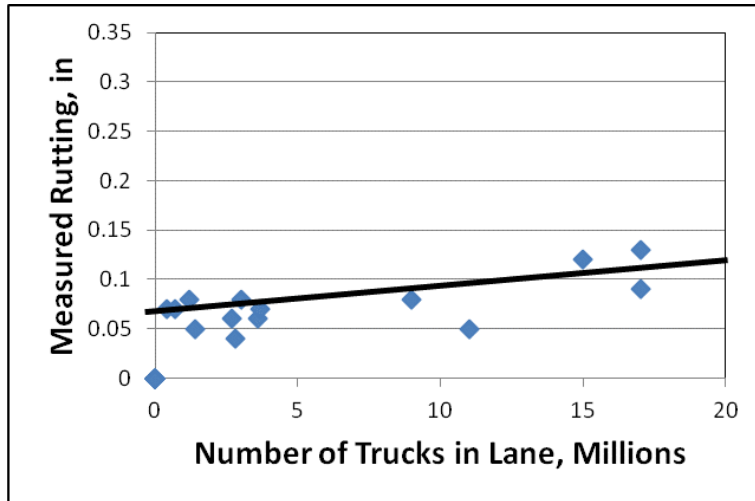


Figure 65. Measured Rutting of ARFC (0.75-inch) for Arizona Composite Pavements

Figure 66 shows the correlation between measured and predicted rutting, both of which were very low, making prediction nearly impossible. The variation of rutting along a project was high and varied widely from year to year. The MEPDG appears to underpredict rutting by less than 0.10 inch and reasonably predict rutting greater than 0.10 inch.

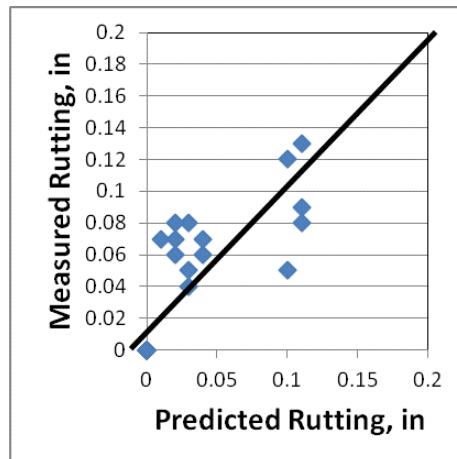


Figure 66. Measured Versus Predicted Rutting for ARFC Surfacing Over JPCP

Based on these results, the rutting prediction for ARFC over a concrete slab appears to be reasonable when using the MEPDG models if the proper inputs are used, including an appropriate binder grade (PG 70-40) and air voids (12 percent appears to work reasonably well).

Transverse Fatigue Cracking of Existing PCC Slab

The key question is when the ARFC/JPCP is modeled in the MEPDG, and fatigue damage and cracking are calculated, do they fall in line with the Arizona-calibrated JPCP curves? The fatigue damage in the JPCP slab resulting from the millions of heavy truck loadings is computed in the MEPDG software over the entire analysis period for each section. This fatigue damage is at the top and bottom of the slab, depending on design and load conditions. If this becomes too high, a fatigue transverse crack forms between the two transverse joints that define a slab, and a full width transverse crack develops, leading to spalling, faulting, and, ultimately, slab replacement.

Table 37 summarizes the data used in the transverse fatigue cracking analysis of Arizona composite pavements. Although these ARFC/JPCP composite pavements were loaded with up to 30 million trucks in the heaviest trafficked lane, fatigue damage to the top and bottom of the slab was not sufficient to predict any fatigue cracking due to the slab design and the ARFC surfacing. Field surveys performed on all of these sections also indicated that no midpanel transverse fatigue cracking existed.

Table 37. Fatigue Damage and Cracking Analysis for ARFC/JPCP Composite Pavements

Section ID	Date PCC/ARFC	Route	Start_MP	End_MP	Pavement Type	Trucks on PCC Millions	Bottom Up Damage	Top Down Damage	Measured Slab Cracking	Predicted Slab Cracking
01-86	2002/2003	10	254.43	256.1	0.75-in ARFC, 14.5 in doweled JPCP, 4-in ATB	0	0.0000	0.0000	0	0
						18	0.0000	0.0060	0	0
02-79	1997/2004	10	157.7	159.2	0.75-in ARFC, 13-in doweled JPCP, 3-in ATB	0	0.0000	0.0000	0	0
						30	0.0000	0.0050	0	0
92-39	1994/1994	10	62	63.48	0.5-in ARFC, 14-in doweled JPCP, 4-in ATB	0	0.0000	0.0000	0	0
						20	0.0000	0.0640	0	0
02-24	2004/2004	10	1.8	11.7	0.75 in ARFC, 13-in dowled JPCP, AB	0	0.0000	0.0000	0	0
						11	0.0000	0.0146	0	0
04-68	2007/2007	40	253.2	254.17	1-in ARFC, 14-in doweled JPCP, 4-in AB	0	0.0000	0.0000	0	0
						5	0.0000	0.0154	0	0
96-36	1999/2003	101	41	42.5	1-in ARFC, 11.5-in non-dow JPCP, 4-AB	0	0.0000	0.0000	0	0
						6	0.0002	0.0354	0	0.13
98-159	2001/2003	101	28	34.5	1-in ARFC, 11.5-in non-dow JPCP, 4-AB	0	0.0000	0.0000	0	0
						4.6	0.0000	0.0057	0	0
99-13	2001/2003	101	24.5	28.25	1-in ARFC, 11.5-in non-dow JPCP, 4-AB	0	0.0000	0.0000	0	0
						3.8	0.0000	0.0045	0	0
97-68	1999/2003	101	22.69	24.36	1-in ARFC, 11-in non-dow JPCP, 4-AB	0	0.0000	0.0000	0	0
						4.5	0.0000	0.0064	0	0
02-63	2005/2005	202	44.6	47.7	1-in ARFC, 13-in non-dow JPCP, 4-in AB	0	0.0000	0.0000	0	0
						1.8	0.0000	0.0018	0	0
03-06	2005/2005	202	31	33.15	1-in ARFC, 13-in non-dow JPCP, 4-in ATB	0	0.0000	0.0000	0	0
						0.6	0.0000	0.0013	0	0
95-22	1997/2004	202	13.23	16.44	1-in ARFC, 12.5-in non-dow JPCP, 4-AB	0	0.0000	0.0000	0	0
						4.4	0.0000	0.0043	0	0
163	1993/1993	93	SPS-1	SPS-1	1 in AC, 15 in RCC	0	0.0000	0.0000	0	0
						8.1	0.0000	0.0000	0	0

In the analysis the researchers used the Arizona fatigue cracking calibration curve previously described. This relationship defines concrete slab fatigue damage and transverse midpanel cracking. Figure 67 shows the results of the analysis (the smooth curve through the data), which indicate that fatigue cracking can develop as load damage increases over time. The Arizona calibration curve is defined as:

$$CRK = \frac{1}{1 + C4(DI_F)^{C5}} \quad (\text{Eq. 13})$$

Where

CRK = low + medium + high cracked slabs as a percentage of all slabs in a mile

DI = Computed Miner's fatigue damage at the top and bottom of the concrete slab at the point of maximum tensile stress caused by axle loads and temperature curl/moisture warping

C4 = 0.19

C5 = -2.067

The Arizona bare JPCP sections and 13 Arizona composite sections are plotted in Figure 67. The data fall right in line with the JPCP sections from Arizona. None of the Arizona ARFC/JPCP composite pavements showed transverse fatigue cracking and none was predicted by the MEPDG because of the relatively thick concrete slabs and the ARFC surfacing that reduces thermal and moisture gradients within the slab, thus limiting slab curling and fatigue damage.

These results in Figure 67 indicate that the ARFC/JPCP composite pavements fatigue damage and cracking are analyzed reasonably well in the MEPDG and that the Arizona calibrated PCC fatigue models are applicable. The researchers concluded that the Arizona JPCP transverse fatigue cracking damage model holds reasonably well for Arizona based on these composite project results.

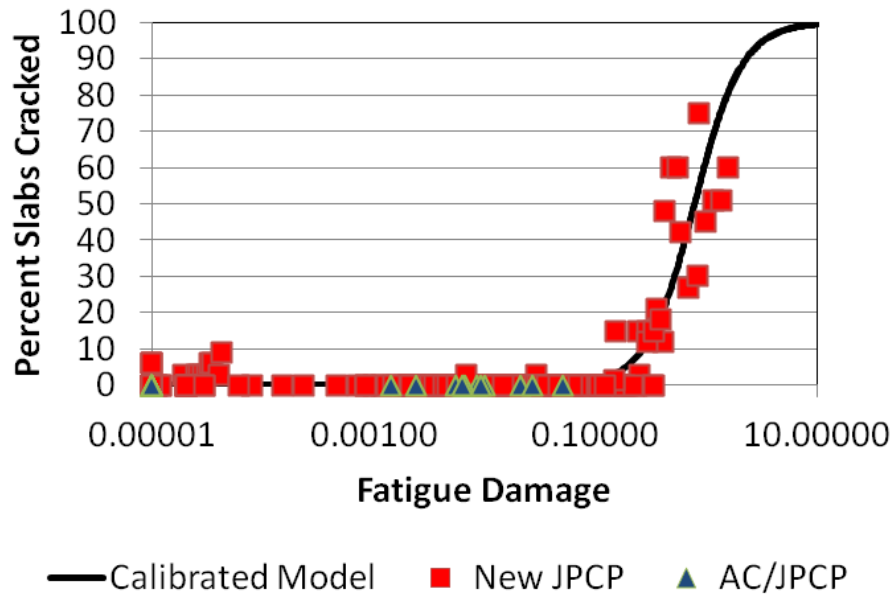


Figure 67. Percentage of Slabs Cracked Versus JPCP Slab Fatigue Damage in JPCP LTPP and PMS Sections and in Composite Pavement

IRI (Smoothness)

The IRI model for flexible pavement is used for composite pavement. The predicted IRI depends mainly on the initial IRI after construction and developing distresses such as rutting and cracking. The researchers determined the initial IRI values from the ADOT PMS database for the closest year after construction; if this information was unavailable, the researchers backcasted from future available measurements. The mean initial IRI after construction for ARFC/JPCP was 53 inches/mi (with a range of 36 to 65 inches/mi), which is very smooth.

Other factors include slab cracking, transverse joint reflection as well as surface rutting. SF is also included with freezing depth, time since construction, and type of subgrade soil. Since rutting and transverse cracking were very low for ARFC/JPCP, the future IRI depends on the initial IRI. If transverse joint reflection cracking developed within a few years, that too would affect IRI in the MEPDG.

Figure 68 plots predicted versus measured IRI. The flexible pavement IRI model appears to reasonably predict the IRI of composite ARFC/JPCP projects over time and traffic with no further modification to the calibration coefficients.

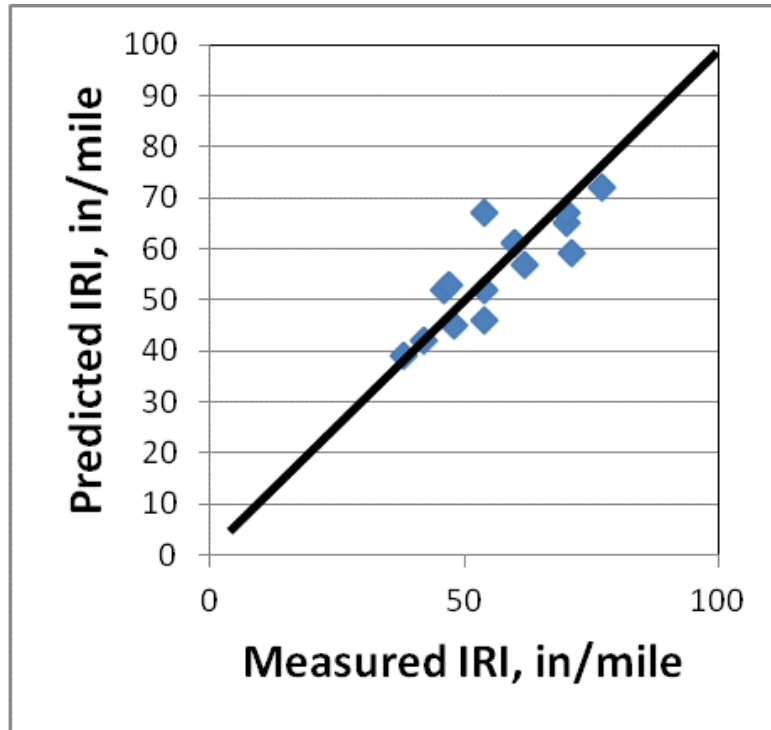


Figure 68. MEPDG Predicted Versus Measured IRI for Composite Pavement Projects (2 to 16 Years)

Joint Reflection Cracking

Field surveys of all ARFC/JPCP sections showed that all transverse joints had reflected through. These reflected joints ranged in age from 7 to 16 years and were mostly under very heavy truck traffic. Nearly all joints showed a low severity deterioration; only one project showed medium severity. The MEPDG empirical model predicts that all of these joints will reflect through within a few years, which occurred. However, a large majority of these reflection cracks did not deteriorate and affect rideability. They are still expected to deteriorate, especially nondoweled transverse joints, which will lead to ARFC replacement.

These results indicate that designers can use the MEPDG to design ARFC/JPCP composite pavements with confidence. The HMA overlay of JPCP mode must be selected to design a composite pavement.

CRCP and ARFC/CRCP Composite

Arizona has constructed two CRCP sections over the years that are available for use in distress and IRI model validation: Loop 101, Milepost (MP) 8 to MP 14.9 (northbound lane), and I-10, MP

70.66 to MP 70.76 (westbound lane), described below. The researchers collected data for these sections through field surveys, ADOT files, and the LTPP database.

Loop 101, MP 8 to 14.9 (between Northern and Bell roads), LTPP section 11.9-12.0

(northbound lane). Built in 1989, this section was bare concrete until 2005 when a 0.75-inch ARFC was placed on Phoenix-area freeways to cut noise level. Other details of this section are:

- 9-inch CRCP, 3-inch AC base, A-6 subgrade.
- Longitudinal steel: #5 bars, spaced at 6 inches and placed at mid-depth with 0.568 percent reinforcement.
- Performance:
 - CRCP exhibited no distress in 2005 when it was resurfaced with 0.75-inch ARFC.
 - Crack spacing: 40 inches. All cracks were very tight.
 - The 2012 survey showed that no transverse cracks had reflected through the entire length of thin ARFC after seven years of heavy traffic. The ARFC exhibited no distress and was in excellent condition.

I-10, MP 70.66 to 70.76, (westbound lane). This very short section was constructed in 1994 as an experimental section and was immediately surfaced with a very thin 0.5-inch ARFC. Other details of this section follow:

- 0.5-inch ARFC at construction.
- 13-inch CRCP, 6-inch aggregate base, A-2-4 subgrade.
- AC shoulder.
- Longitudinal steel: #6 bars, spaced at 6 inches and placed at mid-depth with 0.57 percent reinforcement.
- Performance:
 - Mean reflected crack spacing was about 48 to 60 inches in early 2011. Some of these cracks were about 0.10 inch wide and others were tight.
 - The CRCP exhibited two medium/high punchouts in January 2011 per 528 ft, which translates to 20 per mile.
 - The ARFC exhibited raveling distress and was in fair to poor condition after 16 years of service under heavy truck traffic.

Inputs for the DARWin ME were obtained for these two sections as well as their performance through early 2011. The predicted performance matched the field performance well, as summarized in Table 38. These results suggest that the MEPDG is predicting well the performance of these two Arizona CRCP projects over long service lives and heavy traffic. The Loop 101 CRCP has shown excellent performance over 21 years (tight transverse cracks, no punchouts, smooth), and the MEPDG predicts excellent performance in every way. The I-10 ARFC (0.5 inch)/CRCP has been under much heavier traffic (20 million trucks in the outer lane) and has recently developed wide cracks and structural punchouts. The MEPDG predicts this deterioration as shown by the predicted wide cracks, loss of crack load transfer efficiency, and punchouts. If the I-10 ARFC/CRCP had been designed with a higher steel percentage and an AC base, the pavement would have performed very well over the design period under more than 25 million truck loadings. The ARFC of 0.5 inch is too thin to have any beneficial effect.

Table 38. Measured and Predicted Performance of Loop 101 and I-10 CRCP Sections

Performance Indicator	Loop 101, MP 8 to MP 14.9 NB		I-10, MP 70.66 to MP 70.76 WB	
	Measured	Predicted	Measured	Predicted
Crack spacing	40 inches	44 inches	48- to 60-inch mean	54 inches
Crack width	Could not measure, but all very tight (<0.020 inches)	<0.020 inches	Could not measure, but some >0.040 inches	0.040 inches (very wide; would cause loss of load transfer efficiency)
Crack load transfer efficiency	Very high, 90% to 100%	>92% to 98%	40% to 100%	Could not measure, but some wide and poor (<60%)
Punchouts (M, H)	0 per mile	0 per mile	20 per mile	5 per mile
IRI	47 inch/mi*	53 inch/mi*	90 inch/mi	79 inch/mi
Number of trucks	7 million outer lane		20 million outer lane	
Time period	1989 to 2010 (21 years)		1994 to 2010 (16 years)	

*Measured and predicted on ARFC surface five years after it was placed.

Does the performance of the two Arizona CRCP sections match the Arizona calibration for CRCP conducted under NCHRP 20-07 (calibration done for corrected CTE values)? The fatigue damage in the CRCP slab resulting from the millions of heavy truck loadings is computed in the MEPDG software over the entire analysis period. This fatigue damage is at the top of the slab, 48 inches from the slab edge. If this becomes too high, a fatigue longitudinal crack forms between two transverse cracks, initiating the development of an edge punchout. The NCHRP 20-07 national

calibration of the CRCP punchout model developed a relationship between concrete fatigue damage at the top of the slab and punchouts. This plot, shown in Figure 69 (the smooth curve through the data), shows how the development of structural punchouts can form as load damage increases over time.

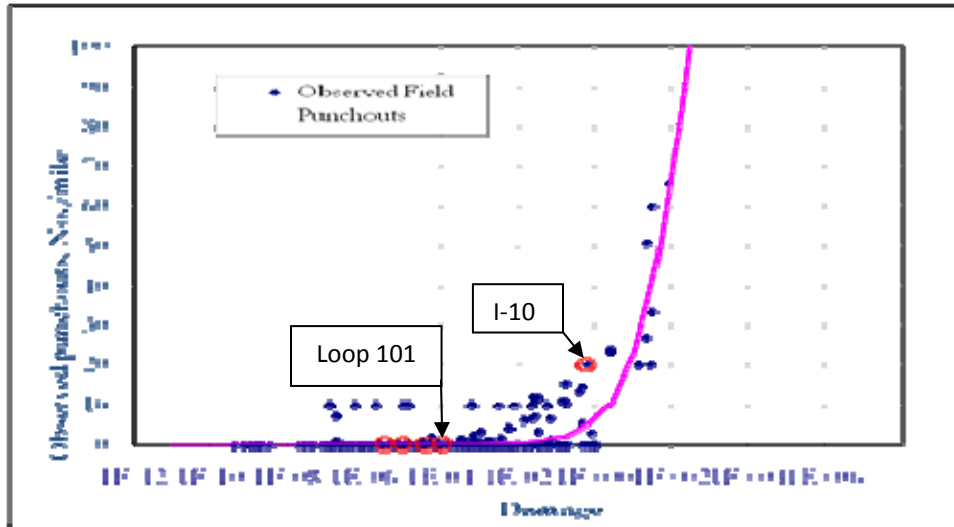


Figure 69. CRCP Observed Punchouts Versus Fatigue Damage for All CRCP Used in the 2007 National Calibration
(Two Arizona CRCP sections circled in red)

The national calibration curve is defined as:

$$PO = \frac{C3}{1 + C4(DAMAGE)^{C5}}$$

(Eq. 14)

Where

PO = number of medium and high punchouts per mile

DAMAGE = computed Miner's fatigue damage at top of concrete slab at
point of maximum tensile stress caused by axle loads and
temperature curl/moisture warping

C3 = 85

C4 = 1.4149

C5 = -0.8061

The Loop 101 and I-10 sections are also plotted in Figure 69. These points are within the same general grouping of U.S. CRCP sections. Loop 101 CRCP is nowhere close to developing punchouts but I-10 CRCP has developed some. While this is very limited CRCP performance data, the researchers concluded that the national CRCP punchout damage model holds reasonably well for Arizona based on the results of these two projects. CRCP may be designed in Arizona using the national calibration factors along with the standard deviation for reliability design.

CHAPTER 4. SENSITIVITY ANALYSIS

To help validate the local Arizona model predictions, the researchers performed a comprehensive, 30-year sensitivity analysis of the new HMA and new JPCP models. The researchers could have chosen a much longer time period, such as 50 years, however the relative results were not expected to change. They developed new HMA pavement and JPCP baseline designs with selected inputs to represent typical Arizona site conditions, design features, construction practices, and pavement materials. Details of the baseline designs for new HMA and new JPCP are presented in Tables 39 and 40, respectively. Key inputs were varied one at a time except where two inputs have known correlations, such as PCC thickness and dowel size. Dowel diameter was increased with PCC thickness using the thickness divided by 8 ratio. Thus, a 12-inch slab would have a 1.50-inch dowel diameter. Next, the researchers plotted the predicted outcomes for each input to illustrate their impact on cracking, faulting, and IRI smoothness, and assessed the reasonableness of the impact on these key performance outputs.

Table 39. Key Inputs in New or Reconstructed HMA Pavement Sensitivity Analysis

Input Parameter	Values		
	Lower End	Mean (Baseline)	Upper End
HMA thickness (inches)	3	6	9
Air voids (%)	6	7	8
Binder content (%)	8	11	14
Binder type (Superpave)	64-22	70-22	76-16
Subgrade (AASHTO soil class)	A-2-4	A-6	—
Initial average annual daily truck traffic (AADTT)	2000	6000	10,000
Climate (weather stations)	Kingman, Page	St. Johns	Douglas, Bisbee
Reliability (%)	50	75	95

Table 40. Key Inputs in New or Reconstructed JPCP Sensitivity Analysis*

Input Parameter	Values		
	Lower End	Mean (Baseline)	Upper End
PCC thickness (inches)	8	10	12
CTE (inch/inch/° F)	4.5	5.0	5.5
AADTT	5000	10,000	15,000
Dowel diameter (inches) (used PCC thickness/8 rule)	1	1.25	1.5
Subgrade (AASHTO soil class)	A-6	A-2-4	—
Shoulder type	HMA	Tied PCC	—
Climate (weather stations)	Tucson	Phoenix	Kingman
Reliability (%)	50	75	95

*Similar results would be obtained for ARFC/JPCP.

Results of the JPCP sensitivity analysis are presented in the following sections. The sensitivity analysis indicates reasonable results that fairly well match the results obtained in field experiments (e.g., thicker slabs show less cracking; larger dowels show less faulting).

NEW HMA SENSITIVITY ANALYSIS RESULTS

Effect of Traffic

Figures 70 through 72 show the effect of average annual daily truck traffic (AADTT) on predicted distress and IRI. The initial year two-directional AADTT varied from 2000 to 10,000, which represents a large range of very heavy truck traffic. The 2000 AADTT results in about 10 million total trucks in the design lane over 20 years. The 10,000 AADTT results in about 48 million trucks in the design lane over 20 years.

The trends of predicted distress and IRI were as expected, with increasing traffic applications resulting in higher levels of predicted distress and IRI. Although the trends were all reasonable, the effect of AADTT on predicted IRI was not significant. These results are in accordance with generally accepted HMA performance in the field.

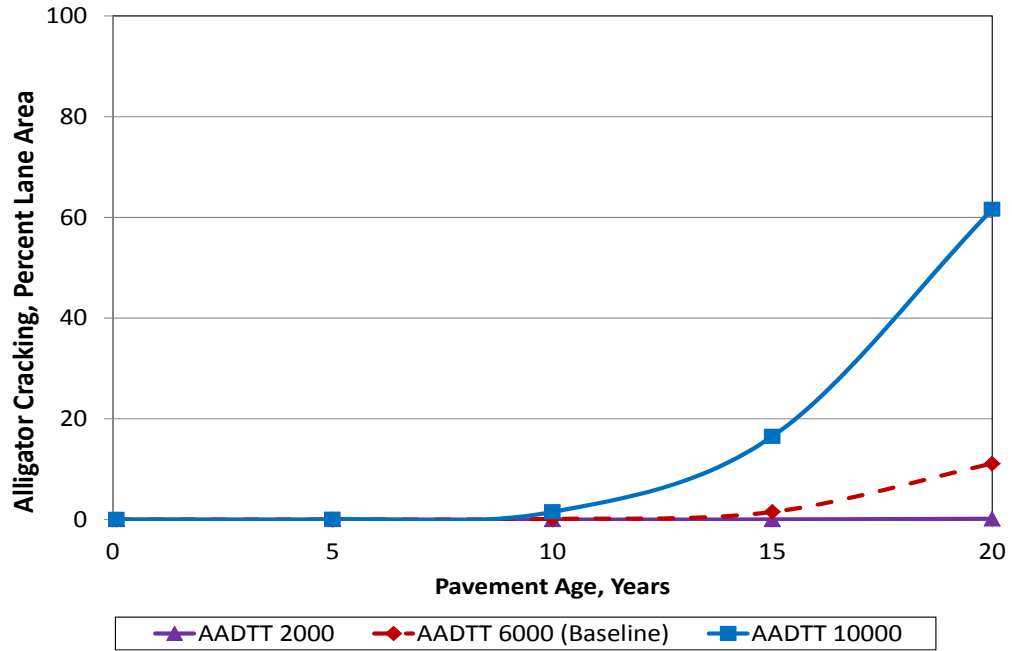


Figure 70. Effect of AADTT on HMA Alligator Fatigue Cracking

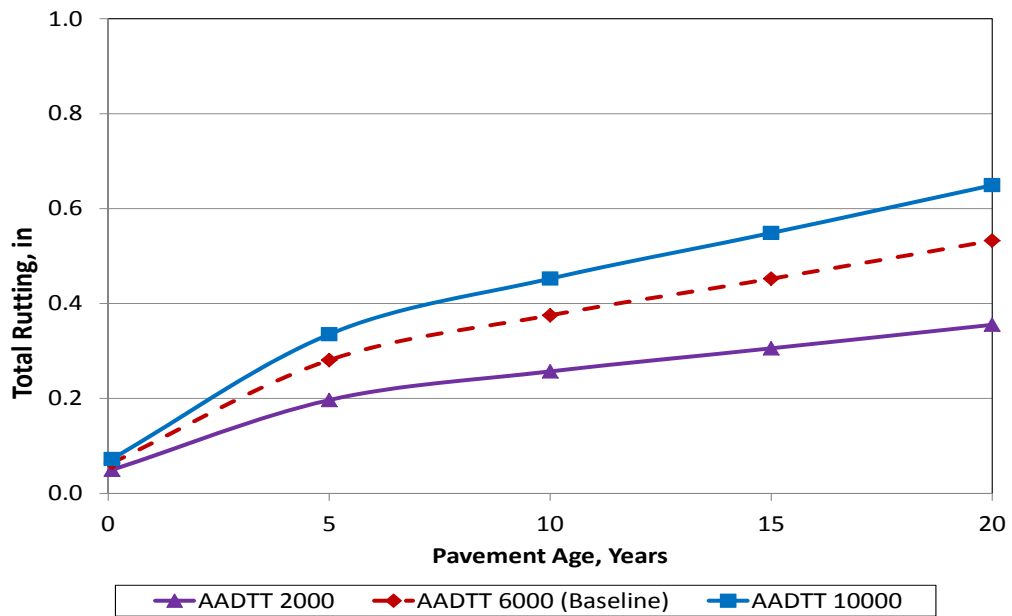


Figure 71. Effect of AADTT on HMA Total Rutting

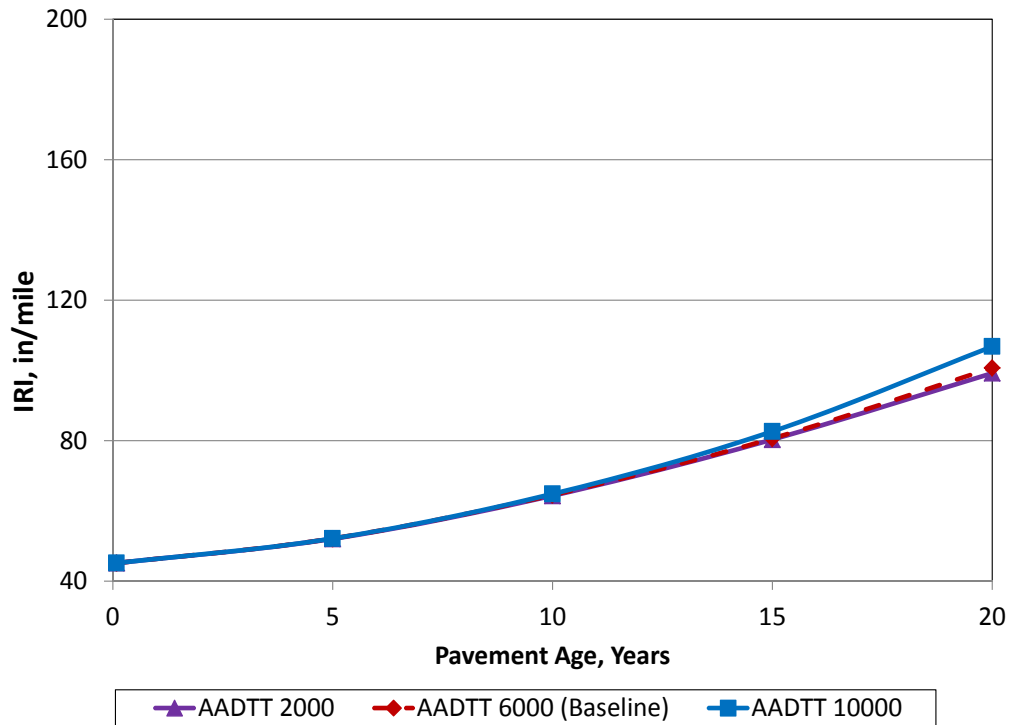


Figure 72. Effect of Initial AADTT on HMA IRI

Effect of HMA Thickness

Figures 73 through 75 show the effect of HMA thickness on predicted distress and IRI. Thicker HMA provides increased structure for applied traffic loads, reduces stresses and the amount of fatigue damage at the bottom of the HMA layer, and also reduces HMA layer deflections. Therefore, increased HMA thickness should result in less alligator cracking, rutting, and IRI.

The three plots show that HMA thickness had the most significant effect on alligator cracking and rutting. Increased HMA thickness resulted in lower alligator cracking and rutting, and had a smaller but significant effect on IRI reduction. These trends are typical and as expected when compared to field pavement performance data from in-service flexible pavements.

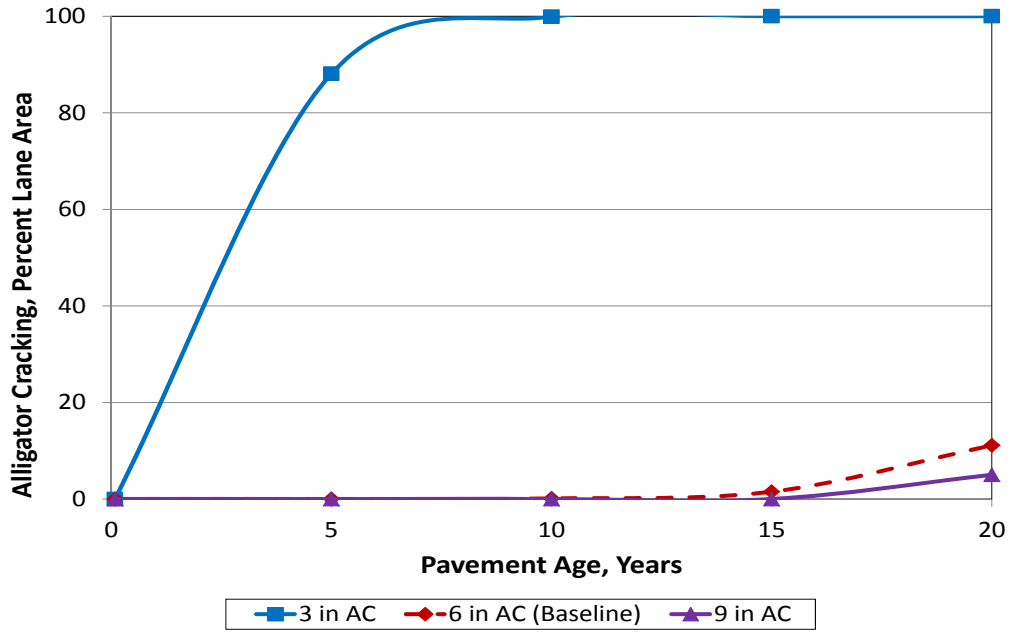


Figure 73. Effect of HMA Thickness on HMA Alligator Fatigue Cracking

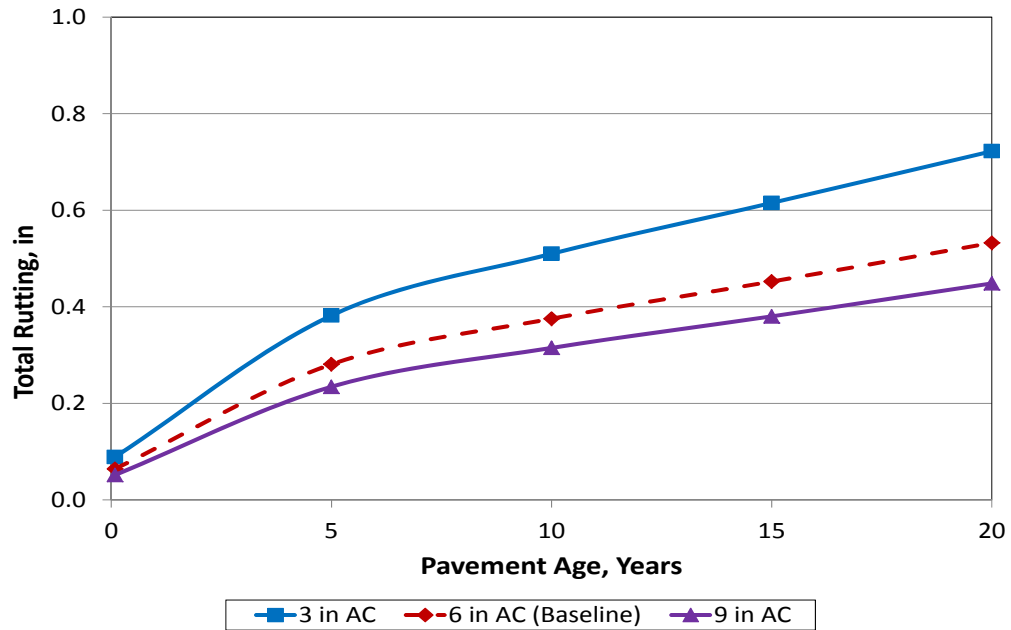


Figure 74. Effect of HMA Thickness on Total Rutting

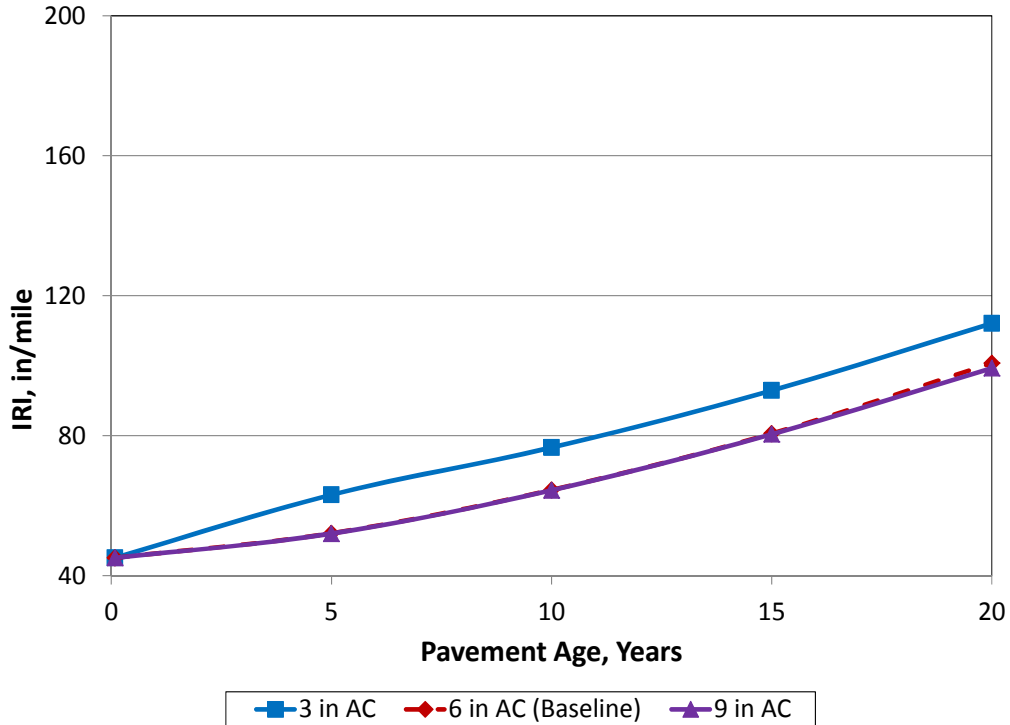


Figure 75. Effect of HMA Thickness on IRI

Effect of HMA Binder Content

Figures 76 through 78 show the effect of HMA binder content on predicted distress and IRI. Higher HMA binder content reduces tensile strain and the amount of fatigue damage at the bottom of the HMA layer thereby reducing alligator cracking. Increased binder content increased rutting as shown. However, binder content has minimal effect on IRI.

The three plots show that HMA binder content had the most significant effect on alligator cracking. Increased binder content resulted in lower alligator cracking and higher rutting. HMA binder content had a small effect on IRI. These trends are typical and as expected when compared to field pavement performance data from in-service flexible pavements.

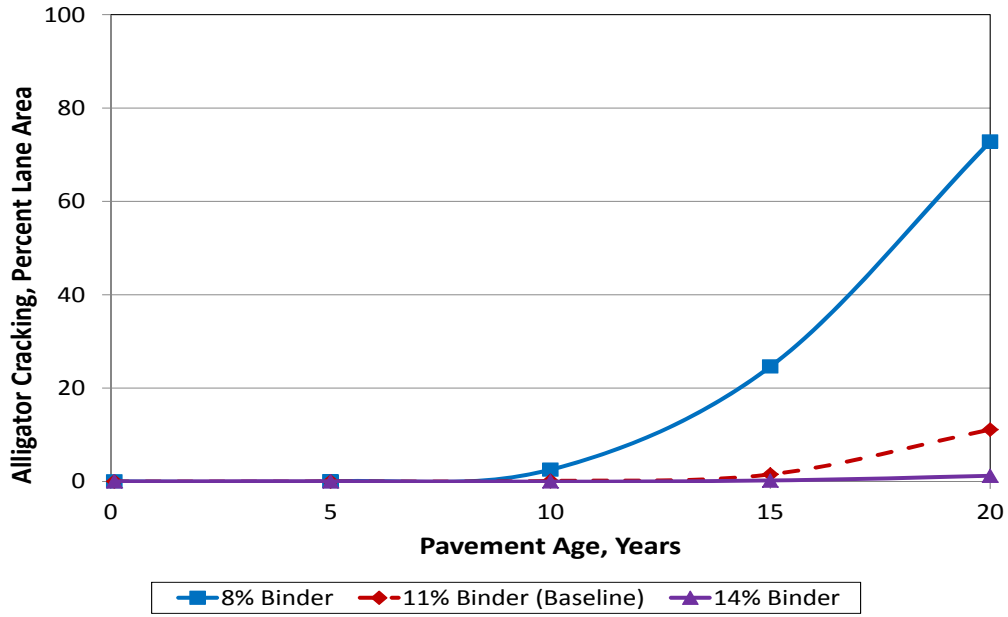


Figure 76. Effect of Binder Content on HMA Alligator Cracking

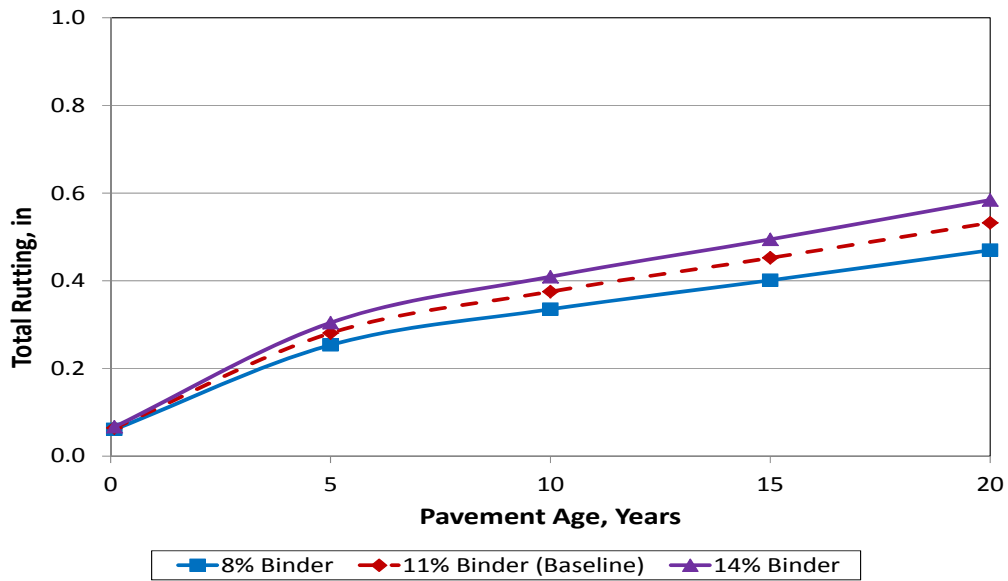


Figure 77. Effect of Binder Content on HMA Total Rutting

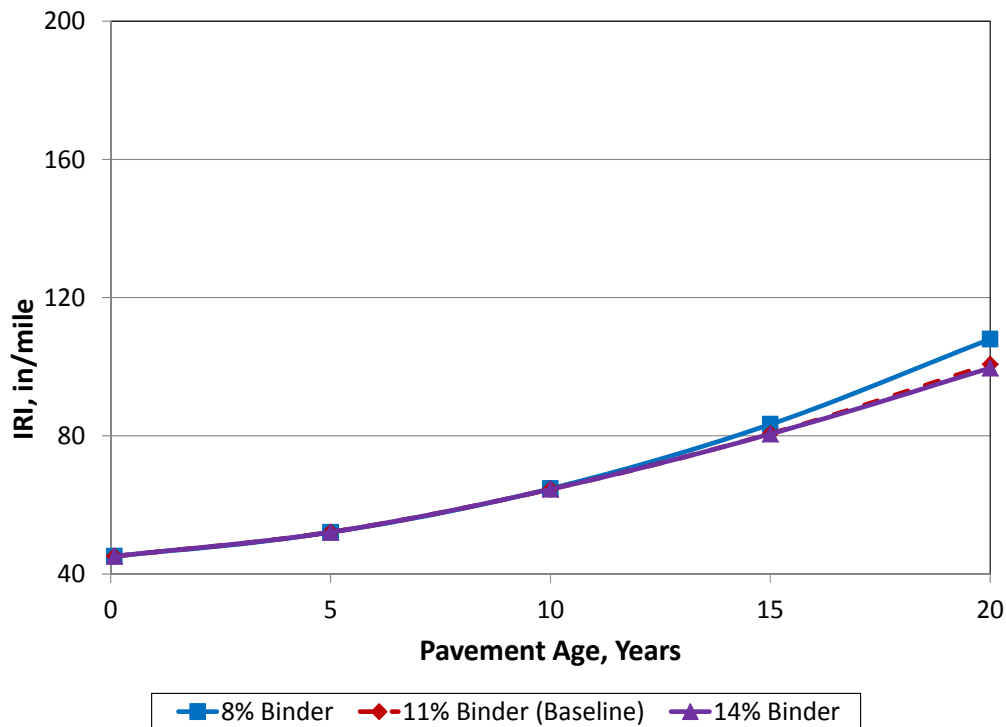


Figure 78. Effect of Binder Content on HMA IRI

Effect of HMA Air Voids

Figures 79 through 81 show the effect of HMA air voids on predicted distress and IRI. Lower HMA air voids increases the dynamic modulus and reduces strain. Therefore, the amount of fatigue cracking at the bottom of the HMA layer is reduced. Decreased air voids have a lower but significant effect on reducing rutting. However, air voids has minimal effect on IRI.

The three plots show that HMA air voids had the most significant effect on alligator cracking. Decreased air voids resulted in lower alligator cracking and rutting. Air voids has minimal effect on IRI. These trends are typical and as expected when compared to field pavement performance data from in-service flexible pavements.

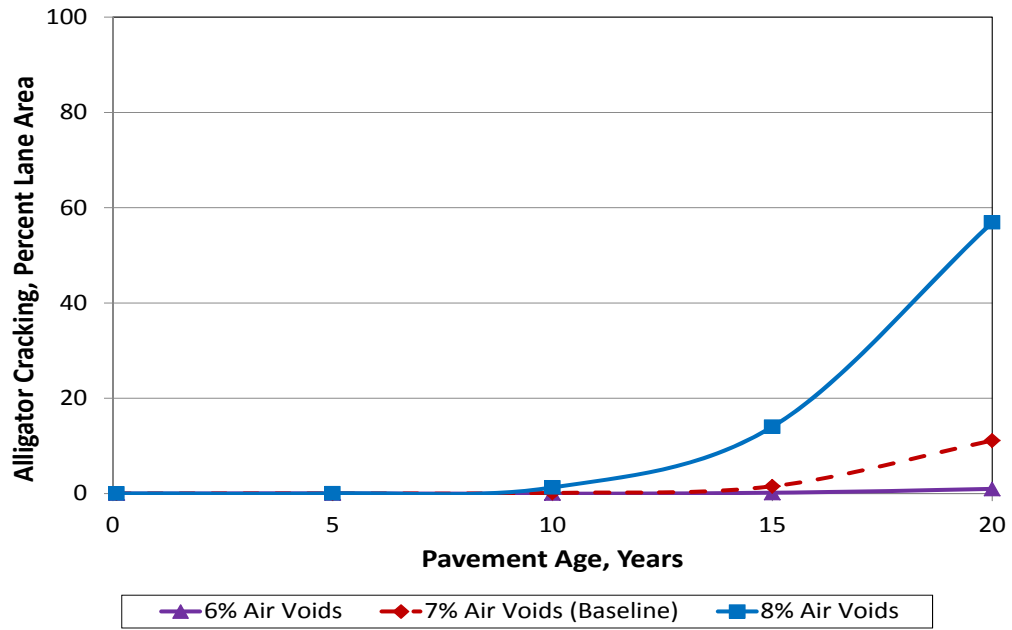


Figure 79. Effect of Air Voids on HMA Alligator Cracking

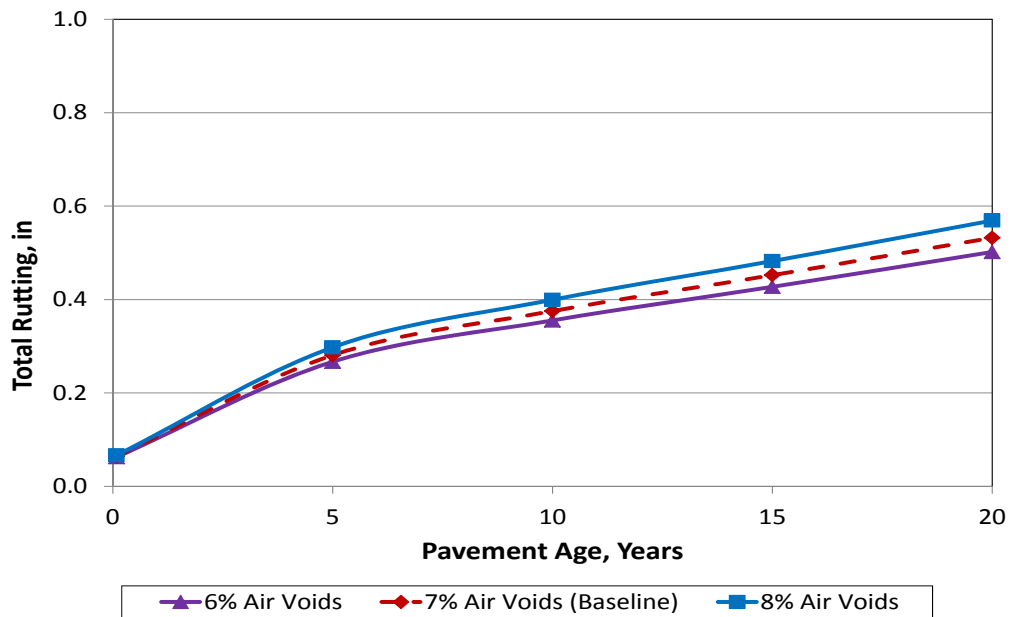


Figure 80. Effect of Air Voids on HMA Total Rutting

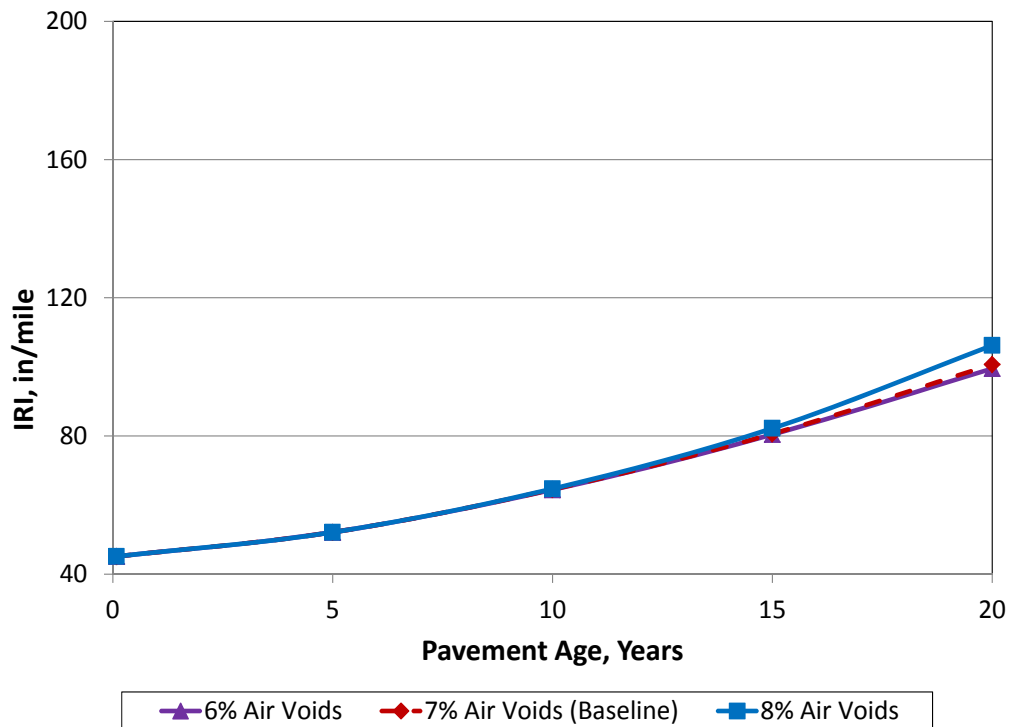


Figure 81. Effect of Air Voids on HMA IRI

Effect of HMA Binder Grade

Figures 82 through 84 show the effect of HMA PG binder on predicted distress and IRI. Higher PG binder reduces both alligator cracking and rutting.

The three plots show that HMA binder grade had the most significant effect on alligator cracking and rutting. For both alligator cracking and rutting performance measures, increased binder grade resulted in lower alligator cracking and rutting. These trends are typical and as expected when compared to field pavement performance data from in-service flexible pavements.

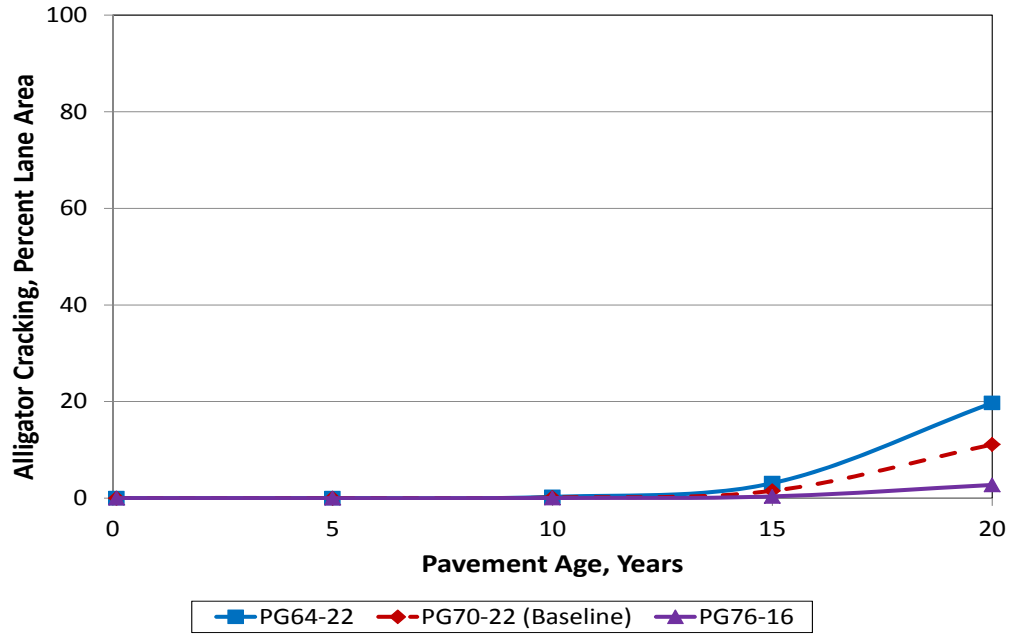


Figure 82. Effect of PG Binder on HMA Alligator Cracking

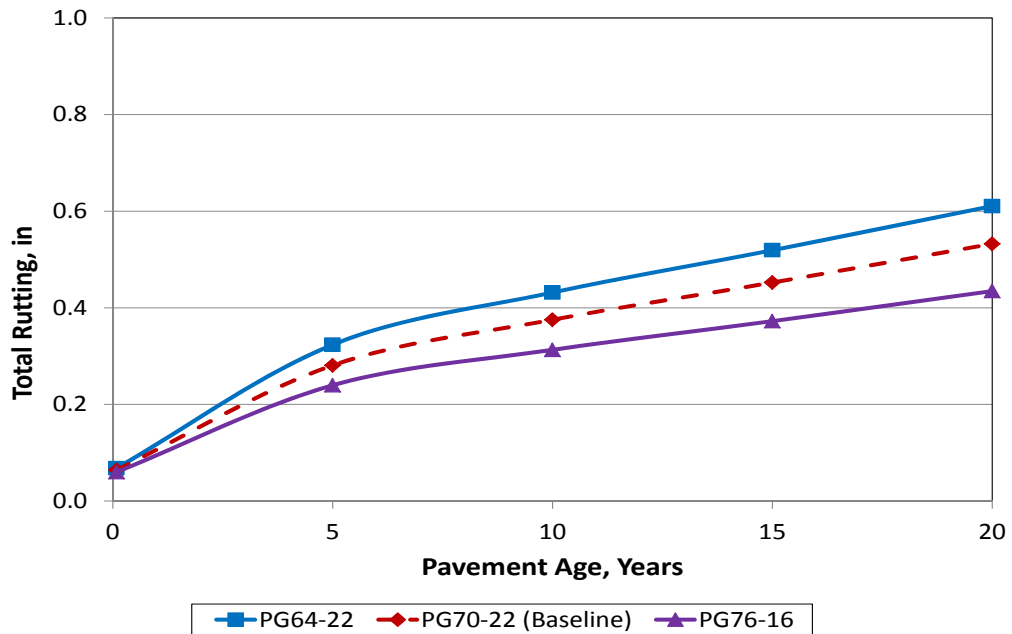


Figure 83. Effect of PG Binder on HMA Total Rutting

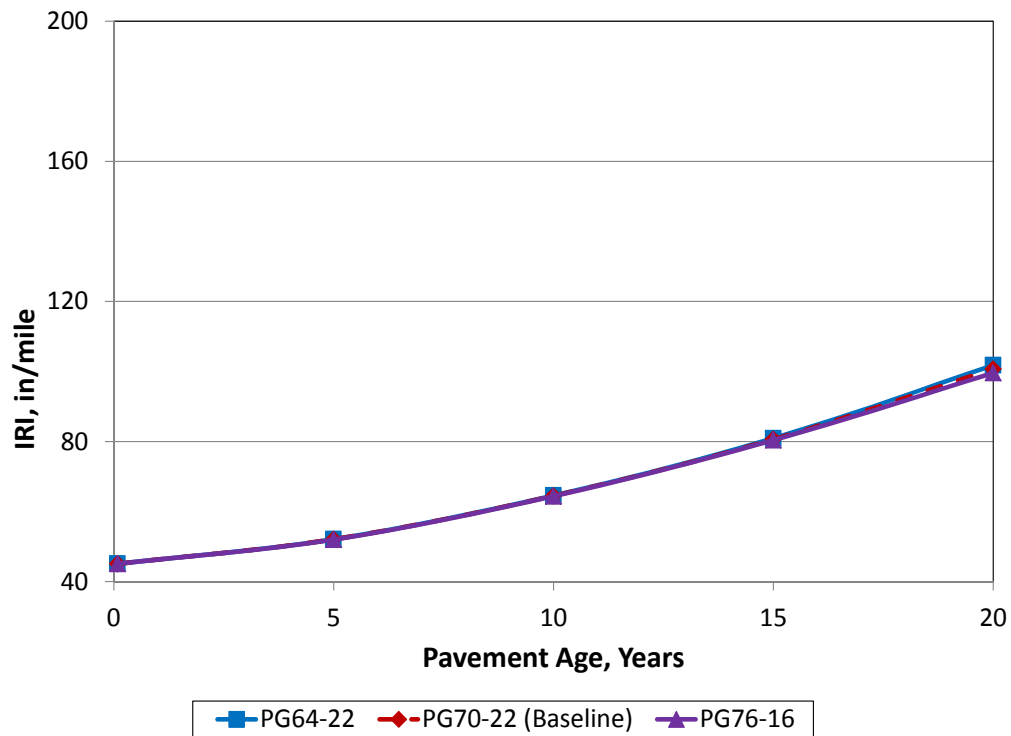


Figure 84. Effect of PG Binder on HMA IRI

Effect of Subgrade Type

Figures 85 through 87 show the effect of subgrade type on predicted distress and IRI. Subgrade support is considered in DARWin-ME through the soil's resilient modulus (at optimum moisture content and density). Typical default mean resilient modulus values were used for these two soils: A-2-4 (coarse-grain subgrade materials) was the highest and A-6 (fine-grain materials) the lowest. The temperature and moisture models used also act upon the soils on a monthly basis, producing varying values. In general, as the resilient modulus increases, load-associated stresses decrease. The three plots show that subgrade type had a small effect on all three performance measures, with A-2-4 performing slightly better than the weaker A-6 materials.

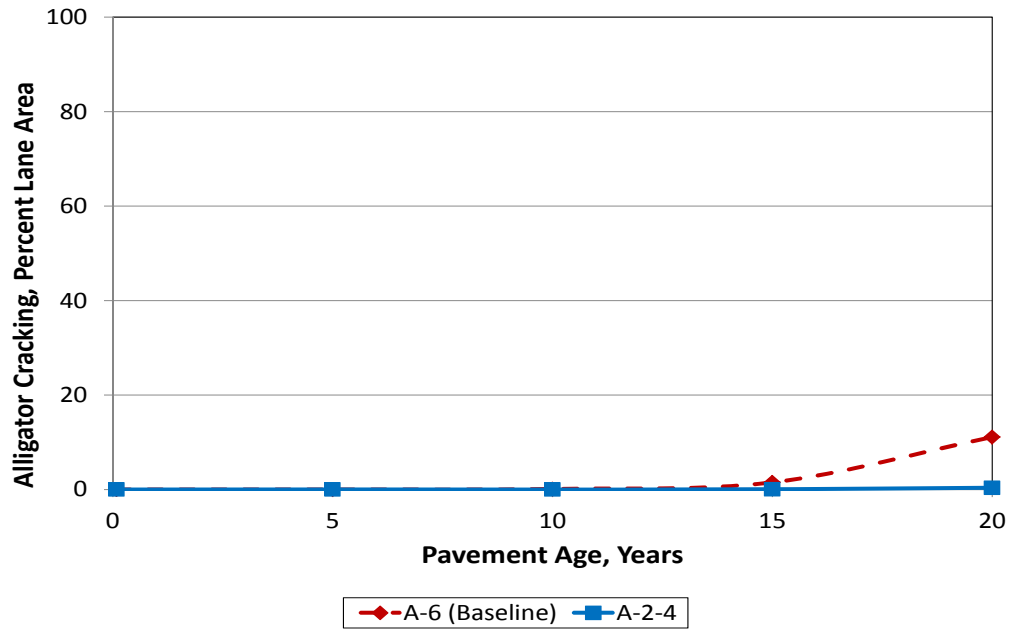


Figure 85. Effect of Subgrade Type on HMA Alligator Cracking

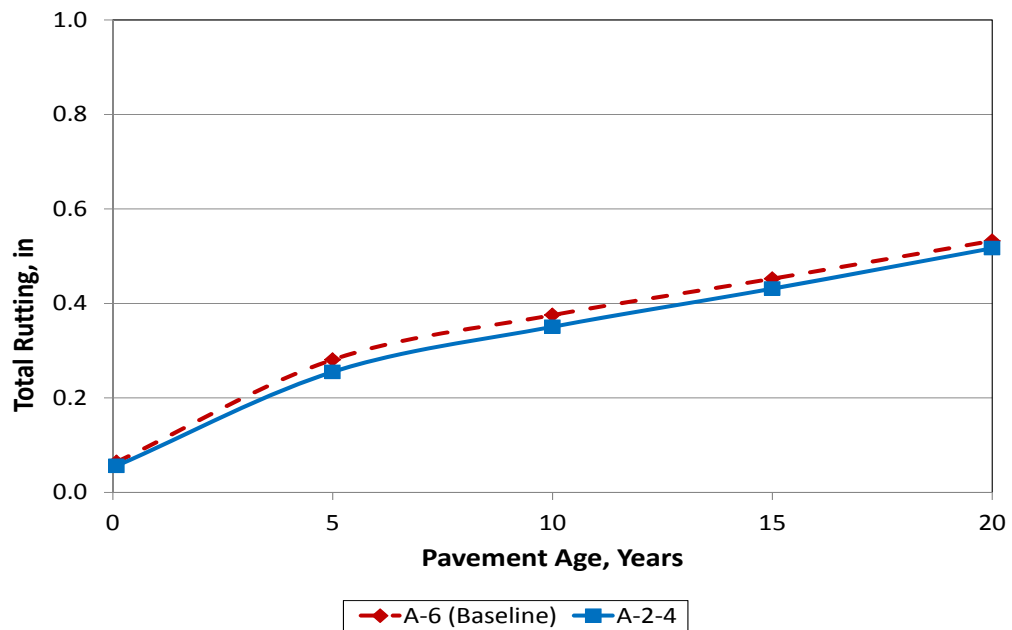


Figure 86. Effect of Subgrade Type on HMA Total Rutting

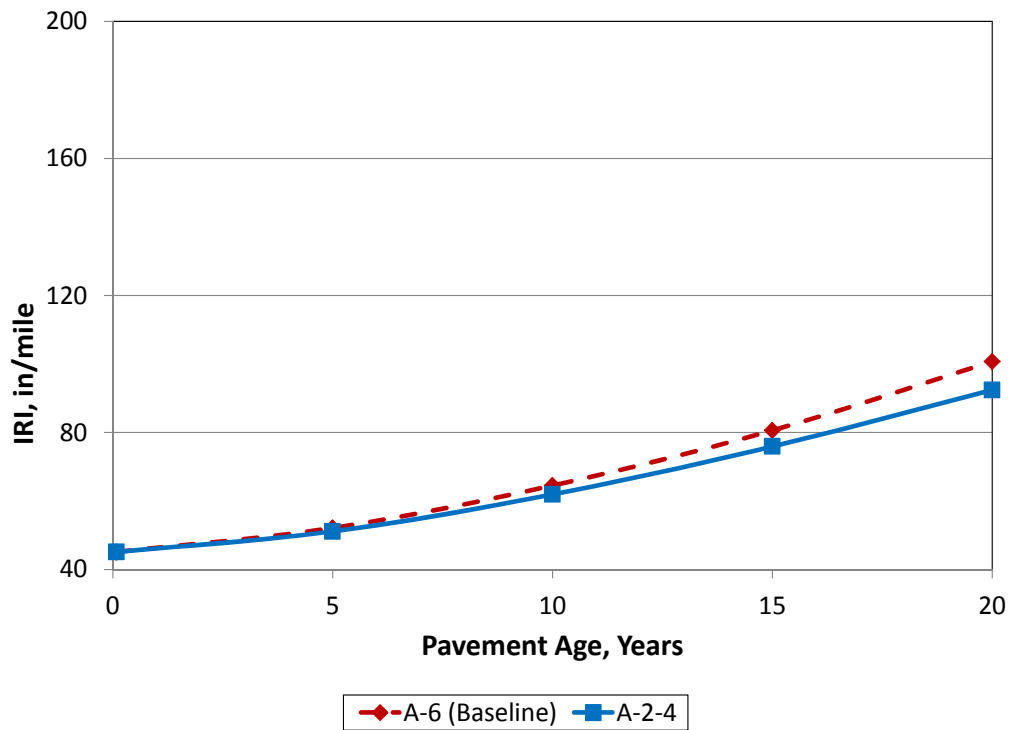


Figure 87. Effect of Subgrade Type on HMA IRI

Effect of Climate

Figures 88 through 90 show the effect of climate on predicted distress and IRI. Results from the Phoenix area were added to these plots to increase the variation in weather. Table 41 summarizes the relationship between elevation, cracking, and rutting. Transverse cracking results from Chapter 3 are also included.

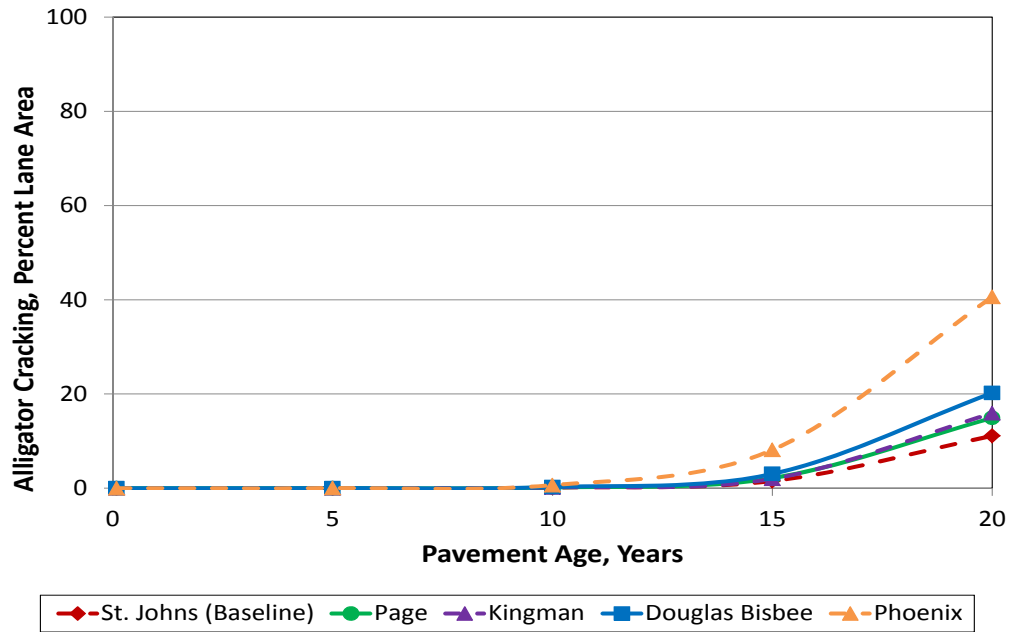


Figure 88. Effect of Climate on HMA Alligator Cracking

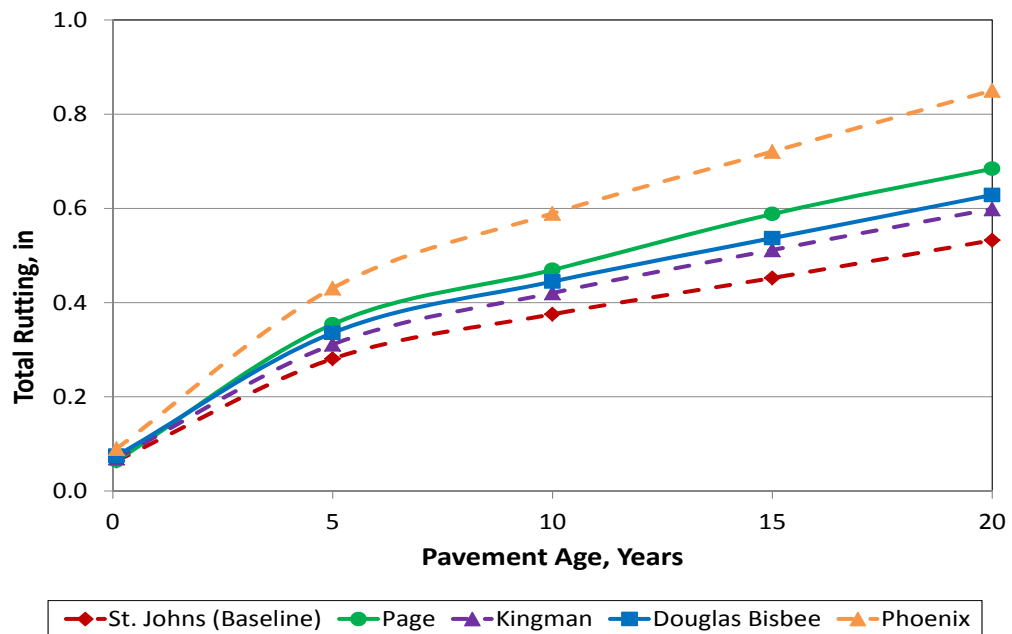


Figure 89. Effect of Climate on HMA Total Rutting

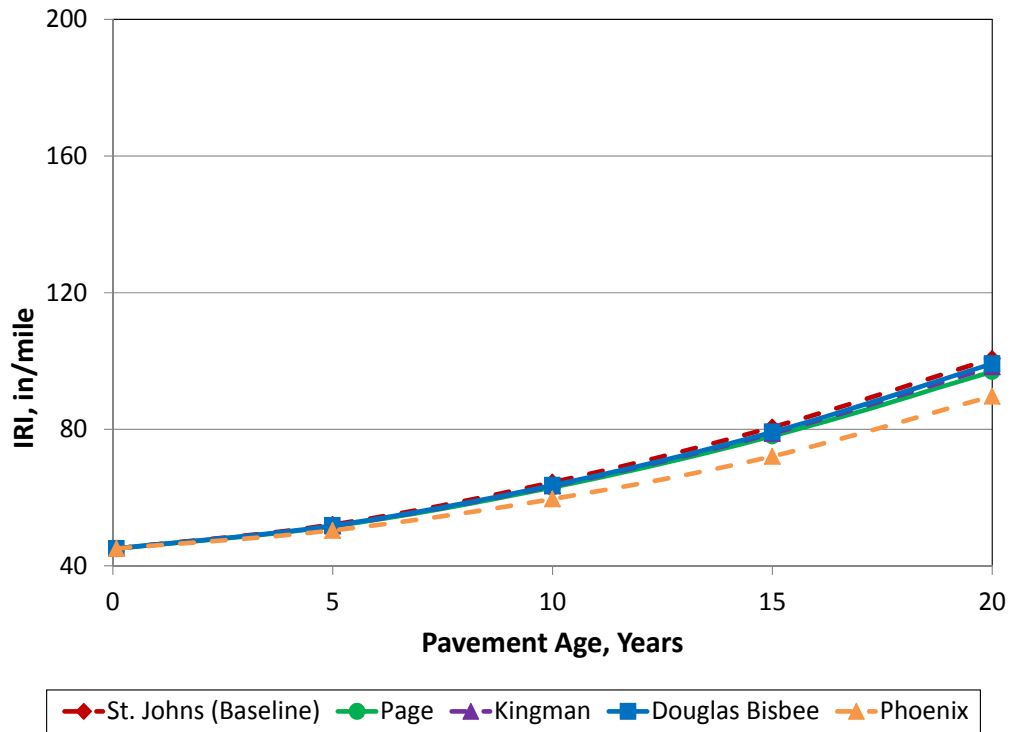


Figure 90. Effect of Climate on HMA IRI

Table 41. Effect of Climate on Predicted Distress and IRI

Site Location	Elevation (ft)	Rutting (inches)	Alligator Cracking (%)	Transverse Cracking (ft)
St. Johns	5722	0.52	11	2112
Bisbee	4105	0.63	20	1966
Kingman	3420	0.60	15	1831
Phoenix	1105	0.85	40	0

Climate varies with elevation, which results in varying amounts of fatigue cracking, rutting, and low-temperature cracking. Generally, as elevation increases, rutting and fatigue cracking decrease and low-temperature transverse cracking increases. These results can be explained partially through temperature considerations and their impact on the HMA dynamic modulus E^* . Higher elevations have colder temperatures and higher E^* , which reduces fatigue damage

and permanent deformation. However, low-temperature cracking becomes more significant in higher elevations.

The trends reported in Figures 88 through 90 are typical and as expected when compared to field pavement performance data from in-service HMA located in different climates.

Effect of Reliability

Figures 91 through 93 show the effect of reliability on predicted distress and IRI. A 50 percent design reliability indicates that the alligator cracking, rutting, and IRI curve ARE being predicted on average. Thus, half of the projects designed should show higher alligator cracking, rutting, and IRI, and half should show lower values.

As the design reliability increases to the 95 percent level, the 95 percent curve increases, indicating that 95 of 100 HMA sections would show this amount or less of alligator cracking, rutting, and IRI. Note that the standard deviation associated with calculating the reliability curves are based on the SEE of the calibration data associated with models. The higher the error, the greater the spread of these curves from 50 to 95 percent for any example and thus the higher the required HMA thickness.

The results show that the design reliability curve for 95 percent is higher than any lower level of reliability. At higher and higher levels of reliability, a thicker pavement or higher support base course will be needed to meet the design reliability requirements.

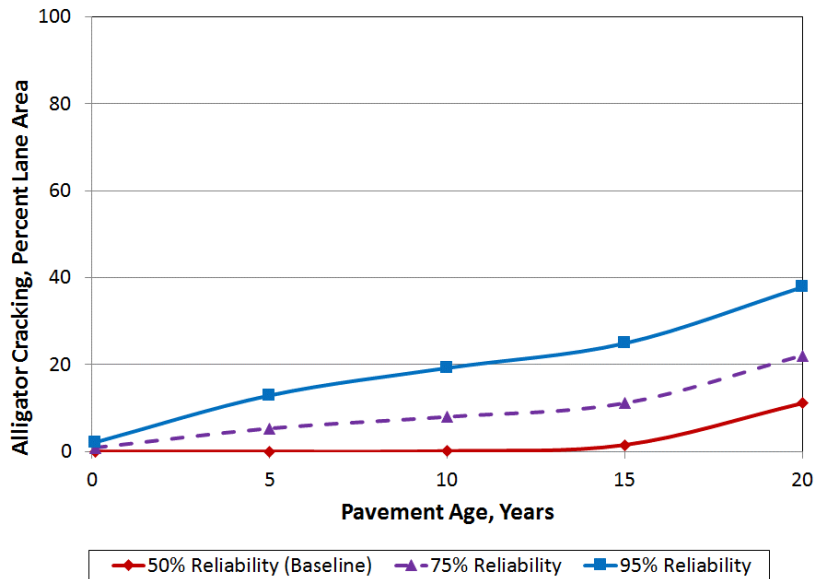


Figure 91. Effect of Reliability on HMA Alligator Cracking

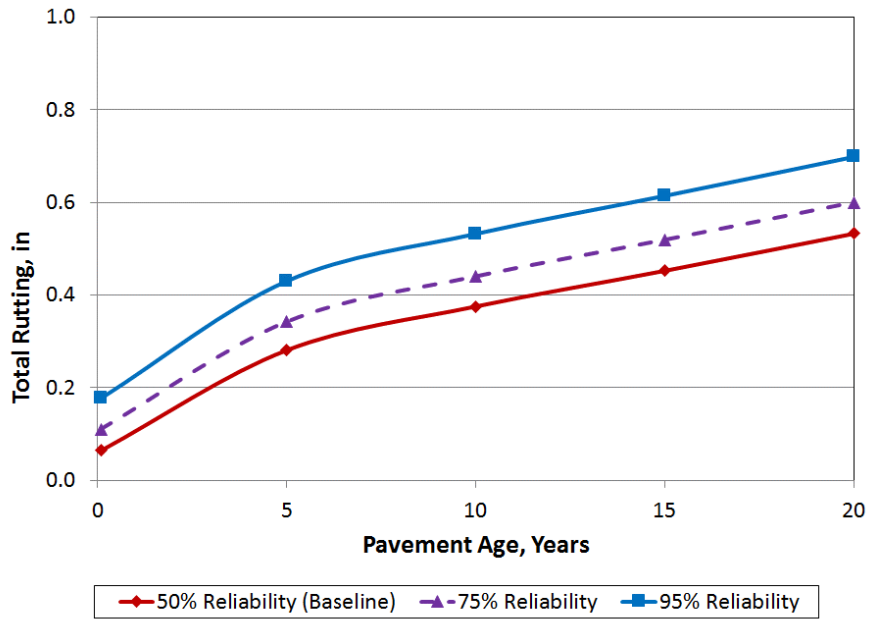


Figure 92. Effect of Reliability on HMA Total Rutting

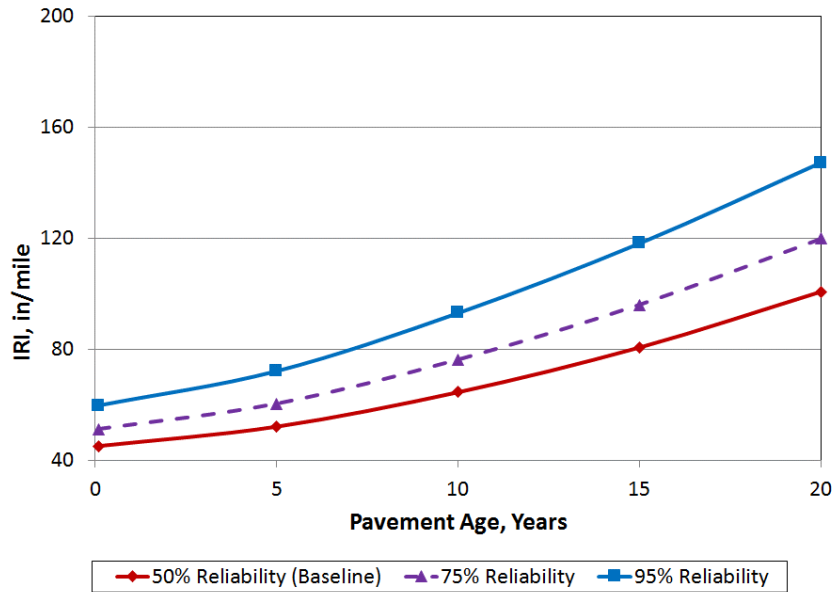


Figure 93. Effect of Reliability on HMA IRI

Overall these analyses suggest that the MEPDG model prediction is consistent in prediction of distress and IRI at least in the same direction as theory and previous experience and field performance have shown. Changes in the design inputs affect HMA alligator cracking, rutting, and IRI smoothness by varying amounts. Knowledge of this cause and effect is useful to design engineers in developing cost-effective pavements.

NEW JPCP SENSITIVITY ANALYSIS RESULTS

Effect of Traffic

Figures 94 through 96 show the effect of AADTT on predicted distress and IRI. The initial year AADTT varied from 5000 to 15,000, which represented a large range of very heavy truck traffic. The 5000 daily trucks results in about 35 million total trucks in the design lane over 30 years; 15,000 daily trucks results in about 104 million trucks in the design lane over 30 years.

The results of this analysis show that, in all cases, the increased number of heavy trucks results in greater slab fatigue cracking, joint faulting, and IRI. These results are in accordance with generally accepted JPCP performance in the field.

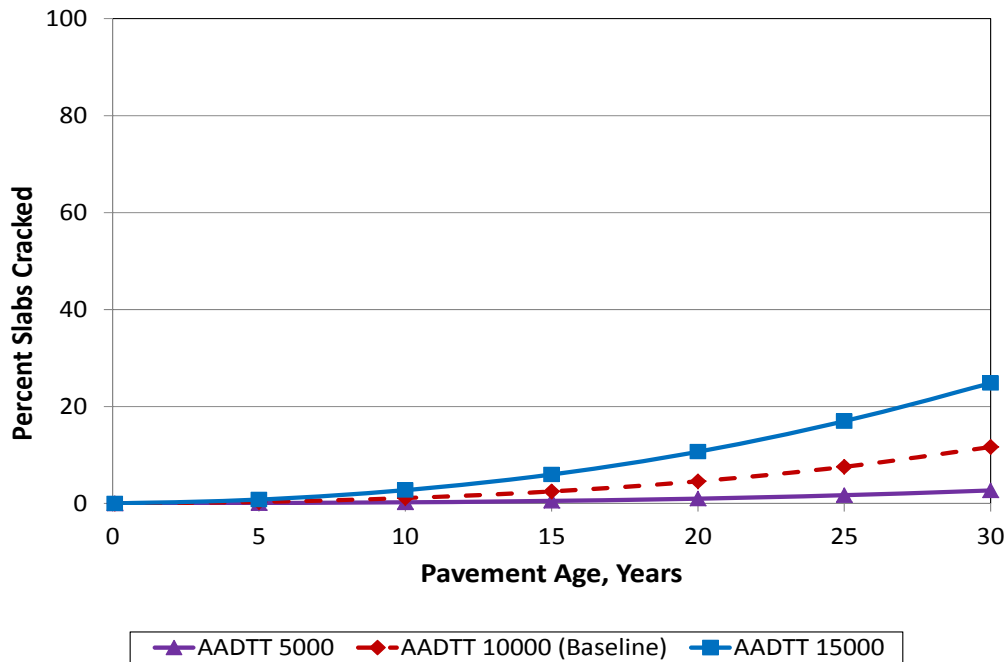


Figure 94. Effect of AADTT on JPCP Transverse Cracking

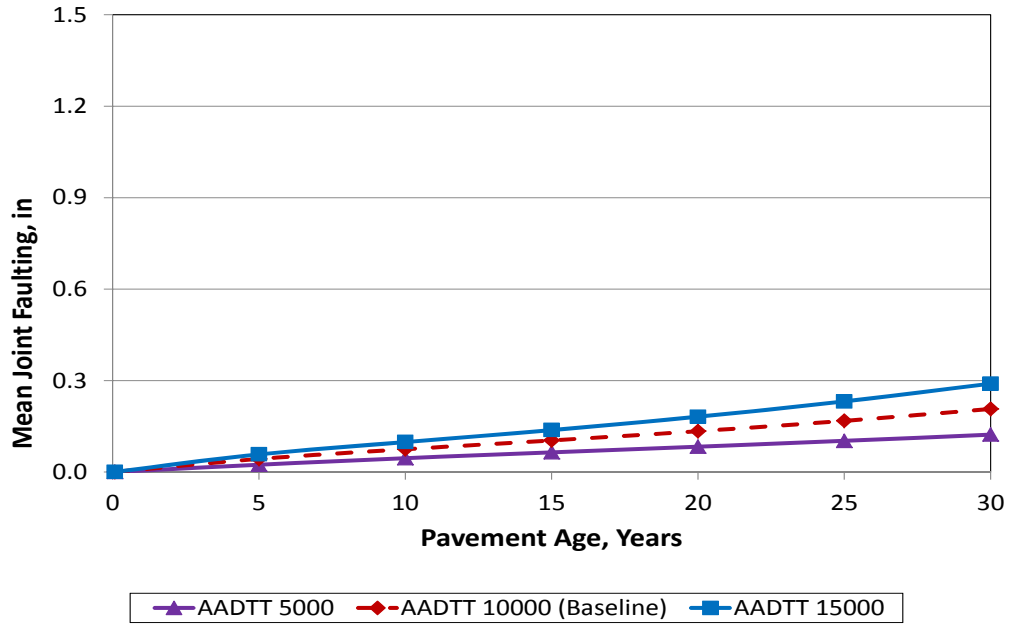


Figure 95. Effect of AADTT on JPCP Mean Joint Faulting

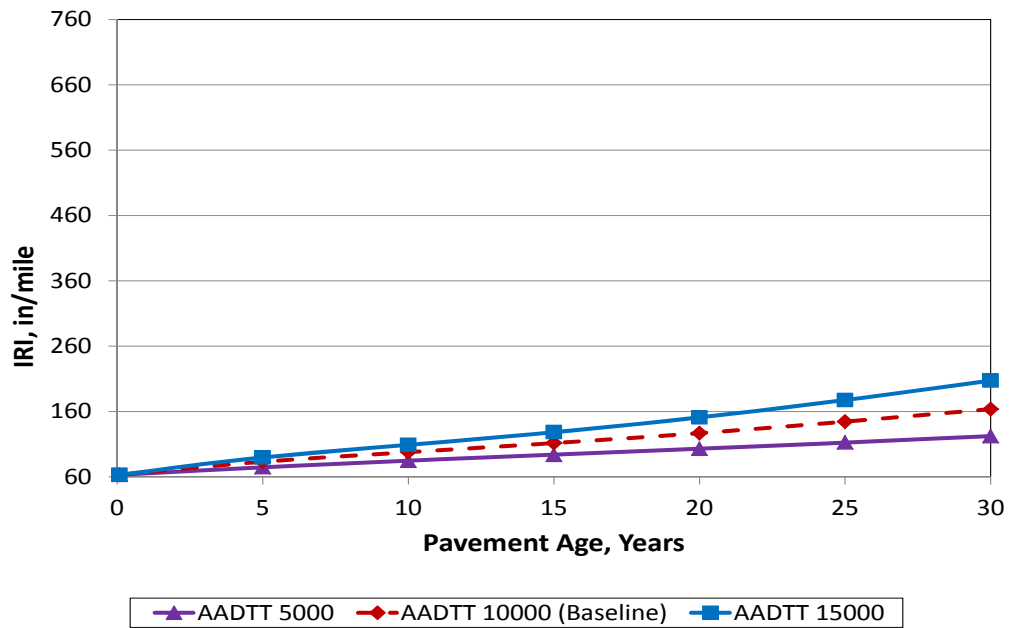


Figure 96. Effect of Initial AADTT on JPCP IRI

Effect of PCC Thickness

Figures 97 through 99 show the effect of PCC thickness on predicted distress and IRI. Thicker PCC slabs provide increased structure for applied traffic loads and thus reduce midpanel stresses and the amount of fatigue damage at the top and bottom of the slab, and deflections at the slab corners and transverse joints causing less erosion. Therefore, increased PCC slab thickness should result in less cracking, faulting, and IRI.

The three plots show that slab thickness had the most significant effect on cracking and IRI. For these performance measures, increased thickness resulted in lower cracking and IRI. For joint faulting, increasing PCC thickness had a smaller but significant effect on reduced faulting. These trends are typical and as expected when compared to field pavement performance data from in-service JPCP.

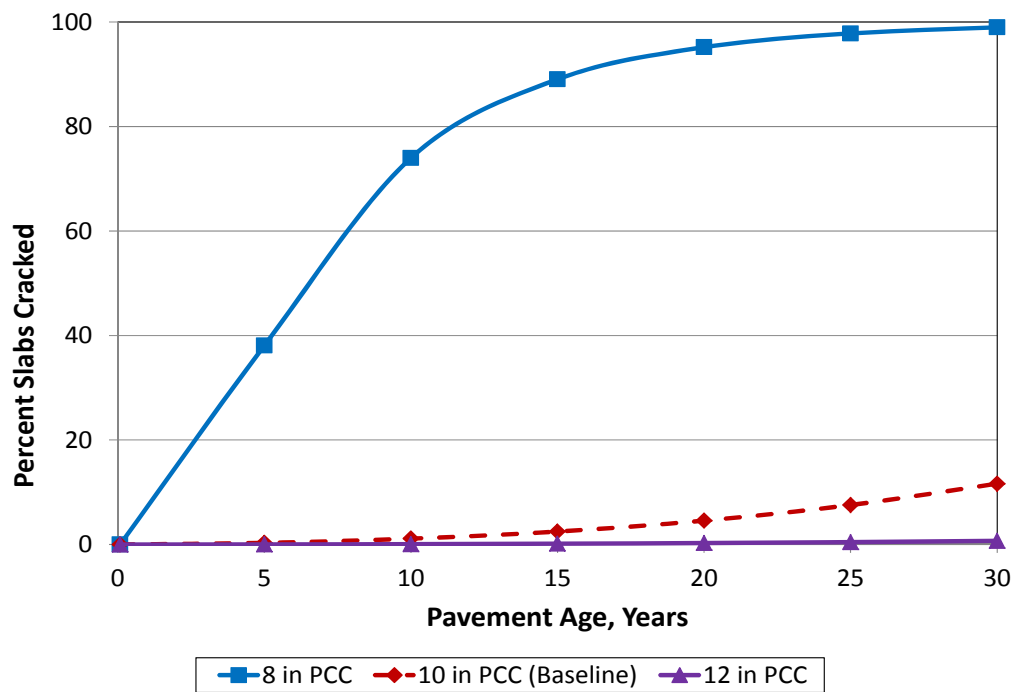


Figure 97. Effect of PCC Thickness on JPCP Transverse Cracking

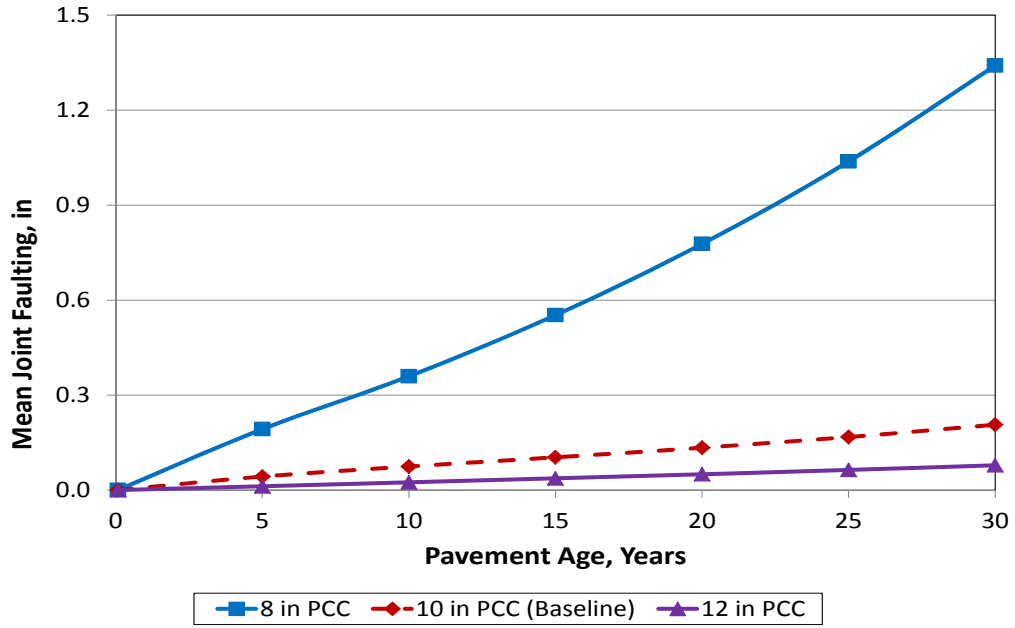


Figure 98. Effect of PCC Thickness on JPCP Mean Joint Faulting

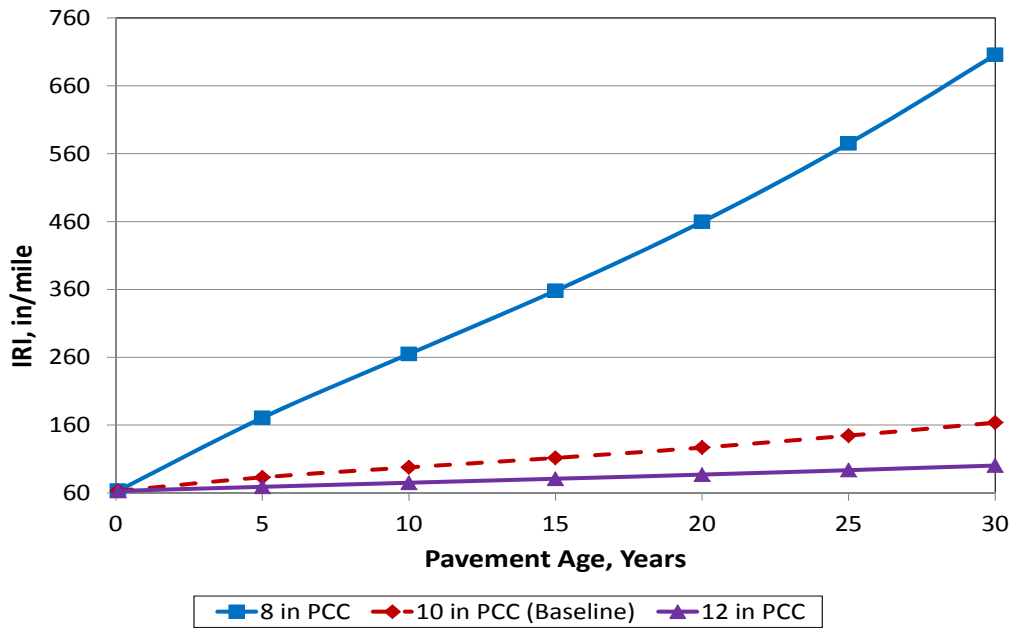


Figure 99. Effect of PCC Thickness on JPCP IRI

Effect of CTE

Figures 100 through 102 show the effect of CTE on predicted distress and IRI. CTE impacts the change in length of concrete when a temperature difference is applied. It affects slab curling and joint opening/closing, thus having an impact on joint faulting and transverse cracking. DARWin-ME is the first pavement design procedure to consider the impact of CTE.

The three plots show that PCC CTE has a very significant effect on all three performance measures. Higher CTE results in higher levels of pavement deterioration in all cases. This result is expected, although little independent field data are available to support such an effect. As CTE influences the magnitude of stresses and deflections/curling of the PCC slab, an increased CTE would be expected to increase stresses and deflections, which normally would result in more cracking and faulting, and thus higher IRI. The increase in pavement life (when IRI reaches 150 inches/mi) is from 4 years to more than 30 years with a reduction in CTE of 5.5 to 4.5×10^{-6} , which could be caused by a change in coarse aggregate.

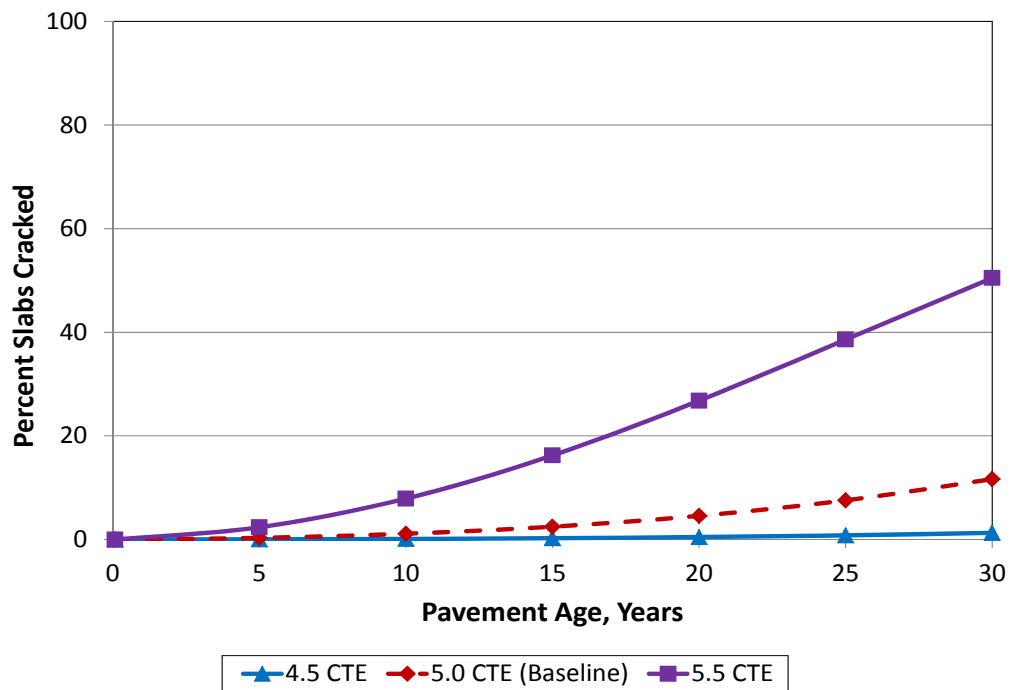


Figure 100. Effect of CTE on JPCP Transverse Cracking

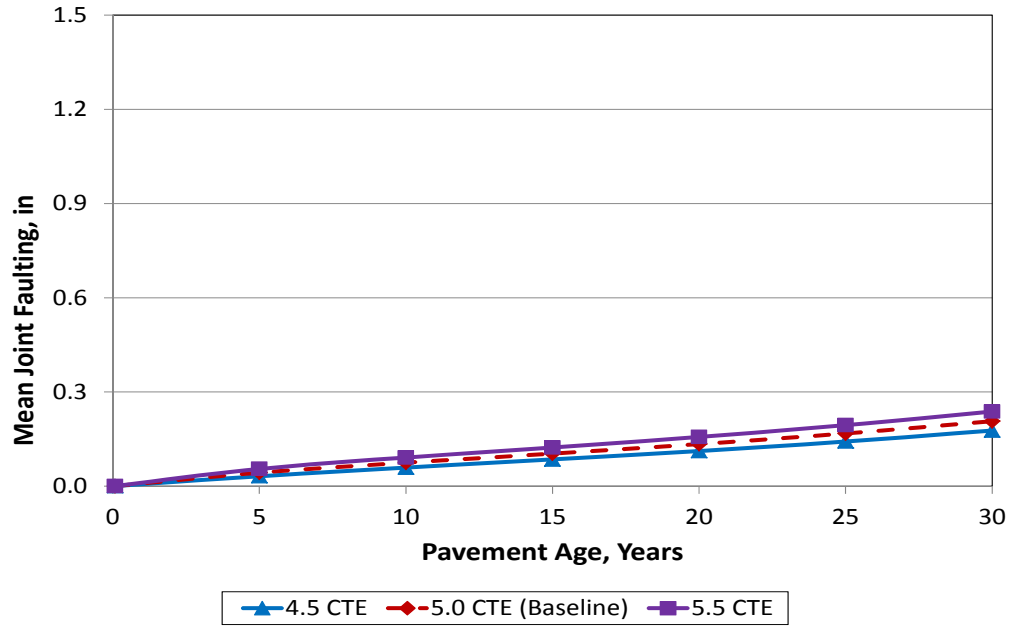


Figure 101. Effect of CTE on JPCP Mean Joint Faulting

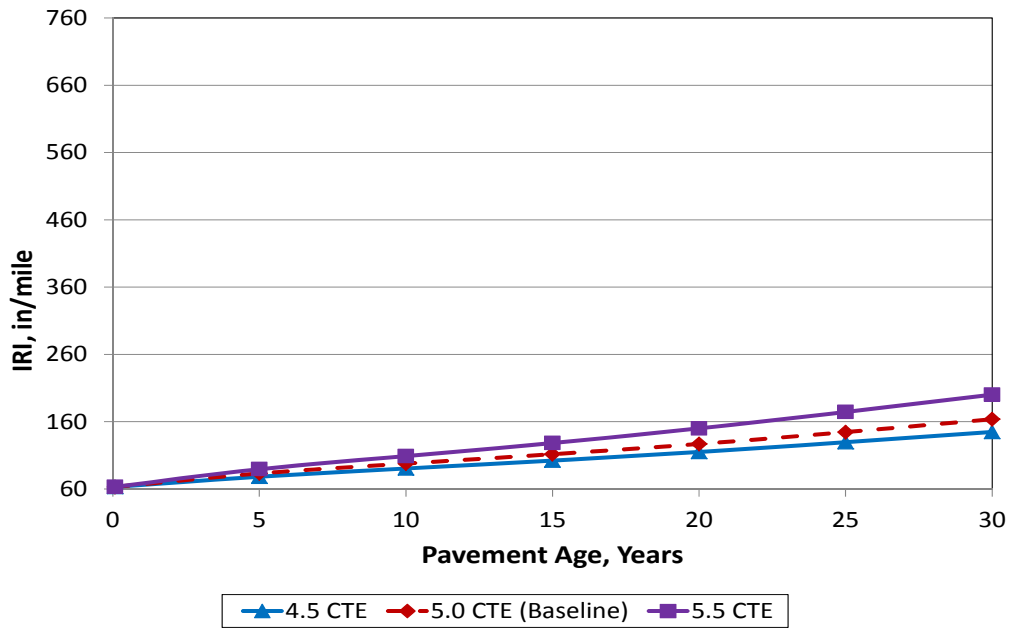


Figure 102. Effect of CTE on JPCP IRI

Effect of Shoulder Type

Figures 103 through 105 show the effect of shoulder type on predicted distress and IRI. DARWin-ME models show that the support provided at the slab and shoulder interface has a significant impact on joint deflections and critical stresses midpanel at the bottom of the PCC slab. For JPCP, support provided at the slab and shoulder interface edge support is highly influenced by the type of shoulder provided. Typically, the best edge support is provided by tied PCC shoulders with high load transfer efficiency. This is followed by PCC shoulders (not tied) and AC shoulders that provide similar levels of support. Note that the longevity of the support provided also has a considerable impact on pavement performance.

Figures 103 through 105 show the effect of shoulder type on predicted cracking, faulting, and IRI, respectively. For all three performance measures, provision of tied PCC shoulders had a positive impact on performance (i.e., reduced cracking, faulting, and IRI). The impact of shoulder type on distress and IRI was most significant for cracking. For both faulting and IRI, the impact was less significant. These trends are as expected when compared to field pavement performance data from in-service JPCP with various shoulder types.

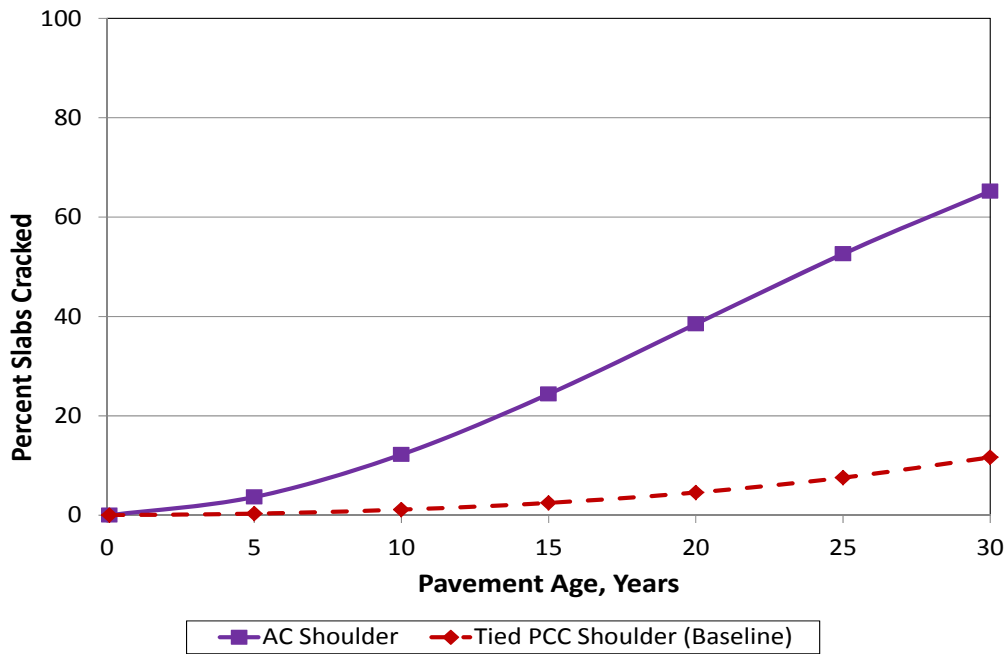


Figure 103. Effect of Shoulder Type on JPCP Transverse Cracking

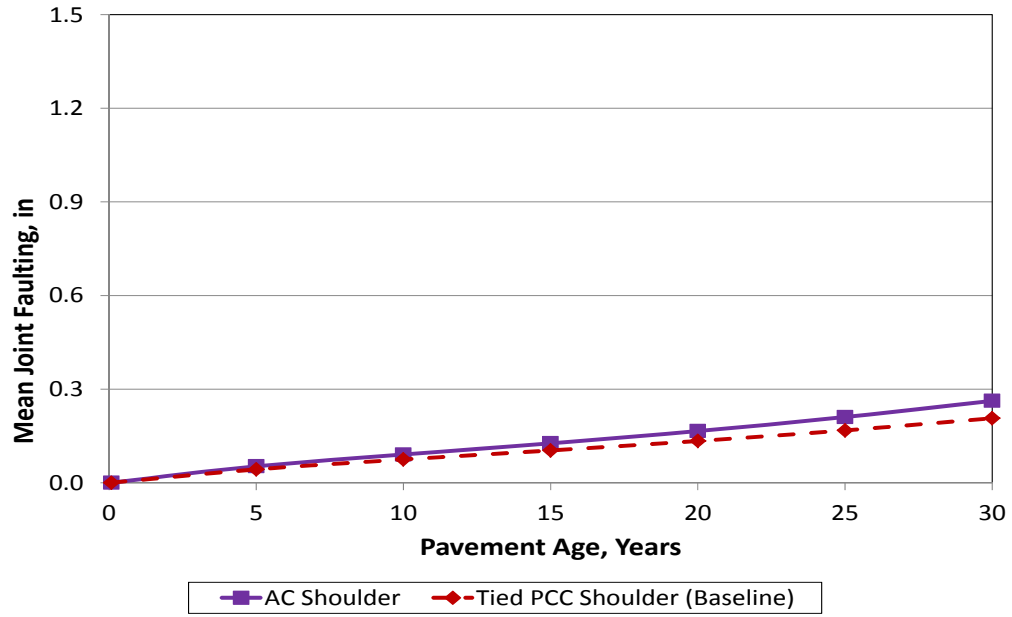


Figure 104. Effect of Shoulder Type on JPCP Mean Joint Faulting

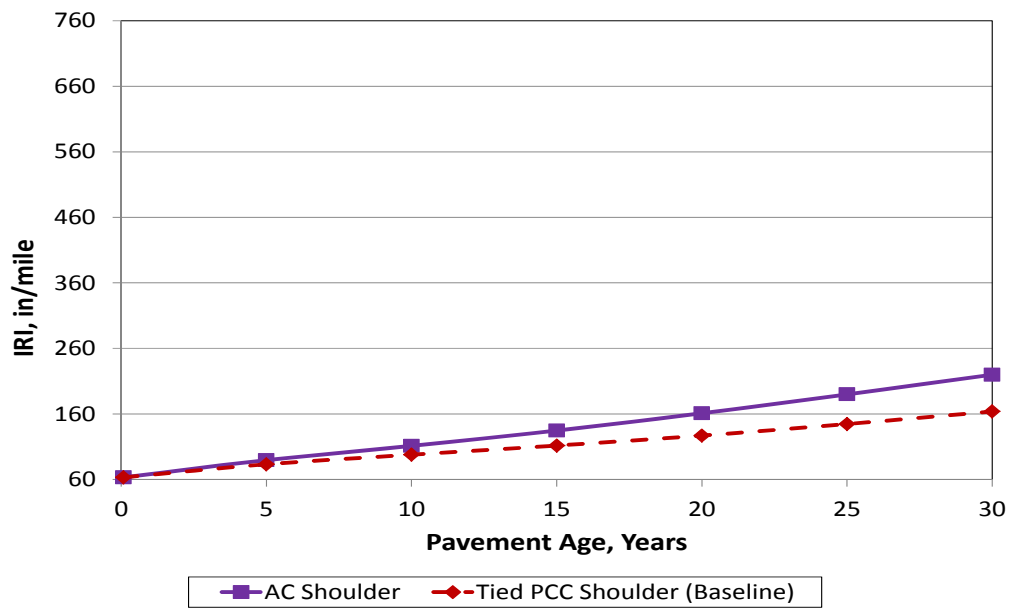


Figure 105. Effect of Shoulder Type on JPCP IRI

Effect of Subgrade Type

Figures 106 through 108 show the effect of subgrade type on predicted distress and IRI. Subgrade support is considered in DARWin-ME through the resilient modulus (at optimum moisture content and density) of the soil. Typical default mean resilient modulus values were used for these two soils, with the coarse-grained subgrade materials (A-2-4) being the highest and the fine-grained (A-6) soil the lowest. The temperature and moisture models of these soils also act upon the soils on a monthly basis, producing different values. In general, as the resilient modulus increases, load-associated stresses decrease, but the thermal curling stress increases. The relative values of these two causes of stress dominate for different designs and climates and result in differing levels of stress (and, thus, different levels of cracking and joint faulting).

The three plots show that subgrade type had a small effect on cracking but more significant effect on joint faulting and IRI. The A-2-4 soil showed lower joint faulting and IRI performance than the A-6 soil. These trends are typical and as expected when compared to field pavement performance data from in-service JPCP.

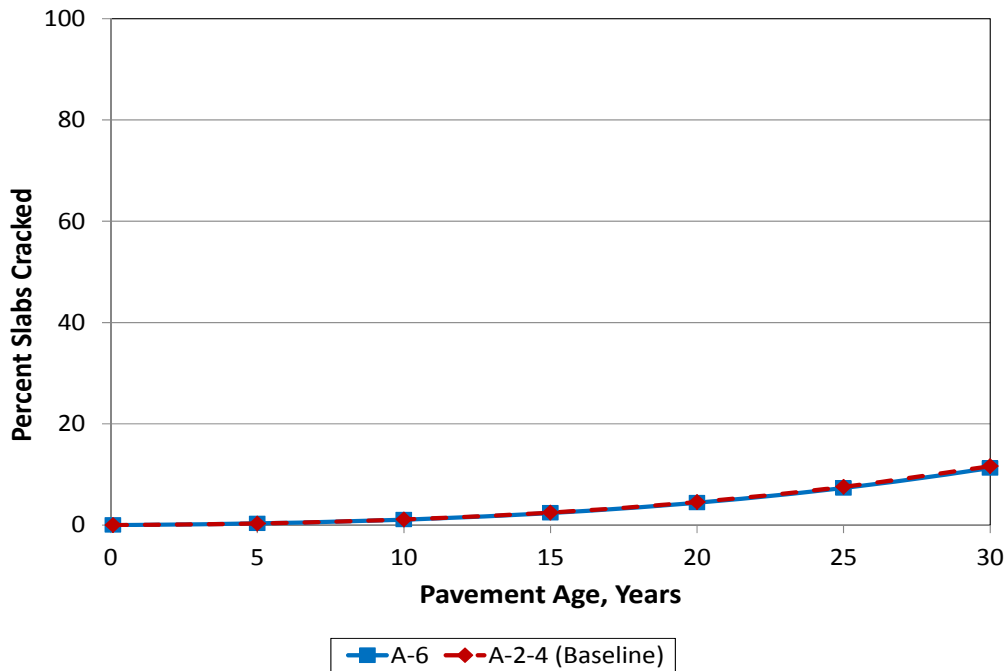


Figure 106. Effect of Subgrade Type on JPCP Transverse Cracking

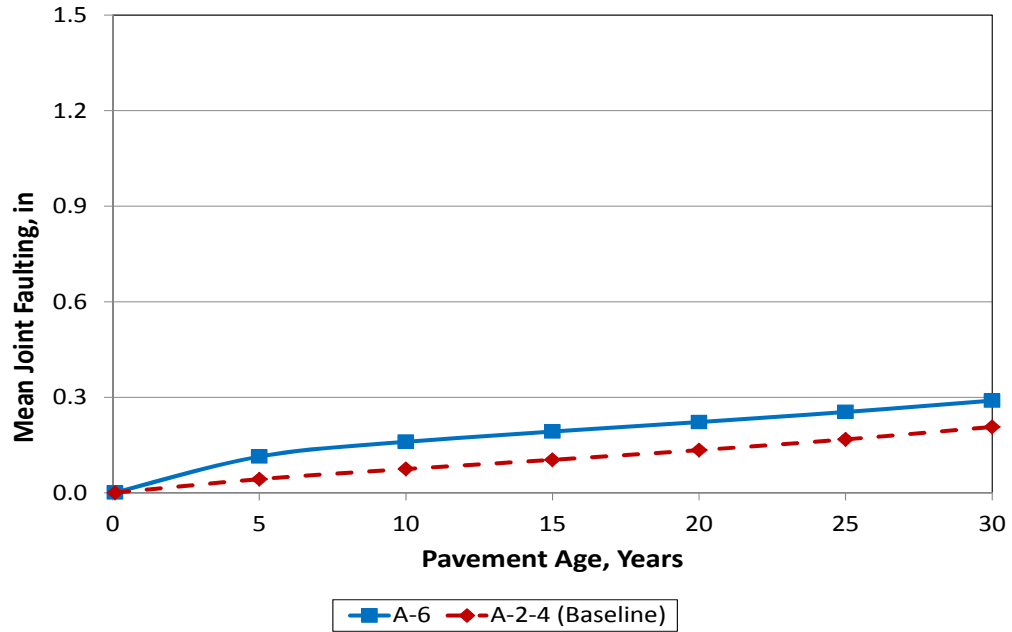


Figure 107. Effect of Subgrade Type on JPCP Mean Joint Faulting

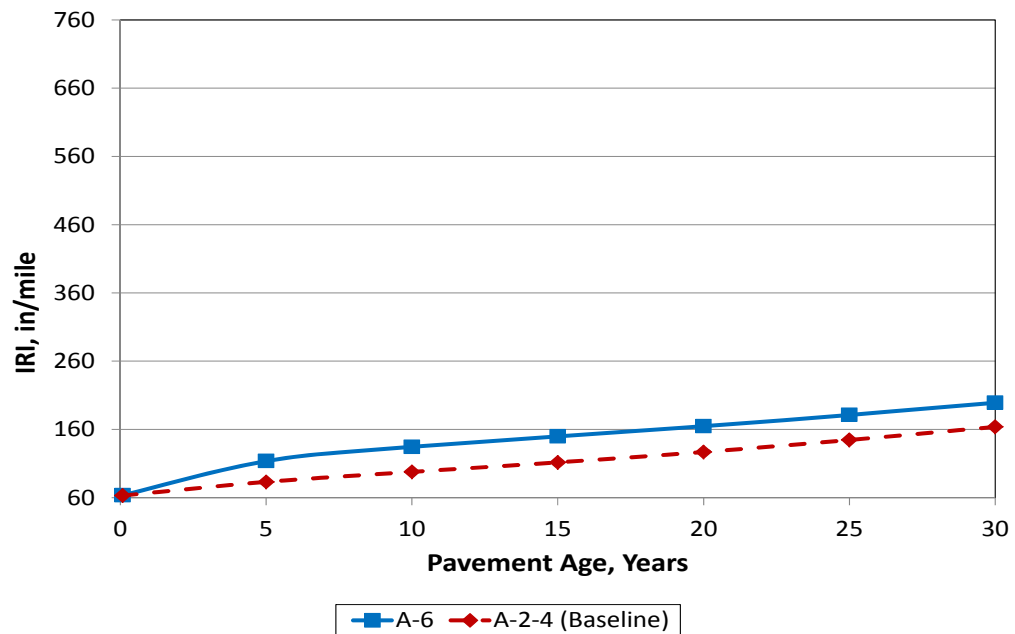


Figure 108. Effect of Subgrade Type on JPCP IRI

Effect of Climate

Figures 109 through 111 show the effect of climate on predicted distress and IRI. Climate ranges from Phoenix at an elevation of 1105 ft to Tucson at 2400 ft to Kingman at 3420 ft. Transverse fatigue cracking is significantly affected with the highest amount occurring in the Kingman climate due to an increased amount of large temperature gradients through the slab as compared to the warmer desert climates.

The figures show that climate has the most significant effect on cracking where the high elevation desert climate (represented by Kingman) was most detrimental due to large temperature gradients and low humidity. Climate had a minimal effect on doweled joint faulting and IRI. These trends are typical and as expected when compared to field pavement performance data from in-service JPCP located in different climates.

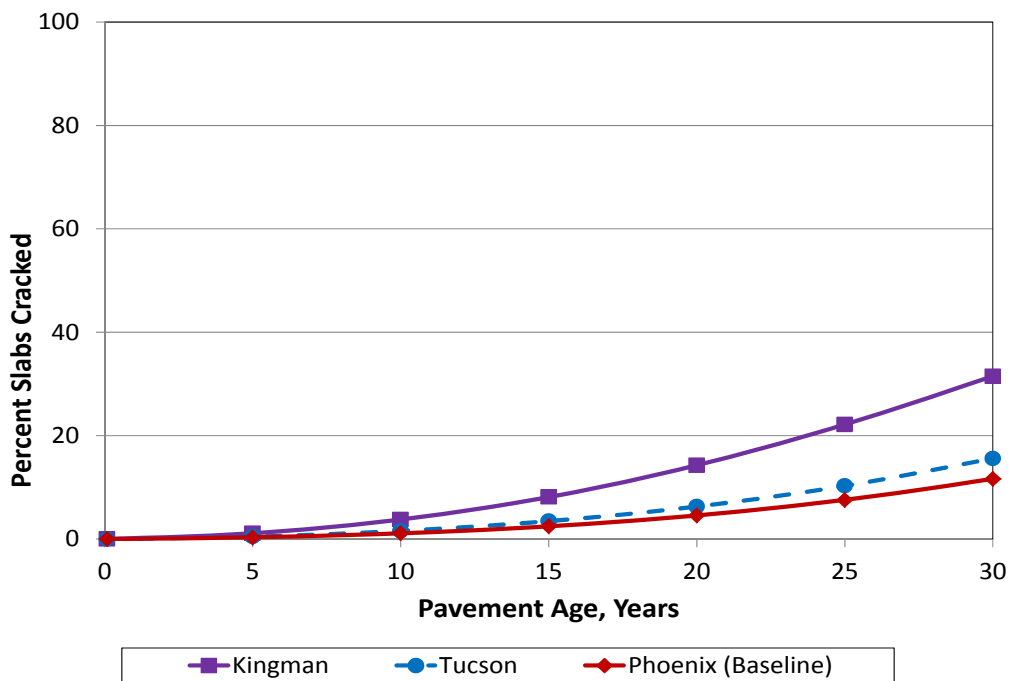


Figure 109. Effect of Climate on JPCP Transverse Cracking

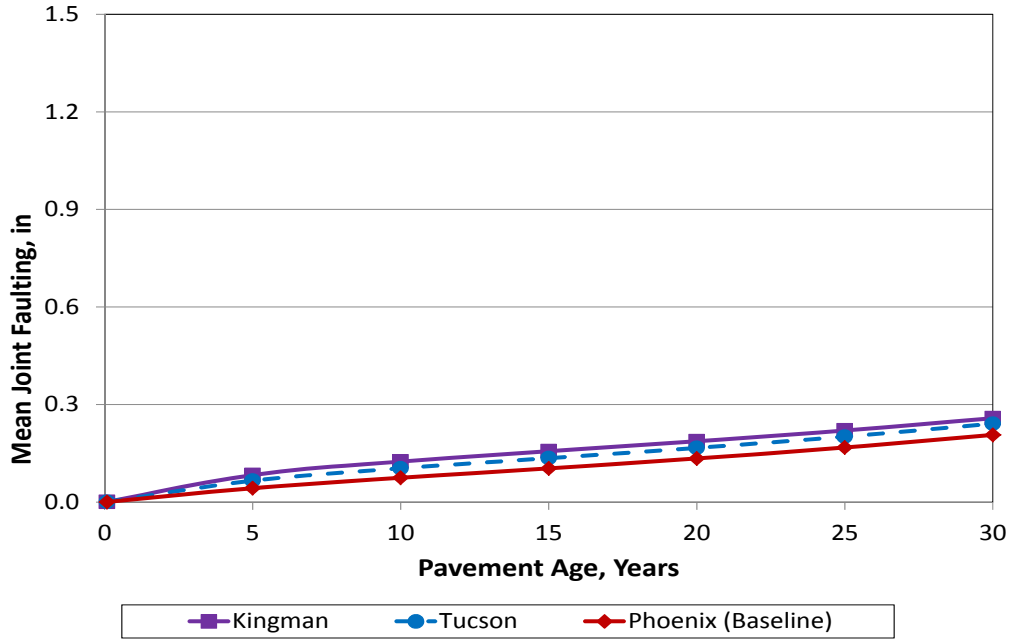


Figure 110. Effect of Climate on JPCP Mean Joint Faulting

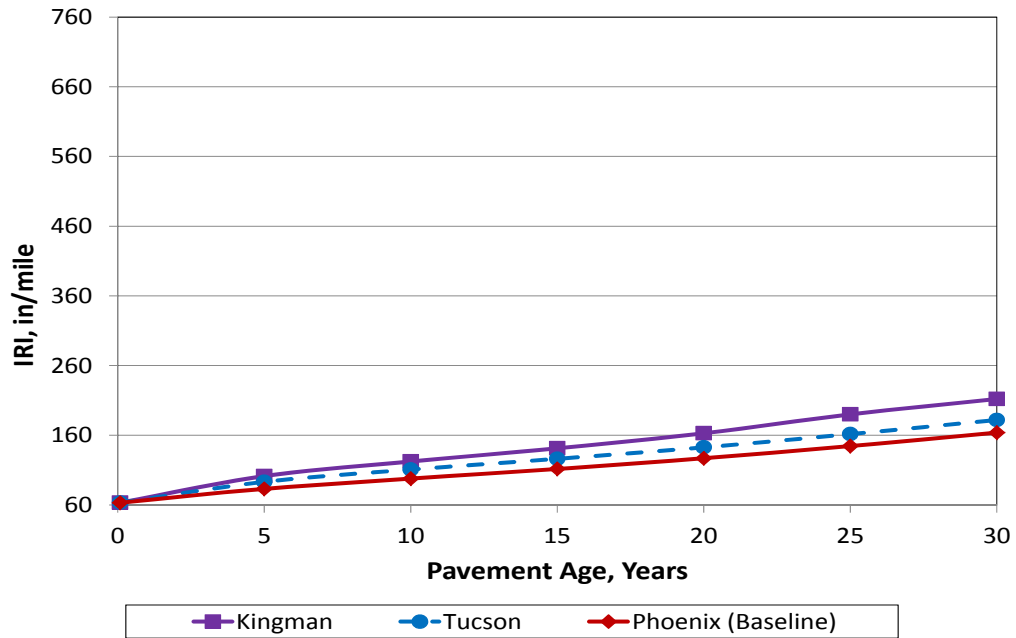


Figure 111. Effect of Climate on JPCP IRI

Effect of Reliability

Figures 112 through 114 show the effect of reliability on predicted distress and IRI. A level of design reliability of 50 percent indicates that the mean slab cracking, joint faulting, and IRI curve are being predicted. Thus, half of the projects designed should show higher cracking, faulting, and IRI, and half should show lower values.

As the design reliability increases to the 95 percent level, the 95 percent curve increases, indicating that 95 of 100 JPCP sections would show this amount or less of cracking, faulting, and IRI. The standard deviation associated with calculating the reliability curves is based on the SEE of the calibration data associated with models. The higher the error, the greater the spread of these curves from 50 to 95 percent for any example.

The results show that the design reliability curve for 95 percent is higher than any lower level of reliability. The consequence for design at higher and higher levels of reliability is that a thicker pavement, larger dowels, or higher support base course will be needed to meet the design reliability requirements.

An overall review of the sensitivity analysis results indicates that DARWin-ME model prediction is consistent with expected trends from empirical observations and pavement engineering theory. The sensitivity analysis provides information about the inputs that have the most impact on pavement deterioration, which this information is useful to design engineers for developing cost-effective designs.

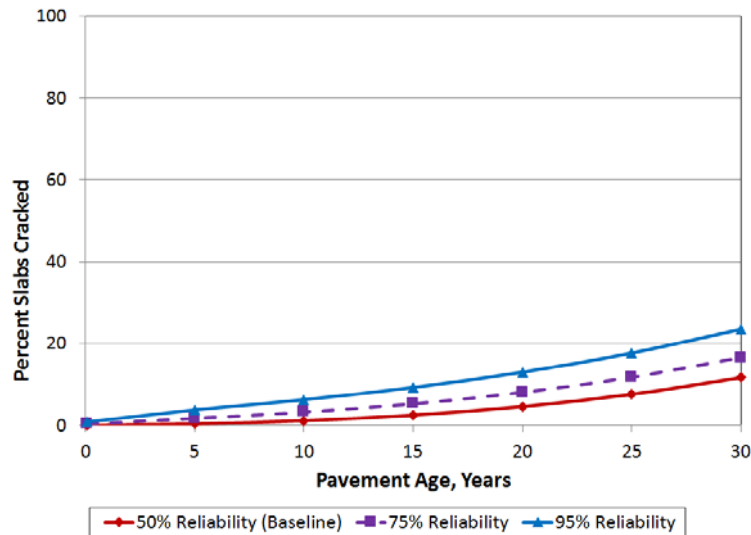


Figure 112. Effect of Reliability on JPCP Transverse Cracking

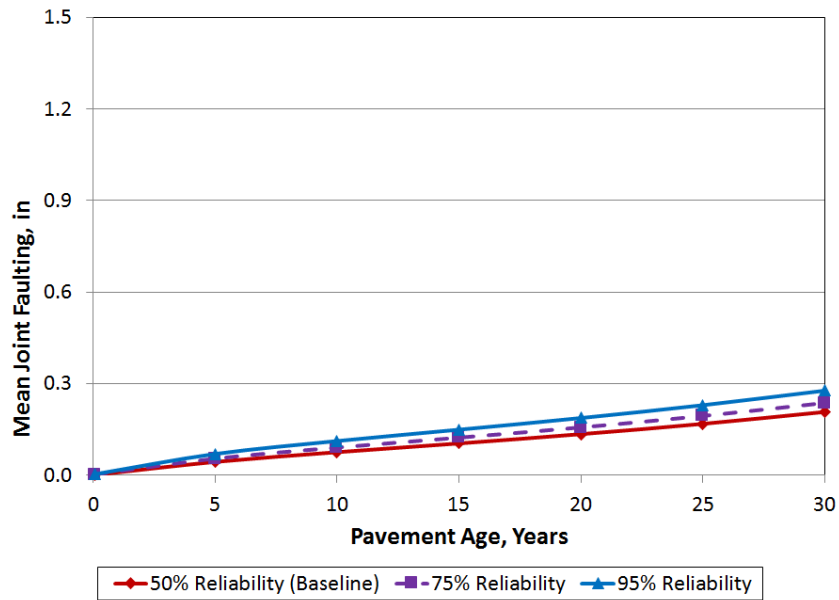


Figure 113. Effect of Reliability on JPCP Mean Joint Faulting

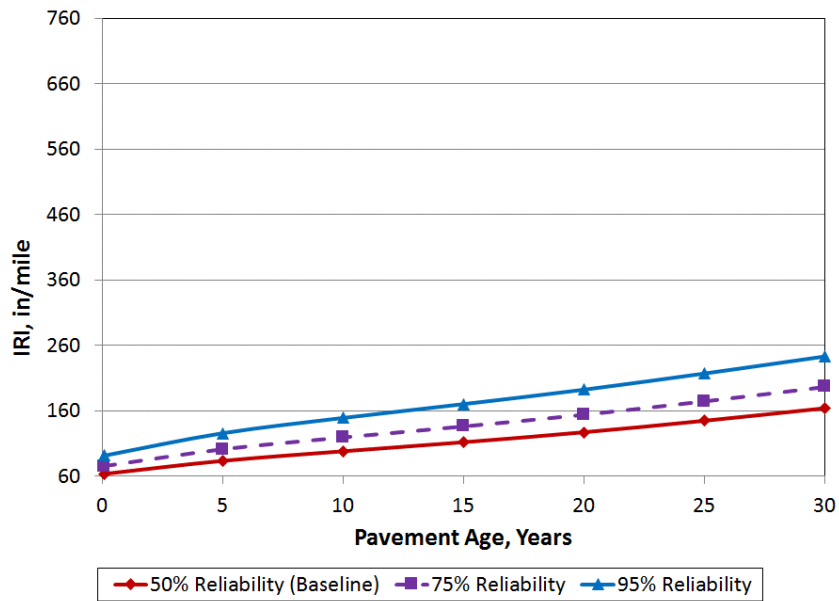


Figure 114. Effect of Reliability on JPCP IRI

CHAPTER 5. VALIDATION OF LOCALLY CALIBRATED DARWin-ME NEW HMA AND JPCP DESIGN PROCEDURES FOR ARIZONA

The Arizona locally calibrated DARWin-ME new HMA and JPCP design procedures were further validated through direct comparison of designs obtained using the *Materials Preliminary Engineering and Design Manual* (ADOT 1989) and the locally calibrated ADOT DARWin-ME. Since DARWin-ME is a far more efficient design tool regarding design optimization, some differences are expected in designs developed using the two different procedures. However, the differences are not expected to be extremely significant.

Pavement designs were developed for two typical ADOT HMA and JPCP projects (obtained from the calibration database). Before comparing the designs, they were evaluated for reasonableness (i.e., if the designs had performed as expected) as follows:

- Performed as expected (i.e., little or no indications of distress after 20 to 30 years of service). For these pavements, new designs developed by the ADOT Pavement Design Guide and ADOT DARWin-ME are expected to be similar to the existing in-service pavements.
- Exhibited early failures (i.e., high levels of distress within 10 to 15 years of a 20- to 30-year design). For these pavements, new designs developed by the ADOT Pavement Design Guide and ADOT DARWin-ME are expected to be an improvement over the existing pavement design (e.g., thicker HMA and PCC layers).

Results are presented in the remainder of this chapter.

NEW HMA PAVEMENT DESIGN COMPARISON

Project Description

Inputs for the new HMA pavement design comparisons were adapted from a project on I-40 near Holbrook, Arizona. This project has HMA over a 10-inch aggregate base placed over an A-6 subgrade.

For this reconstructed project, the researchers established a trial design based on the site, structure, materials, and other properties of the existing pavement (Figure 115). A design period of 20 years was selected based on current ADOT new HMA pavement design practices. Table 42 presents key inputs for both the *Materials Preliminary Engineering and Design Manual* (ADOT 1989) and the locally calibrated ADOT DARWin-ME.

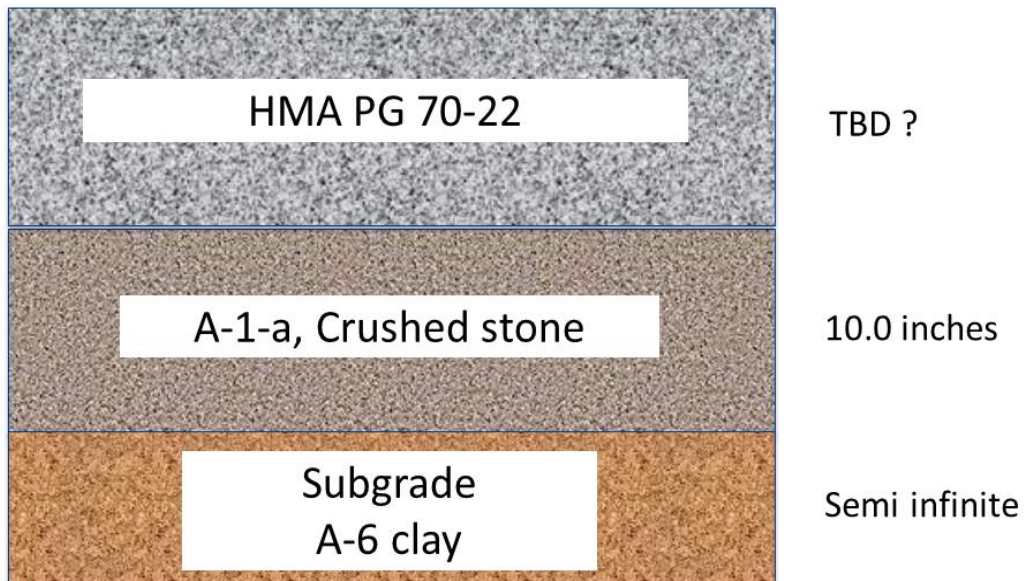


Figure 115. New HMA Project Trial Design Structure
(TBD? = to be determined during design)

Table 42. Key Inputs for New HMA Pavement Project Design Comparison

Input Category	Input Variables	Inputs for <i>Materials Preliminary Engineering and Design Manual</i>	Inputs for Locally Calibrated ADOT DARWin-ME
Structure and materials type and properties	HMA	ADOT AC ½-inch mix (Layer coefficient: 0.44)	Binder grade: PG 70-22 Binder content: 11.3% Air voids: 6%
	Aggregate base	Layer coefficient: 0.14 Drainage coefficients: 0.9	AASHTO Soil Class: A-1-a Aggregate base resilient modulus: 34,000 psi
	Subgrade (AASHTO Soil A-6)	Subgrade resilient modulus @ in situ moisture content (8000 psi)	Subgrade resilient modulus @ optimum moisture content (14900 psi)*
Design	Design period	20 years	20 years
	Design reliability	97%	97%
Traffic	Initial AADTT	7200	7200
	Directional distribution	0.5	0.5
	Lane distribution	0.8	0.8
	Truck growth	3% compound	3% compound
	Cumulative ESAL	37.76 million	—
	Cumulative trucks	—	28.27 million
Performance criteria	Design reliability	97%	97%
	Initial serviceability	4.2	—
	Terminal serviceability	3.0	—
	Overall standard deviation	0.35	—
	Initial IRI (inch/mi)	—	40
	Terminal IRI (inch/mi)	—	150
	Alligator cracking (%)	—	10
	Total rutting (inch)	—	0.55

*The laboratory resilient modulus tests are performed on representative samples in stress and moisture conditions simulating those of the primary moisture seasons (AASHTO 1993). On the other hand, MEPDG requires resilient modulus at optimum moisture and maximum dry density conditions. Therefore, a correction was applied to the laboratory optimum resilient modulus to estimate resilient modulus at field in situ conditions.

Design Analysis

The researchers used DARWin 3.1 software (software version of the AASHTO *Guide for Design of Pavement Structures* [1993]) and AASHTO DARWin-ME in the design analysis. Both software inputs and calibration coefficients were modified as needed to be compatible with the *Materials*

Preliminary Engineering and Design Manual (ADOT 1989) and the locally calibrated pavement models. The trial designs were run for 20 years. The results are presented in Table 43. Figures 116 through 118 show predictions of alligator cracking, total rutting, and IRI from the local DARWin M-E models.

The locally calibrated DARWin-ME procedure produced a thinner pavement section (HMA thickness of 12.25 inch) when compared to the current ADOT pavement design procedure (HMA thickness = 11.0 inch). Based on the design produced, the researchers concluded that the locally calibrated DARWin-ME models and design procedure produce reasonable new HMA pavement designs for this high level of truck traffic.

Table 43. Trial Design Results for New HMA Pavement Projects

Key Variables	<i>Materials Preliminary Engineering and Design Manual</i>	Locally Calibrated ADOT DARWin-ME
Required structural number	6.66	—
Design equivalent single axle loads (ESALs)	37.76 million	37.76 million
Cumulative trucks	—	28.27 million
Reliability	97%	97%
Subgrade R-value (M_R)	8000 psi	14,900 psi
Aggregate base thickness	10 inches	10 inches
Design HMA thickness	12.25 inches	11 inches

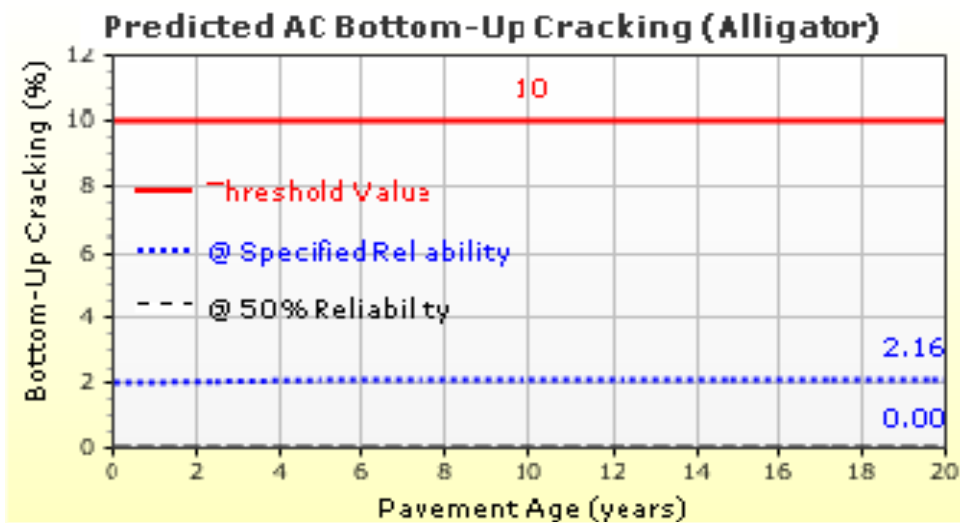


Figure 116. Predicted Alligator Cracking for the New HMA Trial Design Using DARWin-ME

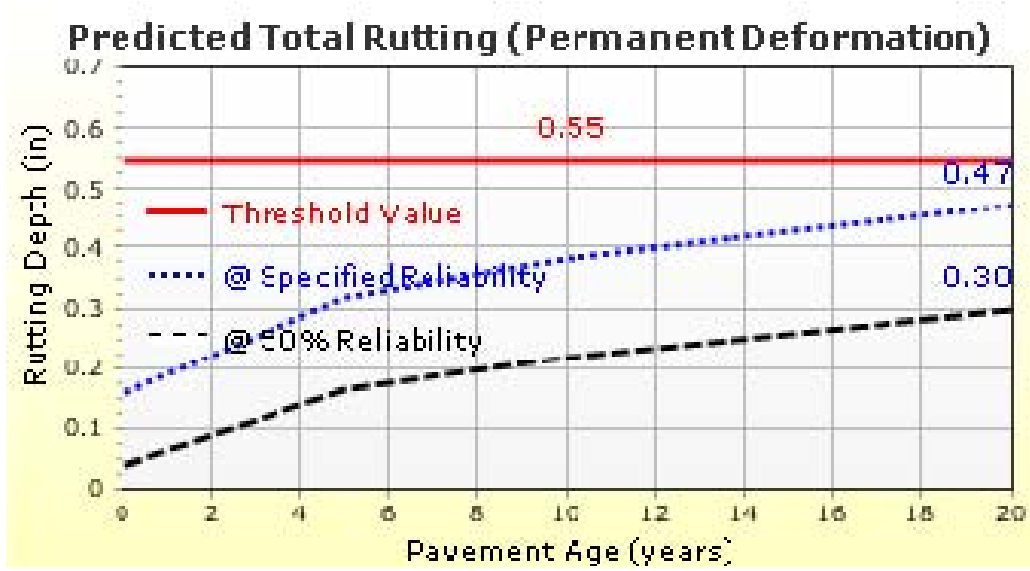


Figure 117. Predicted Rutting for the New HMA Trial Design Using DARWin-ME

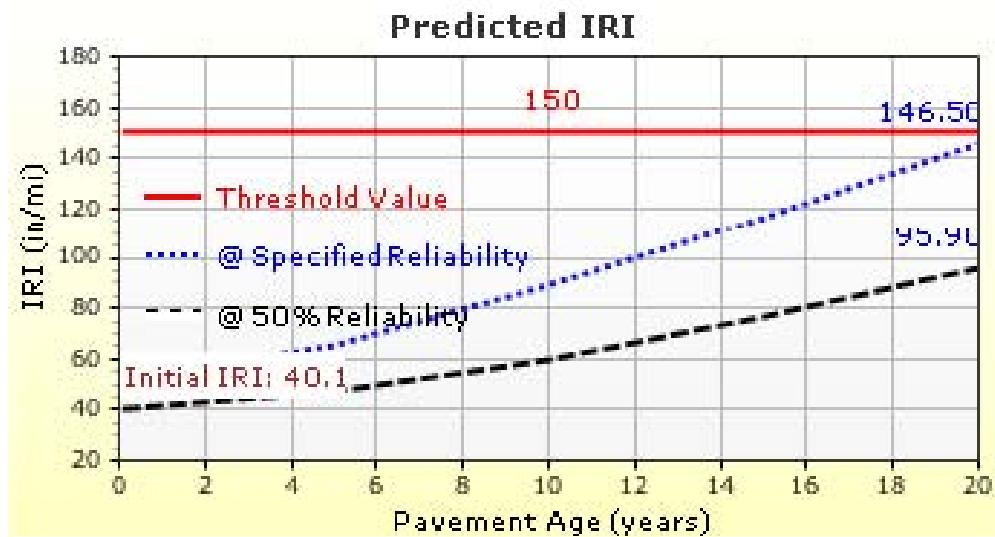


Figure 118. Predicted IRI for the New HMA Trial Design Using DARWin-ME

NEW JPCP DESIGN COMPARISON

Project Description

Inputs for the new JPCP design comparisons were adapted for a project on I-10 west of Phoenix. The section consists of JPCP over a 6-inch aggregate base placed over an A-2-4 subgrade.

For the redesign of this project, the researchers also established a trial design based on the site, structure, materials, and other properties of the existing pavement (Figure 119). A 30-year design period was selected based on current ADOT new HMA pavement design practices. Table 44 presents the key inputs for both the *Materials Preliminary Engineering and Design Manual* (ADOT 1989) and the locally calibrated ADOT DARWin-ME.

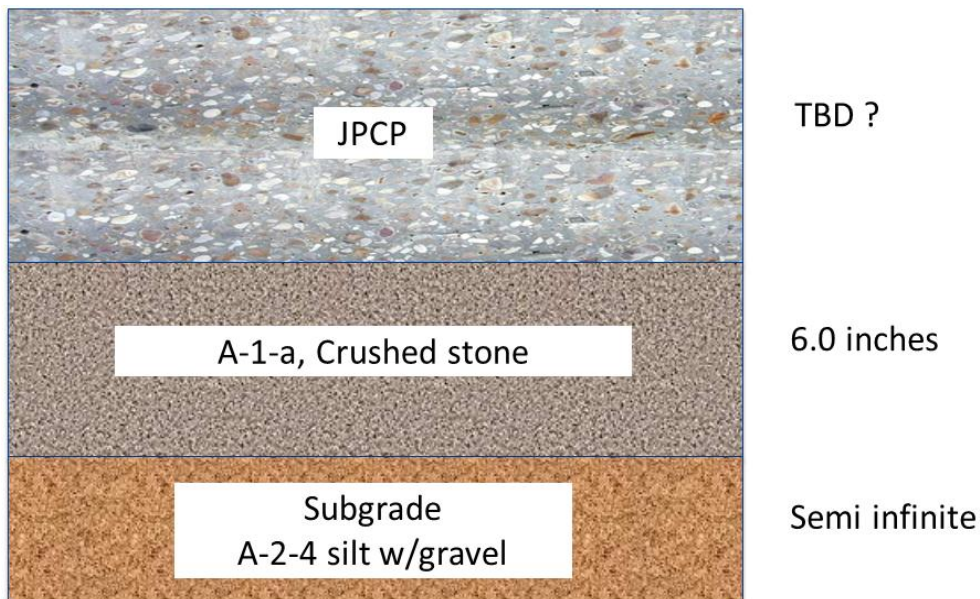


Figure 119. New JPCP Project Trial Design Structure
(TBD? = slab thickness to be determined during design)

Design Analysis

The researchers also used DARWin 3.1 software (software version of the 1993 AASHTO *Guide for Design of Pavement Structures*) and DARWin-ME in this design analysis, and modified both

software inputs and calibration coefficients as needed to be compatible with the *Materials Preliminary Engineering and Design Manual* (ADOT 1989) and the locally calibrated pavement models. Since this is a very heavily trafficked highway, both current Arizona and the DARWin-ME require dowels. The trial designs were run for 30 years. Results are presented in Table 45. Figures 120 through 122 show predictions of transverse slab cracking, faulting, and IRI from the local DARWin M-E models.

The doweled JPCP designs produced from the *Materials Preliminary Engineering and Design Manual* (ADOT 1989) show a 14.75-inch PCC thickness. The locally calibrated DARWin-ME for Arizona produced a doweled 11-inch PCC thickness. This considerably lower PCC thickness was attributed to DARWin-ME model's ability to better optimize designs (material properties and design features). The results presented show that the locally calibrated DARWin-ME models and design procedure do produce reasonable designs for Arizona if the right combination of material inputs and design features is selected.

Table 44. Key Inputs for New JPCP Project Design

Input Category	Input Variables	Inputs for <i>Materials Preliminary Engineering and Design Manual</i>	Inputs for Locally Calibrated ADOT DARWin-ME
Structure and materials type and properties	PCC	28-day flexural strength: 672 psi* 28-day elastic modulus: 4,286,826 psi*	28-day flexural strength: 672 psi* 28-day elastic modulus: 4,286,826 psi* CTE: $4.5 \times 10^{-6} / ^\circ \text{F}$
	Aggregate base	—	Aggregate base (AASHTO A-1-a) Resilient modulus @ optimum moisture content = 34,000 psi
	Subgrade	Modulus of subgrade reaction (k-value): 197 psi/inch	Subgrade type (AASHTO A-2-4) Resilient modulus @ optimum moisture content = 19,600 psi
Design	Joint spacing (ft)	13, 15, 17, 15	15
	Dowel size (inch)	1.50	1.50
	Slab width (ft)	12	12
	Tied shoulder	Yes	Yes, 50% LTE
	Design J factor	2.8	N/A
	Design reliability	97%	97%
	Drainage coefficient	1.0	—
Traffic	Design period	30 years	30 years
	Two-way initial AADTT	10,000	10,000
	Directional distribution	0.5	0.5
	Lane distribution	0.8	0.8
	Truck growth	3% compound	3% compound
	Cumulative ESAL	127.8 million	—
	Cumulative trucks	—	69.51 million
Performance criteria	Initial serviceability	4.2	—
	Terminal serviceability	3.0	—
	Overall standard deviation	0.25	—
	Initial IRI (inch/mi)	—	60
	Terminal IRI (inch/mi)	—	150
	Transverse cracking (%)	—	10
	Joint faulting (inch)	—	0.12

*Computed based on a 28-day compressive strength of 5000 psi.

Table 45. Trial Design Results for New JPCP Project Design

Key Variables	Materials Preliminary Engineering and Design Manual	Locally Calibrated ADOT DARWin-ME
Design ESALs	128 million	128 million
Cumulative trucks	—	69.5 million
Dowel size	Dowelled (J = 2.8)	1.25 inch
Reliability	97%	97%
Aggregate base thickness	6 inch	6 inch
Design PCC thickness	14.75 inch	11 inch

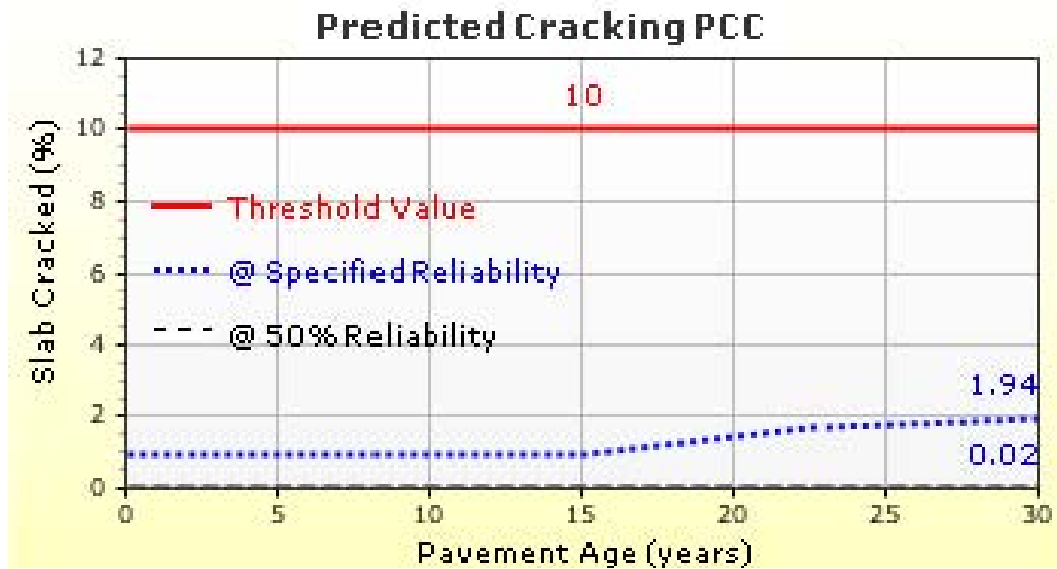


Figure 120. Predicted Transverse Cracking for the New JPCP Trial Design Using DARWin-ME

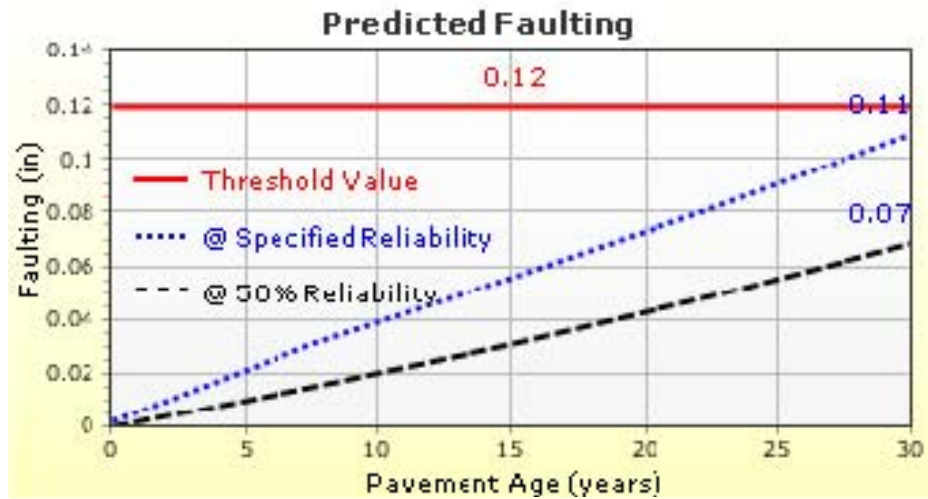


Figure 121. Predicted Faulting for the New JPCP Trial Design Using DARWin-ME

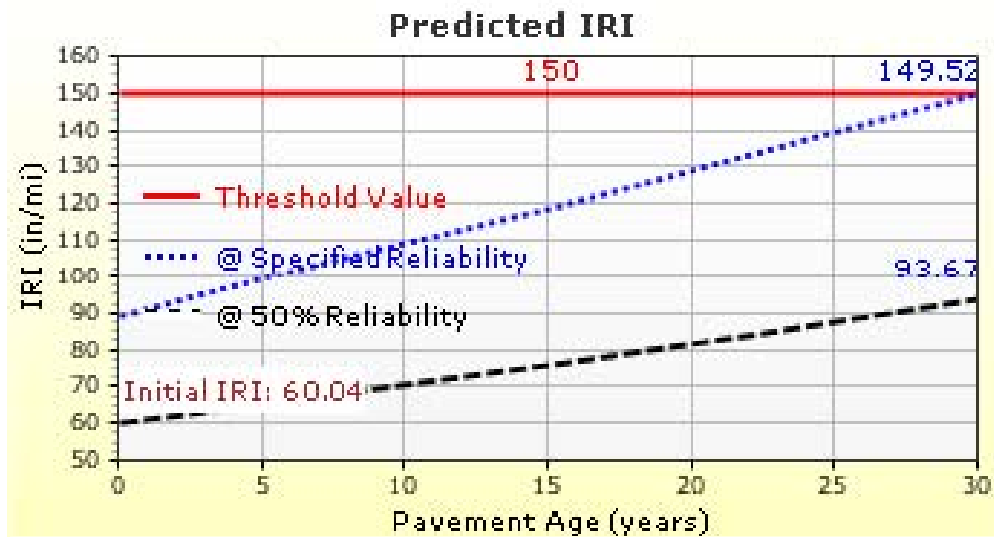


Figure 122. Predicted IRI for the New JPCP Trial Design Using DARWin-ME

CHAPTER 6. PRACTICAL METHODOLOGY TO RECALIBRATE DARWin-ME

The local calibration documented in this report addresses key distresses and IRI associated with HMA (and HMA overlays) and JPCP pavements in Arizona. Low temperature cracking of HMA pavements could not be calibrated at this time, however, and should be further studied and calibrated in the near future. Transverse fatigue cracking in ARFC/JPCP was validated using the calibrated JPCP model. Two sections of CRCP and ARFC/CRCP were evaluated, and results showed no reason not to use the global models at this time. In the future, ADOT may wish to conduct further verifications, calibrations, and validations, including:

- Reverification of the local Arizona distress and IRI models that were addressed under this contract using additional updated performance data or other performance data that becomes available.
- Additional verification and calibration of ARFC/JPCP models for other distresses and IRI.
- Calibration of other pavement structures including unbonded JPCP overlays, diamond grinding projects, or HMA pavement full depth reclamation projects.

The AASHTO *Guide for the Local Calibration of the Mechanistic-Empirical Pavement Design Guide* (2010) provides a comprehensive methodology for recalibrating the DARWin-ME models. The guide presents a detailed, 11-step roadmap for highway agencies to use for local calibration:

- Step 1—Select hierarchical input levels.
- Step 2—Develop experimental factorial design and matrix or sampling template.
- Step 3—Estimate minimum sample size (number of pavement projects) required for each distress/IRI prediction model validation and local calibration.
- Steps 4—Select projects to populate sampling template.
- Step 5—Extract and assess distress and project data.
- Step 6—Conduct field and forensic investigations.
- Step 7—Assess local bias: validation of global calibration values to local conditions, policies, and materials.
- Step 8—Eliminate local bias of distress and IRI prediction models.
- Step 9—Assess the standard error of the estimate.

- Step 10—Reduce standard error of the estimate.
- Step 11—Interpret results and determine adequacy of ADOT MEPDG locally calibrated models.

This process was adopted with modifications as needed for calibrating DARWin-ME for local Arizona conditions. The local calibration framework has been described throughout this report. This chapter describes the guide’s key aspects as adapted as a framework for future model recalibration or pavement calibration in Arizona. The framework presented may be used for future recalibration of the DARWin-ME models and design procedure for Arizona.

STEP 1: SELECT HIERARCHICAL INPUT LEVELS

The MEPDG allows for pavement design inputs (traffic, materials, climate, rehabilitation, etc.) to be obtained at three hierarchical levels as described in Chapter 2.

The AASHTO *Guide for the Local Calibration of the Mechanistic-Empirical Pavement Design Guide* (2010) recommends selecting a hierarchical input level (1, 2, or 3) that is consistent with a highway agency’s day-to-day practices for characterizing pavement design inputs and that is sensitive to predicted performance and thus designs. Recommended hierarchical levels for characterizing pavement materials properties, subgrade properties, and traffic for models recalibration are presented in Tables 46 and 47.

Table 46. Recommended DARWin-ME Hierarchical Input Levels for New HMA and HMA Overlaid Pavements

MEPDG Input Variable	Recommended Hierarchical Input Level
HMA thickness	Trial thickness
HMA CTE	Levels 2 and 3
HMA dynamic modulus	Level 3
HMA air voids in situ (at placement)	Level 3
Effective HMA binder content	Level 3
HMA creep compliance	Level 1
HMA tensile strength	Level 3
Base type/modulus	Level 2
Base thickness	Level 1
Subgrade type/modulus	Level 1
Groundwater table	Level 3
Climate	Level 1
Truck volume	Level 2
Truck axle load distribution	Level 2
Tire load, contact area, and pressures	Level 3
Truck speed	Level 3
Truck wander	Level 3
Initial IRI	Level 2

Table 47. Recommended DARWin-ME Hierarchical Input Levels for New JPCP

MEPDG Input Variable	Recommended Hierarchical Input Level
PCC thickness	Trial selected
PCC modulus of rupture and elasticity	Levels 2 and 3
PCC CTE	Levels 1 and 2
Joint spacing	Level 1
Lane to PCC shoulder long-term LTE	Level 3
Edge support	Level 1
Permanent curl/warp	Level 3
Base type	Level 1
Climate	Level 1 Weather Station
Subgrade type/modulus	Level 1
Truck axle load distribution	Level 2
Truck volume	Level 2
Tire pressure	Level 3
Truck lateral offset	Level 3
Truck wander	Level 3
Initial IRI	Level 2

STEPS 2 AND 3: DEVELOP EXPERIMENTAL DESIGN AND SAMPLING NEEDS

Experimental Design

Step 2 develops a statistical experiment to verify whether the DARWin-ME global models and procedure are adequate for Arizona local conditions and practices, and to calibrate the global models if they are inadequate. To meet these objectives:

1. Define the problem: pavement types and models.
2. Define the population: project locations, materials, site, and design features.
3. Determine the sampling needs and extent: Use statistical procedures presented in the *AASHTO Guide for the Local Calibration of the Mechanistic-Empirical Pavement Design Guide* (2010).
4. Establish the experimental design based on the outcome of Steps 1 through 3.

Examples of the experiment design sampling template and required sampling size are presented in Tables 48 and 49.

Table 48. Sampling Template for New and Rehabilitated HMA Pavements

HMA Thickness (inches)	Granular Base Thickness (inches)*	Subgrade Type	
		Coarse-Grained Soils (AASHTO Class A-1 through A-3)	Fine-Grained Soils (AASHTO Class A-4 through A-7)
<8	<6	1	2
	≥6	3	4
≥8	<6	5	6
	≥6	7	8

*All projects had granular base. Note: An equivalent dense-graded aggregate base was assumed for permeable asphalt-treated bases (PATBs).

Table 49. Estimated Number of Pavement Projects Required for Validation and Local Calibration

Pavement Type	Distress/IRI	Distress/IRI Threshold (at 90% Reliability)	SEE	Minimum Projects Required for Validation and Local Calibration	Minimum Projects Required for Each Pavement Type (n)*
New HMA and HMA overlaid HMA	Alligator cracking	20% lane area	5.01%	16	18
	Transverse thermal cracking	Crack spacing >100 ft of 630 ft/mi	150 ft/mi**	18	
	Rutting	0.4 inch	0.107 inches	14	
	IRI	169 inches/mi	18.9 inches/mi	80	
New JPCP	Faulting	<0.15 inch	0.033 inch	21	21
	Transverse cracking	<10% slabs	4.52%	5	
	IRI	169 inches/mi	17.1 inches/mi	98	

* $n = \left(\frac{Z_{\alpha/2} \sigma}{E} \right)^2$, where $Z_{\alpha/2} = 1.601$ (for a 90 percent confidence interval), α = performance indicator

threshold (design criteria), and E = tolerable bias at 90 percent reliability (1.601*SEE).

**Estimated from other MEPDG implementation projects.

Note: In selecting the overall minimum number of required pavement HMA and JPCP projects, the performance indicator IRI was excluded because the accuracy of the IRI models depends very much on the accuracy of other pavement distress predictions. Sampling a vast number of projects to validate the IRI models is therefore unnecessary if the individual distress prediction models are considered accurate and reasonable.

STEPS 4 AND 5: SELECT HMA AND JPCP PAVEMENT PROJECTS TO POPULATE SAMPLING TEMPLATE, AND EXTRACT AND EVALUATE DISTRESS AND PROJECT DATA

To populate the sampling templates developed in Step 3, projects are selected based on recommendations from the AASHTO *Guide for the Local Calibration of the Mechanistic-Empirical Pavement Design Guide* (2010):

- Projects should be representative of Arizona pavement design and construction practices.
- Projects should be representative of typical pavement condition (i.e., poor, moderate, and good).
- Project age should span the range typical of Arizona practice (i.e., newly constructed, older existing, and rehabilitated).
- Projects must be located throughout the state.

In general, information about local calibration projects is obtained from research experiments and databases and state PMS databases. Criteria for final selection and inclusion into a project database for recalibration of the DARWin-ME models are availability of sufficiently detailed input data (traffic, materials, and construction) with details comparable to the hierarchical levels selected, and distress and IRI data in the formats required by the DARWin-ME models (or convertible to the formats without losing accuracy).

Once pavement selection is completed, pertinent project data are assembled in a project database to be used for recalibration. This effort requires completing a detailed record review, including a review of construction reports and design plans and reports; extracting historic traffic volumes and vehicle class and axle load distributions from traffic databases; and identifying and rectifying anomalies and errors in the assembled data.

STEP 6: CONDUCT FIELD AND FORENSIC INVESTIGATIONS

Projects that may be key to meeting the recalibration objective but lack all pertinent key data (such as PCC strength and CTE) may require a forensic investigation to evaluate the given project and collect additional data as needed to meet project objectives. Tasks performed as part of forensic investigations include windshield distress survey, manual/automated distress survey, nondestructive (FWD) deflection testing, and materials coring and lab texting/examination.

STEP 7: CHARACTERIZE BIAS AND GOODNESS OF FIT OF DARWin-ME GLOBAL MODELS USED UNDER ARIZONA CONDITIONS

Several methods (statistical or otherwise) may be used singly or in combination to verify the MEPDG global models for Arizona local conditions. Statistical methods are used if there was a

good distribution of measured distress and IRI; when measured distress is mostly zero, a nonstatistical approach to model validation is used, which consists of the following steps:

1. Execute the DARWin-ME for each selected pavement project and predict pavement distresses and IRI over a reasonable time period (typically 10 to 40 years).
2. Extract predicted distress and IRI data from the DARWin-ME outputs that match age of measured distress and IRI.
3. Perform statistical or nonstatistical analysis as appropriate to characterize bias and prediction capacity.
4. Determine suitability of the DARWin-ME global models for Arizona local conditions.

Details of the statistical or nonstatistical analysis as needed to verify model suitability are presented in the following sections.

Evaluate Model Prediction Capacity (Goodness of Fit)

The goodness of fit of a given DARWin-ME distress and IRI prediction model must be assessed by determining R^2 and SEE estimated using measured Arizona and DARWin-ME predicted distress and IRI data. Reasonableness of both diagnostic statistics is determined by comparing the Arizona diagnostic statistics with those obtained for the DARWin-ME global models using Arizona data. Nearly all of the calibrated models showed significant improvement in prediction. Engineering judgment must be used to determine the reasonableness of Arizona diagnostic statistics.

Models exhibiting a poor R^2 (i.e., R^2 significantly less than the values presented in Table 50 for the global models) or excessive SEE (significantly higher than the values presented in Table 50 for the global models) typically are considered inadequate for Arizona conditions.

Evaluate Model Bias

Bias is determined by performing linear regression using Arizona measured and DARWin-ME predicted distress and IRI, and performing the following two statistical hypothesis tests. A significance level, α , of 0.05 or 5 percent is typically assumed for all hypothesis testing.

- **Hypothesis 1: Paired t-test.** *This test determines whether the Arizona measured and DARWin-ME predicted distress and IRI represents the same population:*
 1. Assume the following null and alternative hypothesis:
 - a. H_0 : mean measured distress/IRI = mean predicted distress/IRI.
 - b. H_A : mean measured distress/IRI \neq mean predicted distress/IRI.

**Table 50. National Calibration under NCHRP 1-40D of
New HMA Pavement and New JPCP Model Statistics**

Pavement Type	Performance Model	Model Statistics		
		R ²	SEE	Number of Data Points (N)
New HMA	Alligator cracking	0.275	5.01%	405
	Transverse thermal cracking	Level 1*: 0.344 Level 2*: 0.218 Level 3*: 0.057	—	—
	Rutting	0.58	0.107 inch	334
	IRI	0.56	18.9 inches/mi	1926
New JPCP	Transverse slab cracking	0.85	4.52%	1505
	Transverse joint faulting	0.58	0.033 inch	1239
	IRI	0.60	17.1 inches/mi	163

*Level of inputs used for calibration.

2. Compute test p-value. (This can be done using many types of statistical software and spreadsheets such as MS Excel.)
 3. Evaluate results by comparing the computed p-value to the predetermined level of significance (i.e., 0.05).
 4. Interpret results: The null hypothesis H_0 will be rejected if p-value < 0.05. Rejecting H_0 implies that Arizona measured and DARWin-ME distress and IRI are essentially from different populations at the 5 percent significance level, which indicates bias in DARWin-ME predicted distress and IRI because the measured distress and IRI are considered to represent the ground truth for this test analysis.
- **Hypothesis 2: Slope of predicted and measured distress/IRI linear curve.** This test (which is only meaningful if hypothesis 1 was accepted) determines whether a linear regression model ($\text{predicted distress/IRI} = \alpha * \text{measured distress/IRI}$) has a slope (α) of 1.0 at the 5 percent significance level. The test is as follows:
 1. Using the results of the linear regression analysis, test the following null and alternative hypotheses to determine if the linear regression model slope is 1.0:
 - a. H_0 : model slope (α) = 1.0.
 - b. H_A : model slope (α) \neq 1.0.

2. Compute test p-value. (This can be done using many types of statistical software and spreadsheets such as MS Excel.)
3. Evaluate results by comparing computed p-value to the predetermined level of significance for this test (i.e., 0.05).
4. Interpret results: The null hypothesis H_0 is rejected if p-value < 0.05 . Rejecting H_0 implies that the linear model has a slope significantly different from 1.0 at the 5 percent significance level, which indicates that using the DARWin-ME global models outside of the range of Arizona measured distress and IRI will produce biased predictions.

The presence of bias does not necessarily imply that the DARWin-ME global models are defective. It simply means that there is some bias in predicted distress and IRI values when the DARWin-ME is used under Arizona conditions.

Global DARWin-ME models that are biased or have an inadequate prediction capacity or goodness of fit need local calibration according to the procedure in Step 8.

STEP 8: PERFORM LOCAL CALIBRATION TO REDUCE BIAS AND IMPROVE GOODNESS OF FIT

Local calibration uses both linear and nonlinear regression procedures:

1. Split the assembled pavement projects data into two separate databases for calibration and validation. Typically a 90/10 percent split is adopted. A 90/10 percent split implies approximately 90 percent of all projects will be used to create a local calibration database while the remaining 10 percent of projects will be used to create a validation database. Projects must be selected at random while maintaining a general balance of pavement type, design features, material properties, traffic, construction year, location/climate, and so on. In essence the 10 percent validation database must represent the same population as the 90 percent calibration database.
2. Perform a preliminary or tentative local calibration of the DARWin-ME models using the 90 percent local calibration as follows:
 - a. Run the DARWin-ME for all projects in the 90 percent local calibration database.
 - b. Assemble critical DARWin-ME inputs (HMA thickness); DARWin-ME outputs (predicted damage, distress, and IRI); and measured distress and IRI required for local calibration in an optimization database.
 - c. Determine DARWin-ME models calibration coefficients that can be modified as part of the local calibration. (See appendix.)

- d. Perform optimization using linear and nonlinear regression techniques as needed to select local calibration coefficients that maximize R^2 , minimize SEE, and eliminates bias.
3. Validate the tentative locally calibrated MEPDG models as follows:
 - a. Run the DARWin-ME for all projects in the 10 percent validation database using the local calibration coefficients previously determined.
 - b. Assemble critical DARWin-ME inputs (HMA thickness); DARWin-ME outputs (predicted damage, distress, and IRI); and measured distress and IRI required for local calibration in an optimization database.
 - c. Determine goodness of fit and presence or absence of bias.
 4. Modify the tentative locally calibrated DARWin-ME models as needed until an adequate model/solution is obtained (i.e., reasonable goodness of fit and no bias).
 5. Develop final locally calibrated DARWin-ME models using 100 percent of all projects.

Once local calibration is complete (DARWin-ME's local calibration coefficients are adjusted), users must decide whether to develop new standard error models for use in reliability analysis.

In general if a small data set is used in local calibration, the global standard error models must be left unchanged as there is not sufficient data to characterize models' standard error. However, with larger datasets, developing new standard error models is recommended (guidance provided in the AASHTO *Guide for the Local Calibration of the Mechanistic-Empirical Pavement Design Guide* [2010]).

STEPS 9 THROUGH 11: ASSESS AND REDUCE STANDARD ERROR, AND INTERPRET RESULTS AND DETERMINE ADEQUACY OF LOCALLY CALIBRATED DARWin-ME MODELS

The final steps are to determine if the new local models meet engineering expectations by performing a comprehensive sensitivity analysis and design comparisons with existing ADOT pavement designs or in-service pavements. The standard error provides an overall assessment of the ability to predict the distress or IRI. It should be compared to the national or global standard error. The local calibration standard error may be lower than the global value, however, and that may be reasonable, but be careful to not accept too low of value that results in an inadequate structural design.

Sensitivity Analysis

Sensitivity analysis involves the following steps:

1. Develop a baseline pavement design (a typical ADOT pavement design that reflects current and future design and construction practices along with site conditions).
2. Identify key DARWin-ME inputs (e.g., thickness, strength, traffic volume and climate).
3. Determine typical mean and likely range of key inputs. The typical mean values are used in the baseline design.
4. Run the DARWin-ME software for the baseline design.
5. Run the DARWin-ME software changing each key input value individually within the likely range of values.
6. Characterize change in distress and IRI values as the key input values change from the mean.
7. Evaluate change in distress and IRI for reasonableness. (Does it meet engineering expectations?)

If the change in distress and IRI meets engineering expectations, then the locally calibrated models are considered reasonable. Otherwise, the models' local coefficients may need to be further adjusted to make predictions more reasonable.

Design Comparisons

Design comparisons involve using the new locally calibrated models within DARWin-ME to produce typical ADOT designs and determining if the new designs meet engineering expectations. Existing ADOT designs or information from as-constructed pavements in Arizona can be used for these comparisons. Again, if the new DARWin-ME designs do not meeting engineering expectations (HMA or PCC sections are too thin or too thick), it may be necessary to adjust the design reliability levels.

CHAPTER 7. ARIZONA INPUT DEFAULTS AND CALIBRATION COEFFICIENTS FOR MEPDG

This chapter summarizes the information related to Arizona pavement site conditions, materials, design features, and construction practices gathered for the ADOT DARWin-ME implementation effort. Data were gathered from various sources, including ADOT construction quality assurance/quality control (QA/QC) databases and LTPP.

DEFAULT LEVEL 3 INPUTS

HMA Materials

Default Level 3 inputs (HMA gradation, in-situ air voids, effective volumetric binder content, and unit weight) for HMA materials were developed from ADOT’s QA/QC databases. These inputs were computed from more than 300 lab and field measured data, including distributions, mean, ranges, and standard deviation. The computed defaults are presented in Table 51.

PCC Materials

Default Level 3 inputs (compressive strength, flexural strength, elastic modulus, CTE, and mixture constituents) for PCC materials inputs were developed from LTPP materials databases. The PCC defaults were computed using lab measured data from the LTPP GPS experiments, which is more representative of ADOT practices. A summary of the computed defaults are presented in Tables 52 through 56.

Table 51. Default Level 3 Inputs for HMA Materials

Material	ADOT Material Designation	Gradation (%)				In situ Air Voids (%)	Unit Weight (pcf)	Effective Binder Content (%)
		Passing ¾-inch Sieve	Passing ⅜-inch Sieve	Passing No. 4 Sieve	Passing No. 200 Sieve			
1/2-inch HMA mix	M 12	100.0	79.2	51.3	4.3	7.7	139.8	11.9
	M 12F	100.0	82.2	59.8	4.1	7.7	138.7	12.6
	M 12K	100.0	78.9	49.5	4.6	7.3	141.9	11.1
3/4-inch HMA mix	M 34	97.6	73.1	55.8	4.4	7.6	141.9	10.8
	M 34A	98.3	72.7	54.2	4.3	7.0	142.0	11.3
	M 34B	99.8	77.3	60.8	4.9	7.5	138.1	10.7
	M 34F	98.9	73.7	58.7	4.3	6.9	142.0	11.4
	M 34K	99.1	67.4	43.0	4.7	6.8	144.8	10.0
	M 34KA	99.2	69.4	42.0	4.3	7.0	146.3	8.9
	M 34KB	98.0	67.8	43.8	4.5	6.7	154.5	4.6
ATB mix	M BM	92.9	67.4	51.5	3.8	6.9	143.1	10.9
Road mix	M RD	100.0	71.5	36.3	2.5	7.9	134.0	15.0
ACFC	ACFC	100	99	41.1	1.48	—	—	—
AR-ACFC	AR-ACFC	100	99	37.7	1.4	—	—	—
RF	RF	100	99	35	0.9	—	—	—

Table 52. Default Level 3 PCC Compressive Inputs

SHRP ID	Test No.	Compressive Strength (Long Term) (psi)	Compressive Strength (28 days) (psi*)
0601	1	5,540	3,847
0601	2	7,040	4,889
0603	1	6,070	4,215
0603	2	6,800	4,722
0604	1	6,170	4,285
0604	2	8,310	5,771
0605	2	5,440	3,778
0607	2	5,810	4,035
0608	1	6,620	4,597
0608	2	6,930	4,813
0659	2	6,800	4,722
0660	1	6,020	4,181
0662	1	5,450	3,785
0662	2	8,210	5,701
7079	1	6,460	4,486
7079	2	7,110	4,938
7614	1	6,020	4,181
7614	2	5,090	3,535
Average		6,438	4,471

*Converted using DARWin-ME strength growth relationship.

Table 53. Default Level 3 PCC Flexural Strength Inputs

Project ID	Route ID	Compressive Strength (28 days) (psi)	Unit Weight (lb/yd ³)	Water/Cement Ratio	Cementitious Materials (lb)
H087502C	L202	5090	147	0.47	581
H323002C	L101	4900	149	0.46	586
H406001C	L101	5307	152	0.47	581
H458401C	I-40	4664	148	0.49	595
H473301C	L101	5280	148	0.48	588
H484501C	L101	5217	N/A	N/A	N/A
H538101C	L202	5707	150	0.36	586
H575601C	L101	5513	149	0.47	581
H591501C	L202	4988	150	0.40	581
H601401C	I-10	5383	151	0.40	581
Mean		5205	149	0.44	584

Note: These are current PCC strength values since incentives were introduced.

Table 54. Default Level 3 PCC Elastic Modulus Inputs

SHRP ID	Test No.	Poisson Ratio	Unit Weight (pcf)	Elastic Modulus (Long Term) (psi)	Elastic Modulus (28-day) (psi)
7079	1	0.21	145	4,150,000	3,458,333
7079	2	0.10	149	3,750,000	3,125,000
7613	1	0.26	145	3,400,000	2,833,333
7613	2	0.12	149	4,850,000	4,041,667
7614	1	0.13	147	4,000,000	3,333,333
7614	2	0.10	149	4,900,000	4,083,333
Average		0.15	147	4,175,000	3,479,167

Table 55. Default Level 3 PCC CTE Inputs

SHRP ID	CTE (° F/° F/inch)	Coarse Aggregate Type	Mean CTE (° F/° F/inch)
0213	4.8	Granite	4.78
0214	4.8	Granite	
0215	4.5	Granite	
0216	4.42	Granite	
0217	4.8	Granite	
0218	4.8	Granite	
0219	4.8	Granite	
0220	4.8	Granite	
7613	4.63	Granite	
7614	5.5	Granite	
0221	4.4	Limestone	4.4
0222	4.4	Limestone	
0223	4.4	Limestone	
0224	4.4	Limestone	

Note: These are the corrected CTE values obtained from the FHWA laboratory.

Table 56. Default Level 3 PCC Mixture Constituents Inputs

SHRP ID	Coarse Content (lb/yd ³)	Fine Content (lb/yd ³)	Cement Content (lb/yd ³)	Water Content (lb/yd ³)	Water-to-Cement Ratio
7079	1311	1809	706	283	0.40
7614	1858	1265	513	240	0.47

Chemically Treated Aggregate (Cement Aggregate Mixture) Base Materials

Default Level 3 inputs (elastic modulus) for key cement aggregate mixture materials (used as cement-treated bases) were developed from only a few pavement projects available in the LTPP materials database. These computed defaults are presented in Table 57.

Table 57. Default Level 3 Inputs for Cement Aggregate Mixture Materials

SHRP ID	Test No.	Compressive Strength (Long Term) (psi)	Elastic Modulus (Long Term) (psi)
0604	2	720	1,529,470
0605	2	610	1,407,796
0607	2	790	1,602,096
0608	1	810	1,622,248
0608	2	920	1,728,896
7614	1	2,370	2,774,911
7614	2	2,550	2,878,359
Average		1,253	1,934,825

Unbound Aggregate Base Materials

Default Level 3 inputs (gradation and Atterberg limits) for unbound aggregate base and subbase materials were developed from more than 300 lab and field measured data in ADOT's QA/QC databases. These inputs are summarized in Table 58.

Table 58. Default Level 3 Inputs for Unbound Aggregate Materials

Material Property	ADOT Material Code		
	Aggregate Base	Aggregate Subbase	Embankment
Plasticity index	2.5	8.4	8.8
Plastic limit	5.4	19.6	14.6
Liquid limit	7.9	28.1	23.4
Passing No. 200	6.3	6.9	32.2
Passing No. 100	9.3	9.6	41.5
Passing No. 50	15	14.2	50.3
Passing No. 40	19.1	17.4	54.4
Passing No. 30	24.4	21.5	58.9
Passing No. 16	32.9	28.4	65.7
Passing No. 10	39.7	33.9	70.9
Passing No. 8	42.1	35.7	72.6
Passing No. 4	52.5	44.8	78.7
Passing 3/8	68.2	59.9	89.3
Passing 1/2	76.8	67.3	91.3
Passing 3/4	92.9	81.2	94
Passing 1	99.5	90.4	95.6
Passing 1-1/2	99.9	98.4	97.4
Passing 2	99.97	99.8	98.3
Passing 2-1/2	99.98	99.98	98.9
Passing 3	99.99	100	99.3
Passing 3-1/2	100	100	100

Subgrade Soil Materials

Default Level 3 inputs (gradation, Atterberg limits, and resilient modulus at optimum moisture content) for subgrade materials were developed from DARWin-ME, LTPP, and ADOT projects. Default gradations and Atterberg limits were obtained from DARWin-ME (global defaults).

Resilient modulus at optimum moisture content was obtained through backcalculation from nearly all Arizona sections. The researchers used field FWD tests to backcalculate the in situ subgrade elastic modulus for each flexible pavement, which was then adjusted to obtain estimates of Mr at optimum moisture content (Table 59). Field FWD tests were also used to backcalculate the in situ subgrade dynamic k-value for each rigid pavement, which was then used to obtain the Mr at optimum moisture content through iteration of the DARWin-ME to match the output k-value with the field backcalculated k-value. Table 59 summarizes the mean Mr values at optimum moisture content for each AASHTO soil classification.

Table 59. Default Level 3 Inputs for Subgrade Materials Mr at Optimum Moisture Content

AASHTO Soil Classification	Resilient Modulus at Optimum Moisture (psi)		
	Base/Subbase for Flexible and Rigid Pavements	Embankment and Subgrade for Flexible Pavements	Embankment and Subgrade for Rigid Pavements
A-1-a	34,000	18,700	18,700
A-1-b	34,000	18,700	18,700
A-2-4	N/A	15,000	19,600
A-2-5	N/A	15,300	15,900
A-2-6	N/A	15,800	15,000
A-2-7	N/A	16,500	16,000
A-3	N/A	15,000	15,000
A-4	N/A	14,400	16,500
A-5	N/A	14,500	14,500
A-6	N/A	14,900	14,600
A-7-5	N/A	15,000	15,000
A-7-6	N/A	14,800	16,300

Note: These resilient modulus values were obtained from averaging over all sections for flexible and rigid pavements used in the Arizona calibration database. The FWD backcalculated in situ elastic solid subgrade modulus for flexible pavement was adjusted to optimum moisture and a lab value by multiplying by 0.55 for fine-grained soils and 0.67 for coarse-grained soils as done for the national calibration. The FWD backcalculated in situ k-value for rigid pavement was used to establish through iteration the proper input resilient modulus at optimum moisture. Some soils were missing in the testing and were assigned values.

Traffic

Default traffic inputs for DARWin-ME were developed under the ADOT project, *Development of a Traffic Data Input System in Arizona for the MEPDG* (Darter et al. 2010). The project objectives were to:

- Identify the needs of various sections within ADOT in terms of traffic data specifically related to the 1993 AASHTO *Guide for Design of Pavement Structures* and the MEPDG.
- Evaluate the current ADOT practice in terms of obtaining, compiling, and managing traffic data.
- Critically investigate the existing traffic data collection infrastructures, such as weigh-in-motion (WIM) stations, and determine their validity and usefulness for the MEPDG.
- Develop a detailed action plan for ADOT to continuously obtain all necessary traffic data and compile that information for effective use in the MEPDG. The action plan should also include a detailed cost estimate.

The default vehicle class distributions, axle load distributions, and other key traffic inputs from the ADOT project, *Development of a Traffic Data Input System in Arizona for the MEPDG* (Darter et al. 2010), were used to locally calibrate the DARWin-ME models. The project's final report contains all the information required to obtain default traffic inputs.

Climate

Default climate inputs were obtained from NCDC climate data from several Arizona weather stations. Many weather stations were missing some of the hourly data. Each weather station was checked and fixed if deficient. The default climate data is included in DARWin-ME by default.

DARWin-ME ARIZONA LOCAL CALIBRATION COEFFICIENTS

The researchers conducted an extensive local calibration and validation effort to ensure that the distress and IRI models were unbiased (i.e., did not, on average, over- or underpredict rutting, fatigue cracking, and IRI). The Arizona specific local calibration coefficients have been entered into the most current version of the DARWin-ME software, however, Arizona designers will need to update the local calibration coefficients with each new version that AASHTO provides. The coefficients used are always output with every run of the software and located under the Calibration tab in the Excel output and at the end of the PDF output file.

Tables 60 through 62 summarize the 2012-derived local calibration coefficients for the HMA/HMA overlays and JPCP. Composite pavements should follow the JPCP local calibration coefficients for concrete and HMA local calibration coefficients for HMA pavements. There was insufficient data to calibrate CRCP models, but there is no reason to believe the global coefficients will not be adequate in Arizona. The Arizona local calibration coefficients may be changed in the future as ADOT conducts additional local calibration efforts.

Table 60. DARWin-ME Local Calibration Coefficients for New HMA and HMA Overlaid HMA Pavement

Model or Submodel Type	Model Coefficients	ADOT Local Calibration	Change from Global Models
Fatigue damage model (AC fatigue)	K1	0.007566	No
	K2	3.9492	No
	K3	1.281	No
	BF1	249.0087232	Yes
	BF2	1	No
	BF3	1.233411397	Yes
Alligator cracking model (AC cracking bottom)	C1	1	No
	C2	4.5	Yes
	C4	6000	No
	AC cracking bottom standard deviation	$1.1+22.9/(1+\exp(-0.1214-2.0565*\text{LOG}_{10}(\text{BOTTOM}+0.0001)))$	Yes
Reflection cracking model	a	$3.5+0.75\text{heff}$	No
	b	$-0.688584-3.37302*\text{heff}^{0.915469}$	No
	c	2.55	Yes
	d	1.23	Yes
AC rutting	K1	-3.35412	No
	K2	1.5606	No
	K3	0.4791	No
	BR1	0.69	Yes
	BR2	1	No
	BR3	1	No
	AC rutting standard deviation	$0.0999*\text{Pow}(\text{RUT},0.174)+0.001$	Yes
Base rutting (granular subgrade rutting)	K1 (base)	2.03	No
	BS1 (base)	0.14	Yes
	Base rutting standard deviation	$0.05*\text{Pow}(\text{BASERUT},0.115)+0.001$	Yes
Subgrade rutting (fine subgrade rutting)	K1 (subgrade)	1.35	No
	BS1 (subgrade)	0.37	Yes
	Subgrade rutting standard deviation	$0.05*\text{Pow}(\text{SUBRUT},0.085)+0.001$	Yes
HMA transverse cracking model (thermal fracture)	Thermal fracture level 1K	1.5	No
	Thermal fracture level 1 standard deviation	$0.1468 * \text{THERMAL} + 65.027$	No
	Thermal fracture level 2K	0.5	No
	Thermal fracture level 2 standard deviation	$0.2841 * \text{THERMAL} + 55.462$	No
	Thermal fracture level 3K	1.5	No
	Thermal fracture level 3 standard deviation	$0.3972 * \text{THERMAL} + 20.422$	No
HMA IRI model	C1 (for rutting)	1.2281	Yes
	C2 (for fatigue)	0.1175	Yes
	C3 (for transverse)	0.008	No
	C4 (for SF)	0.0280	Yes

Table 61. DARWin-ME Local Calibration Coefficients for New JPCP

Model or Submodel Type	Model Coefficients	ADOT Local Calibration	Change from NCHRP 1-40D Global Models
PCC fatigue model	C1	2	No
	C2	1.22	No
JPCP transverse cracking model	C4	0.19	Yes
	C5	-2.067	Yes
	PCC cracking standard deviation	$\text{Pow}(9.87 * \text{CRACK}, 0.4012) + 0.5$	Yes
Faulting model	C1	0.0355	Yes
	C2	0.1147	Yes
	C3	0.00436	Yes
	C4	1.1E-07	Yes
	C5	20000	Yes
	C6	2.0389	Yes
	C7	0.1890	Yes
	C8	400	No
	PCC faulting standard deviation	$\text{Pow}(0.037 * \text{FAULT}, 0.6532) + 0.001$	Yes
JPCP IRI model	J1 (for cracking)	0.60	Yes
	J2 (for spalling)	3.48	Yes
	J3 (for faulting)	1.22	Yes
	J4 (for SF)	45.20	Yes
	PCC IRI JPCP standard deviation	5.4	No

Table 62. DARWin-ME Local Calibration Coefficients for New CRCP

Model or Submodel Type	Model Coefficients	ADOT Local Calibration	Change from NCHRP 1-40D Global Models
PCC fatigue model	C1	2	No
	C2	1.22	No
CRCP punchout model	C3	85	Yes
	C4	1.4149	Yes
	C5	-0.8061	Yes
	PCC punchout standard deviation	$1.5 + 2.9622 * \text{Pow}(\text{PO}, 0.4356)$	Yes
CRCP IRI model	C1	3.15	No
	C2	28.35	No
	PCC IRI CRCP standard deviation	5.4	No

CHECKLIST OF ALL INPUTS

Below are summaries of key data inputs for flexible (new HMA and HMA overlays of existing HMA) pavements (Table 63) and new JPCP (Table 64).

Table 63. Checklist of Flexible Pavement Inputs

Input Parameter		<i>ADOT User's Guide (2012)</i>	Comment
General information	Design life	Table 1, page 13	
	Base/subgrade construction data	Table 2, page 14	
	Pavement construction date		
	Traffic opening date		
Performance criteria	Initial IRI	Table 7, page 19	
	Reliability level	Table 8, page 22	
	Terminal IRI	Table 6, page 18	Not used
	Top-down fatigue cracking		
	Bottom-up fatigue cracking		
	Transverse cracks		
	Total rut depth		
	HMA rut depth		
Reflective cracking		Regression	
Traffic, site features	Average annual daily truck traffic	Table 9, page 27	
	Number of lanes in design direction		
	Percent of two-directional trucks in design direction		
	Percent of trucks in design lane		
	Operational speed		
General traffic, axle configuration	Average axle width	Table 26, page 49	Default value
	Dual tire spacing		Default value
	Dual tire pressure		
	Tandem axle spacing		Default value
	Tridem axle spacing		Default value
	quad axle spacing		Default value
Traffic, lateral wander	Mean wheel location	Page 49	N/A
	Wander, standard deviation		Default value
	Design lane width		N/A
Traffic, wheelbase	Average spacing	Table 27, page 49	N/A
	Percent trucks		
Traffic, volume	Normalized vehicle class distribution	Table 11, page 30	
	Growth rate and function	Page 32	
	Monthly adjustment factors	Table 10, page 28	
	Number of axles per truck type	Table 25, page 48	Default value
	Hourly distribution factors	Table 12, page 31	N/A
	Single axles	Tables 13 to 24, pages 36 to 47	
	Tandem axles		
	Tridem axles		
Quad axles			

Table 63. Checklist of Flexible Pavement Inputs (Continued)

Input Parameter		ADOT User's Guide (2012)	Comment
Climate	Weather station	Figure 18, page 55	
	Location: latitude, longitude, elevation		
	Depth to water table	Figure 19, page 56	
HMA layers	Summary	Table 31, page 58	
	Thickness		
	Dynamic modulus; Level 1	Table 35, page 64	
	Creep compliance; Level 1	Page 67	
	Tensile strength; Level 1	Page 66	
	Asphalt binder grade	Page 65	
	Gradation	Table 36, page 65	
	Effective asphalt content by volume		
	Air voids	Table 37, page 66	
	Unit weight		
	Poisson's ratio	Table 38, page 67	Default Value
	Surface shortwave absorptivity	Page 67	Default Value
	Thermal conductivity	Page 68	Default Value
	Heat capacity	Page 68	Default Value
	Coefficient of thermal contraction	Page 68	Default Value
Existing HMA – backcalculated modulus			
Unbound aggregate and soil layers	Summary	Table 34, page 61	
	Thickness		
	AASHTO soil classification		
	Resilient modulus	Table 50, page 77 Table 51, page 82	
	Poisson's ratio	Table 52, page 83	Default Value
	Coefficient of lateral pressure	Table 53, page 84	Default Value
	Specific gravity	Page 82	Default Value
	Saturated hydraulic conductivity	Page 82	Default Value
	Soil-water characteristic curve	Page 82	Default Value
	Water content; optimum	Page 82	
	Dry unit weight; modified proctor	Page 82	
	Gradation		
	Plasticity index	Table 52, page 83	
Liquid limit	Table 53, page 84		
Local calibration factors	Alligator cracking; bottom-up cracking	Table 62, page 110	
	HMA rutting	Table 63, page 111	
	Aggregate base rutting; coarse subgrade	Table 63, page 111	
	Subgrade rutting; fine subgrade	Table 63, page 111	
	HMA IRI regression equation	Table 64, page 112	
Reflection cracking	Table 62, page 110		

Table 64. Checklist of Rigid Pavement Inputs

Input Parameter		ADOT User's Guide (2012)	Comment
General information	Design life	Table 1, page 13	
	Pavement PCC construction date		
	Traffic opening date		
Performance criteria	Initial IRI	Table 7, page 19	
	Reliability Level	Table 8, page 22	
	Terminal IRI	Table 6, page 18	
	JPCP transverse fatigue cracking		
	JPCP transverse joint faulting		
	JPCP transverse joint load transfer		
	CRCP punchouts		
	CRCP crack width		50% Rel
CRCP crack load transfer	50% Rel		
Traffic, site features	AADTT	Table 9, page 27	
	Number of lanes in design direction		
	Percent of two-directional trucks in design direction		
	Percent of trucks in design lane		
	Operational speed		
General traffic, axle configuration	Average axle width	Table 26, page 49	Default Value
	Dual tire spacing		Default Value
	Dual tire pressure		
	Tandem axle spacing		Default Value
	Tridem axle spacing		Default Value
	Quad axle spacing		Default Value
Traffic, lateral wander	Mean wheel location	Page 49	NA
	Wander, standard deviation		Default Value
	Design lane width		NA
Traffic, wheelbase	Average spacing	Table 27, page 49	NA
	Percent trucks		
Traffic, volume	Normalized vehicle class distribution	Table 11, page 30	
	Growth rate and function	Page 32	
	Monthly adjustment factors	Table 10, page 28	
	Number of axles per truck type	Table 25, page 48	Default Value
	Hourly adjustment factors	Table 12, page 31	NA
	Single axles	Tables 13 to 24, pages 36 to 47	
	Tandem axles		
	Tridem axles		
	Quad axles		

Table 64. Checklist of Rigid Pavement Inputs (Continued)

Input Parameter		ADOT User's Guide (2012)	Comment
Climate	Weather station	Figure 18, page 55	
	Location: latitude, longitude	Long-Lat.com	
	Elevation of project	Long-Lat.com	
	Depth to water table	Figure 19, page 56	
HMA layers	Summary	Table 31, page 58	
	Thickness		
	Dynamic modulus; Level 1	Table 35, page 64	
	Creep compliance; Level 1	Page 67	
	Tensile strength; Level 1	Page 66	
	Asphalt binder grade	Page 65	
	Gradation	Table 36, page 65	
	Effective asphalt content by volume		
	Air voids	Table 37, page 66	
	Unit weight		
	Poisson's ratio	Table 38, page 67	Default value
	Surface shortwave absorptivity	Page 67	Default value
	Thermal conductivity	Page 68	Default value
	Heat capacity	Page 68	Default value
	Coefficient of thermal contraction	Page 68	Default value
Existing HMA – backcalculated modulus			
Unbound aggregate and soil layers	Summary	Table 34, page 61	
	Thickness		
	AASHTO soil classification		
	Resilient modulus	Table 50, page 77 Table 51, page 82	
	Poisson's ratio	Table 52, page 83	Default value
	Coefficient of lateral pressure	Table 53, page 84	Default value
	Specific gravity	Page 82	Default value
	Saturated hydraulic conductivity	Page 82	Default value
	Soil-water characteristic curve	Page 82	Default value
	Water content, optimum	Page 82	
	Dry unit weight; modified proctor	Page 82	
	Gradation	Table 52, page 83 Table 53, page 84	
	Plasticity index		
Liquid limit			
Local calibration factors	JPCP IRI		
	JPCP transverse fatigue cracking		
	JPCP transverse joint faulting		
	CRCP IRI		
	CRCP punchouts		
	CRCP crack width		

CHAPTER 8. SUMMARY AND RECOMMENDATIONS

The complete implementation process has involved several major efforts to assure ADOT that the MEPDG models will predict distress and IRI that matches Arizona experience:

- Develop a user's guide with procedures for creating proper inputs that use the MEPDG to design new, reconstructed, and rehabilitated pavement structures.
- Use Arizona performance data to verify, validate, and calibrate the MEPDG models (if necessary) to remove bias (consistent over- or underprediction) and improve accuracy of prediction. This was accomplished through the verification, validation, and recalibration of Arizona calibration coefficients. In nearly all cases, this effort improved the accuracy of the distress and IRI models and removed the over- and underprediction of bias.
- Develop recommended levels of design reliability and model standard deviations specific to each distress and IRI model that are required to design a pavement with a desired level of reliability.
- Conduct design comparisons and sensitivity studies that help to establish confidence in the pavement design results achieved by the MEPDG.

Summary

The *ADOT User's Guide* (2012) presents the following information to help ADOT pavement design engineers and others use the AASHTO DARWin-ME pavement design guide and software:

- An overview of the AASHTO DARWin-ME procedure.
- Help information for installing the software.
- Guidelines for obtaining all needed inputs.
- Design guidance for using the software with the following pavement types:
 - New or reconstructed HMA pavement.
 - New or reconstructed JPCP and CRCP.
 - New or reconstructed composite pavement (ARFC overlay on JPCP or CRCP).
 - HMA rehabilitation: HMA overlay on existing HMA.
 - HMA rehabilitation: HMA on existing JPCP.
 - JPCP rehabilitation: CPR diamond grinding and JPCP overlay on an existing HMA or JPCP pavement.

- Examples of pavement design using the design guide software.
 - New or reconstructed HMA pavement.
 - New or reconstructed JPCP.
 - New or reconstructed ARFC/JPCP.
 - HMA overlay on existing HMA.

The MEPDG prediction models were verified, validated, and, if necessary, recalibrated using Arizona pavement sections. One hundred and eighty HMA, JPCP, ARFC/JPCP, and rehabilitated pavements were included in a valuable database that represents Arizona pavement performance over many years. This database was used to verify, validate, and recalibrate the prediction models to make them more accurate and unbiased (neither over- nor underprediction). They were also used to establish Arizona design inputs and the appropriate standard deviation or error of each model for use in reliability design, which will make it possible to design a pavement in Arizona with the desired reliability at the most optimum cost possible.

Table 65 shows the global model goodness of fit statistics and the Arizona specific calibration goodness of fit statistics. The improvement in these models through verification, validation, and calibration with Arizona data is well-documented in this table; the calibrated models will provide much more accurate, reliable, and cost-effective designs than the global calibrations.

Table 65. Comparison of MEPDG Global and Arizona-Specific Model Goodness of Fit Statistics

Pavement Type	Distress/IRI Models	Global Models		ADOT Calibrated Models	
		Global R ² (%)*	Global Model SEE*	Arizona R ² (%)	Arizona SEE
New HMA and HMA Overlay	Alligator cracking	8	14%	58	13%
	Transverse thermal cracking	N/A	N/A	Not calibrated	Not calibrated
	Total rutting	5	0.31 inch	21	0.12 inch
	IRI	30	19 inches/mi	80	8 inches/mi
New JPCP	Transverse cracking	20	9%	78	6%
	Transverse joint faulting	45	0.03 inch	52	0.03 inch
	IRI	35	25 inches/mi	81	10 inches/mi
ARFC/JPCP	Transverse cracking	Same as JPCP	Same as JPCP	Same as JPCP	Same as JPCP
	Rutting	Same as HMA	Same as HMA	Same as ADOT HMA	Same as ADOT HMA
	IRI	Same as HMA	Same as HMA	Same as ADOT HMA	Same as ADOT HMA
New CRCP	Punchouts	68%	5 PO/mi	Same as global	2 ADOT CRCP matched global predictions
	Slab/base friction	Established values	N/A	Same as global	N/A

*Global calibration coefficients using the Arizona database.

Information presented in Table 35 shows that the local models also have improved goodness of fit statistics. The results of the design comparisons also show reasonable distress and IRI predictions by the Arizona locally calibrated MEPDG.

The Arizona calibrated models had a lower model prediction error, improved accuracy and reliability, and reasonable sensitivity to changes in inputs. The locally calibrated MEPDG models for Arizona are considered reasonable and are recommended for use in pavement design.

Recommendations

The following improvements are recommended to further improve pavement design using AASHTO DARWin-ME:

- **Evaluation of Arizona State University (ASU) lab testing data for binder and HMA mixtures for use as defaults to improve estimation of HMA dynamic modulus.** ASU conducted substantial testing under the ADOT project, *Development of Performance Related Specifications for Asphalt Pavements in the State of Arizona* (Witczak 2008), that may better characterize HMA mixes.
- **Further evaluation of the low-temperature cracking model and its calibration in Arizona.** This model was not calibrated under this study due to lack of creep compliance and indirect tensile strength data for ADOT HMA mixes. In addition, there was insufficient information to properly characterize observed HMA transverse cracking distress (such as thermal fracture and shrinkage). However in Colorado and Wyoming, DARWin-ME implementation efforts produced a local calibration coefficient K value of 7.5. This may be a reasonable value for ADOT to use while additional research is conducted to more fully establish proper local calibration coefficients.
- **Research into the cause of transverse cracking of HMA pavements in desert warm nonfreezing areas.** There is substantial transverse cracking in nonfreeze areas that is not considered in the DARWin-ME. These cracks lead to roughness and increased IRI that is not considered in design. The mechanism may be shrinkage of the HMA mixture due in part to absorption of binder into the porous aggregates.
- **Major increase in the collection and analysis of truck traffic data.** Sufficient current WIM axle weight data and truck classification data are not available. This will require additional WIM sites across the state.
- **Consideration of AR mixtures.** These materials were not included in the DARWin-ME development. Since Arizona uses substantial quantities of AR mixes in new construction and overlays, better characterization would be useful in design.

REFERENCES

- American Association of State Highway and Transportation Officials (AASHTO). 1993. *Guide for Design of Pavement Structures*. Washington, D.C.: American Association of State Highway and Transportation Officials.
- American Association of State Highway and Transportation Officials (AASHTO). 2008. *Mechanistic-Empirical Pavement Design Guide, A Manual of Practice*, July 2008, Interim Edition. Washington, D.C.: American Association of State Highway and Transportation Officials.
- American Association of State Highway and Transportation Officials (AASHTO). November 2010. *Guide for the Local Calibration of the Mechanistic-Empirical Pavement Design Guide*. Washington, D.C.: American Association of State Highway and Transportation Officials.
- Arizona Department of Transportation (ADOT). March 1989. *Materials Preliminary Engineering and Design Manual*. Phoenix: Arizona Department of Transportation.
- Darter, M. I., L. Titus-Glover, and D. J. Wolf. 2010. *Development of a Traffic Data Input System in Arizona for the MEPDG*. Publication FHWA-AZ-13-672. Phoenix: Arizona Department of Transportation.
- National Cooperative Highway Research Program (NCHRP). 2004. *2002 Design Guide: Design of New and Rehabilitated Pavement Structures*. Project 1-37A. Publication FHWA-RD-00-129. Washington, D.C.: National Cooperative Highway Research Program.
<http://onlinepubs.trb.org/onlinepubs/archive/mepdg/guide.htm>
- National Cooperative Highway Research Program (NCHRP). 2007. *Version 1.0 – Mechanistic-Empirical Pavement Design Guide Software*. Washington, D.C.: National Cooperative Highway Research Program.
http://onlinepubs.trb.org/onlinepubs/nchrp/nchrp_rrd_308.pdf
- Smith, K. D., D. G. Peshkin, A. L. Mueller, E. Owusu-Antwi, and M. I. Darter. 1991. *Evaluation of Concrete Pavements in the Phoenix Urban Corridor*. Publication FHWA-AZ91-264-1. Phoenix: Arizona Department of Transportation.
- Witczak, M. W. 2008. *Development of Performance Related Specifications for Asphalt Pavements in the State of Arizona*. Publication FHWA-SPR-08-402-2. Phoenix: Arizona Department of Transportation.

APPENDIX: DARWin-ME HMA PAVEMENT AND JPCP PERFORMANCE PREDICTION MODELS

A brief description of the *Mechanistic-Empirical Pavement Design Guide* (MEPDG) models used to predict performance is presented in this appendix. Additional information is available in the original MEPDG documentation (NCHRP 2004, 2007; AASHTO 2008).

NEW AND RECONSTRUCTED HMA PAVEMENTS

Alligator Cracking

Alligator cracking prediction in the MEPDG comprises several submodels and algorithms for estimating critical horizontal strain at the bottom of the HMA layers, empirical models relating strain to allowable number of load repetitions, and transfer functions for computation incrementally of HMA bottom-up fatigue damage by dividing the actual number of axle loads by the allowable number of axle loads, and an alligator cracking model based on estimated fatigue damage levels. Eq. 15 through Eq. 22 present the key models used by the MEPDG for predicting alligator cracking (AASHTO 2008).

Fatigue Damage Model

This model computes accumulated fatigue damage DI in the HMA over time.

$$DI = \sum (\Delta DI)_{j,m,l,p,T} = \sum \left(\frac{n}{N_{f-HMA}} \right)_{j,m,l,p,T} \quad (\text{Eq. 15})$$

Where

N = actual number of axle load applications within a specific time period

j = axle load interval

m = axle load type (single, tandem, tridem, quad, or special axle configuration)

l = truck type using the truck classification groups included in the MEPDG

p = month

T = median temperature for the five temperature intervals or quintiles used to
subdivide each month (° F)

N_{f-HMA} = allowable number of axle load applications for a flexible pavement and
HMA overlays to fatigue cracking

Allowable Number of Axle Load Applications Model

$$N_{f-HMA} = k_{f1} (C)(C_H) \beta_{f1} (\epsilon_t)^{k_{f2} \beta_{f2}} (E_{HMA})^{k_{f3} \beta_{f3}} \quad (\text{Eq. 16})$$

Where

N_{f-HMA} = allowable number of axle load applications for a flexible pavement and HMA overlays to fatigue cracking

ϵ_t = tensile strain at critical locations and calculated by the structural response model (inch/inch)

E_{HMA} = dynamic modulus of the HMA measured in compression (psi)

k_{f1}, k_{f2}, k_{f3} = global field calibration parameters ($k_{f1} = 0.007566$, $k_{f2} = -3.9492$, and $k_{f3} = -1.281$)

$\beta_{f1}, \beta_{f2}, \beta_{f3}$ = local or mixture-specific field calibration constants; for the global calibration effort, these constants were set to 1.0

$$C = 10^M \quad (\text{Eq. 17})$$

$$M = 4.84 \left(\frac{V_{be}}{V_a + V_{be}} - 0.69 \right) \quad (\text{Eq. 18})$$

Where

V_{be} = effective asphalt content by volume (percent)

V_a = percent air voids in the HMA mixture (in situ only, not mixture design)

C_H = thickness correction term as follows:

$$C_H = \frac{1}{0.000398 + \frac{0.003602}{1 + e^{(11.02 - 3.49 H_{HMA})}}} \quad (\text{Eq. 19})$$

Where

H_{HMA} = total HMA thickness (inch)

For the HMA alligator cracking allowable number of axle load applications model, the MEPDG allows the following model coefficients to be modified as needed as part of Arizona local calibration to improve alligator cracking prediction accuracy and remove bias:

k_{f1} , k_{f2} , k_{f3} = global field calibration parameters ($k_{f1} = 0.007566$, $k_{f2} = -3.9492$, and $k_{f3} = -1.281$)

θ_{f1} , θ_{f2} , θ_{f3} = Arizona local or mixture specific field calibration constants were set to 249.0087, 1.0, and 1.2334

Alligator Cracking Model

This S-shaped model predicts alligator fatigue bottom-up cracking FC_{Bottom} in the traffic lane due to accumulated fatigue damage DI_{Bottom} .

$$FC_{Bottom} = \left(\frac{1}{60} \right) \left(\frac{C_4}{1 + e^{(C_1 C_1^* + C_2 C_2^* \text{Log}(DI_{Bottom}))}} \right) \quad (\text{Eq. 20})$$

Where

FC_{Bottom} = Area of alligator cracking that initiates at the bottom of the HMA layers (percent of total lane area)

DI_{Bottom} = Cumulative damage index at the bottom of the HMA layer

$C_{1,2,4}$ = Transfer function regression constants; $C_4 = 6,000$; $C_1 = 1.00$; and $C_2 = 1.00$

$$C_1^* = -2C_2^* \quad (\text{Eq. 21})$$

$$C_2^* = -2.40874 - 39.748(1 + H_{HMA})^{-2.856} \quad (\text{Eq. 22})$$

Where

H_{HMA} = total HMA thickness (inches)

For the HMA alligator cracking model, the MEPDG allows the following model coefficients to be modified as needed as part of Arizona local calibration to improve alligator cracking prediction accuracy and remove bias:

$C_{1,2,4}$ = Transfer function regression constants ($C_1=1.0$; and $C_2=4.5$, $C_4= 6,000$;))

Transverse Cracking (Low Temperature Induced)

This model predicts transverse cracking in HMA pavement that is specifically caused by low-temperature contraction of asphalt binders that lead to tensile stresses and transverse crack formation. Hourly HMA temperatures are calculated along with HMA properties such as creep compliance to estimate tensile stress in the HMA surface. These cracks can be initially spaced at more than 100 ft to as low as 20 ft (very severe) after a period of several years, and can deteriorate and create significant roughness leading to increased IRI.

Transverse cracking prediction begins with characterizing the amount of crack propagation induced by a given thermal cooling cycle using the Paris law of crack propagation (AASHTO 2008).

$$\Delta C = A (\Delta K)^n \quad (\text{Eq. 23})$$

Where

ΔC = change in the crack depth due to a cooling cycle

ΔK = change in the stress intensity factor due to a cooling cycle

A, n = fracture parameters for the HMA mixture

Experimental results indicate that reasonable estimates of A and n can be obtained from the indirect tensile creep-compliance and strength of the HMA in accordance with Eq. 24 and Eq. 25 (AASHTO 2008).

$$A = 10^{k_i \beta_i (4.389 - 2.52 \text{Log}(E_{HMA} \sigma_m^n))} \quad (\text{Eq. 24})$$

And set

$$n = 0.8 \left[1 + \frac{1}{m} \right]$$

Where

k_t = coefficient determined through global calibration for each input level

(Level 1 = 5.0; Level 2 = 1.5; and Level 3 = 3.0)

E_{HMA} = HMA indirect tensile modulus (psi)

σ_m = mixture tensile strength (psi)

M = the m-value derived from the indirect tensile creep compliance curve measured in the laboratory

β_t = local or mixture calibration factor

Stress intensity factor, K , was incorporated in the MEPDG through the use of a simplified equation developed from theoretical finite element studies (Eq. 25).

$$K = \sigma_{ip} \left(0.45 + 1.99(C_o)^{0.56} \right) \quad (\text{Eq. 25})$$

Where

σ_{ip} = far-field stress from pavement response model at depth of crack tip (psi)

C_o = current crack length (ft)

The amount of transverse cracking is predicted by the MEPDG using an assumed relationship between the probability distribution of the log of the crack depth to HMA layer thickness ratio and the percent of cracking. Equation 26 shows the expression used to determine the amount of thermal cracking (AASHTO 2008).

$$TC = \beta_{t1} N \left[\frac{1}{\sigma_d} \text{Log} \left(\frac{C_d}{H_{HMA}} \right) \right] \quad (\text{Eq. 26})$$

Where

TC = Thermal cracking (ft/mi)

β_{t1} = Regression coefficient determined through global calibration (400)

$N[z]$ = Standard normal distribution evaluated at $[z]$

σ_d = Standard deviation of the log of the depth of cracks in the pavement

(0.769) (inches)

C_d = Crack depth (inches)

H_{HMA} = Thickness of HMA layers (inches)

For the HMA transverse cracking model, the MEPDG allows the following model coefficients to be modified as needed as part of local calibration to improve transverse cracking prediction accuracy and remove bias:

β_{t1} = Regression coefficient determined through global calibration (400)

Rutting

This model predicts the amount of permanent deformation (rutting) in each pavement and subgrade layer and accumulates total rutting. Rutting prediction in the MEPDG comprises several submodels and algorithms for estimating incrementally critical vertical permanent or plastic axial strain in the HMA and unbound aggregate bases materials and subgrade soils. The MEPDG assumes rutting does not occur in chemically stabilized materials or layers.

Total rutting is the sum of all plastic vertical strain accumulated in each pavement layer due to applied axle loading. Eq. 27 through Eq. 34 present the key models used by the MEPDG for predicting rutting (AASHTO 2008):

HMA Rutting Model

For all HMA mixtures types, the MEPDG field calibrated form of the laboratory derived relationship from repeated load permanent deformation tests is shown in Eq. 27.

$$\Delta_{p(HMA)} = \varepsilon_{p(HMA)} h_{HMA} = \beta_{1r} k_z \varepsilon_{r(HMA)} 10^{k_{1r}} n^{k_{2r} \beta_{2r}} T^{k_{3r} \beta_{3r}} \quad (\text{Eq. 27})$$

Where

$\Delta_{p(HMA)}$ = accumulated permanent or plastic vertical deformation in the HMA layer or sublayer (inches)

$\varepsilon_{p(HMA)}$ = accumulated permanent or plastic axial strain in the HMA layer or sublayer (inch/inch)

$\epsilon_{r(HMA)}$ = resilient or elastic strain calculated by the structural response model at the mid-depth of each HMA sublayer (inch/inch)

$h_{(HMA)}$ = thickness of the HMA layer/sublayer (inches)

n = number of axle load repetitions

T = mix or pavement temperature (° F)

k_z = depth confinement factor

$k_{1r,2r,3r}$ = global field calibration parameters (from the NCHRP 1-40D recalibration; $k_{1r} = -3.35412$, $k_{2r} = 1.5606$, $k_{3r} = 0.4791$)

θ_{1r} , θ_{2r} , θ_{3r} = local or mixture field calibration constants; for the global calibration, these constants were all set to 1.0

$$k_z = (C_1 + C_2 D) 0.328196^D \quad (\text{Eq. 28})$$

$$C_1 = -0.1039(H_{HMA})^2 + 2.4868H_{HMA} - 17.342 \quad (\text{Eq. 29})$$

$$C_2 = 0.0172(H_{HMA})^2 - 1.7331H_{HMA} + 27.428 \quad (\text{Eq. 30})$$

Where

D = depth below the surface (inches)

H_{HMA} = total HMA thickness (inches)

For the HMA rutting model, the MEPDG allows the following model coefficients to be modified as part of the Arizona local calibration to improve rutting prediction accuracy and remove bias:

$k_{1r,2r,3r}$ = global field calibration parameters (from the NCHRP 1-40D recalibration; $k_{1r} = -3.35412$, $k_{2r} = 1.5606$, $k_{3r} = 0.4791$)

θ_{1r} , θ_{2r} , θ_{3r} = Arizona local or mixture field calibration constants; for the global calibration, these constants were all set to 0.69, 1.0, and 1.0.

Aggregate Base and Subgrade Soils Rutting Model

Eq. 31 shows the field-calibrated mathematical equation used to calculate plastic vertical deformation within all unbound pavement sublayers and the foundation or embankment soil.

$$\Delta_{p(soil)} = \beta_{s1} k_{s1} \varepsilon_v h_{soil} \left(\frac{\varepsilon_o}{\varepsilon_r} \right) e^{-\left(\frac{\rho}{n}\right)^\beta} \quad (\text{Eq. 31})$$

Where

$\Delta_{p(soil)}$ = permanent or plastic deformation for the layer or sublayer (inches)

n = number of axle load applications

ε_o = intercept determined from laboratory repeated load permanent deformation tests (inch/inch)

ε_r = resilient strain imposed in laboratory test to obtain material properties ε_o , β , and ρ , in/in

ε_v = average vertical resilient or elastic strain in the layer or sublayer, and calculated by the structural response model (inch/inch)

h_{soil} = thickness of the unbound layer or sublayer (inches)

k_{s1} = global calibration coefficients; $k_{s1}=2.03$ for granular materials and 1.35 for fine-grained materials

β_{s1} = local calibration constant for the rutting in the unbound layers (base or subgrade); the local calibration constant was set to 1.0 for the global calibration effort. β_{s1} represents the subgrade layer while β_{B1} represents the base layer

$$\text{Log}\beta = -0.61119 - 0.017638(W_c) \quad (\text{Eq. 32})$$

$$\rho = 10^9 \left(\frac{C_o}{1 - (10^9)^\beta} \right)^{\frac{1}{\beta}} \quad (\text{Eq. 33})$$

$$C_o = \text{Ln} \left(\frac{a_1 M_r^{b_1}}{a_9 M_r^{b_9}} \right) = 0.0075 \quad (\text{Eq. 34})$$

Where

W_c = water content (percent)

M_r = resilient modulus of the unbound layer or sublayer (psi)

$a_{1,9}$ = regression constants; $a_1=0.15$ and $a_9=20.0$

$b_{1,9}$ = regression constants; $b_1=0.0$ and $b_9=0.0$

For the unbound aggregate base and subgrade rutting model, the MEPDG allows the following model coefficients to be modified as needed as part of Arizona local calibration to improve rutting prediction accuracy and remove bias:

θ_{s1} = local calibration constant for the rutting in the unbound layers (base or subgrade); the Arizona local calibration constant was set to $\theta_{s1} = 0.14$ and $\theta_{B1} = 0.37$. θ_{s1} represents the subgrade layer while θ_{B1} represents the base layer.

HMA Smoothness (IRI)

This model predicts the IRI in the traffic lane over time. HMA smoothness prediction in the MEPDG is based on the principle that smoothness degradation (increasing IRI) from an initial as-constructed smoothness level is due mostly to the development of critical surface distresses and subgrade foundation movement. Eq. 35 and Eq. 36 were developed using data from the LTPP program to predict the IRI over time for new HMA pavements (AASHTO 2008).

$$IRI = IRI_o + C1(SF) + C2(FC_{Total}) + C3(TC) + C4(RD) \quad (\text{Eq. 35})$$

Where

IRI_o = initial IRI after construction (inch/mi)

SF = site factor, refer to Eq. 23

FC_{Total} = area of fatigue cracking (combined alligator, longitudinal, and reflection cracking in the wheel path) (percent of total lane area). All load-related cracks are combined on an area basis – length of cracks is multiplied by 1 ft to convert length into an area basis

TC = length of transverse cracking (including the reflection of transverse cracks in existing HMA pavements) (ft/mi).

RD = average rut depth (inches)

$$C1 = 0.0150$$

$$C2 = 0.4000$$

$$C3 = 0.0080$$

$$C4 = 40.000$$

SF = site factor

SF is calculated in accordance with the following equation:

$$SF = FROSTH + SWELLP * AGE^{1.5} \quad (\text{Eq. 36})$$

Where

$$FROSTH = \text{LN}([\text{PRECIP}+1] * \text{FINES} * [\text{FI}+1])$$

$$SWELLP = \text{LN}([\text{PRECIP}+1] * \text{CLAY} * [\text{PI}+1])$$

$$\text{FINES} = \text{FSAND} + \text{SILT}$$

AGE = pavement age (years)

PI = subgrade soil plasticity index

PRECIP = mean annual precipitation (inches)

FI = mean annual freezing index (° F days)

FSAND = amount of fine sand particles in subgrade (percent of particles between 0.074 and 0.42 mm)

SILT = amount of silt particles in subgrade (percent of particles between 0.074 and 0.002 mm)

CLAY = amount of clay size particles in subgrade (percent of particles less than 0.002 mm)

For the HMA IRI model, the MEPDG allows modifications to the following model coefficients as part of the Arizona local calibration to improve IRI prediction accuracy and remove bias:

$$C1 = 1.2281$$

$$C2 = 0.1175$$

$$C3 = 0.0080$$

$$C4 = 0.0280$$

NEW AND RECONSTRUCTED JPCP

The JPCP MEPDG models developed originally under NCHRP Project 1-37A have been recalibrated twice since the completion of Project 1-37A to improve global models prediction accuracy and remove bias. Other reasons for recalibration included correcting systematic errors in key MEPDG inputs that were discovered since the 2004 and 2007 completion of NCHRP Projects 1-37A and 1-40D projects, respectively. The latest round of the JPCP models was completed under NCHRP 20-07 in 2011 using the correct CTE values. They are of interest in Arizona since the correct CTE values are being used in the local calibration.

Transverse Slab Cracking

The MEPDG predicts both bottom-up and top-down modes of transverse slab cracking. The estimates of bottom-up and top-down transverse slab cracking combined to predict total transverse slab cracking. For both modes of cracking, the MEPDG estimates critical stresses at the portland concrete cement (PCC) surface or bottom that is then related to an allowable number of load repetitions before the slab cracks using empirical relationships. The allowable number of load repetitions is then used for computing incrementally PCC top-down and bottom-up fatigue damage by dividing the actual number of axle loads by the allowable number of axle loads. Top-down and bottom-up transverse cracking is then estimated based on estimates of fatigue damage.

The two estimates of slab cracking are combined in a manner that excludes the possibility of both modes of cracking occurring on the same slab as under typical service conditions; the potential for either mode of cracking is present in all slabs but although slabs may crack either from the bottom up or top down, both do not occur simultaneously. Eq. 37 through Eq. 40 present the key models used by the MEPDG for predicting cracking (AASHTO 2008).

Top-Down and Bottom-Up Transverse Slab Cracking Model

$$CRK = \frac{1}{1 + C4(DI_F)^{C5}} \quad (\text{Eq. 37})$$

Where

CRK = predicted amount of bottom-up or top-down cracking (fraction).

DI_F = fatigue damage calculated using the procedure described in this section.

$C4 = 0.6$ (NCHRP 20-07)

$C5 = -2.05$ (NCHRP 20-07)

For the JPCP cracking model, the MEPDG allows the following model coefficients to be modified as needed as part of Arizona local calibration to improve cracking prediction accuracy and remove bias:

$$C4 = 0.19$$

$$C5 = -2.067$$

PCC Fatigue Damage

The general expression for fatigue damage accumulations considering all critical factors for JPCP transverse cracking follows (based on Miner's hypothesis):

$$DI_F = \sum \frac{n_{i,j,k,l,m,n,o}}{N_{i,j,k,l,m,n,o}} \quad (\text{Eq. 38})$$

Where

DI_F = total fatigue damage (top-down or bottom-up)

$n_{i,j,k,\dots}$ = applied number of load applications at condition i, j, k, l, m, n

$N_{i,j,k,\dots}$ = allowable number of load applications at condition i, j, k, l, m, n

l = age (accounts for change in PCC modulus of rupture and elasticity, slab or base contact friction, traffic loads)

j = month (accounts for change in base elastic modulus and effective dynamic modulus of subgrade reaction)

k = axle type (single, tandem, and tridem for bottom-up cracking; short, medium, and long wheelbase for top-down cracking)

l = load level (incremental load for each axle type)

m = equivalent temperature difference between top and bottom PCC surfaces

n = traffic offset path

o = hourly truck traffic fraction

Allowable Number of Load Repetitions

The applied number of load applications ($n_{i,j,k,l,m,n}$) is the actual number of axle type k of load level l that passed through traffic path n under each condition (age, season, and temperature difference). The allowable number of load applications is the number of load cycles at which fatigue failure is expected on average and is a function of the applied stress and PCC strength. The allowable number of load applications is determined using the following globally calibrated PCC fatigue equation:

$$\log(N_{i,j,k,l,m,n}) = C_1 \cdot \left(\frac{MR_i}{\sigma_{i,j,k,l,m,n}} \right)^{C_2} \quad (\text{Eq. 39})$$

Where

$N_{i,j,k,\dots}$ = allowable number of load applications at condition i, j, k, l, m, n

MR_i = PCC modulus of rupture at age i (psi)

$\sigma_{i,j,k}$ = applied stress at condition i, j, k, l, m, n

C_1 = calibration constant, 2.0

C_2 = calibration constant, 1.22

For the JPCP transverse cracking allowable number of load repetitions model, the MEPDG allows the following model coefficients to be modified as needed as part of Arizona local calibration to improve cracking prediction accuracy and remove bias. However, these were not changed.

C_1 = calibration constant, 2.0

C_2 = calibration constant, 1.22

Total Transverse Cracking Model

The fatigue damage calculation is a process of summing damage from each damage increment. Once top-down and bottom-up damage are estimated, the corresponding cracking is computed using Eq. 37 and the total combined cracking determined using Eq. 40.

$$TCRACK = \left(CRK_{Bottom-up} + CRK_{Top-down} - CRK_{Bottom-up} \cdot CRK_{Top-down} \right) \cdot 100 \quad (\text{Eq. 40})$$

Where

$TCRACK$ = total transverse cracking (percent, all severities)

$CRK_{Bottom-up}$ = predicted amount of bottom-up transverse cracking (fraction)

$CRK_{Top-down}$ = predicted amount of top-down transverse cracking (fraction)

Eq. 40 assumes that a slab may crack from either bottom up or top down, but not both.

Transverse Joint Faulting

The mean transverse joint faulting is predicted incrementally on a monthly basis. The magnitude of increment is based on current faulting level, the number of axle loads applied, pavement design features, material properties, and climatic conditions. Total faulting is determined as a sum of faulting increments from all previous months (i.e., since traffic opening) using the following equations (AASHTO 2008):

$$Fault_m = \sum_{i=1}^m \Delta Fault_i \quad (\text{Eq. 41})$$

$$\Delta Fault_i = C_{34} * (FAULTMAX_{i-1} - Fault_{i-1})^2 * DE_i \quad (\text{Eq. 42})$$

$$FAULTMAX_i = FAULTMAX_0 + C_7 * \sum_{j=1}^m DE_j * \text{Log}(1 + C_5 * 5.0^{EROD})^{C_6} \quad (\text{Eq. 43})$$

$$FAULTMAX_0 = C_{12} * \delta_{\text{curling}} * \left[\text{Log}(1 + C_5 * 5.0^{EROD}) * \text{Log}\left(\frac{P_{200} * \text{WetDays}}{P_s}\right) \right]^{C_6} \quad (\text{Eq. 44})$$

Where

$Fault_m$ = mean joint faulting at the end of month m (inches)

$\Delta Fault_i$ = incremental change (monthly) in mean transverse joint faulting
during month i (inches)

$FAULTMAX_i$ = maximum mean transverse joint faulting for month i (inches)

$FAULTMAX_0$ = initial maximum mean transverse joint faulting (inches)

$EROD$ = base or subbase erodibility factor

DE_i = differential density of energy of subgrade deformation accumulated during month i

$\delta_{curling}$ = maximum mean monthly slab corner upward deflection PCC due to temperature curling and moisture warping

P_s = overburden on subgrade (pounds)

P_{200} = percent subgrade material passing No. 200 sieve

$WetDays$ = average annual number of wet days (greater than 0.1 inch rainfall)

$C_1 = 1.0184$

$C_2 = 0.91656$

$C_3 = 0.0021848$

$C_4 = 0.000884$

$C_5 = 250$

$C_6 = 0.4$

$C_7 = 1.83312$

Note that C_{12} and C_{34} are defined by Eq. 45 and Eq. 46.

$$C_{12} = C_1 + C_2 * FR^{0.25} \quad (\text{Eq. 45})$$

$$C_{34} = C_3 + C_4 * FR^{0.25} \quad (\text{Eq. 46})$$

Where

FR = base freezing index defined as percentage of time the top base temperature is below freezing (32° F) temperature.

For the JPCP transverse joint faulting model, the MEPDG allows the following model coefficients to be modified as needed as part of the Arizona local calibration to improve faulting prediction accuracy and remove bias:

$$C1 = 0.0355$$

$$C2 = 0.1147$$

$$C3 = 0.00436$$

$$C4 = 1.1 \times 10^{-07}$$

$$C5 = 20000$$

$$C6 = 2.0389$$

$$C7 = 0.189$$

$$C8 = 400$$

Smoothness (IRI)

JPCP smoothness is predicted as a function of the initial as-constructed smoothness and any change in pavement longitudinal profile over time and traffic due to distress development and progression and foundation movements. The IRI model was calibrated and validated using LTPP data that represented variety of design, materials, foundations, and climatic conditions. The following is the final globally calibrated model (AASHTO 2008):

$$IRI = IRI_i + C1*CRK + C2*SPALL + C3*TFAULT + C4*SF \quad (\text{Eq. 47})$$

Where

IRI = predicted IRI (inch/mi)

IRI_i = initial smoothness measured as IRI (inch/mi)

CRK = percent slabs with transverse cracks (all severities)

SPALL = percentage of joints with spalling (medium and high severities)

TFAULT = total joint faulting cumulated per mi (inches)

$$C1 = 0.8203$$

$$C2 = 0.4417$$

$$C3 = 0.4929$$

$$C4 = 25.24$$

SF = site factor

$$SF = AGE (1+0.5556*FI) (1+P_{200}) * 10^{-6} \quad (\text{Eq. 48})$$

Where

AGE = pavement age (years)

FI = freezing index (° F days)

P_{200} = percent subgrade material passing No. 200 sieve

The transverse cracking and faulting are obtained using the MEPDG models described earlier. The transverse joint spalling is determined in accordance with Eq. 49, which was calibrated using LTPP and other data (AASHTO 2008):

$$SPALL = \left[\frac{AGE}{AGE + 0.01} \right] \left[\frac{100}{1 + 1.005^{(-12 * AGE + SCF)}} \right] \quad (\text{Eq. 49})$$

Where

$SPALL$ = percentage joints spalled (medium and high severities)

AGE = pavement age since construction (years)

SCF = scaling factor based on site, design, and climate

$$SCF = -1400 + 350 \cdot AC_{PCC} \cdot (0.5 + PREFORM) + 43.4 f'_c \wedge^{0.4} - 0.2 (FT_{cycles} \cdot AGE) + 43 H_{PCC} - 536 WC_{PCC} \quad (\text{Eq. 50})$$

Where

AC_{PCC} = PCC air content (percent); 6 percent

AGE = time since construction (years)

$PREFORM$ = 1 if preformed sealant is present; 0 if not

f'_c = PCC compressive strength (psi)

FT_{cycles} = average annual number of freeze-thaw cycles

H_{PCC} = PCC slab thickness (inches)

WC_{PCC} = PCC water/cement ratio

For the JPCP IRI model, the MEPDG allows the following model coefficients to be modified as part of the Arizona local calibration to improve IRI prediction accuracy and remove bias:

$$C1 = 0.60$$

$$C2 = 3.48$$

$$C3 = 1.22$$

$$C4 = 45.20$$

SUMMARY

Tables 66 and 67 present the local calibration coefficients for HMA pavements and JPCP, respectively, that can be modified to improve model prediction accuracy and eliminate bias.

Table 66. HMA Pavement Local Calibration Coefficients

Distress/IRI	Local Calibration Coefficients That Improve Prediction Accuracy	Local Calibration Coefficients That Eliminate Bias
Rutting	$k_{1r}, \beta_{S1}, \beta_{B1}$	$\beta_{2r}, \beta_{3r}, k_{2r}, k_{3r}$
Alligator cracking	C_2, k_{f1}	C_1, k_{f2}, k_{f3}
Transverse cracking	β_{t1}	β_{t1}
IRI	C_2, C_3, C_4	C_1

Table 67. JPCP Local Calibration Coefficients

Distress/IRI	Local Calibration Coefficients That Improve Prediction Accuracy	Local Calibration Coefficients That Eliminate Bias
Faulting	$C_2, C_3, C_4, C_5, C_6, C_7$	C_1
Transverse cracking	C_2, C_5	C_1, C_4
IRI	C_1, C_2, C_3	C_4

